UNLV | UNIVERSITY LIBRARIES

UNLV Retrospective Theses & Dissertations

1-1-2003

The relationship of cell morphology, density, and mechanical properties in a rigid polyurethane foam

Michelle Cameron Nelson
University of Nevada, Las Vegas

Follow this and additional works at: https://digitalscholarship.unlv.edu/rtds

Repository Citation

Nelson, Michelle Cameron, "The relationship of cell morphology, density, and mechanical properties in a rigid polyurethane foam" (2003). *UNLV Retrospective Theses & Dissertations*. 1605.
http://dx.doi.org/10.25669/zb4u-7ua4

This Thesis is protected by copyright and/or related rights. It has been brought to you by Digital Scholarship@UNLV with permission from the rights-holder(s). You are free to use this Thesis in any way that is permitted by the copyright and related rights legislation that applies to your use. For other uses you need to obtain permission from the rights-holder(s) directly, unless additional rights are indicated by a Creative Commons license in the record and/or on the work itself.

This Thesis has been accepted for inclusion in UNLV Retrospective Theses & Dissertations by an authorized administrator of Digital Scholarship@UNLV. For more information, please contact digitalscholarship@unlv.edu.

THE RELATIONSHIP OF CELL MORPHOLOGY, DENSITY, AND MECHANICAL PROPERTIES IN A RIGID POLYURETHANE FOAM

by

Michelle Cameron Nelson

Bachelor of Science
University of Nevada, Las Vegas
2001

A thesis submitted in partial fulfillment
of the requirements for the

Master of Science Degree in Mechanical Engineering
Department of Mechanical Engineering
Howard R. Hughes College of Engineering

Graduate College
University of Nevada, Las Vegas
December 2003

Reproduced with permission of the copyright owner. Further reproduction prohibited without permission.

UMI Number: 1417782

Copyright 2004 by
Nelson, Michelle Cameron

All rights reserved.

INFORMATION TO USERS

The quality of this reproduction is dependent upon the quality of the copy submitted. Broken or indistinct print, colored or poor quality illustrations and photographs, print bleed-through, substandard margins, and improper alignment can adversely affect reproduction.

In the unlikely event that the author did not send a complete manuscript and there are missing pages, these will be noted. Also, if unauthorized copyright material had to be removed, a note will indicate the deletion.

UMI®

UMI Microform 1417782
Copyright 2004 by ProQuest Information and Learning Company.
All rights reserved. This microform edition is protected against unauthorized copying under Title 17, United States Code.

ProQuest Information and Learning Company
300 North Zeeb Road
P.O. Box 1346
Ann Arbor, MI 48106-1346

Reproduced with permission of the copyright owner. Further reproduction prohibited without permission.

Copyright by Michelle Cameron Nelson 2004
All Rights Reserved

Reproduced with permission of the copyright owner. Further reproduction prohibited without permission.

UNLV
UNIVERSITY OF NEVADA LAS VEGAS

Thesis Approval
The Graduate College
University of Nevada, Las Vegas

November 13, 2003

The Thesis prepared by

Michelle Cameron Nelson

Entitled

The Relationship of Cell Morphology, Density, and Mechanical Properties in a Rigid Polyurethane Foam

is approved in partial fulfillment of the requirements for the degree of

Master of Science in Mechanical Engineering

Examination Committee Chair

Dean of the Graduate College

Examination Committee Member

Examination Committee Member

Graduate College Faculty Representative

1017-53

Reproduced with permission of the copyright owner. Further reproduction prohibited without permission.

ABSTRACT

The Relationship of Cell Morphology, Density, and Mechanical Properties in a Polyurethane Foam System

by

Michelle Cameron Nelson

Dr. Brendan O'Toole, Examination Committee Chair
Associate Professor of Mechanical Engineering
University of Nevada, Las Vegas

Polyurethane foam, used as a supporting or insulating material, is sometimes formed in complex molds with significant variations in geometry and size. This work investigates the relationships between cell morphology, density, and mechanical properties in a molded polyurethane material using relatively small cylindrical molds. Understanding these relationships will help mechanical designers analyze and predict the responses of foam components accurately.

Three mold sizes are used to study changes in cell morphology (cell area, cell diameter, aspect ratio, cell angle, cell edge length, cell face thickness, and cell edge thickness), density, and mechanical properties (Young's modulus, peak yield, and collapse stress) with respect to vertical and radial positions. In addition, five time periods (1-day, 2-days, 7-days, 30-days, and 90-days) are used to determine aging effects on density and compressive mechanical properties of small diameter molds. Finally, theoretical equations are used to compare the experimental and theoretical density and mechanical properties.

Reproduced with permission of the copyright owner. Further reproduction prohibited without permission.

TABLE OF CONTENTS

ABSTRACT iii

LIST OF FIGURES vi

LIST OF TABLES ix

ACKNOWLEDGMENTS x

CHAPTER 1: INTRODUCTION 1
- Purpose of Study 1
- Research Objectives/ Questions 2
- Study Procedures and Methodology 3
- Paper Format 5

CHAPTER 2: MECHANICAL PROPERTIES AND CHEMISTRY BACKGROUND ... 6
- Mechanical Properties of Foam 6
- Previous Research at Sandia National Laboratories 7
- Previous Research at University of Nevada, Las Vegas 11
  - Mechanical Engineering Department 11
  - Chemistry Department 16
- Closely Related Research 17

CHAPTER 3: CELL MORPHOLOGY BACKGROUND AND THEORY 19
- Foam Geometry and Cell Morphology 19
- Linking Morphology to Mechanical Properties 27
  - Theoretical Equations for Density and Mechanical Properties 30
  - Previous Research on Morphology 33

CHAPTER 4: EXPERIMENTAL PROCEDURES 37
- Polyurethane Foam Fabrication 37
- Processing 42
  - Mechanical Testing Sample Preparation 48
  - Scanning Electron Microscope Sample Preparation 49
- Testing 57
  - Mechanical Testing 58
  - Imaging Analysis 61
  - Density Gradients 63

Reproduced with permission of the copyright owner. Further reproduction prohibited without permission.

CHAPTER 5: RESULTS 64
Experimental Density and Mechanical Results 65
Average Density and Mechanical Properties for Each Designation Batch 68
Density and Mechanical Property Gradients as a Function of Vertical Position 72
Effect of Mold Order on Density and Mechanical Properties 81
Discussion of Density and Mechanical Results 84
Cell Morphology Results 86
Level Changes in Cell Morphology 94
Radial Changes in Cell Morphology 104
Discussion of Cell Morphology Results 111
Theoretical Density and Mechanical Results 112
Volume Fraction 113
Density 115
Modulus 116
Collapse Stress 118
Discussion of Theoretical Results 121

CHAPTER 6: LINKING DENSITY AND MECHANICAL PROPERTIES TO CELL MORPHOLOGY 123

CHAPTER 7: CONCLUSIONS 130

APPENDIX A: MATERIALS AND EQUIPMENT 133

APPENDIX B: FOAM PROCESSING LOG 137

APPENDIX C: RADIAL DENSITY GRADIENT SAMPLE PREPARATION 141

APPENDIX D: DENSITY AND MECHANICAL PROPERTIES 143

APPENDIX E: CELL MORPHOLOGY IMAGES, TABLES, AND GRAPHS 171

APPENDIX F: THEORETICAL CALULATIONS 207

APPENDIX G: PERMISSION TO USE COPYRIGHTED MATERIAL 224

REFERENCES 226

VITA 229

Reproduced with permission of the copyright owner. Further reproduction prohibited without permission.

LIST OF FIGURES

CHAPTER 1: INTRODUCTION
Figure-1.1 Measurements to Describe Foam Morphology 3

CHAPTER 2: MECHANICAL PROPERTIES AND CHEMISTRY BACKGROUND
Figure-2.1 Stress-Strain Curve for ReCrete Polyurethane Foam in Compression 7

CHAPTER 3: CELL MORPHOLOGY BACKGROUND AND THEORY
Figure-3.1 Kelvin Geometry (One Cell Forms the Repeating Unit Structure) 20
Figure-3.2 Weaire Phelan Geometry (A Combination of Multiple Cells Having Two Different Geometries Forms the Repeating Unit Structure) 20
Figure-3.3 Pentagonal Dodecahedron 21
Figure-3.4 Gibson and Ashby's Cubic Model Cell for Closed Foams 22
Figure-3.5 (a) Open-Celled Foam (b) Closed-Celled Foam 24
Figure-3.6 Measurements to Describe Foam Morphology 26
Figure-3.7 (a) Optical Image of Foam Structure, (b) SEM Image of Foam Structure 28
Figure-3.8 Confocal Image of Foam Structure 29

CHAPTER 4: EXPERIMENTAL PROCEDURES
Figure-4.1 (a) 1-L container and Scale, (b) Manual Mixing, (c) Electric Overhead Mixer, (d) Pouring Chemical Formulation into Molds 38
Figure-4.2 (from left to right) Small Mold, Tall Mold, and Reference Mold 39
Figure-4.3 1500-cc Batch Worksheet 41
Figure-4.4 (from left to right) Small Mold and Specimen, Tall Mold and Specimen, and Reference Mold and Specimen 42
Figure-4.5 Cutting Schematic of Small Cylindrical Columns (a) 31.75-mm Samples (b) 63.5-mm Samples 43
Figure-4.6 Cutting Schematic of Tall Cylindrical Columns as 31.75-mm Samples .. 44
Figure-4.7 Delta 12-in Disk Sander 45
Figure-4.8 Reference Mold Cut into Sections (a) Side View (b) Top View of Bottom Section 46
Figure-4.9 Craftsman 8-in Drill Press and Hole Saw 47
Figure-4.10 (a) Mitutoyo Absolute Digimatic Calipers (b) Mettler Toledo Digital Scale 47
Figure-4.11 Mechanical Testing Samples with Reflective Strips (left to right) 25.4-mm Height and 50.8-mm Height 48
Figure-4.12 Storage of Aged Samples 49
Figure-4.13 (a) Epoxy Mold with Foam and Weight, (b) Foam with Epoxy Reinforcement 50

Reproduced with permission of the copyright owner. Further reproduction prohibited without permission.

Figure-4.14 Schematic of Perpendicular and Parallel Samples 51
Figure-4.15 Position of Foam in Vice (a) Perpendicular Slice, (b) Parallel Slice 52
Figure-4.16 Sample Sliced with Band Saw (a) Perpendicular Slice, (b) Parallel Slice 52
Figure-4.17 (a) JOEL-5600 SEM and (b) Cressington Sputter Coater 53
Figure-4.18 Parallel and Perpendicular Samples Affixed to Metal Cylinders with Graphite Tape (shown after being sputter coated with 24kt gold) 53
Figure-4.19 (a) Metal Cylinder Holder, (b) Microscope Stage 54
Figure-4.20 Screen Capture of JOEL SEM Software 55
Figure-4.21 Imaging the Perpendicular Foam Slice 56
Figure-4.22 Imaging the Parallel Foam Slice 56
Figure-4.23 United Axial Loading Machine 59
Figure-4.24 Calculation Young's Modulus from the Stress-Strain Curve 60
Figure-4.25 Image Pro Screen 62
Figure-4.26 Manual Measurements 63

CHAPTER 5: RESULTS
Figure-5.1 Actual Stress-Strain Curves for a Small, Tall, and Reference Mold 67
Figure-5.2 Average Density vs. Batch 69
Figure-5.3 Percent Differences for Aged Density 69
Figure-5.4 Average Normalized Modulus vs. Batch 70
Figure-5.5 Average Normalized Peak Yield vs. Batch 71
Figure-5.6 Average Normalized Collapse Stress vs. Batch 71
Figure-5.7 Diagram of Levels for the Small, Tall, and Reference Molds 72
Figure-5.8 Average Density vs. Level: Small and Reference Molds 25.4-mm Samples 73
Figure-5.9 Average Density vs. Level: Tall Molds 25.4-mm Samples 74
Figure-5.10 Average Density vs. Level: Small Mold 50.8-mm Samples 74
Figure-5.11 Average Normalized Modulus vs. Level: Small and Reference Molds 25.4-mm Samples 76
Figure-5.12 Average Normalized Peak Yield vs. Level: Small and Reference Molds 25.4-mm Samples 76
Figure-5.13 Average Normalized Collapse Stress vs. Level: Small and Reference Molds 24.5-mm Samples 77
Figure-5.14 Average Normalized Modulus vs. Level: Tall Molds 25.4-mm Samples 78
Figure-5.15 Average Normalized Peak Yield vs. Level: Tall Molds 25.4-mm Samples 78
Figure-5.16 Average Normalized Collapse Stress vs. Level: Tall Molds 25.4-mm Samples 79
Figure-5.17 Average Normalized Modulus vs. Level: Small Molds 50.8-mm Samples 80
Figure-5.18 Average Normalized Peak Yield vs. Level: Small Molds 50.8-mm Samples 80
Figure-5.19 Average Normalized Collapse Stress vs. Level: Small Molds 50.8-mm Samples 81

Reproduced with permission of the copyright owner. Further reproduction prohibited without permission.

Figure-5.20 Average Density vs. Mold Order 82
Figure-5.21 Average Normalized Modulus vs. Mold Order 83
Figure-5.22 Average Normalized Peak Yield vs. Mold Order 83
Figure-5.23 Average Normalized Collapse Stress vs. Mold Order 84
Figure-5.24 Location and Names of Samples to be Imaged 86
Figure-5.25 Location and Names of Images taken on Parallel and Perpendicular Slices 87
Figure-5.26 Small Mold Parallel Images 89
Figure-5.27 Tall Mold Parallel Images 90
Figure-5.28 Reference Mold Parallel Images 91
Figure-5.29 Tall Mold Bottom Sample Perpendicular Images 91
Figure-5.30 Visual Representation of Measurements 93
Figure-5.31 Average Area vs. Sample 94
Figure-5.32 Average Maximum Diameter, Average Minimum Diameter, and Average Mean Diameter vs. Sample 96
Figure-5.33 Average Aspect Ratio vs. Sample Number 98
Figure-5.34 Average Angle vs. Sample Number 100
Figure-5.35 Average Cell Edge Length, Cell Face Thickness, and Edge Thickness vs. Sample Number 103
Figure-5.36 Average Area vs. Radial Position 105
Figure-5.37 Average Maximum Diameter, Average Minimum Diameter, and Average Mean Diameter vs. Radial Position 107
Figure-5.38 Average Aspect Ratio vs. Radial Position 108
Figure-5.39 Average Angle vs. Radial Position 108
Figure-5.40 Average Cell Edge Length, Cell Face Thickness, and Edge Thickness vs. Radial Position 110
Figure-5.41 Theoretical Volume Fraction 114
Figure-5.42 Theoretical and Experimental Density 116
Figure-5.43 Theoretical and Experimental Normalized Modulus 117
Figure-5.44 Theoretical and Experimental Normalized Collapse Stress (σ_{pl}) 120
Figure-5.45 Theoretical and Experimental Normalized Collapse Stress (σ_{el}) 121

CHAPTER 6: LINKING DENSITY AND MECHANICAL PROPERTIES TO CELL MORPHOLOGY

Figure-6.1 Actual Stress-Strain Curve of Batch C5 (S-2-1) 126
Figure-6.2 Average Theoretical and Experimental Radial Density 128

Reproduced with permission of the copyright owner. Further reproduction prohibited without permission.

LIST OF TABLES

CHAPTER 3: CELL MORPHOLOGY BACKGROUND AND THEORY
Table 3.1 Characterization Chart for Foams 23

CHAPTER 4: EXPERIMENTAL PROCEDURES
Table 4.1 Definitions of Measurements 62

CHAPTER 5: RESULTS
Table-5.1 Chapter 5 Outline 64
Table-5.2 Analyzed Foam Batches 65
Table-5.3 Reference Batch Average Values and Standard Deviations 66
Table-5.4 Differences in Vertical Density for Different Molds 75
Table-5.5 Differences in Properties for Different Mold Orders 82
Table-5.6 Measured Properties 92
Table-5.6 Percent Differences between Theoretical and Experimental Modulus .. 118

CHAPTER 6: LINKING DENSITY AND MECHANICAL PROPERTIES TO CELL MORPHOLOGY
Table-6.1 Percentage Differences in Properties per Level 124
Table-6.2 Percent Differences in Radial Density 128

Reproduced with permission of the copyright owner. Further reproduction prohibited without permission.

ACKNOWLEDGEMENTS

Thank you to my advisor, Dr. Brendan O'Toole, who saw potential in an undergraduate student and hired me on the foams project in the summer of 1999. I am glad I was able to witness the beginning of this project and possibly its end. It has been an interesting journey and I've enjoyed most of it. Thanks so much for your time, support, and guidance. I'd also like to thank my committee members, Dr. Mohamed Trabia, Dr. William Culbreth, and Dr. Malcolm Nicol, who have provided constructive criticism to insure my thesis is the best I can make it.

Thanks to Leroy Whinnery and Steven Goods at Sandia National Labs for taking time to provide the team at UNLV with knowledge of your previous works and for helping me learn how to make and prepare the foam used for this project. Without your assistance none of this would have been possible. Thanks also to the DOE Cooperative Agreement DE-FC08-98NV13410 for financial support

I'd like to thank all the individuals who helped me with aspects of this thesis. Ray Kozak who spent many hours with me in the engineering shop milling samples for SEM. Dr. Robert Fairhurst who spent many hours with me imaging the foam samples. Heidi Aquino who took time out of her busy schedule to help me with epoxying samples, SEM imaging, and for just being my friend and listening to my problems and triumphs. I'd also like to thank Dacia Jackovich who spent endless hours analyzing images and testing foam samples. I couldn't have finished on time without your help. I'd also like to thank her for being by my side since the beginning of my thesis and helping me with anything I needed

Reproduced with permission of the copyright owner. Further reproduction prohibited without permission.

to get done. Thanks for being a great friend, giving me encouragement, and a sense to take breaks and have fun once in a while.

Finally, I would like to thank my husband, Edward Hawkins, for providing love and support though all of these years I've spent in college. He provided a voice of reason and lent his shoulder when I cried. I would have been lost without his strength.

Reproduced with permission of the copyright owner. Further reproduction prohibited without permission.

CHAPTER 1

INTRODUCTION

1.1 Purpose of Study

Replacement foam for stockpile applications is currently being studied by the Department of Energy. In stockpiles, foam is used to protect electronics and to provide energy absorption. The stockpile is twenty to thirty years old, some components are degrading, and others are replaced by improved components. The foam itself degrades or the electronic modules fail and/or become obsolete and must be replaced. TDI (Toluene Di-Isocyanate) is an older type of foam commonly used in the stockpile. This foam is characterized fairly well, and its mechanical properties as a function of strain rate and density are documented and understood to some degree [1]. It is becoming increasingly difficult to produce new foam products with this material because of regulatory constraints. The PU foam industry is moving away from TDI foams because they can be hazardous to handle during fabrication [2] and can be harmful to the environment [3]. One new foam, ReCrete, is considered a promising candidate for replacement because it is considered safer to manufacture than TDI. [4]. It is important to study mechanical properties, morphology, and chemistry as a function of time to determine if ReCrete is comparable to TDI. It is known that density will affect the mechanical properties of rigid polyurethane foam [5]. The density of polyurethane foam is influenced by the cell morphology or microstructure, which consists of cell size, cell edge length, cell face

Reproduced with permission of the copyright owner. Further reproduction prohibited without permission.

thickness, cell edge thickness and the anisotropy of the cells. Therefore, the morphology plays an important role in the deformation behavior of the foam under loading. The chemical makeup of the cell walls affects the stiffness and strength of the polymer material as well, and chemical changes can play a major role in how these properties change with time. Previous work has shown that mold size and processing temperature affect the compressive mechanical properties of ReCrete foam [6, 7, 8]. Density differences do not account for all of the variations in the mechanical properties. One objective of this work is to determine if the cell morphology is causing the mechanical property changes. A parallel project in the UNLV Chemistry Department is investigating whether there are significant chemical changes that may also be affecting the mechanical properties. The polyurethane foam studied in this work is processed under room temperature conditions to examine cell morphology, density, mechanical properties, and chemistry.

1.2 Research Objectives/Questions

1. How does cell morphology (cell size, cell edge length, cell face thickness, edge thickness and the anisotropy of the cells) relate to density and mechanical properties?
2. Does the cell morphology, density or mechanical properties change significantly from the bottom to the top of the mold or from the center to the outside of the mold?
3. Do the mechanical properties change significantly during the first ninety days of aging at room temperature?

Reproduced with permission of the copyright owner. Further reproduction prohibited without permission.

1.3 Study Procedures and Methodology

Studies are performed to relate theoretical and experimental results, in addition to relating morphology to density and mechanical results. A theoretical study is conducted to estimate the density and mechanical properties of polyurethane foam using cell edge length, cell face thickness, cell edge thickness, and the area fraction of the solid contained in the cell edges. Three of these measurements mentioned are shown in Figure-1.1 in addition to the cell diameter. The area fraction is calculated from these and other measurements.

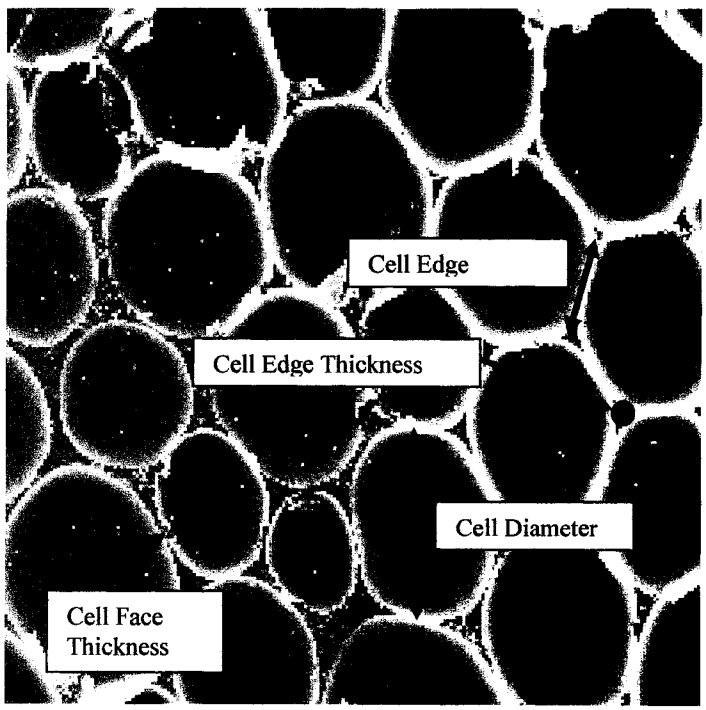

Figure-1.1: Measurements to Describe Foam Morphology

For experimental analysis, several batches of foam are made in short tubes (28.7-mm diameter and 154.2-mm height) and tall tubes (28.7-mm diameter and 457.2-mm height)

Reproduced with permission of the copyright owner. Further reproduction prohibited without permission.

at room temperature free rise conditions. This means that the foam rises in a tube that is open at the top so that the foam is unrestricted in the z-direction. These batches are used for mechanical testing of 25.4-mm and 50.8-mm gauge length samples and for a cell morphology analysis. The mechanical tests for the 25.4-mm samples are performed at 1-day, 2-day, 7-day, 30-day, and 90-day intervals. However, the 50.8-mm samples are tested at just the 2-day interval. In addition, a reference batch at room temperature free rise conditions is fabricated in a large mold (178-mm diameter and 178-mm height) for a theoretical comparison of the density, mechanical properties, and cell morphology. The reference batch has minimal mold effects on the foam. This batch is used for mechanical testing of 25.4-mm gauge length samples at the 3-day interval and for cell morphology analysis of its middle section.

This work includes the collection of compressive mechanical properties (Young's modulus, peak yield, and collapse stress), cell morphology (cell diameter, cell edge length, cell face thickness, edge thickness, aspect ratio, angle, and area of the cells) as it relates to levels and radial positions, and theoretical calculations of the volume fraction, density, Young's modulus, and collapse stress. Measurements of cell morphology are taken for sections that are perpendicular and parallel to the rise direction of the foam. Coring analysis is a macroscopic way of determining density gradients in the foam presented in previous work [6, 7, 8] and will be compared to the theoretical density calculated using cell morphology.

Reproduced with permission of the copyright owner. Further reproduction prohibited without permission.

1.4 Paper Format

This thesis consists of seven chapters. Chapter 1 provides an introduction to the thesis including detail on research objectives, study procedures, and methodology. Chapter 2 provides an introduction to mechanical testing theory on foams and includes a background on the mechanical and chemistry aspects of the foam. The third chapter provides a background on the morphology and imaging as well as definitions and discussions on foam geometry and cell morphology. In addition, this chapter presents theoretical equations that are used to calculate density and mechanical data using cell morphology measurements. Chapter 4 presents the procedures for experimental testing and analysis. This includes fabrication, processing, and testing. Chapter 5 details and discusses the experimental results gathered from morphology analysis and mechanical testing. A discussion of linking mechanical properties to morphology is provided in Chapter 6. Finally, conclusions are supplied in Chapter 7.

Reproduced with permission of the copyright owner. Further reproduction prohibited without permission.

CHAPTER 2

MECHANICAL PROPERTIES AND CHEMISTRY BACKGROUND

2.1 Mechanical Properties of Foam

This section is devoted to explaining and defining the mechanical properties of foam. There are three types of foams, elastomeric, elastic-plastic, and brittle foam. Elastomeric foam deforms elastically during the plateau (collapse), and the deformation is recoverable but non-linear. Foam that is elastic-plastic collapses plastically, and the strain is no longer recoverable during the plateau (collapse). Elastic-plastic foams (ceramic foam) experience brittle crushing during the plateau (collapse) [5]. The foam dealt with in this thesis is called ReCrete which was developed at Sandia National Labs in Livermore, California. Goods and Whinnery et al. show that Crete and, therefore ReCrete is an elastomeric foam [1]. However, from other sources it makes more sense to consider ReCrete as an elastic-plastic foam. The stress-strain curve of the ReCrete foam is shown in Figure-2.1.

All foams have three important stages during axial compression as shown on a stress-strain curve. These are linear elasticity, collapse plateau, and densification. The modulus of elasticity is defined as the initial slope in the linear elastic portion of the stress-strain curve as shown in Figure-2.1. The modulus is calculated as the stress divided by the strain of the linear portion of the stress-strain curve. The second stage of foam deformation is characterized by a relatively large deformation that occurs at a constant

Reproduced with permission of the copyright owner. Further reproduction prohibited without permission.

stress. During this stage, the individual cell walls in the foam are buckling (or collapsing). This constant stress is referred to as the collapse stress or the collapse plateau which is also shown in Figure-2.1. In some instances, the foam experiences a yield strength that is slightly higher than the collapse stress. The peak yield stress is defined as the maximum stress before the collapse phase begins. The final stage of foam deformation begins after all of the individual cells have collapsed. At this stage, the foam density has increased significantly because the axial compression may be up to 60-70% and there is very little expansion in the radial direction. After this densification, the stress rises rapidly with very small increase in strain [5].

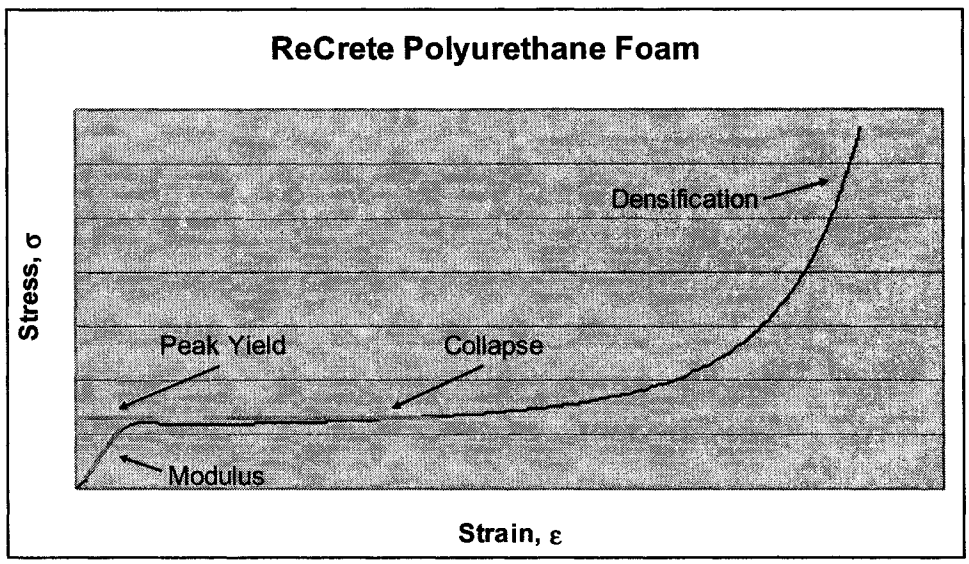

Figure-2.1: Stress-Strain Curve for ReCrete Polyurethane Foam in Compression

2.2 Previous Research at Sandia National Laboratories

Crete and ReCrete are two types of foam developed and tested by Steven Goods and Leroy Whinnery at Sandia National Labs (SNL) located in Livermore, California. [1, 4,

Reproduced with permission of the copyright owner. Further reproduction prohibited without permission.

9]. The objective of studies performed at SNL includes creating a new foam that will replace TDI (BKC 44402) and to perform tests on the new foams to insure they will hold up in a weapon system application. Tension, compression, and impact tests are performed to determine mechanical properties and energy absorption. Goods and Whinnery also developed a formula to normalize the foam's mechanical properties to density [1, 9]. Lastly, experimental work is related to theoretical values of Young's modulus and collapse stress found by using equations presented by Gibson and Ashby [1, 9]. In addition to performing tests on Crete and ReCrete, TDI samples are subjected to thermal aging to see how the mechanical properties of the foam age [10].

The studies at SNL focus on foams with fairly uniform densities by using "cored" samples. This is accomplished by using a large mold to form the foam and then cutting out blocks from this molded sample. The blocks are then shaped into right circular cylinders with the cylinder axis parallel to the direction of the foam rise. All samples have a diameter of 28.7-mm and a height of 50.8-mm. None of the cylinders are taken within 3-mm below the surface or contain skin. This type of sample is called a "cored" sample because it is cored out from foam that is molded [1, 9, 10].

Crete and ReCrete are formulations of rigid polyurethane foam that were both created at SNL. "As with other polyurethane foams, the reaction of the water with isocyanate produces carbon dioxide that expands the foam" [9]. The only difference between the two formulations is the use of different isocyanates. Crete is made with Isonate 143L whereas ReCrete is made with Rubinate 1680. Both were created for the same reason, namely to replace the TDI prepolymer [1, 4, 10].

Reproduced with permission of the copyright owner. Further reproduction prohibited without permission.

Tensile and compressive tests are performed on foam samples of densities ranging from 0.12- g/cm^3 to 0.60-g/cm^3. By doing this, a power law relationship is developed between the mechanical properties and the densities. Equation 2.1 states that the modulus is proportional to the density with an exponent of 1.7. In addition, Equation 2.2 states the elastic collapse stress is proportional to the density with an exponent of 2.1. Tensile and compressive tests show that the stress-strain curves are fairly close to one another and can be considered identical. Therefore, Equation 2.1 can be used to normalize both tensile and compressive moduli. It is also important to note that Equation 2.2 is used to normalize yield stress as well as collapse stress. These equations are of particular importance to rule out differences in density when trying to compare moduli of different density foams [9].

$$E = \rho^{1.7} \qquad \text{Equation 2.1}$$

$$\sigma_{el} = \rho^{2.1} \qquad \text{Equation 2.2}$$

When comparing the tensile, compressive, and impact testing stress-strain curves, it is evident that at a particular density, the compressive strength is lower than the tensile strength, which is still lower than the impact strength [1]. However, impact testing causes the foam to fail catastrophically unlike the failure modes for the slow strain rate compressive testing [1]. In addition, the tensile and compressive testing shows that the total energy absorption is much greater in compression than tension [9]. Interestingly, the energy absorption through impact testing begins to decline after a certain density is reached whereas through the compressive testing, the energy continues to climb with increasing density [1].

Reproduced with permission of the copyright owner. Further reproduction prohibited without permission.

Thermal aging is performed on TDI (BKC 44402) at room temperature, 60°C, and 80°C conditions. Samples aged for three months show that mass decreases for samples aged at 60°C and 80°C, but the mass actually increases for samples aged at room temperature. Mass decreases are attributed to loss in surfactant whereas mass increases are attributed to a possible absorption of moisture in the air. After aging samples for one year it is shown that the impact properties decrease, but there is no clear effect for the quasi-static mechanical properties. Impact testing reveals losses in toughness but minimal changes in crush strength. Compression testing does not show clear evidence that aging has any effect on the modulus or collapse stress. Tensile testing is the same with regard to modulus, fracture strength and fracture strain. This thesis shows the effects of three months room temperature aging on the mechanical properties of ReCrete. It is uncertain whether the same results will surface since the samples used in the SNL study are cored and in this study are molded [10].

Work at SNL also shows that mechanical properties correlate fairly well with theoretical data when the density of the foam is known. The use of equations developed by Gibson and Ashby show that the elastic modulus and elastic collapse stress of experimental tests matches fairly well with theoretical calculations. This shows that it is possible to relate experimental and theoretical properties. However, will this still hold true when the density of the material is not known and is in fact calculated using measurements of the foam's cell walls and struts? In addition, is it possible to theoretically predict properties for a smaller area of foam such as a 10-mm^2 area? This thesis will try to answer these important questions [9].

Reproduced with permission of the copyright owner. Further reproduction prohibited without permission.

2.3 Previous Research at University of Nevada, Las Vegas

Polymer foam work performed at the University of Nevada, Las Vegas (UNLV) is conducted by two separate and corresponding departments. The mechanical engineering and chemistry departments work together to perform linked experiments relating the chemical and mechanical properties of the foam. The first subsection below describes work performed by the mechanical engineering department, and the second subsection includes work performed by the chemistry department.

2.3.1 Mechanical Engineering

This project is different from the SNL work because it is focusing on foams that are molded into containers, which contain density gradients. The foam also contains skin, which is a small layer of unfoamed polyurethane that surrounds the outer side of each foam cylinder. This type of sample is called a "molded" sample because it is molded in place and not cored before being tested for mechanical properties. The density gradients and skin might affect the mechanical properties (modulus, yield, and collapse) of the polyurethane foam. In addition, the cylindrical molds affect the temperature distribution and flow of the polymer material during the foaming process. This may also affect the morphology and chemistry of the foam [6]. In addition to using molded samples, all experiments are performed by the University of Nevada, Las Vegas with free rise polyurethane foam. This is foam that is poured into a mold with an open top so that the foam can rise freely in the vertical direction.

Prior to any experiments being performed using molded samples, a theoretical study was completed to calculate the mechanical properties of samples with skin. This study treats the skin and foam core as a two-part composite material using the rule of mixtures

Reproduced with permission of the copyright owner. Further reproduction prohibited without permission.

equation [11]. It is shown that the composite compressive modulus and tensile strength increases linearly as a function of skin volume fraction. The skin volume fraction for most rigid polyurethane foams is very small. The smallest molded samples in this thesis have a skin volume fraction of approximately 0.35%. It is not expected that the skin will have a major effect on the foam modulus or collapse strength at this low volume fraction but it may influence the mode of failure initiation. Nevertheless, some foam structures (like architectural columns) are produced in a two-step process with a thick solid polyurethane skin and a foam core. Considering this type of cross-section, the load carried by the skin, or in this case the solid polyurethane section, will carry most of the load. Of course, this is an extreme case but it shows that the composite's strength improves with added skin [12].

In addition to performing studies with molded samples, the project has extensively focused on the effects of mold sizes and processing temperatures on the foam's density and mechanical properties. Three documented studies were performed at the University of Nevada, Las Vegas. The first examines the effects of mold size on the vertical and radial density of polyurethane foam [7]. The second examines the effects of processing temperature on the density and mechanical properties of polyurethane foam [8]. The final is a combination of the two previous studies by looking at the combined effects of mold size and processing temperatures on density and mechanical properties [6].

In the paper entitled, "Effect of Mold Size on the Average Density and Density Gradients in a Polyurethane Foam System," three different mold sizes are studied to understand density gradients more clearly. The foam is prepared under room temperature conditions and poured into any of the three molds with inner diameters of approximately

Reproduced with permission of the copyright owner. Further reproduction prohibited without permission.

28.7-mm, 85.5-mm, and 174.6-mm. It is shown that smaller diameter molds yield foam with a higher mean density and larger radial density gradients. Findings also show that density increases slightly from the top of the mold to the bottom and that the vertical density gradient increases with mold size. Interestingly, the vertical density gradient of the small molds is almost nonexistent with just a 2% change in density from the top to the bottom of the mold. Finally, the last conclusion gathered from the study is that as the mold size increases, the size of the uniform density zone in the center of the mold increases. Overall, it is shown that a specimen uniform in the radial direction is produced from molds with large diameters and a specimen uniform in the vertical direction is produced from molds with small diameters [7].

Processing temperatures are initially studied and explained in, "Correlation of Processing Temperature, Density Gradients, and Mechanical Properties in a Molded Polyurethane Foam System". The processing temperature of a normal batch of polyurethane foam is ambient conditions (~25°C). This is the temperature at which the foam is mixed and allowed to rise in prepared molds for 30-minutes before being placed in an oven for 4-hours for post cure (66°C). The effect of processing temperature is studied by varying the mold temperature during this 30-minute rise time. During this 30-minute cure time, the foam is subjected to different processing temperatures by being poured into molds that are preheated in a water bath or an ice bath. The water bath is set to a particular temperature, and the foam cures in the molds while in the water bath. The ice bath has the same premise as the water bath except that cubes of ice are used to keep the tubes at 0°C and fluctuations in the temperature cannot be controlled. The processing temperatures chosen for this paper include a 0°C ice bath and several temperatures in a

Reproduced with permission of the copyright owner. Further reproduction prohibited without permission.

water bath (25°C, 40°C, and 90°C). In addition, the room temperature condition (25°C air) is studied as a reference [8].

This experiment shows that processing temperatures have an effect on the density and mechanical properties of polyurethane foam. When exposed to all processing temperatures the mean densities are above the density of the foam processed in a large mold at room temperature, which is most likely due to differences in mold size. It is also shown that the mean density and deviations in density decrease with increased processing temperatures. The mean density is also fairly uniform in the vertical direction for all temperatures except 0°C which has noticeably large variations in cell size and density. It is noticed that the radial density gradients are smaller as the processing temperature increases [8].

The actual collapse strength and modulus decrease with an increase in processing temperature, but this is attributed to the decrease in mean density. When the mechanical property values are normalized, taking into account differences in density, there is only a slight increase in the collapse strength. However, there is an increase in the foam modulus especially for the 25°C air. The 25°C and 40°C water bath batches show a slight increase but lower than the 25°C air. The 0°C and 90°C saw the least increase in modulus and a high increase in deviation but still had properties above the large reference mold at room temperature. At the conclusion of the paper it is thought that "the increased properties may be caused by the foam skin, density gradients, or differences in the foam microstructure" [8].

The final topic which links the two above is addressed in "Temperature and Mold Size Effects on Density Gradients and Mechanical Properties in a Polyurethane Foam

Reproduced with permission of the copyright owner. Further reproduction prohibited without permission.

System". This study involves the use of three different diameter molds (29-mm, 41-mm, and 51-mm), and five different processing temperatures (25°C, 40°C, 65°C, and 85°C and a reference batch made in a 4-L mold at room temperature). This study is performed to provide a greater understanding of the combined effects of mold size and processing temperatures over a smaller range of mold sizes and temperatures [6].

On average, increasing both the processing temperature and the mold size decreases the mean density. Mean densities range from 0.106-g/cc to 0.15-g/cc compared to the reference density of 0.101-g/cc. Interestingly, the radial density gradient increases from the small to the medium mold but decreases from the medium to the large mold. The radial density gradients also decrease as the processing temperatures increase. The vertical density gradients are minimal in all three tubes ranging from 0.09% to 2.4%. The vertical gradients decreased as the processing temperature increases and the mold size decreases [6].

As with the previous study, all processing temperatures yield foam with higher modulus, peak yield, and collapse strength values than the reference batch, which is due to the differences in mold size. Actual properties decrease as processing temperature increases. Normalized properties show the modulus decreases and the yield and collapse show a wave-like or scattered appearance with increasing processing temperatures. When the mold size increases the modulus, yield, and collapse stress increase slightly [6].

Through these studies it was determined that a more in depth analysis of the radial density needed to be performed. It was decided that the foam morphology should be studied to show differences among foams prepared at different processing temperatures and mold sizes. This thesis is the beginning of that study by first focusing on the small

Reproduced with permission of the copyright owner. Further reproduction prohibited without permission.

tubes and determining if the foam morphology can be understood both quantitatively and qualitatively.

2.3.2 Chemistry

In "Structural Characterization of Polyurethane Foam and Implications of Aging," chemical and structural analysis is performed on foam that is processed at 25°C and 85°C temperature conditions [13]. Photoacoustic infrared spectroscopy, IR imaging and thermal analyses are used to determine why the modulus of the foam material decreases with increasing processing temperatures. It is shown that one of the constituents used to process the foam, Rubinate 1680, which contains unstable uretoneimine linkages and unreacted diisocyanate, chemically changes at different processing temperature. This finding correlates to the changes in the modulus at different processing temperatures. It is concluded that high processing temperatures result in the breaking of the uretoneimine rings, which creates less rigid foam with a higher degree of crosslinking [13].

Aging of the foam samples over a three month period is also discussed in the paper and experiments show that the chemistry changes over time. Rubinate 1680 is shown to have continuing reactivity during the three month period using infrared analysis. Interestingly, the foam processed at 25°C shows more variation than the 85°C processed foam in DSC (differential scanning colorimetry), TMA (Thermal Mechanical Analysis), and IR (Infared Spectroscopy). It is advised by the UNLV Chemistry Department that more processing temperatures be explored to reveal if foams with better chemical properties can be discovered [13].

Morphological studies are also performed on foams processed at 25°C, 40°C, and 85°C using both SEM and optical microscopes. The observations suggest that a radial

Reproduced with permission of the copyright owner. Further reproduction prohibited without permission.

temperature gradient is responsible for the changes in chemical properties from the center to the outside of the sample. The 25°C foam sample exhibits cells of various sizes, the 85°C sample exhibits cells of a more uniform size. The 40°C sample exhibits a distribution somewhere in between the ones seen in the 25°C and 85°C samples. In a 25°C or 85°C sample the center has cells that are larger and more uniform than the side. This indicates that there are differences in morphology from the center to the side of the molded samples. Parallel images of the skin also show that, as the processing temperature increases, the cell size increases. This indicates that the density near the edge of the molded foam samples is lower as the processing temperature increases [13].

Even though the chemistry department touches on the morphology of the foams, it is the goal of this thesis to expand on their work. Instead of taking random images from samples, this study will systematically show images of the foam at certain distances into the core. Both parallel and perpendicular images will be shown and documented in addition to analyzing the images quantitatively and qualitatively.

2.4 Closely Related Research

Research performed by Harbron, Page, and Scarrow in the paper, "Methods of Minimizing Density Gradients in Rigid Polyurethane Foams," closely matches work performed at SNL and UNLV. The study focuses on changing the chemical formulation and the mold temperature simultaneously to reduce the radial and vertical density gradients of the foam. Foam made in a large container is sectioned into four levels with eleven samples per level. Each sample is 25.4-mm in height and 20.3-mm in diameter [14].

Reproduced with permission of the copyright owner. Further reproduction prohibited without permission.

Elemental analysis shows that there is no chemical change between the center samples at different levels. This means that the vertical density gradient is not caused by chemical changes in the foam. It is also shown that while there is overlap in densities from the bottom three levels, the top level is separate [14].

It is shown that varying the catalysts (i.e. gelling vs. high activity blowing vs. balanced) or by using high functionality isocyanates lowers the density gradients. Combining both of these variants, it is shown that the reduction of the density gradients is even more pronounced. However, when this is done, the foam is more difficult to mix and it rises quickly [14].

Three temperatures (20°C, 42-43°C, and 50°C) are used to examine the effect of mold temperatures on the density gradients of foam. It is shown that as the mold temperature increases, the density gradient decreases. This result is replicated by the study performed at UNLV [6]. This means that the rising foam in the room temperature mold creates the largest density gradient. This is another reason why this thesis is focusing on the room temperature foam first [14].

Reproduced with permission of the copyright owner. Further reproduction prohibited without permission.

CHAPTER 3

CELL MORPHOLOGY BACKGROUND AND THEORY

3.1 Foam Geometry and Cell Morphology

This section is mostly based on the work presented by Gibson and Ashby and can be found in more detail in their book entitled, "Cellular Solids: Structure and Properties" [5]. Ideas from the book are presented here to give an overview of foam geometry and cell morphology.

Foam morphology refers to the structure or form of foam. In other words, it is a description of the foam on a microscopic level. Foam consists of a connection of cells that are created by cell edges and cell faces. A unit cell consists of a single cell or a group of cells that can be connected repeatedly to simulate a large foam structure. The properties of a unit cell represent the properties of a uniform foam sample [5]. A cell can be thought of as a bubble with the geometry of Kelvin or Weaire Phelan shown in Figure-3.1 and Figure-3.2, respectively. Both of these geometries have been viewed in real life and are used as unit cells to describe the structure of foam cells [15]. Kelvin geometry consists of tetrakaidecahedral cells that have 14-sides with slightly curved faces, Weaire Phelan geometry consists of two types of cells, a 14-sided cell and a 12-sided cell. The Kelvin unit cell is one tetrakaidecahedral cell while the Weaire Phelan unit cell is a combination of six 14-sided cells and two 12-sided cells [5]. In an experiment where foam of equal-sized bubbles were made by blowing them from a nozzle immersed in a

Reproduced with permission of the copyright owner. Further reproduction prohibited without permission.

soap solution, Kelvin geometry was observed close to the edge of the container while the Weaire Phelan geometry was observed toward the center of the container [15]. This is perhaps why there is a density change from the center to the outside of the structure.

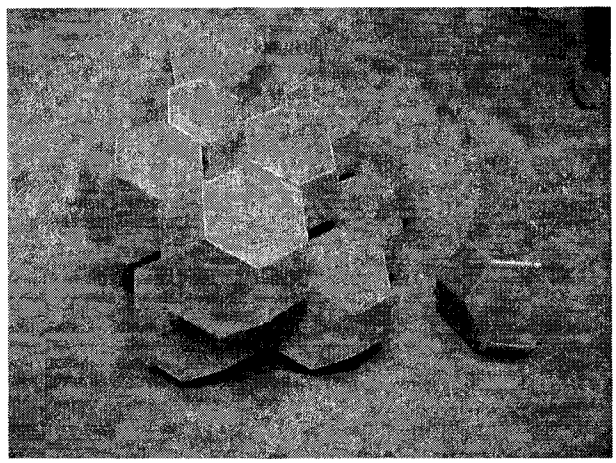

Figure-3.1: Kelvin Geometry (One Cell Forms the Repeating Unit Structure)

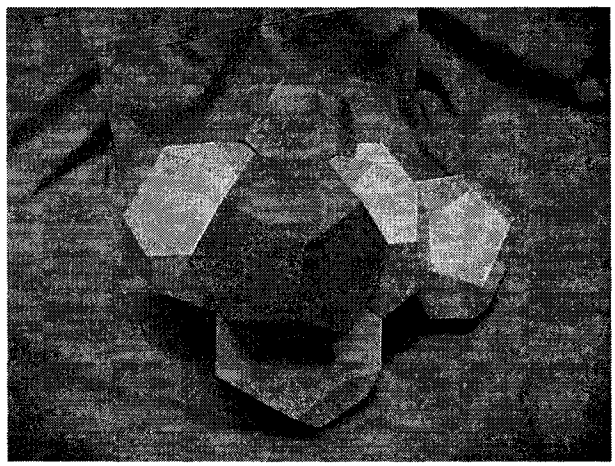

Figure-3.2: Weaire Phelan Geometry (A Combination of Multiple Cells Having Two Different Geometries Forms the Repeating Unit Structure)

Reproduced with permission of the copyright owner. Further reproduction prohibited without permission.

Another type of cell called the pentagonal dodecahedron has also been observed in foam structures and is shown in Figure-3.3 [16]. Even though this cell is shown as an actual foam structure, the pentagonal dodecahedron is not a space filling cell and cannot be packed consecutively without distortion of the pentagonal faces [5]. As Figure-3.3 reveals, some of the pentagonal faces in the foam cell are undeniably distorted. This is why the pentagonal dodecahedron is not used as a geometrical structure to theoretically calculate density.

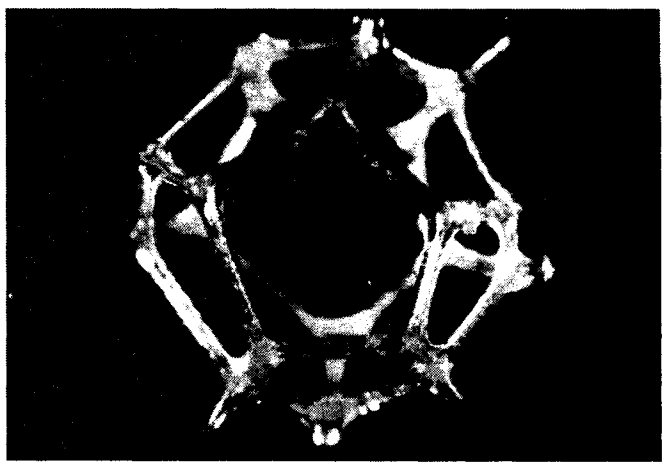

Figure-3.3: Pentagonal Dodecahedron [16]

While it is important to know the structure of actual foam cells, it is also important to realize that studies performed on these complex geometries that are used to relate mechanical properties to morphology can be meticulous. This is why Gibson and Ashby base the relationships of morphology to mechanical properties on what they call a cubic model cell shown in Figure-3.4. For closed-cell foams the cubic model contains cell walls with a length of "l", cell edges with a thickness "t_e" and cell faces with a thickness "t_f". In

Reproduced with permission of the copyright owner. Further reproduction prohibited without permission.

other studies, it is shown that the mechanical response of this cubic cell simulates the response of most foam materials especially well. This cell geometry, however, is not a realistic match of the geometry of an actual foam cell. The cubic model cell is also not a true unit cell because it cannot be combined in a repetitive fashion to create a larger structure as shown with the Kelvin and Weaire Phelan cells [5].

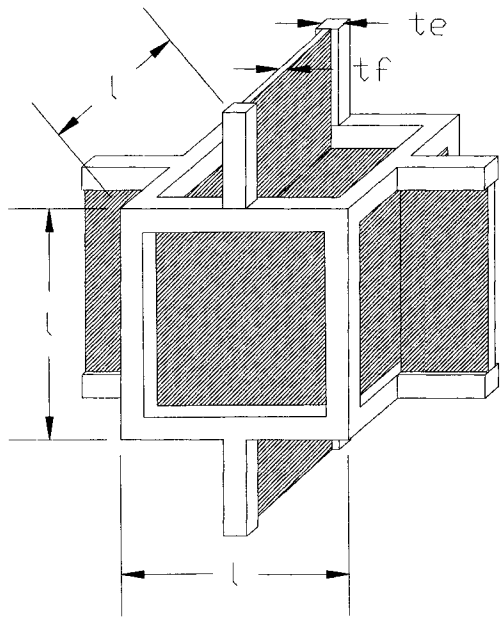

Figure-3.4: Gibson and Ashby's Cubic Model Cell for Closed Foams

A characterization chart for foams, created by Gibson and Ashby, is used to provide relevant morphological information and is shown in Table-3.1. A clear description of foam is given when the information of Table-3.1 is provided. The material in this paper, of course, is always rigid polyurethane foam [5].

There are two types of densities defined in reference to foams. The first is the density of the cellular material as shown in Table-3.1 and is designated by ρ^*. This density is

Reproduced with permission of the copyright owner. Further reproduction prohibited without permission.

relatively easy to calculate since only the volume and mass of the foam are needed. The second type of density is the density of the solid material that makes up the foam's edges and faces. This density is designated by ρ_s and has a greater value than ρ^* because it does not contain large air pockets, i.e. cells [5].

Table-3.1: Characterization Chart for Foams

Material	Rigid Polyurethane Foam
Density of Foam	ρ^*
Density of Solid	ρ_s
Cell Type	Closed
Edge Connectivity	Z_e
Face Connectivity	Z_f
Mean Edges/ Face	n
Mean Faces/ Cell	f
Cell Shape	
Symmetry of Structure	
Cell Edge Thickness	t_e
Cell Face Thickness	t_f
Cell Edge Length	l
Fraction of Material in Cell Edges	ϕ
Largest Principal Cell Dimension	L1
Smallest Principal Cell Dimension	L3
Intermediate Principal Cell Dimension	L2
Shape Anisotropy Ratios	R12= L1/L2 and R13= L1/L3
Standard Deviation of Cell Size	
Other Specific Features	Variations in Density, Cell Size, etc.

There are two types of foam, open-celled and closed-celled foams as shown in Figure-3.5 (a) and (b), respectively. ReCrete polyurethane foam is considered a closed-celled foam. This means that the foam consists of enclosed cells that are created by the

Reproduced with permission of the copyright owner. Further reproduction prohibited without permission.

connection of cell faces and cell edges. Closed cell foams are sometimes referred to as rigid foams. Another type of foam is an open-celled foam, which consists of cell edges only. The cells in this type of foam are not enclosed and do not have cell faces [5]. Open cell foams are sometimes called flexible foams [17]. An example of a flexible foam is the padding in a seat cushion.

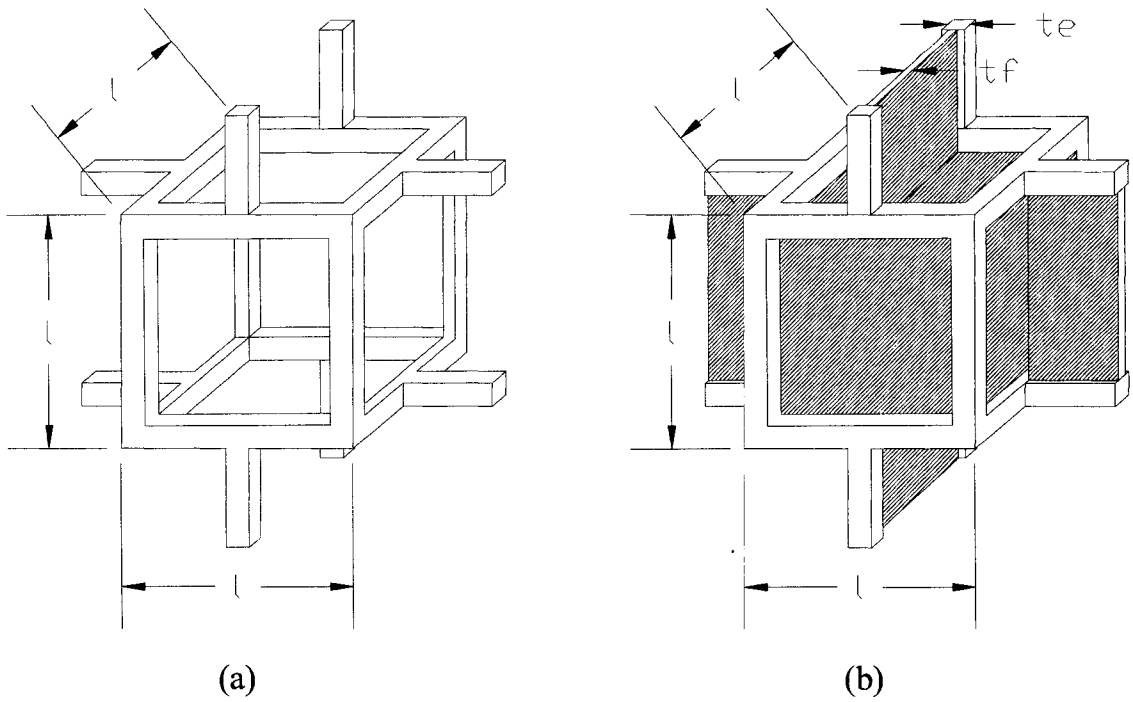

Figure-3.5: (a) Open-Celled Foam (b) Closed-Celled Foam

Edge connectivity (Z_e) and face connectivity (Z_f) are the average number of edges that meet at one vertex and the average number of faces that meet at one edge, respectively. These two values, in addition to n and f, are used to help determine cell shape and to calculate certain physical properties. The mean number of edges per face is denoted as n and the mean number of faces per cell is denoted as f. For a

Reproduced with permission of the copyright owner. Further reproduction prohibited without permission.

tetrakaidecahedra cell, $Z_e = 4$, $Z_f = 3$, $n = 5.14$, $f = 14$ and for a rhombic dodecahedra $Z_e = 5.33$, $Z_f = 3$, $n = 4$, $f = 12$. Since most foams are a combination of these two cells it has been determined that $Z_f = 3$, $n = 5$, $f = 14$. For density and mechanical calculations, only Z_f and n are needed in order to calculate the volume fraction [5].

The symmetry of the foam is important to give a good picture of the foam's structure. Usually foams are axisymmetric because they are elongated in the rise direction. However, foam can also be classified as orthotropic, different dimensions in all directions, and isotropic, uniform cells in all directions [5].

Cell edge thickness (t_e), cell face thickness (t_f), and cell edge length (l) all describe the dimensions of the cell material as shown in Figure-3.6. Cell edge thickness is the thickness of the strut material and can be found by drawing a circle enclosing the strut area and then measuring its diameter [18]. Cell face thickness is the thickness of the cell faces and can be measured at the center of where two cells meet. Cell edge length is the distance of a cell face from cell edge to cell edge. All three of these measurements are imperative to make theoretical calculations based on cell morphology [5].

Foam cells are made of cell walls and cell edges, and it is important to define how much material is in the walls as compared to the edges. The variable that defines this is (ϕ) which is the fraction of material in cell edges [5]. It can be found theoretically by using an equation that relates t_e, Z_f, n, t_f, and l as shown below:

$$\phi := \frac{(t_e)^2}{(t_e)^2 + \frac{Z_f}{n} \cdot t_f \cdot l} \qquad \text{Equation 3.1}$$

Reproduced with permission of the copyright owner. Further reproduction prohibited without permission.

It can also be calculated experimentally using computer software. As with the variables used to calculate this fraction, it is imperative to find (ϕ) to make theoretical calculations based on cell morphology.

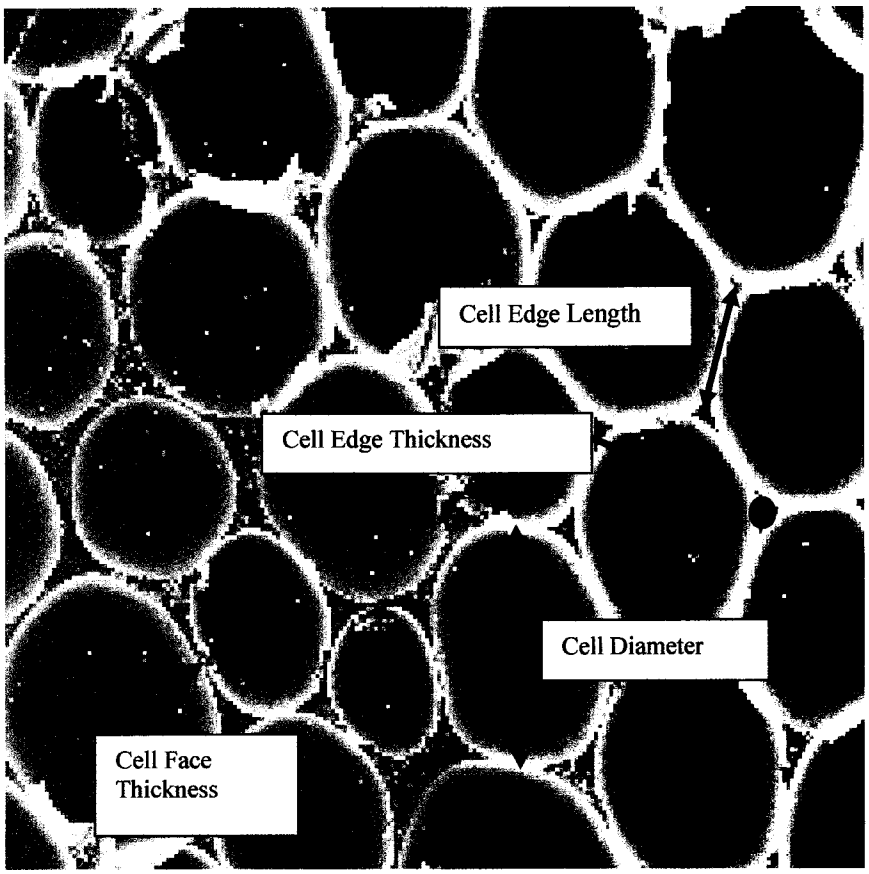

Figure-3.6: Measurements to Describe Foam Morphology

Anisotropy of the cells can be calculated using ratios of principal cell dimensions. The largest principal cell dimension (L1) is the average vertical diameter of the cells parallel to the rise direction. The smallest principal cell dimension (L3) is the average horizontal diameter of the cells parallel to the rise direction. The intermediate principal cell dimension (L2) is the average diameter of the cells perpendicular to the rise

Reproduced with permission of the copyright owner. Further reproduction prohibited without permission.

direction. The cells that are perpendicular to the rise direction should be relatively circular. That is why there is not a separate calculation for the x- and y-axes. Once the principal cell dimensions are calculated, shape anisotropy ratios can be calculated as, R12= L1/ L2 and R13= L1/ L3. The cells are more anisotropic as the anisotropy ratio deviates from the value of one [5].

Standard deviation of cell size should be calculated to give an accurate picture of the foam structure. This value shows how even or uneven the distribution of cell size is throughout the sample. If the standard deviation is large, then the "sample does not represent a normal distribution" [16].

3.2 Linking Morphology to Mechanical Properties

In "Characterization of Polymeric Cellular Structures" an overview of imaging analysis for cell morphology is discussed [16]. There are two types of characterization, qualitative and quantitative. There are a number of different methods to determine quantitative measurements like cell diameter, cell wall thickness, and cell edge thickness. However, no two methods always produce the same values. For example, there are many different ways to determine a cell's diameter and it is therefore important to document the procedure used so that it can be accurately compared and reproduced [16].

Image analysis software is now available and provides a better means to analyze bigger populations. Instead of manually calculating features such as cell diameters with a test piece on an optical microscope, a projection onto a calibrated screen, or by measurement from a photomicrograph, it is now possible to take a digitized image, enhance it and then use segmentation to separate the image into details of interest. It is then possible to choose from a list of structural parameters that are of interest. Using

Reproduced with permission of the copyright owner. Further reproduction prohibited without permission.

image analysis software allows more quantitative analysis to be performed on a greater number of cells [16].

Another important aspect of imaging is the use of microscopes. An image is not as easy to analyze when the 3-D structure of the foam is seen as in an optical microscope image. However, the Scanning Electron Microscope (SEM) creates a 2-D image that is easily analyzed using imaging software. This is accomplished because the SEM uses scattered or emitted electrons to produce an image which means the foam specimen needs to be coated in 24kt gold [19]. This provides a clear image of the surface without interference of multiple layers. It is possible to create a 2-D optical image but this involves cutting the foam to a single mono-cell layer which is quite challenging since the foam tends to disintegrate due to cutting at such a small thickness [16].

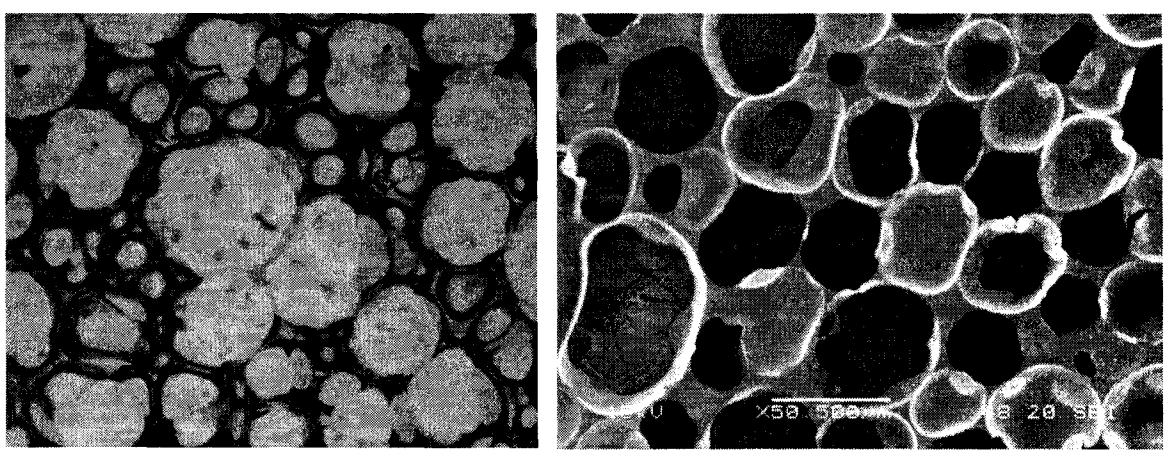

(a) (b)

Figure-3.7: (a) Optical Image of Foam Structure, (b) SEM Image of Foam Structure

Reproduced with permission of the copyright owner. Further reproduction prohibited without permission.

Figure-3.7 shows an optical and SEM image. This demonstrates clearly that the optical image is more difficult to analyze because it shows multiple layers of the foam's structure. Other applicable microscopes that can be used that produce good images include fluorescence, reflected (incident) radiation, confocal, phase contrast, and interference optics [20]. Confocal, although able to produce quite good images, has very slow imaging time compared to the optical and SEM. A few images could possibly take up to a week to produce. SEM and optical images take about two-minutes to produce. Figure-3.8 shows an image of polyurethane foam taken with a confocal microscope.

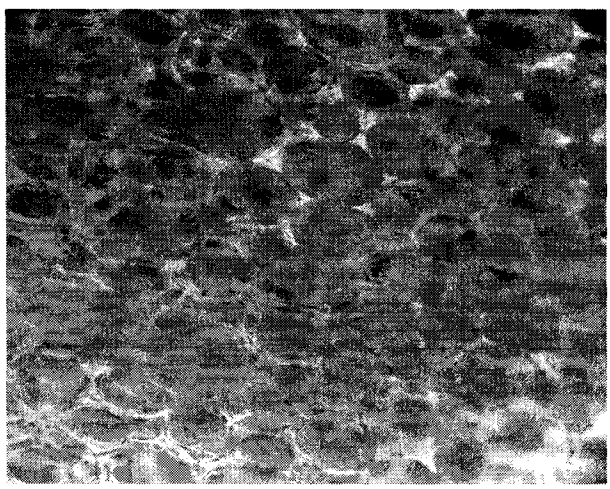

Figure-3.8: Confocal Image of Foam Structure

One important fact to consider when performing or viewing research on cell morphology is that there is not an "established and thoroughly tested and accepted method for the quantitative characterization of cell structure variable which is applicable to a statistically valid sample of the cell population" [16]. This means that there is no standardized way to calculate quantitative measurements of a foam's cell structure.

Reproduced with permission of the copyright owner. Further reproduction prohibited without permission.

Unfortunately, there is also "ambiguity associated with the assignment of any one specific cell feature.... influencing a given behavior" [16]. Though, it is understood that a wide variety of cell features must be included in equations that predict mechanical properties [20]. In addition, it is possible to perform morphological measurements on foam samples and have no correlation which is most likely due to a non-representative sampling [20].

3.2.1 Theoretical Equations for Density and Mechanical Properties

Theoretical calculations on the density and mechanical properties of rigid polyurethane foam are performed in this paper using equations presented by Gibson and Ashby [5]. These equations are also used by other authors including Hong-Ru Lin where SEM is used to determine cell thickness, cell length, and cell edge thickness to calculate the volume fraction and relative yield strength [18]. Another paper by N. Chan and K.E. Evans uses Gibson and Ashby's Young's modulus equation in addition to the suggested characterization chart to evaluate different foams under SEM [21]. The equations presented by Gibson and Ashby are used to theoretically calculate foamed material properties.

This study calculates the theoretical volume fraction, density, Young's modulus, and collapse stress using measurements taken from SEM images. The theoretical values are then compared to the values calculated experimentally. Gibson and Ashby's equations for relative values are rearranged to solve for the density, Young's modulus, and collapse stress. To do this, values for the density, Young's modulus, and collapse stress of the cell wall properties need to be determined. Fortunately, these values have been

Reproduced with permission of the copyright owner. Further reproduction prohibited without permission.

experimentally determined for rigid polyurethane foam and are shown in Equation 3.2 [5].

$$\rho_s := 1.2\cdot 10^6 \frac{g}{m^3} \qquad 1.6\cdot 10^9 < E_s < 2.7\cdot 10^9 \frac{N}{m^2} \qquad \sigma_{ys} := 127\cdot 10^6 \frac{N}{m^2} \qquad \text{Equation 3.2}$$

Density of the foam is calculated using cell edge thickness, cell face thickness, and cell edge length. Gibson and Ashby present several equations for calculating density based upon the geometry of the foam. This study focuses on three of their equations. The first one, shown as Equation 3.3, is based on an approximation that most foams have the following properties: Z_f=3, n=5, f=14, and C_4=10, where C_4 is a constant [5]. The second equation, shown as Equation 3.4, is based on the assumption that all cells contained in the foam are rhombic dodecahedra (Z_e=5.33, Z_f=3, n=4, f=12) [5]. Finally, the third equation, shown as Equation 3.5, is based on the assumption that all cells contained in the foam are tetrakaidecahedra (Z_e=4, Z_f=3, n=5.14, f=14) [5]. All three equations are used to compare theoretical density to the experimental density.

$$\rho^* := 1.2\cdot\left[\frac{(t_e)^2}{l^2} + 0.7\cdot\frac{t_f}{l}\right]\cdot\rho_s \qquad \text{Equation 3.3}$$

$$\rho^* := 1.90\cdot\frac{t}{l}\cdot\rho_s \qquad \text{Equation 3.4}$$

$$\rho^* := 1.18\cdot\frac{t}{l}\cdot\rho_s \qquad \text{Equation 3.5}$$

Reproduced with permission of the copyright owner. Further reproduction prohibited without permission.

Once the theoretical density is calculated, the theoretical mechanical properties can be found. Standard beam theory is used to derive the mechanical property equations using the model of the unit cell shown in Figure-3.5 (a). The open and closed cell equations differ only by the inclusion of the volume fraction, membrane stresses and gas pressure. However, gas pressures are ignored in man made foams because the initial fluid pressure is usually equal to the atmospheric pressure [5].

Equation 3.6 shows an approximate value for Young's modulus for closed cells including membrane stresses [5]. In addition, Equation 3.7 shows the value of the volume fraction. Typically, the volume fraction for rigid polyurethane foams is 0.8-0.9 [22]. The volume fraction is defined as the volume of the solid material contained in the cell edges divided by the total volume of the solid contained in the sum of the cell edges and cell faces [5].

$$E^{*} := \left[\phi^{2} \cdot \left(\frac{\rho^{*}}{\rho s} \right)^{2} + (1 - \phi) \cdot \frac{\rho^{*}}{\rho s} \right] \cdot E_{s} \qquad \text{Equation 3.6}$$

$$\phi := \frac{(t_e)^2}{(t_e)^2 + \frac{Z_f}{n} \cdot t_f \cdot l} \qquad \text{Equation 3.7}$$

The collapse stress is calculated using Equation 3.8 or Equation 3.9. Since the yield stress for the cell walls is not as well researched, the inclusion of the membrane stresses may not make a big difference in the calculated value of collapse stress [5]. However, calculations will include the membrane stress terms. There is some confusion as to whether the elastic collapse or plastic collapse should be used to describe the collapse

Reproduced with permission of the copyright owner. Further reproduction prohibited without permission.

stress of ReCrete so, both equations are used to calculate the values to determine which best matches the experimental values.

$$\sigma^*_{el} := 0.03 \cdot \left(\frac{\rho^*}{\rho_s}\right)^2 \cdot \left[1 + \left(\frac{\rho^*}{\rho_s}\right)^{0.5}\right]^2 \cdot E_s \qquad \text{Equation 3.8}$$

$$\sigma^*_{pl} := \left[0.3 \cdot \left(\phi \cdot \frac{\rho^*}{\rho_s}\right)^{\frac{3}{2}} + 0.4 \cdot (1 - \phi) \cdot \frac{\rho^*}{\rho_s}\right] \cdot \sigma_{ys} \qquad \text{Equation 3.9}$$

3.2.2 Previous Research on Morphology

Several studies try to relate mechanical properties to cell morphology using various methods and have presented interesting results. "The Structure and Property Relationships of Commercial Foamed Plastics" focuses on the behavior of the foam cells under loading and relating the cell structure to mechanical properties. In addition to using SEM to study the morphology of the foam, tensile and compressive testing is performed on the PVC commercial foam and polystyrene foam ranging in density from 0.03 to 0.08-g/cc. Interestingly, the compressive stress-strain curves show that the peak yield point is much more obvious with foams at higher densities. This means that foams with a higher density have yield points that peak and then stress lowers sharply before entering the collapse stress [18].

The morphological study in the paper focuses on finding the volume fraction and relative yield strength using Gibson and Ashby's equations. Only cell edge thickness, face thickness, and cell edge length are measured from SEM images. The other variables

Reproduced with permission of the copyright owner. Further reproduction prohibited without permission.

needed for calculating the volume fraction and yield strength are known by assuming the foam cells are tetrakaidecahedra. The shape anisotropy ratios are also calculated [18].

Results show that, when the theoretical calculations are plotted against experimental results, there is a better correlation at higher densities. However, this conclusion comes from testing only three densities. It is also shown that the shape anisotropy ratio, R13, decreases with increasing density. This means that the cells become less elongated as the density increases [18]. This could be due to the amount of force needed by the gas inside the cell to deform the cell into an elongated bubble [23]. Especially since this paper states that the cell wall thickness is found to increase with foam density [18].

Another important study performed by H.T. Huber and L.J. Gibson consider anisotropy as the main focus of the paper, "Anisotropy of Foams". This work shows the important effect anisotropy (elongation of the cells) has on the mechanical properties of the foam. Image analysis and mechanical testing are performed on specimens taken from a large mold where the SEM and mechanical samples to be compared are taken at a close distance to one another. Mechanical properties are measured in the rise direction and at two orthogonal directions normal to the rise direction of the foam [23].

Compressive stress-strain curves show that when the foam is loaded in the rise direction, its modulus, peak yield, and collapse stress are greater than if it were loaded in a direction normal to the rise. It is also evident from these graphs that when polyurethane foam is loaded in the rise direction it produces a peak similar to that of more dense foams discussed in reference 18 and when the foam is less dense it produces a stress-strain curve similar to one with lower density also discussed in reference 18. It is extremely

Reproduced with permission of the copyright owner. Further reproduction prohibited without permission.

interesting that density and anisotropy changes could create similar stress-strain curves [23].

Shape anisotropy ratios documented in the study range from 1.1 to 1.6 whereas the average for polymer foams is 1.3. It is shown that anisotropy increases as average cell size increases. In addition, anisotropy decreases with density. The modulus is the property most affected by the anisotropy ratio. It tends to increase with an increasing anisotropy ratio and can multiply up to four times as documented in the paper. The plastic collapse is less sensitive to the anisotropy ratio but can multiply up to 2.2 times as the ratio increases. The elastic collapse has a weak dependence upon anisotropy only being able to multiply by 1.3 times with an increasing anisotropy ratio. All of these results indicate that the anisotropy ratio has an effect on the mechanical properties of foam [23].

The study performed by Schwartz and Bomberg show histograms and averages of the cell areas and cell aspect ratios of foams prepared with different blowing agents. Measurements of edge thickness and cell face thickness are also made using a thinning technique and optical interference technique, respectively. The study involves imaging parallel and perpendicular samples at different levels within a sample taken from the foam core. It is found that the areas of the cells are similar for all levels but that the aspect ratios show greater differences for different levels. In addition, samples in the rise direction (parallel direction), show larger average aspect ratios and areas than the samples in the normal direction (perpendicular direction). Average cell lengths range from 181 to 192-um, edge thickness is about 36-um, and cell face thickness ranges from 1.7 to 2.8-um [24].

Reproduced with permission of the copyright owner. Further reproduction prohibited without permission.

From reviewing articles making reference to imagining, most seem to compare just the measurement data instead of using equations to calculate actual properties. In the article by Hong-Ru Lin measurements of cell edge length, cell face thickness, and edge thickness are made, but these values are not used to find the relative density which is one of two main variables to find the relative collapse stress. Instead relative density is found by knowing the foam's density and dividing it by the foam's solid density which is usually found in other texts that provide these values for several different materials. Instead, values measured for the article are used just to calculate the volume fraction of the material. Calculated values of the volume fraction are 8.1%, 54.4%, and 41.3% for foams of densities 0.03, 0.06, and 0.08-g/cc [18].

Reproduced with permission of the copyright owner. Further reproduction prohibited without permission.

CHAPTER 4

EXPERIMENTAL

4.1 Polyurethane Foam Fabrication

The polyurethane foams in this study are fabricated using five constituents: Voranol 490, DC 193 Surfactant, Polycat 17 Amine Catalyst, Distilled Water, and Rubinate 1680. For this study 1500-cm^3 and 3000-cm^3 batches are fabricated. These batch sizes require the following:

	1500-cm^3	3000-cm^3
Voranol 490 (g)	84.24	168.48
DC 193 Surfactant (g)	2.13	4.26
Polycat 17 Amine Catalyst (g)	0.49	0.98
Distilled Water (g)	0.98	1.96
Rubinate 1680 (g)	128.51	257.02

The first chemical, Voranol, is carefully poured into a 1-L plastic container shown in Figure-4.1 (a) to its target mass on a Mettler Toledo Digital Scale. The next three chemicals, Surfactant, Polycat, and water, are all weighed out in the same 1-L container making sure that each is poured into a different location in the container. This assures that the chemicals will not react prematurely. The four chemicals are mixed manually in the 1-L container with a metal spatula for 2-minutes as shown in Figure-4.1 (b). During this process, the sides of the container are scraped and the mixing is slow to avoid inducing

Reproduced with permission of the copyright owner. Further reproduction prohibited without permission.

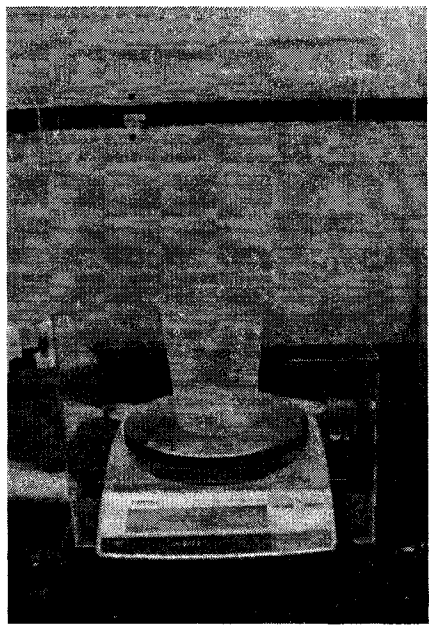

(a)

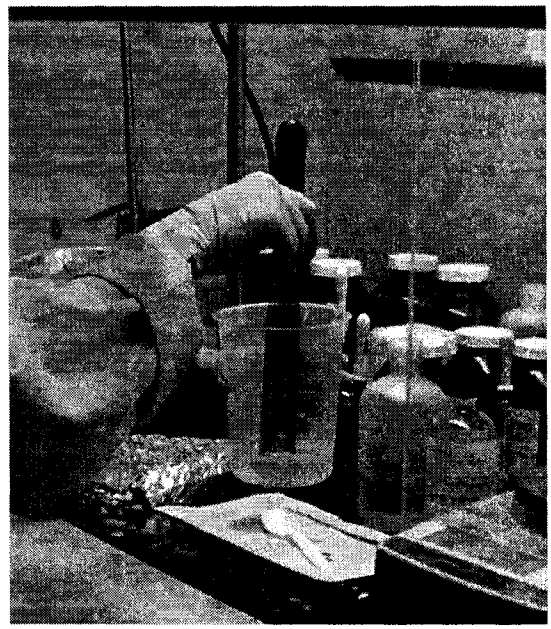

(b)

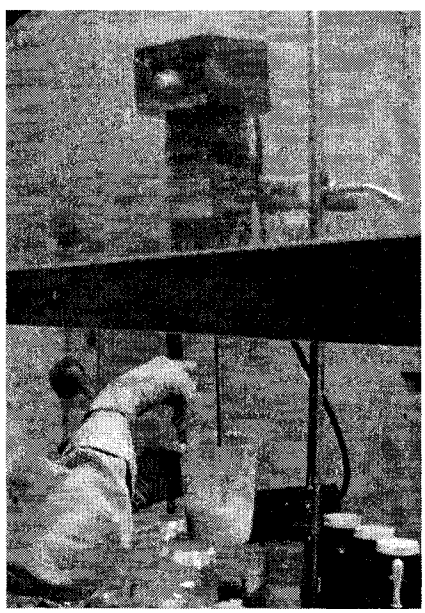

(c)

(d)

Figure-4.1: (a) 1-L container and Scale, (b) Manual Mixing, (c) Electric Overhead Mixer, (d) Pouring Chemical Formulation into Molds

Reproduced with permission of the copyright owner. Further reproduction prohibited without permission.

bubbles into the mixture. A Puritan Wooden Applicator stick is used to scrape excess chemicals from the metal spatula after mixing is complete. The final chemical, Rubinate, is then poured into the same 1-L container to its target mass. The five constituents are now combined using an electric Arrow Overhead Mixer with a Conn Blade as shown in Figure-4.1 (c). The blade is placed on the bottom of the container to minimize bubbles, and a metal spatula is used to scrape the sides of the container. The chemicals are mixed for 90-seconds and then poured directly into the prepared molds as shown in Figure-4.1 (d).

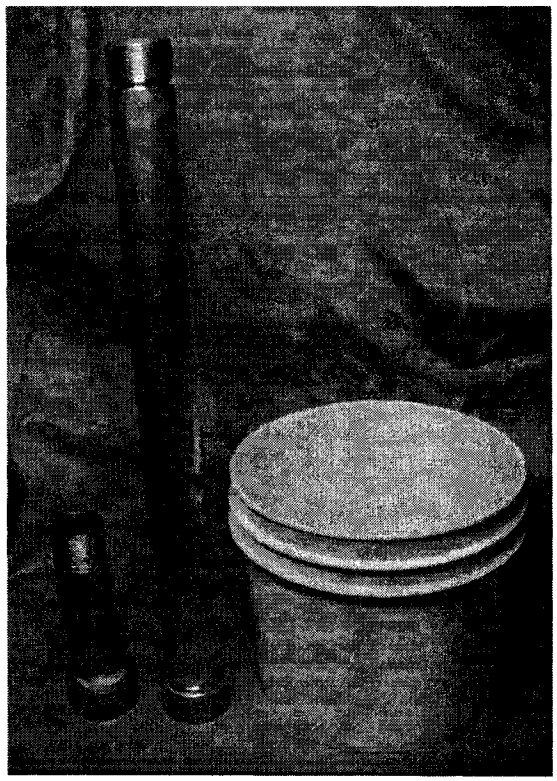

Figure-4.2: (from left to right) Small Mold, Tall Mold, and Reference Mold

Reproduced with permission of the copyright owner. Further reproduction prohibited without permission.

Three types of molds are used for this project. The first two types of molds are made from aluminum and both have an inner diameter of 28.7-mm. The first mold has a height of 139.7-mm and is designated as the "small" mold. The second mold has a height of 457.2-mm and is designated as the "tall" mold. Finally, the third type of mold is made from plastic and has a decreasing diameter from top to bottom, 203-mm to 175-mm. This mold is designated as the "reference" mold. The molds are prepared for fabrication by applying PTM&W Industries Mold Release to the inside of the mold. This mold release helps in the extraction of the foam from the molds. Figure-4.2 shows all three molds.

When a batch of polyurethane foam is fabricated, the date is recorded in addition to the name of the person actually pouring and mixing the chemicals and the person who is helping. Each batch is assigned its own number so that data can be collected and stored in an organized fashion. The hood temperature and humidity are measured by a VWR Thermo-hygro hygrometer and then recorded. The times that the chemical mix is finished, moved to the oven, and removed from the oven are also recorded. See Figure-4.3 for an example of the "Batch Worksheet Form". A log book has been maintained that documents all of the foam manufactured at UNLV starting in July 2000. This log is shown in Appendix B.

Once the polyurethane foam is mixed and then poured into a mold, it rises for 30-minutes under a laboratory hood. This is done to ensure fumes from the chemical reaction during the foaming process are contained. The foam is then placed in a Blue M Oven for 4-hours at 66°C for post cure. This ensures that the chemical reactions are mostly completed. The oven temperature for post curing was chosen by SNL and has not been altered for this project.

Reproduced with permission of the copyright owner. Further reproduction prohibited without permission.

DATE:					
BATCH NUM:					
CHEMICALS:					
ASSISTANTS:					
ADDTL INFO:					
B150 TEMP:		B150 HUMIDITY:			
B150 BAROMETRIC PRESSURE:					
Polyurethane RE-CRETE Foam Formula Generator					
Free Rise					
Polyol Master Batch -- Part Volume					
USE CAUTION IF POUR SIZE > 1000g					
Note: It is recommended that the mix size be greater than or equal to 200g					
Please enter the Part Volume desired (cc)				1500	
Computed Factor	2				
Part Volume		(cc)		1500	
Polymer Foam Density		(lb/ft3)		6.00	
		(g/cc)		0.096	
Packing Factor		(1 <= PF <= 2)		1.0	
					ACTUAL
Voranol 490		(g)		84.24	
DC 193 Surfactant		(g)		2.13	
Polycat 17 Amine Catalyst		(g)		0.49	
Distilled Water		(g)		0.98	
Rubinate 1680		(g)		128.51	
Mix Size		(g)		216.35	
Pour Size		(g)		158.66	
TIME CHEMICAL MIX WAS FINISHED:					
TIME FOAM WAS PUT INTO OVEN:					
TIME FOAM WAS TAKEN OUT OF OVEN:					
MIX TIME W/ SPATULA		MIX TIME W/MIXER			

Figure-4.3: 1500-cc Batch Worksheet

Reproduced with permission of the copyright owner. Further reproduction prohibited without permission.

4.2 Processing

Once the foam has been removed from the oven, it is extracted from the molds. This is done after the molds have cooled for handling. The foam is extracted from the small and tall aluminum molds by screwing off the threaded cap and pushing lightly on the bottom of the specimen. The foam is removed from the plastic 4-L reference molds by using high-pressure air to loosen the foam from the sides of the mold. The small aluminum mold yields a cylindrical column 139.7-mm in height and 28.5-mm in diameter. The tall aluminum mold yields a cylindrical column 457.2-mm in height and 28.5-mm in diameter. The plastic reference mold yields a cylindrical column 177.8-mm in height and approximately 182-mm in diameter. Figure-4.4 shows pictures of all three foam molds and columns.

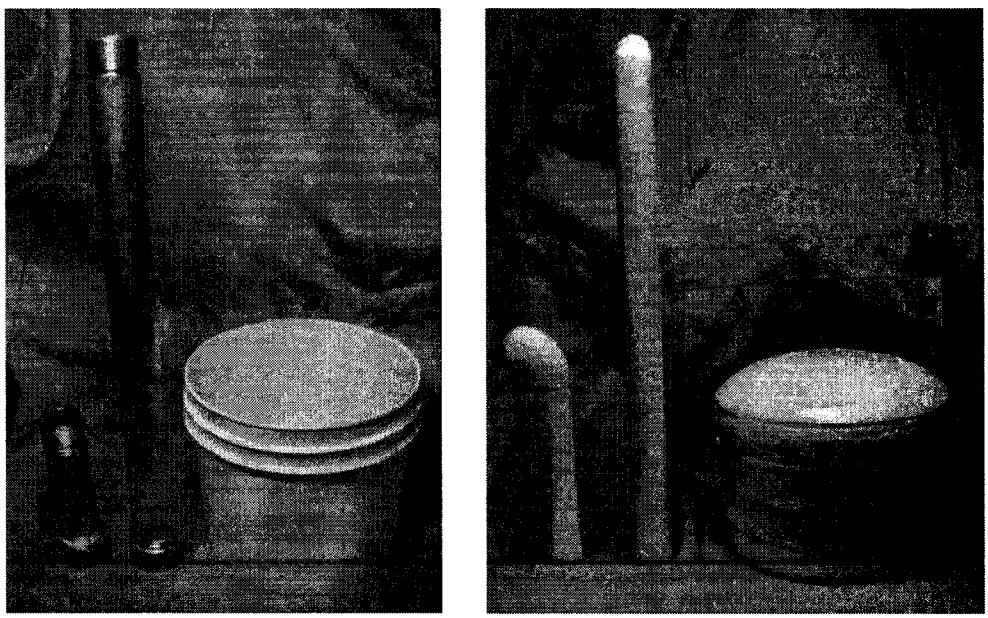

Figure-4.4: (from left to right) Small Mold and Specimen, Tall Mold and Specimen, and Reference Mold and Specimen

Reproduced with permission of the copyright owner. Further reproduction prohibited without permission.

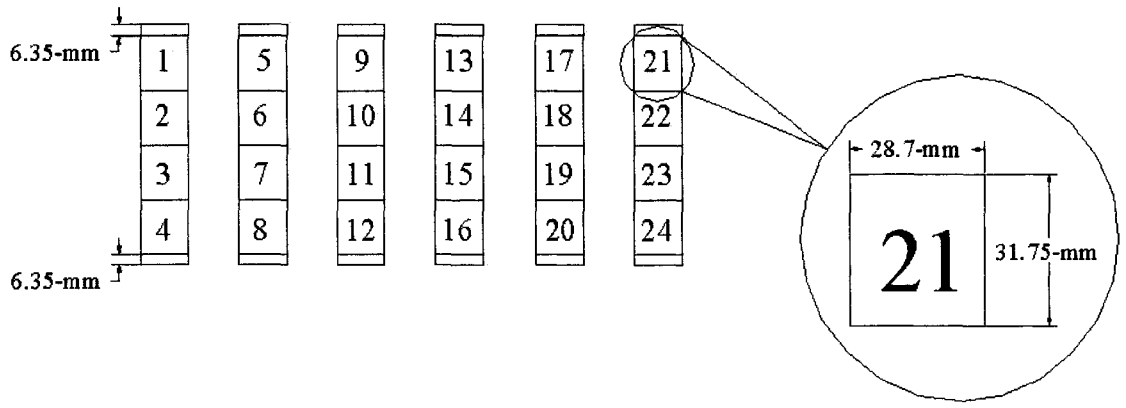

(a)

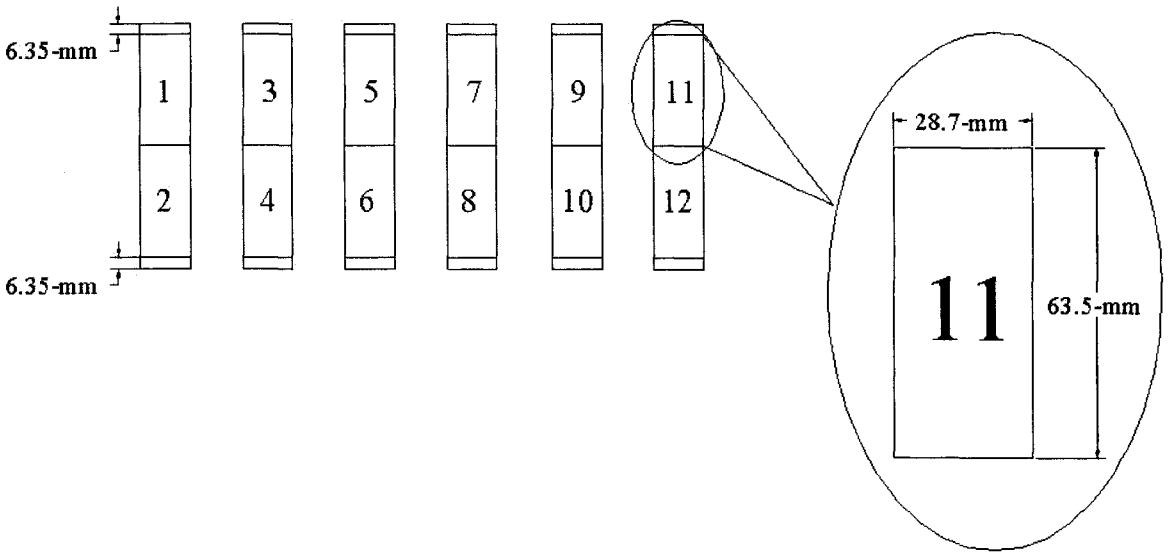

(b)

Figure-4.5: Cutting Schematic of Small Cylindrical Columns (a) 31.75-mm Samples

(b) 63.5-mm Samples

Reproduced with permission of the copyright owner. Further reproduction prohibited without permission.

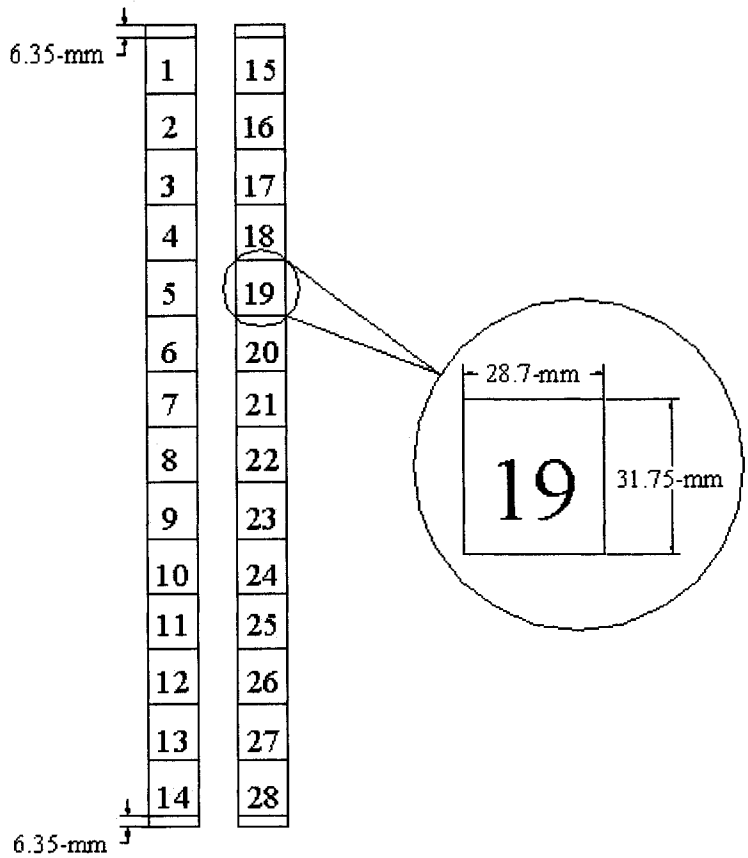

Figure-4.6: Cutting Schematic of Tall Cylindrical Columns as 31.75-mm Samples

The cylindrical column extracted from the small aluminum molds is cut with a Craftsman 11-in Band Saw into four 31.75-mm or two 63.5-mm high samples leaving 6.35-mm of material at the top and bottom of the column. The cylindrical column extracted from the tall aluminum molds is cut in the same manner as the small molds except now fourteen 31.75-mm samples are cut. Figure-4.5 and Figure-4.6 show a schematic of where each cylindrical column is cut into smaller pieces (cylindrical samples) from the small and tall molds, respectively. The numbers denote the level where each sample is taken. The smallest level number is always considered the top sample of each cylindrical specimen.

Reproduced with permission of the copyright owner. Further reproduction prohibited without permission.

Once the cylindrical samples are cut from the cylindrical columns, each one is sanded on the top and bottom with a Delta 12-in Disk Sander as shown in Figure-4.7. This ensures that each sample is a right circular cylinder approximately 25.4-mm in height for the 31.75-mm pieces and 50.8-mm for the 63.5-mm pieces.

The cylindrical column extracted from the 4-L plastic reference mold is cut with a band saw into four 43.65-mm vertical sections and into four 38.1-mm horizontal sections as shown in Figure-4.8. Each horizontal section is trimmed with a band saw to yield 31.75-mm high sections. A Craftsman 8-in Drill Press and a hole saw shown in Figure-4.9 are used to make 48 total cylindrical samples from the reference mold, 12 from each level as shown in Figure-4.8 (b). The cylindrical samples are sanded with a disk sander to a height of approximately 25.4-mm.

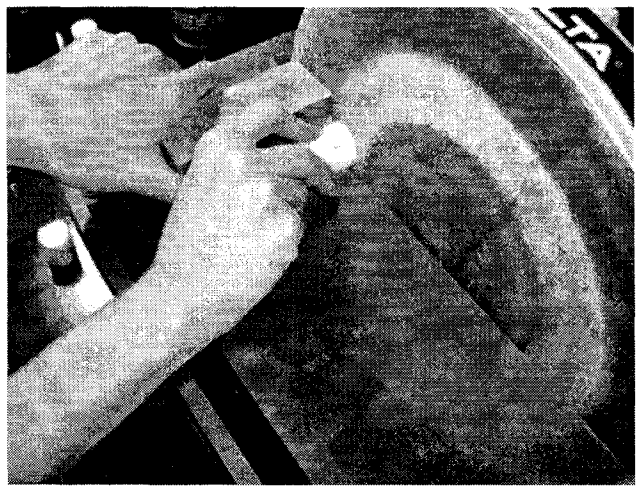

Figure-4.7: Delta 12-in Disk Sander

Reproduced with permission of the copyright owner. Further reproduction prohibited without permission.

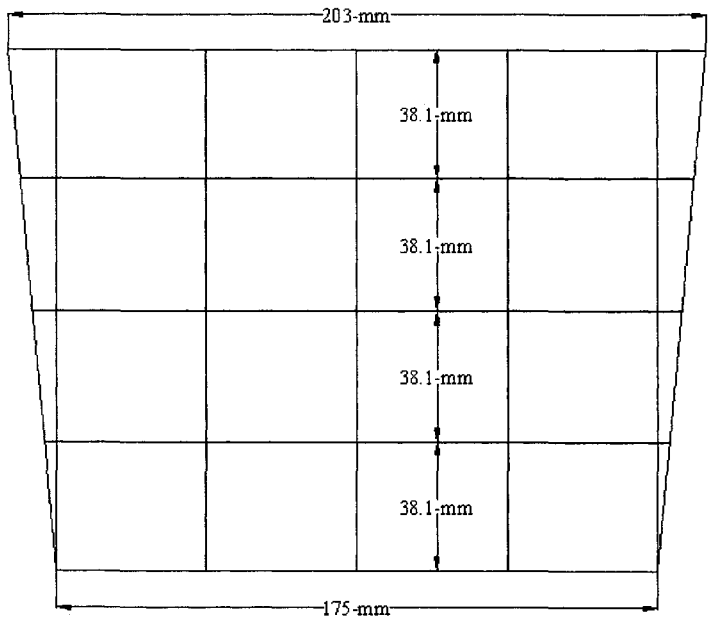

(a)

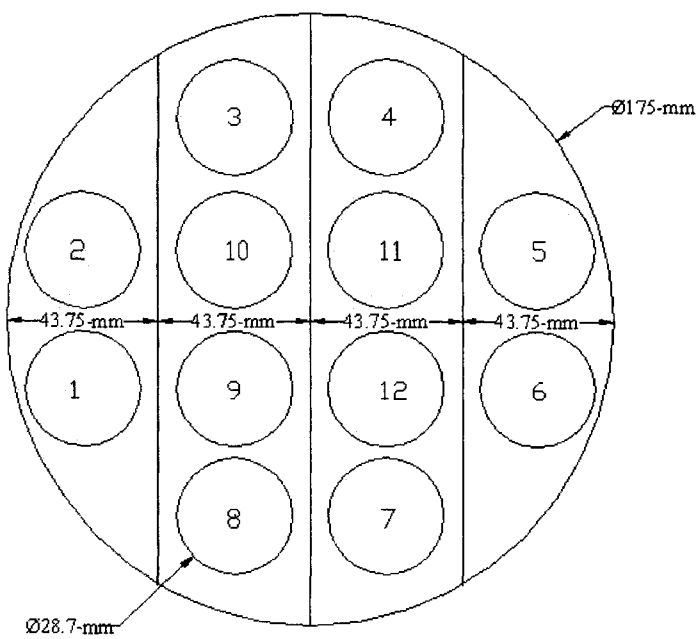

(b)

Figure-4.8: Reference Mold Cut into Sections (a) Side View (b) Top View of Bottom Section

Reproduced with permission of the copyright owner. Further reproduction prohibited without permission.

Densities of all samples are calculated according to ASTM Standard D1622-93 [25]. All cylindrical samples are measured with Mitutoyo Absolute Digimatic Calipers for diameter and height measurements and weighed with a Mettler Toledo Digital Scale for accurate mass measurements as shown in Figure-4.10. Four height and diameter measurements are taken and averaged for a mean measurement. The densities of all samples are calculated with these measurements. These samples are the basis for which the cell morphology samples, mechanical testing samples, and density gradient samples are derived.

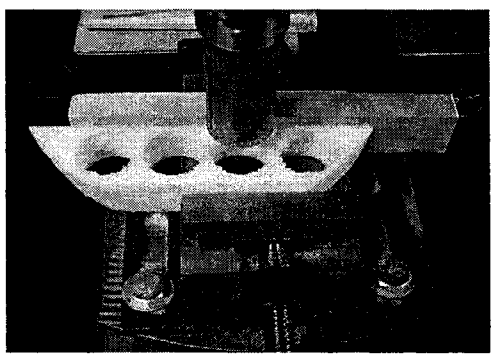

Figure-4.9: Craftsman 8-in Drill Press and Hole Saw

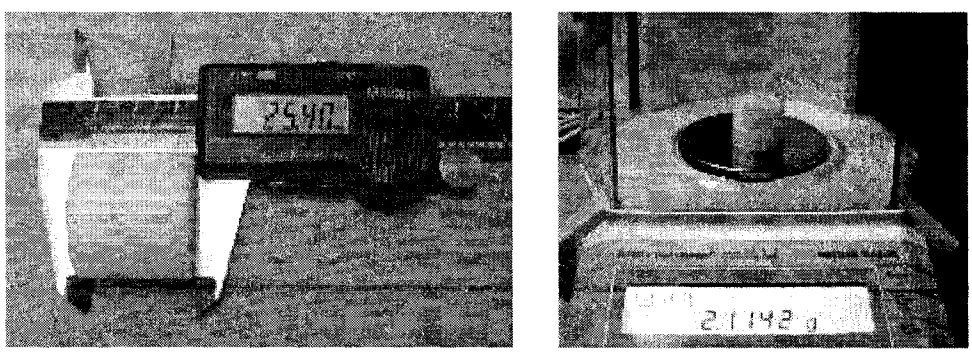

(a) (b)

Figure-4.10: (a) Mitutoyo Absolute Digimatic Calipers (b) Mettler Toledo Digital Scale

Reproduced with permission of the copyright owner. Further reproduction prohibited without permission.

4.2.1 Mechanical Testing Sample Preparation

Samples are ready to be tested for mechanical properties after density calculations are recorded. All samples from the small molds, tall molds, and reference molds are 28.7-mm in diameter. Samples from the tall molds and reference molds are always 25.4-mm in height whereas samples from the small molds are either 25.4-mm or 50.8-mm in height. This is to better understand the vertical differences in samples taken from the small molds.

For mechanical testing, each sample requires two 2-mm thick reflective strips placed approximately 13-mm apart for the 25.4-mm high samples and 38-mm for the 50.4-mm high samples. The strips are also centered on the sample as shown in Figure-4.11. These reflective strips are used by the United Laser to calculate strain.

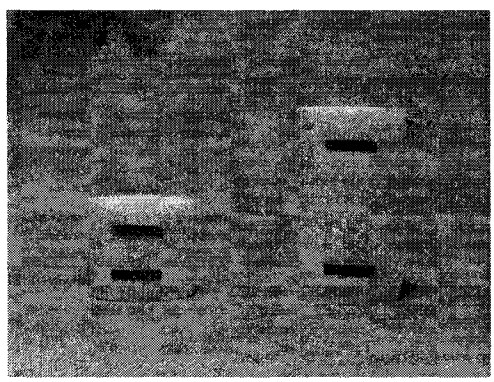

Figure-4.11: Mechanical Testing Samples with Reflective Strips

(left to right) 25.4-mm Height and 50.8-mm Height

Density is always measured and recorded within twenty-four hours of being tested. For those samples being aged, density is also measured within thirty-six hours of being

Reproduced with permission of the copyright owner. Further reproduction prohibited without permission.

fabricated or in other words chemically mixed. This allows comparisons to be made on how the density changes over time. Five time periods are used for this study, which include 1-day, 2-day, 7-day, 30-day, and 90-day. All aged samples are stored in a cardboard box as shown in Figure-4.12. This is done to insure light is not affecting the surface of the foam samples.

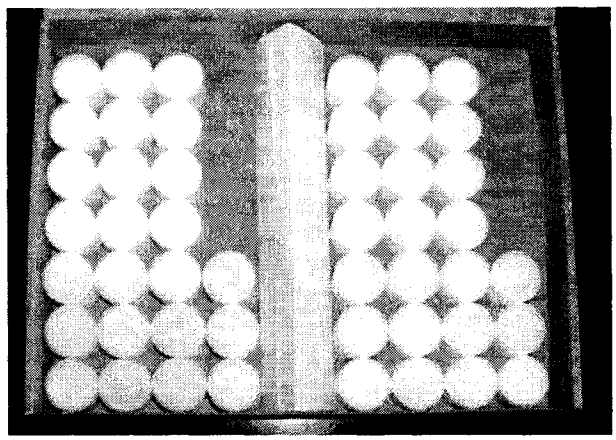

Figure-4.12: Storage of Aged Samples

4.2.2 Scanning Electron Microscope Sample Preparation

Scanning Electron Microscope (SEM) imaging is performed on thin slices of polyurethane foam, which are either parallel or perpendicular to the rise direction. One parallel slice and one perpendicular slice is taken from the 25.4-mm high cylindrical samples from levels one through four of the small aluminum molds and from level one, eight, and fourteen of the tall aluminum molds. All perpendicular slices are taken from the top of each cylindrical sample, and all parallel samples are taken from the center of each cylindrical sample. This configuration ensures that the vertical and radial differences can be recorded. A cylindrical sample is cut with a hole saw from the center of the

Reproduced with permission of the copyright owner. Further reproduction prohibited without permission.

reference batch so that a perpendicular and parallel slice can also be taken from the reference batch in the same manner as the small and tall molded cylinders.

A Lagun Mill is used to create a smooth surface on the slice of foam to be imaged. Since the foam needs to be held in a vice while being milled, the foam is encapsulated with Buehler EPOXICURE epoxy at a 5:1 ratio so that the foam does not deform. Buehler Disposable 38.1-mm inner diameter epoxy molds are used, and an aluminum weight approximately 65-grams is placed on top of the foam to keep it from floating as shown in Figure-4.13 (a). The epoxy is poured approximately 6.35-mm from the bottom of the foam as seen in Figure-4.13 (b).

Each slice is faced with a mill and cut with a band saw and is approximately 3-mm in thickness. The first slice cut from the sample is in the perpendicular direction, and the parallel sample is cut afterward. Figure-4.14 shows a schematic of the perpendicular and parallel samples. Both samples are cut with a 6-flute end mill at a rate of 4200-rpm. This tool and cutting speed were determined after cutting and imaging foam samples using a

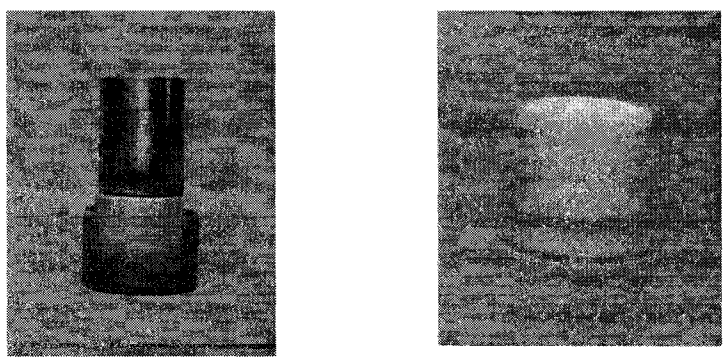

(a) (b)

Figure-4.13: (a) Epoxy Mold with Foam and Weight, (b) Foam with Epoxy Reinforcement

Reproduced with permission of the copyright owner. Further reproduction prohibited without permission.

variety of speeds and tools. Two mill bits and several cutting speeds were investigated to determine which tool and cutting speed provided the cleanest cut for imaging with the SEM. Foam samples were prepared using a two-flute or 6-flute end mill and speeds including 2300-rpm, 3300-rpm, and 4200-rpm. It was shown that faster speeds and more flutes on the end mill yielded better results. Figure-4.15 (a) shows the position of the foam sample when a perpendicular sample is cut and Figure-4.15 (b) shows the position of the foam sample when a parallel sample is cut. Several leveling blocks are used to raise the foam to the top of the vice for both sample cuts. Once the sample is milled, it is cut to the 3-mm thickness with a band saw shown in Figure-4.16 (a) and (b).

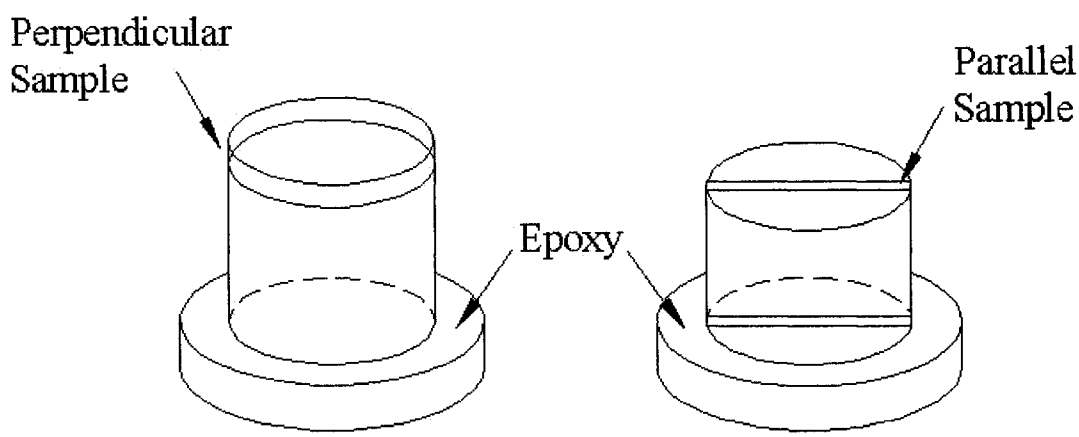

Figure-4.14: Schematic of Perpendicular and Parallel Samples

Reproduced with permission of the copyright owner. Further reproduction prohibited without permission.

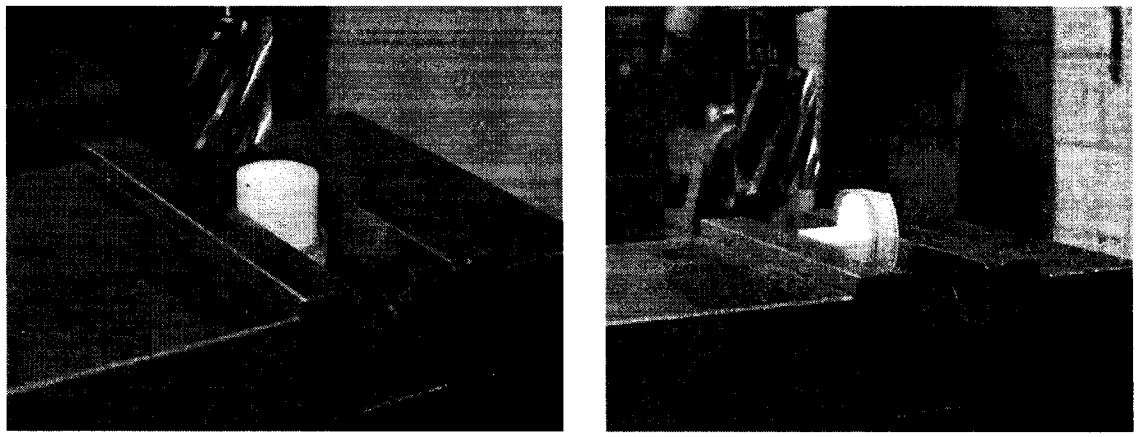

(a) (b)

Figure-4.15: Position of Foam in Vice (a) Perpendicular Slice, (b) Parallel Slice

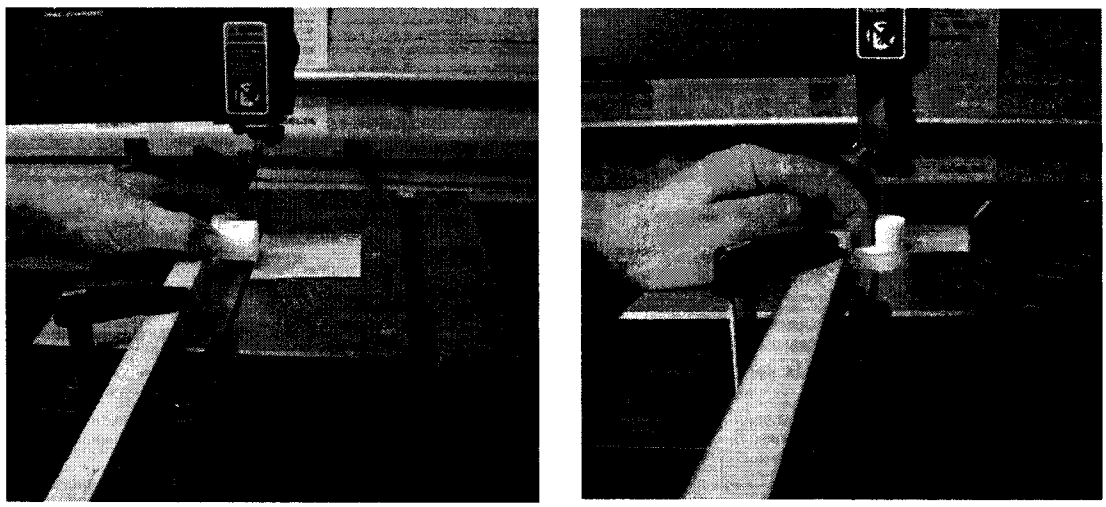

(a) (b)

Figure-4.16: Sample Sliced with Band Saw (a) Perpendicular Slice, (b) Parallel Slice

Figure-4.17 (a) shows the setup of the JEOL-5600 SEM, which is located in the Geosciences building on the University of Nevada, Las Vegas campus. Since the foam does not have metallic properties, the sample surface must be sputter coated in 24kt gold. Figure-4.17 (b) shows the Cressington Sputter Coater used for SEM samples. Samples

Reproduced with permission of the copyright owner. Further reproduction prohibited without permission.

are first blown with canned air to remove any dust, and double-sided graphite tape is used to affix the foam sample to a metal cylinder as shown in Figure-4.18. The foam is sputter coated in 24kt gold after it is affixed to the metal cylinder.

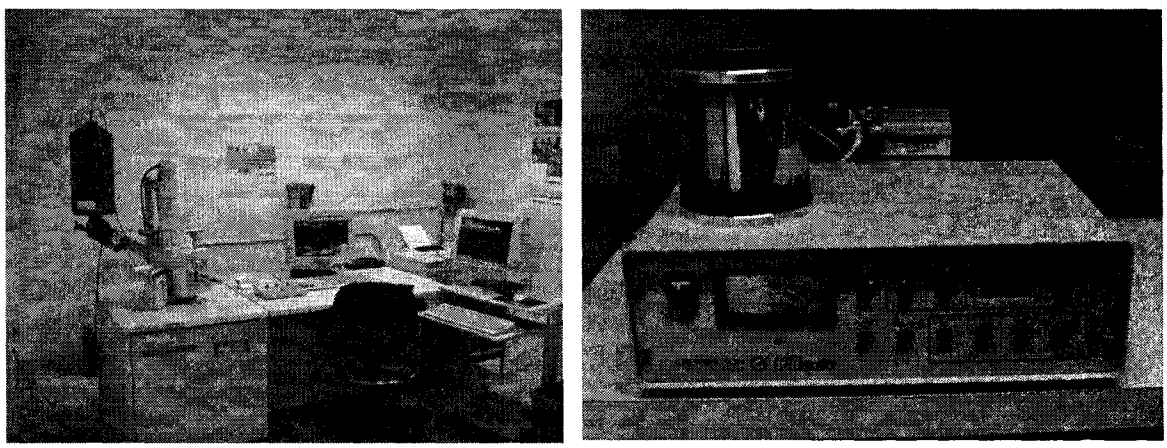

(a) (b)

Figure-4.17: (a) JOEL-5600 SEM, and (b) Cressington Sputter Coater

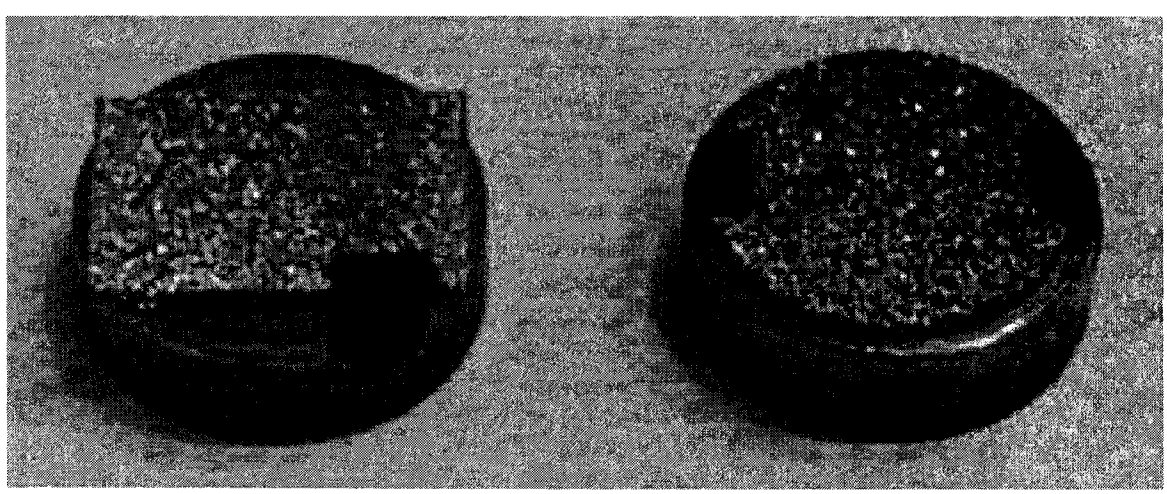

Figure-4.18: Parallel and Perpendicular Samples Affixed to Metal Cylinders with Graphite Tape (shown after being sputter coated with 24kt gold)

Reproduced with permission of the copyright owner. Further reproduction prohibited without permission.

The metal cylinder is inserted into a holder shown in Figure-4.19 (a) that is then mounted on the microscope's stage as shown in Figure-4.19 (b). Once the stage is closed and vented, imaging can take place with the JOEL SEM software as seen in Figure-4.20. This is a screen capture of the software taking an image of one of the foam surfaces. The stage is manually moved to different locations of the foam surface using x- and y-coordinates.

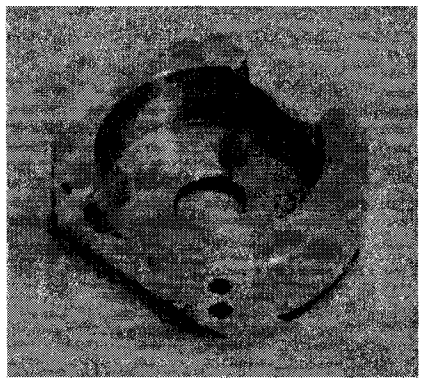

(a)

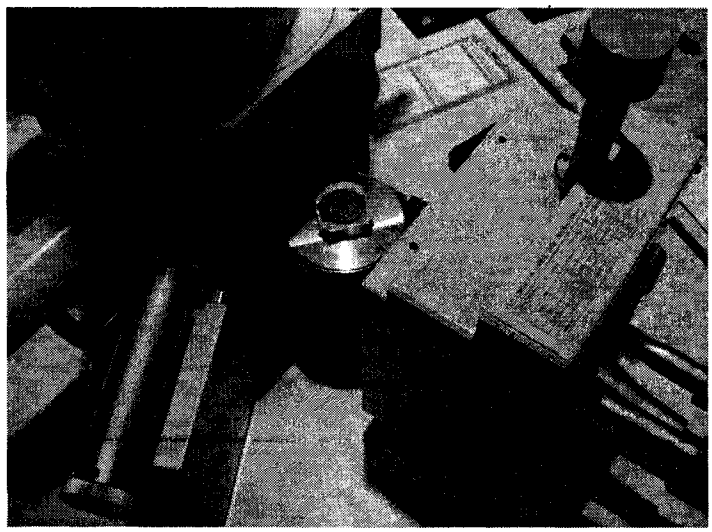

(b)

Figure-4.19: (a) Metal Cylinder Holder, (b) Microscope Stage

Reproduced with permission of the copyright owner. Further reproduction prohibited without permission.

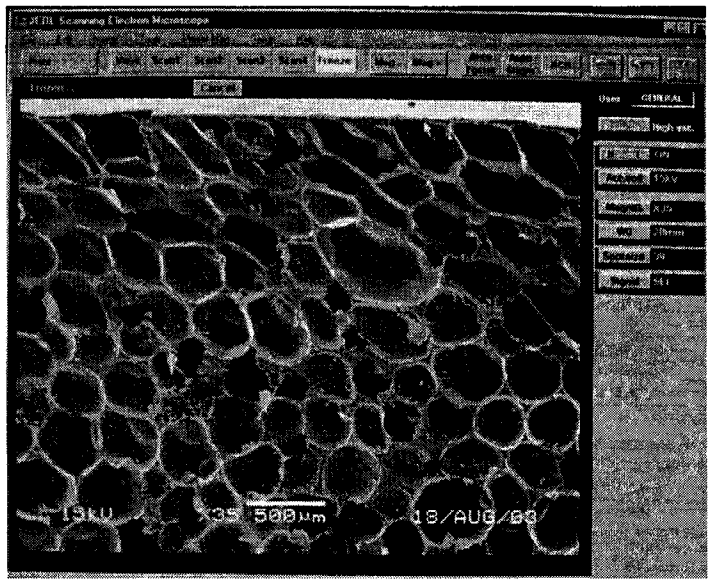

Figure-4.20: Screen Capture of JOEL SEM Software

The perpendicular foam slices are 28.7-mm diameter slices and are centered on the stage manually. Images are then taken from the center to the outside of the sample. The sample is rotated, re-centered, and images are taken again from the center to the outside of the sample. From the center position, the first image is taken at a 5.0-mm radial interval. The remaining images are taken at intervals of 4.0-mm. This reduces the number of images taken and reduces uncertainty by assuming each image is approximately at the same interval away from the center. See Figure-4.21 for a drawing of the perpendicular foam pieces.

The parallel foam slices are 28.7-mm long and approximately 12.7-mm wide. Images taken from the slices are also taken at the same intervals as the perpendicular slices. The images are taken horizontally across the slice in rows starting with the upper left corner after centering the sample. See Figure-4.22 for a drawing of the parallel foam pieces.

Reproduced with permission of the copyright owner. Further reproduction prohibited without permission.

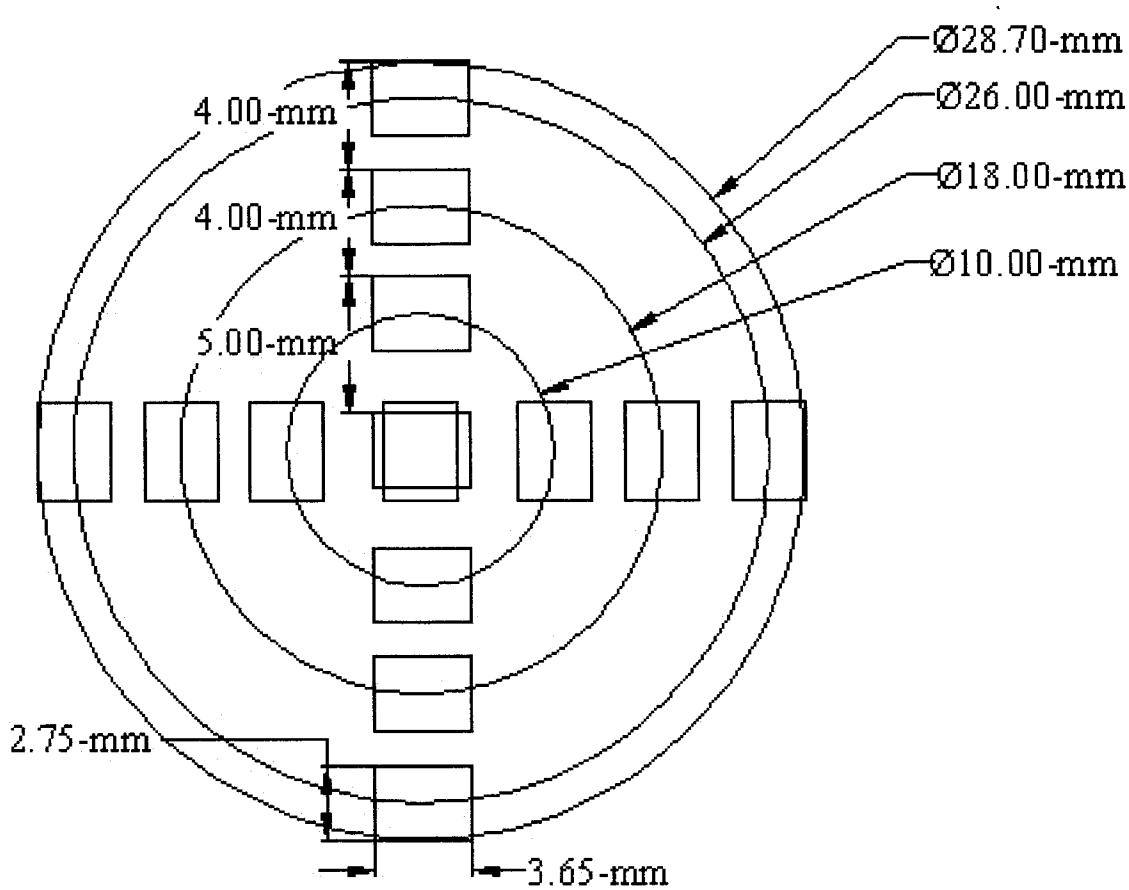

Figure-4.21: Imaging the Perpendicular Foam Slice

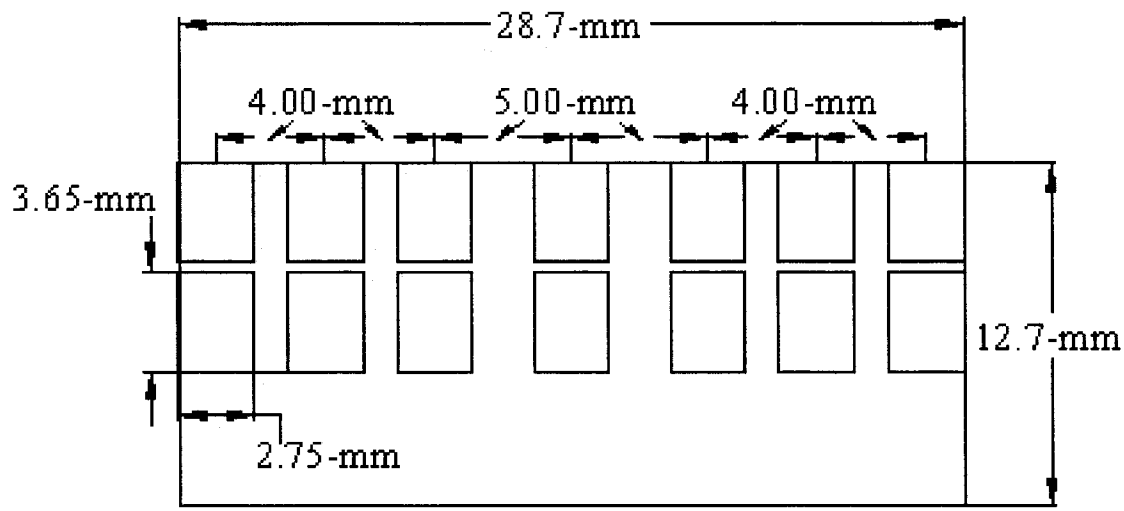

Figure-4.22: Imaging the Parallel Foam Slice

Reproduced with permission of the copyright owner. Further reproduction prohibited without permission.

The intervals chosen for image analysis are fairly close to the intervals used to determine density using the coring method. To insure the intervals are accurate, whole numbers are used and therefore, matching the coring intervals exactly is not possible. Radial intervals used for coring were 0.0-mm, 5.5-mm, 8.5-mm, and 11.0-mm from the center of the sample. Radial intervals used for imaging are 0.0-mm, 5.0-mm, 9.0-mm, and 13.0-mm from the center of the sample. The first three intervals of each method are fairly close to one another, however the last interval is not. This is because the coring method is limited and the SEM image can be taken closer to the edge of the sample.

Each perpendicular sample is considered to be symmetric about its x- and y-axis and each parallel sample is considered to be symmetric about its y-axis. This allows the four images taken from each radial position to be averaged from the perpendicular samples. In addition, the four images taken at the same interval on the parallel sample can be averaged. This means that four data points are collected from each perpendicular and parallel sample, from the center to outside of the sample. This data will include the average area, mean diameter, maximum diameter, minimum diameter, aspect ratio, angle, cell edge length, cell face thickness, and cell edge thickness. From this data, changes in cell morphology can be quantified and the volume fraction, density, Young's modulus, and collapse stress can be calculated in reference to the four intervals.

4.3 Testing

Three types of testing are used to compile experimental results for this paper. These include microscope images, mechanical testing, and density gradient testing. Microscope images provide the means to analyze the microstructure of the foam in several different

Reproduced with permission of the copyright owner. Further reproduction prohibited without permission.

locations throughout a molded foam sample. Mechanical testing provides the modulus, yield stress, and collapse stress for four sections of the small and reference molded foam samples or fourteen sections of a tall molded foam sample and will be compared with the microstructure of the foam to correlate any differences. Radial density gradient analysis provides the density at four radial positions throughout a sample and vertical density gradient analysis provides the density at each level throughout a mold. Both density gradients will be compared with the results from the microscope images and theoretical calculations.

4.3.1 Mechanical Testing

A United Axial Loading Machine shown in Figure-4.23 is used to test the polyurethane foam samples in compression according to ASTM Standard D1621-94 [26]. The machine uses a 4.4-kN Load Cell to record the amount of force on the sample, and a United Laser Extensometer is used to record the displacement of the sample. The cross-head speed used for all tests is 1.27-mm/min. Each sample's height, cross-sectional area, and mass are entered into the software program. The software uses this data input and the data it collects from the load cell and laser to output the stress and strain of each sample into an M.S. Excel spreadsheet. The data for each sample is then graphed, and a modulus, yield stress, and collapse stress are calculated manually by examining the stress-strain graph.

The modulus is calculated as the initial linear portion of the stress-strain graph. The first 100 data points recorded by the laser and load cell usually equate to the linear portion, however in some instances this is not the case. Sometimes the linear portion is preceded by a curve and then ends with a slight curve leading to the yield. The points

Reproduced with permission of the copyright owner. Further reproduction prohibited without permission.

making up these curves are usually deleted from the linear portion so that a linear regression can be performed to produce the modulus. Figure-4.24 shows the original curve with the first 100 recorded data points and then the curve with the first and last few points deleted for the linear regression. The correlation factor, R^2, is usually not lower than 0.97 and is quite often around 0.99. The peak yield point is taken as the highest stress value after the linear portion and before the stress begins to decrease. The collapse stress is taken as the average value of the plateau region that occurs after the peak yield.

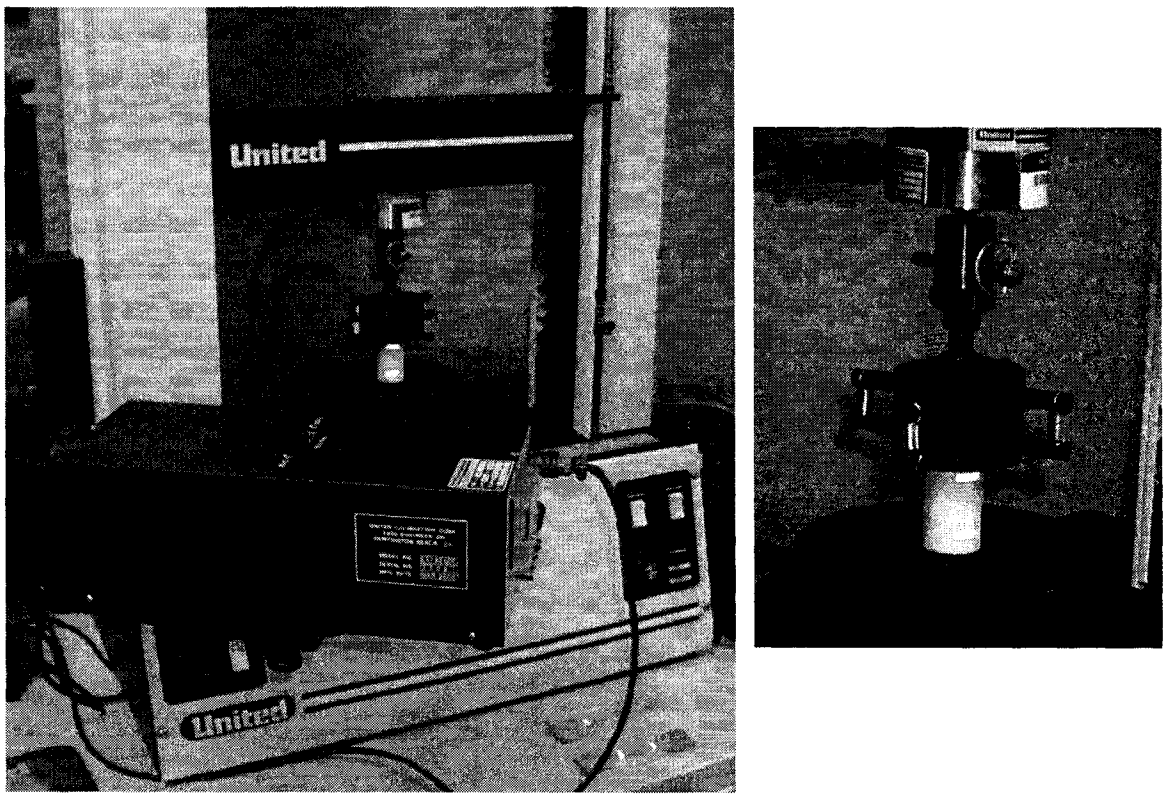

Figure-4.23: United Axial Loading Machine

Reproduced with permission of the copyright owner. Further reproduction prohibited without permission.

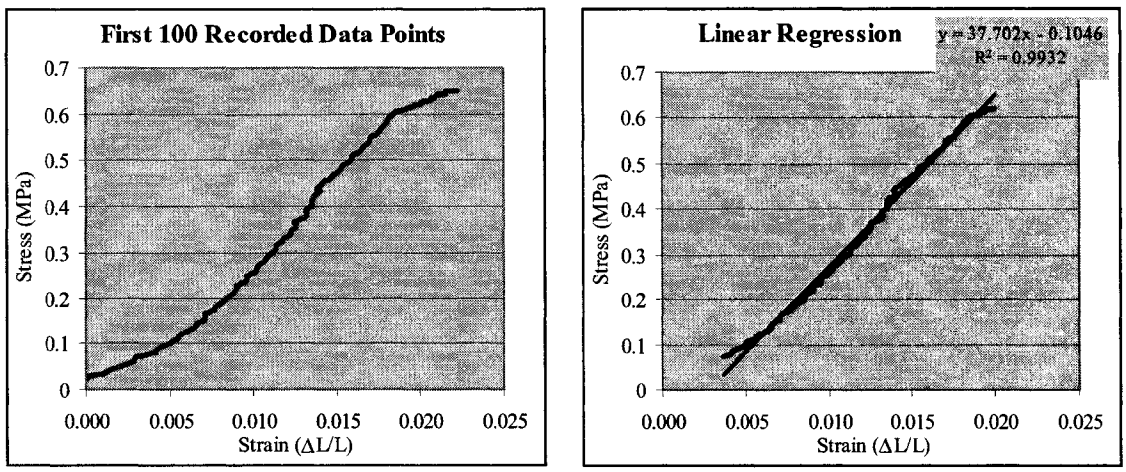

Figure-4.24: Calculation Young's Modulus from the Stress-Strain Curve

It is important to note the accuracy of the experimental measurements. The load cell is accurate to within +/-0.1%, which equates to approximately 4.4-N. The laser is more difficult to quantify but several conditions may create variations in the data. For instance, readings are not so accurate for small gauge samples or very stiff samples [27]. The samples used for this work are not very stiff, but they are on the low end of the recommended gauge length. In addition, the molded foam samples used in this study contain a thin layer of skin on the outside which may detach from the core and slide relative to the rest of the sample creating variations in measurements. A more in depth discussion of the United testing machine and laser can be found in reference 6 or 27.

Once the modulus, peak yield, and collapse stress values are determined, all are normalized using equations set forth by Goods and Whinnery et al [1]. The basic equations are presented as Equation-2.1 and Equation-2.2. These equations are modified to provide Equation-4.1 and Equation-4.2 where E_{exp} and σ_{exp} are raw values determined by the stress-strain curve, ρ is the density of the material, and E_{norm} and σ_{norm} are the

Reproduced with permission of the copyright owner. Further reproduction prohibited without permission.

normalized modulus and stress, respectively. Equation-4.1 provides the normalized value of the modulus whereas Equation-4.2 provides the normalized values for peak yield and collapse stress.

$$E_{norm} = E_{exp}\,(0.1/\rho)^{1.7} \qquad \text{Equation-4.1}$$

$$\sigma_{norm} = \sigma_{exp}\,(0.1/\rho)^{2.1} \qquad \text{Equation-4.2}$$

4.3.2 Imaging Analysis

The Scanning Electron Microscope (SEM) is used to obtain images in bitmap form. The images are uploaded to an image software analysis package, Image-Pro Plus 4.5, as seen in Figure-4.25. The images are first calibrated, and then a histogram band is created by thresholding. Cell size is determined by moving the vertical bar on the histogram. Once this is done it is possible to calculate the average cell area, aspect ratio, angle with the horizontal axis, maximum diameter, minimum diameter, and mean diameter. Table-4.1 provides definitions of the measurements, which are obtained from the software manual. To calculate measurements, the software only uses whole cells and therefore removes any cells on the boarder of the image from the analysis. Abnormally large cells are usually disregarded by the software since they usually touch the boarder.

The cell edge length, cell face thickness, and cell edge thickness are all calculated manually using the measurement tools provided by the software. For each image at least 15-20 manual measurements are taken and averaged for each length or thickness. Definitions of these manual measurements are shown in Figure-4.26. Since these manual measurements are very small, pixel size might have an effect on the measured results. All of the information gathered using thresholding and manual measurements are transferred to an M.S. Excel spreadsheet for further analysis of the raw data.

Reproduced with permission of the copyright owner. Further reproduction prohibited without permission.

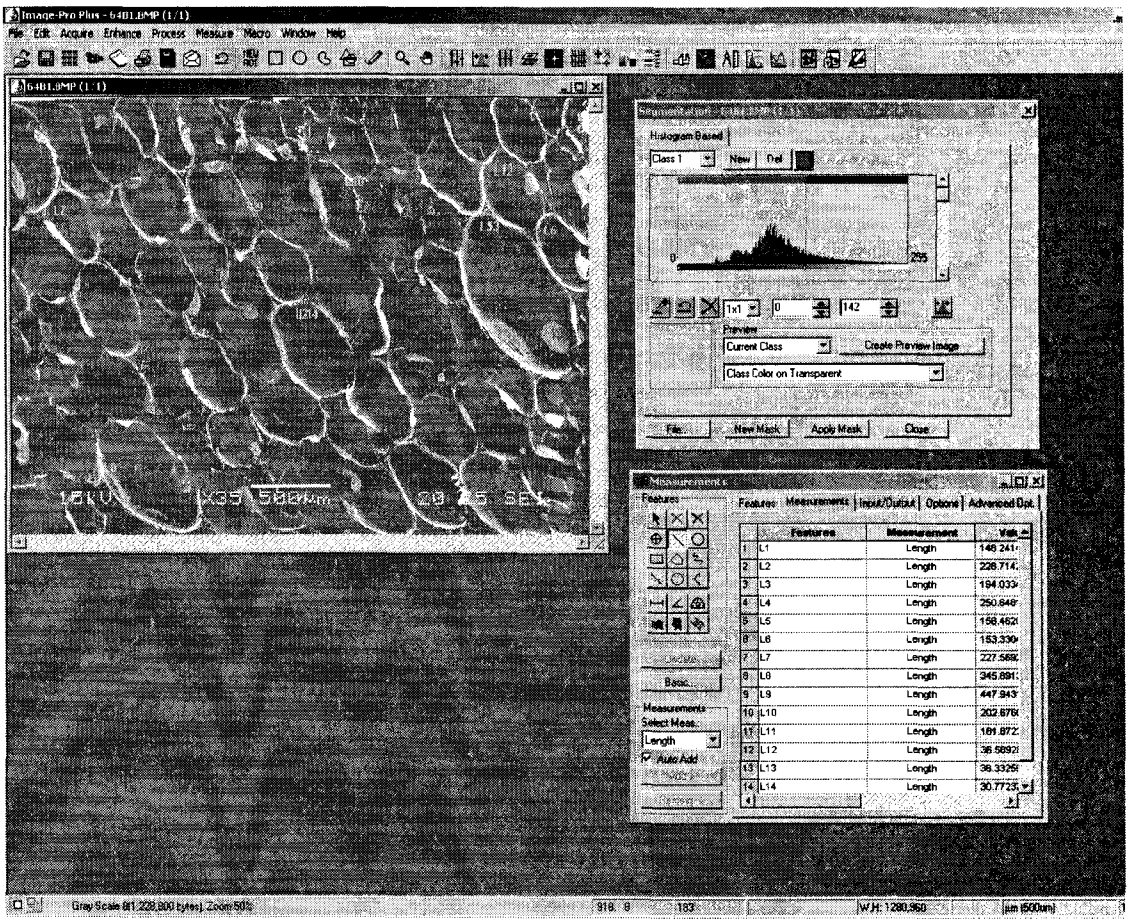

Figure-4.25: Image Pro Screen

Table-4.1: Definitions of Measurements

Area	Reports the area of each object (including holes)
Aspect	Reports the ratio between the major axis and the minor axis of the ellipse equivalent to the object
Angle	Reports the angle between the horizontal axis and the major axis of the ellipse equivalent to the object. The horizontal angle is 0-degrees
Diameter (max)	Reports the length of the longest line joining two outline points and passing through the centroid
Diameter (min)	Reports the length of the shortest line joining two outline points and passing through the centroid
Diameter (mean)	Reports the average length of the diameters measured at two degree intervals joining two outline points and passing through the centroid

Reproduced with permission of the copyright owner. Further reproduction prohibited without permission.

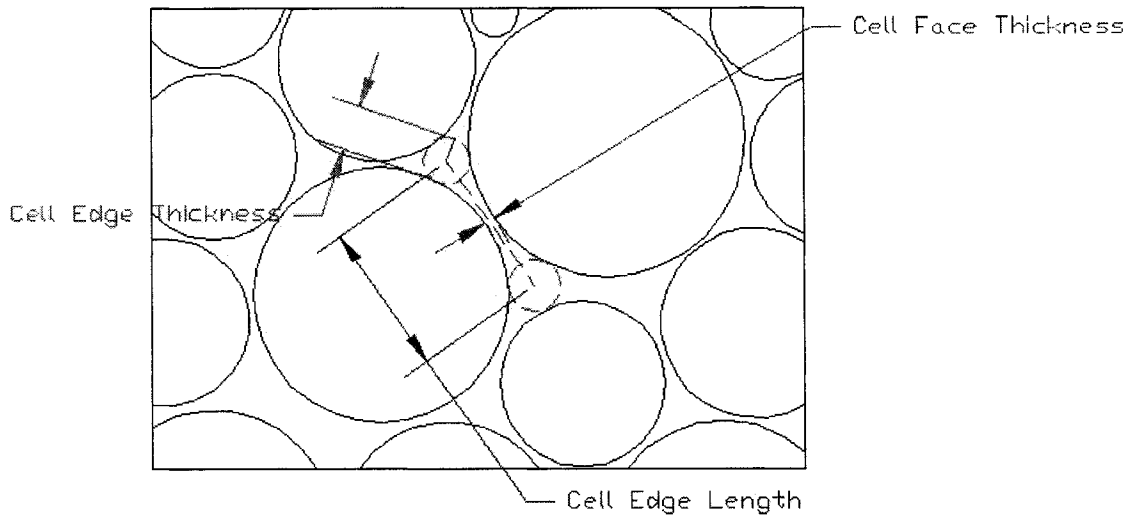

Figure-4.26: Manual Measurements

4.3.3 Density Gradients

Two types of density gradients are important to study. One of them is a radial density gradient and the other is a vertical density gradient. The radial density gradient is a measurement of the density change between the center and outside of a foam sample and is thoroughly explained in Appendix C. There are four data points representing the radial density gradient for the small molds, the first point representing the center and the last point representing the outer edge of the samples. The vertical density gradient is a measurement of the density change between the top of a molded cylinder to the bottom of the molded cylinder. Since four samples are obtained from each small molded cylinder and fourteen samples are obtained from each tall molded cylinder, four and fourteen density points are plotted for the vertical density gradient, respectively.

Reproduced with permission of the copyright owner. Further reproduction prohibited without permission.

CHAPTER 5

RESULTS

This chapter is quite long and is broken into three sections, "Experimental Density and Mechanical Results", "Cell Morphology Results", and "Theoretical Density and Mechanical Results". Each of these sections has subsections which discuss important aspects of each section. At the end of each section is a subsection that discusses the important findings. An outline of this chapter is shown below in Table-5.1.

Table-5.1: Chapter 5 Outline

5.1 Experimental Density and Mechanical Results
5.1.1 Average Density and Mechanical Properties for Each Designation Batch
5.1.2 Density and Mechanical Property Gradients as a Function of Vertical Position
5.1.3 Effect of Mold Order on Density and Mechanical Properties
5.1.4 Discussion of Density and Mechanical Results
5.2 Cell Morphology Results
5.2.1 Level Changes in Cell Morphology
5.2.2 Radial Changes in Cell Morphology
5.2.3 Discussion of Cell Morphology Results
5.3 Theoretical Density and Mechanical Results
5.3.1 Volume Fraction
5.3.2 Density
5.3.3 Modulus
5.3.4 Collapse Stress
5.3.5 Discussion of Theoretical Results

Reproduced with permission of the copyright owner. Further reproduction prohibited without permission.

5.1 Experimental Density and Mechanical Results

Several batches are fabricated for analysis of density and mechanical properties. At least two batches are fabricated for each condition, with exception of the reference batch. Table-5.2 shows the batches that are analyzed and under which conditions. Designation numbers are used from here on to refer to batches under certain conditions that are listed in the table. The first letter in the designation number refers to the type of mold used (i.e. S=Small Mold, T=Tall Mold, and R=Reference Mold). The second number refers to the gauge length of the sample analyzed (i.e. 2=50.8-mm gauge and 1=25.4-mm gauge). Finally, the third number refers to the days the samples are aged before testing.

Table-5.2: Analyzed Foam Batches

Designation Number	Batch Numbers	Type of Mold	Sample Gauge	Tested After	Total Number of Samples
S-2-1	C1 and C5	Small	50.8-mm	1-day	24
S-2-2	C4 and C8	Small	50.8-mm	2-days	24
S-1-1	C3 and C7	Small	25.4-mm	1-day	48
S-1-2	C2 and C6	Small	25.4-mm	2-days	48
S-1-7	C13 and C14	Small	25.4-mm	7-days	48
S-1-30	C15 and C16	Small	25.4-mm	30-days	48
S-1-90	C11 and C12	Small	25.4-mm	90-days	48
T-1-2	C9 and C10	Tall	25.4-mm	2-days	56
R-1-3	D2	Reference	25.4-mm	3-days	48

The main objective of analyzing this data is to show how the values are or are not changed in reference to different levels, molds, and the number of days from fabrication to testing. This section is divided into four subsections; averages, levels, mold order, and discussion. Each of the first three discusses the differences in density, modulus, peak yield, and collapse stress.

Reproduced with permission of the copyright owner. Further reproduction prohibited without permission.

To help to provide physical significance of future discussions, Figure-5.1 shows actual stress-strain curves for foam processed in a small mold, a tall mold, and a reference mold. These stress-strain curves show mechanical properties of the foam that are not normalized for density. Therefore, values presented in these graphs will be higher than the values presented in future tables and graphs. This is because the higher density of the foam produces higher values of mechanical properties, which when normalized for a lower density will yield lower normalized properties.

Appendix D included in this thesis is a compilation of charts and graphs that show individual average values for each designation number broken into averages, levels, and mold order. All graphs in Appendix D include first and second standard deviations for each average value. Stress-strain curves that show the actual raw data are also provided. The information in Appendix D is provided for completeness and is not included in this section because of its cumbersome nature.

Values of density, modulus, peak yield, and collapse for the reference batch are sometimes shown as dotted lines on the graphs in this section. The standard deviations for the reference batch are typically lower than for the batches in the small or tall molds. This is possibly due to the fact that more samples are taken from one mold or the fact that the radial density gradient is not as significant [6]. Table-5.3 shows average values and standard deviations calculated from the reference batch.

Table-5.3: Reference Batch Average Values and Standard Deviations

	Density (g/cc)	Modulus (MPa)	Peak Yield (MPa)	Collapse (MPa)
Average	0.1015	35.7	0.97	0.88
Standard Deviation	0.0038	3.9	0.07	0.05
% Deviation	3.8%	10.9%	7.2%	5.7%

Reproduced with permission of the copyright owner. Further reproduction prohibited without permission.

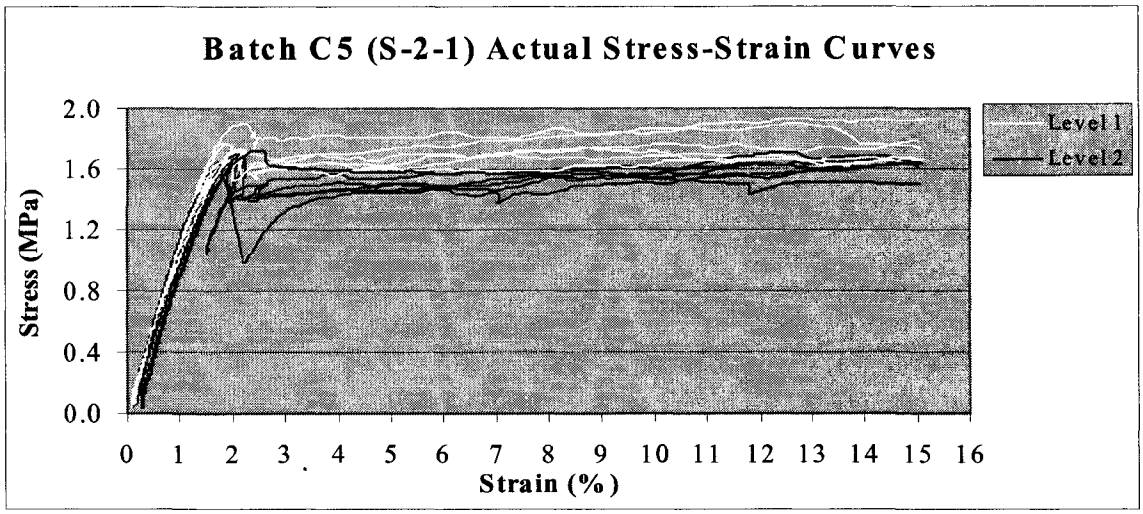

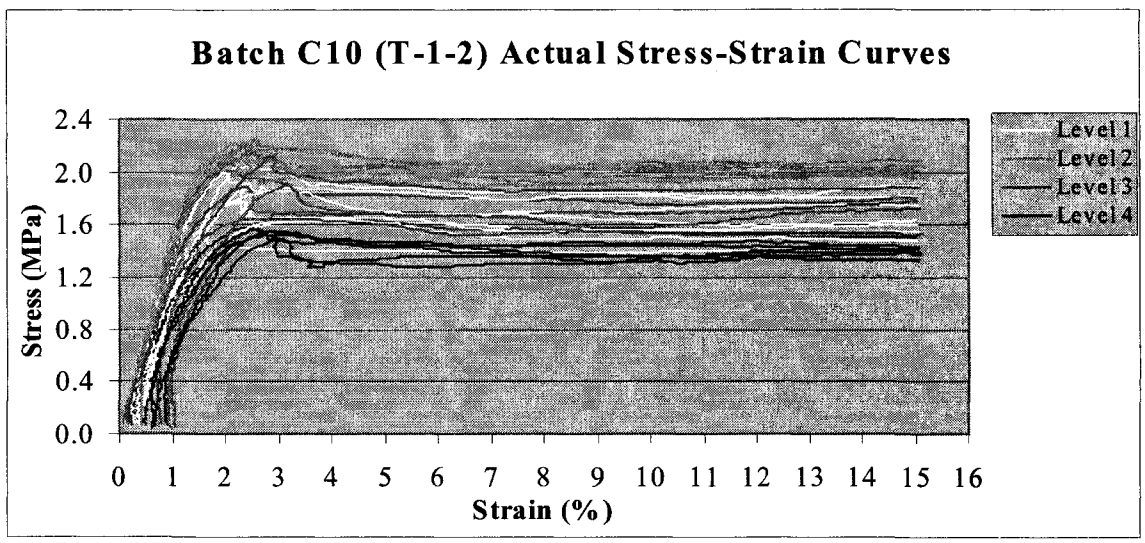

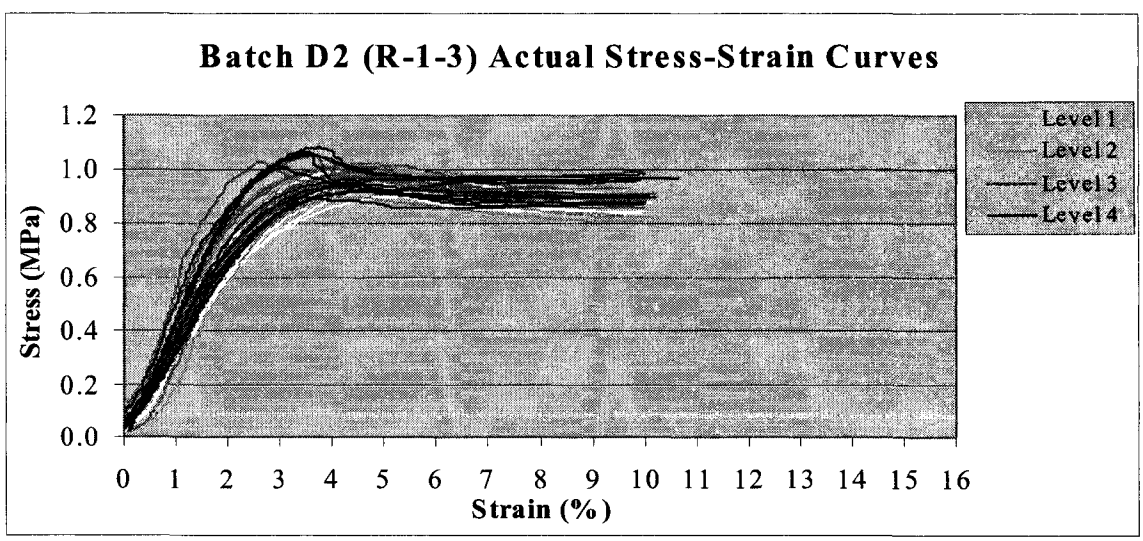

Figure-5.1: Actual Stress-Strain Curves for a Small, Tall, and Reference Mold

Reproduced with permission of the copyright owner. Further reproduction prohibited without permission.

5.1.1 Average Density and Mechanical Properties for Each Designation Batch

Figure-5.2 shows the average density for each batch and illustrates that the reference batch, shown by the dotted straight line, has a density much lower than the batches fabricated in the small or tall molds. The reference batch also yields a density very close to the target formulation density used to normalize the mechanical data showing that this mold really does act like a reference. All of the densities shown for the aged batches are the densities before the batches are aged. Figure-5-3 shows the percent differences between the original and aged densities. The density decreases 0.33% between the first and seventh day, decreases 0.37% between the first and thirtieth day, and decreases 0.16% between the first and ninetieth day. As described in reference 10, the increase in density could be due to moisture absorption and the decrease in density could be due to a loss in Surfactant. As the data shows, there is more of a change in density during the first thirty days. However, the density change is below 1.0% which is seen as an insignificant change. Even though the density does not change significantly, the aged density is used to normalize the mechanical data.

The average normalized modulus for each batch is shown in Figure-5.4. All of the average values of moduli are shown to be much greater than the reference batch modulus, shown as the dotted straight line. In fact, the moduli of the foam made in the small and tall molds are twice as large as the reference batch. This shows that the average modulus increases for molds with small diameters regardless of the height. Batches S-2-1 and S-2-2, which indicate the small molds with 50.8-mm gauge samples, both have a lower modulus and a much lower standard deviation than the other batches. This could be because the molds are separated into two sections instead of four and that there is less of

Reproduced with permission of the copyright owner. Further reproduction prohibited without permission.

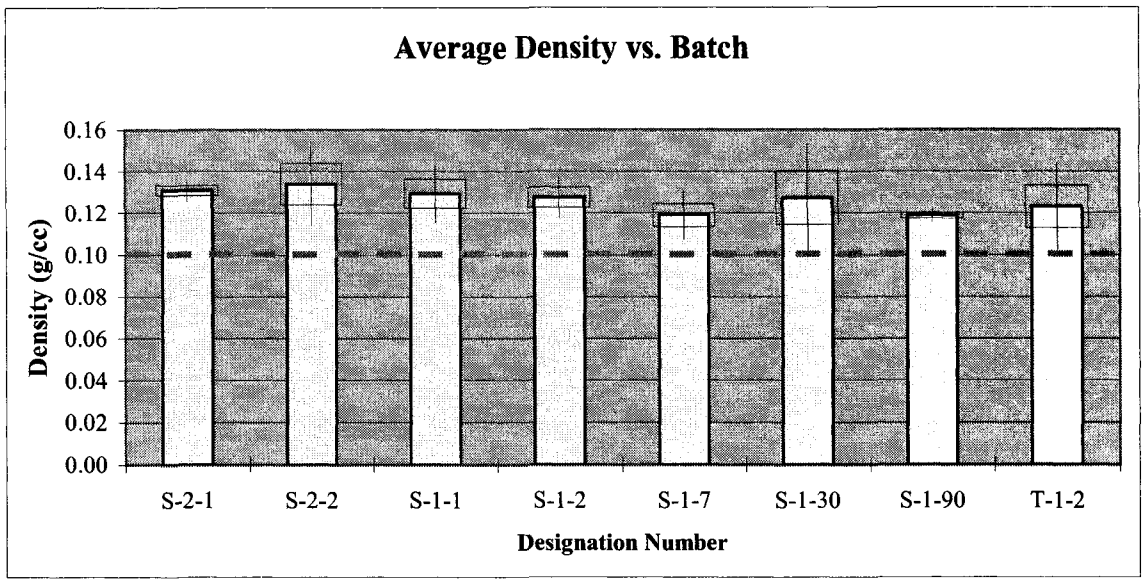

Figure-5.2: Average Density vs. Batch

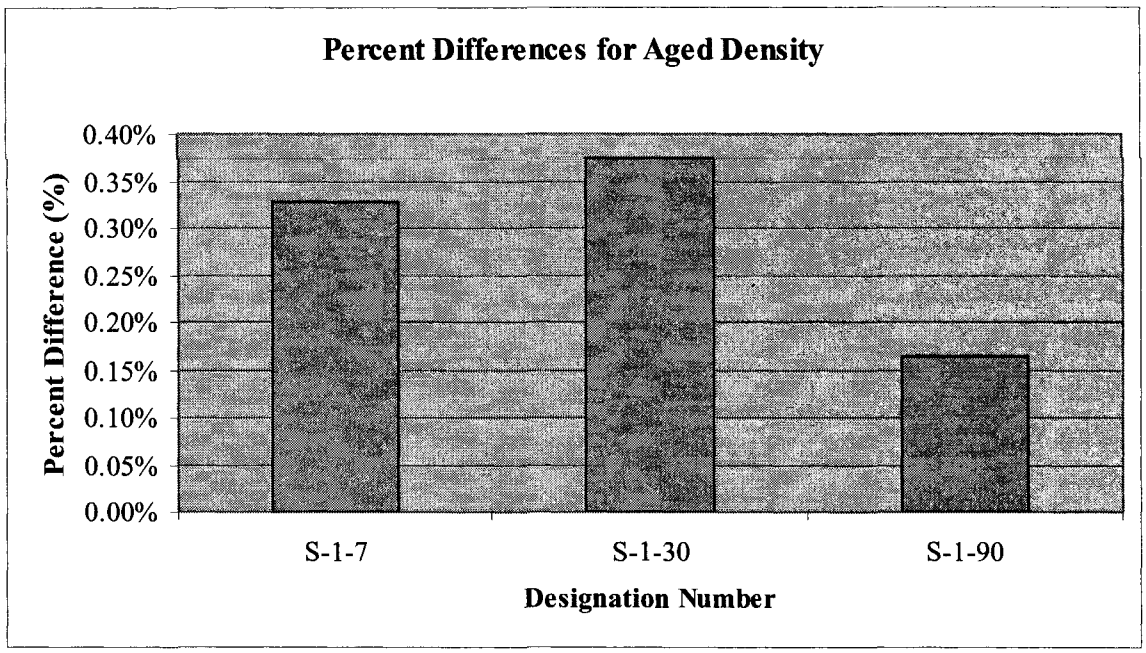

Figure-5.3: Percent Differences for Aged Density

an effect of levels on the average values. The large standard deviations of the 25.4-mm samples could also be due to the gauge length being so close to the low end of the

Reproduced with permission of the copyright owner. Further reproduction prohibited without permission.

recommended gauge length for the United Laser. All of the other batches, including the small and tall molds with 25.4-mm samples, are all at relatively the same average, except perhaps S-1-90. The aged batches show that the modulus slightly increases from the first to the second day and then slowly decreases after ninety days, however this is not definite since the standard deviations are so high.

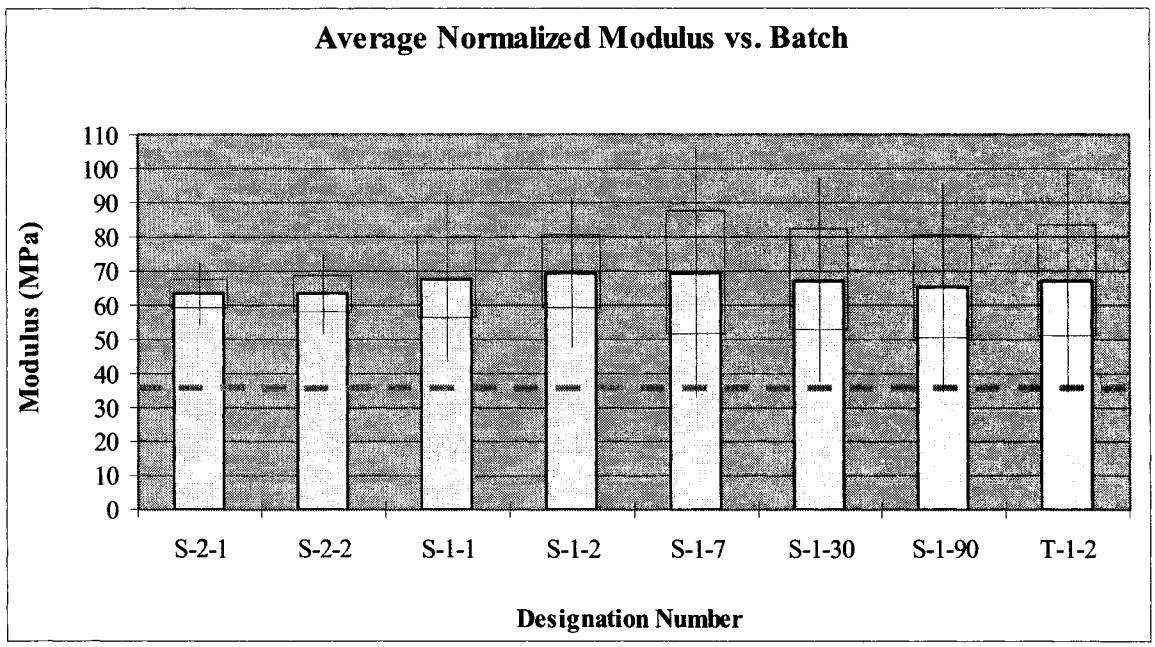

Figure-5.4: Average Normalized Modulus vs. Batch

The average normalized peak yield and collapse stress are shown by Figure-5.5 and Figure-5.6, respectively. All of the peak yield values are relatively the same except for the S-2-1 and S-2-2 batches which are slightly lower and the T-1-2 batch, which is slightly higher. However, this cannot be stated as significant because the first standard deviations overlap. It is important to note that again the standard deviations for the S-2-1 and S-2-2 batches are low. The reference batch shows a peak yield, which is relatively

Reproduced with permission of the copyright owner. Further reproduction prohibited without permission.

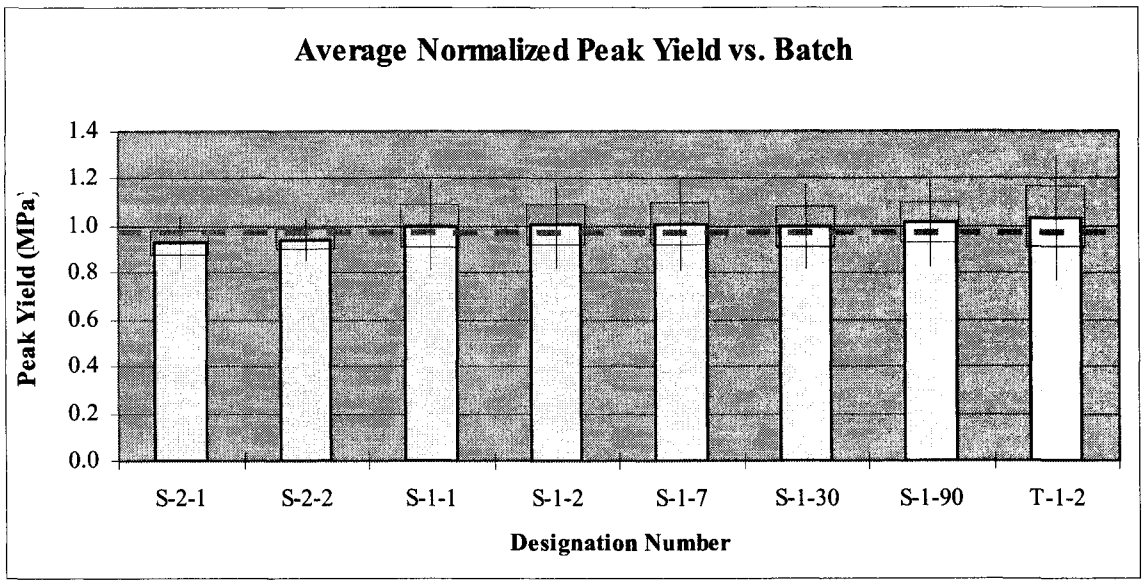

Figure-5.5: Average Normalized Peak Yield vs. Batch

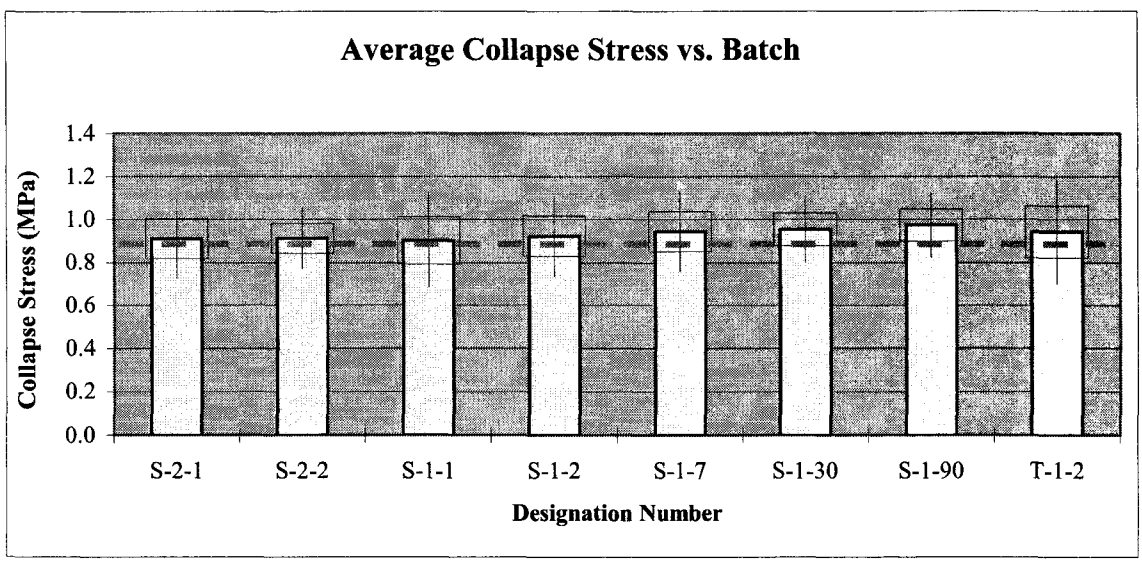

Figure-5.6: Average Normalized Collapse Stress vs. Batch

close to all the other batches shown. This indicates that the normalized peak yield is not significantly affected by the height of the mold or by being aged. The collapse stress of the reference batch is also close to the values of the other batches. The aged batches have

Reproduced with permission of the copyright owner. Further reproduction prohibited without permission.

a slightly higher value than all of the non-aged batches but again, the standard deviations overlap. However, it can be stated that the collapse stress increases after thirty to ninety days above that of the reference batch.

5.1.2 Density and Mechanical Property Gradients as a Function of Vertical Position

Vertical positions are defined as levels within the molds. Figure-5.7 shows the small, tall, and reference molds broken into levels. The top section is always designated as "Level 1". The small and reference molds with 25.4-mm samples have four levels, the small mold with 50.8-mm samples has two levels, and the tall mold has fourteen levels.

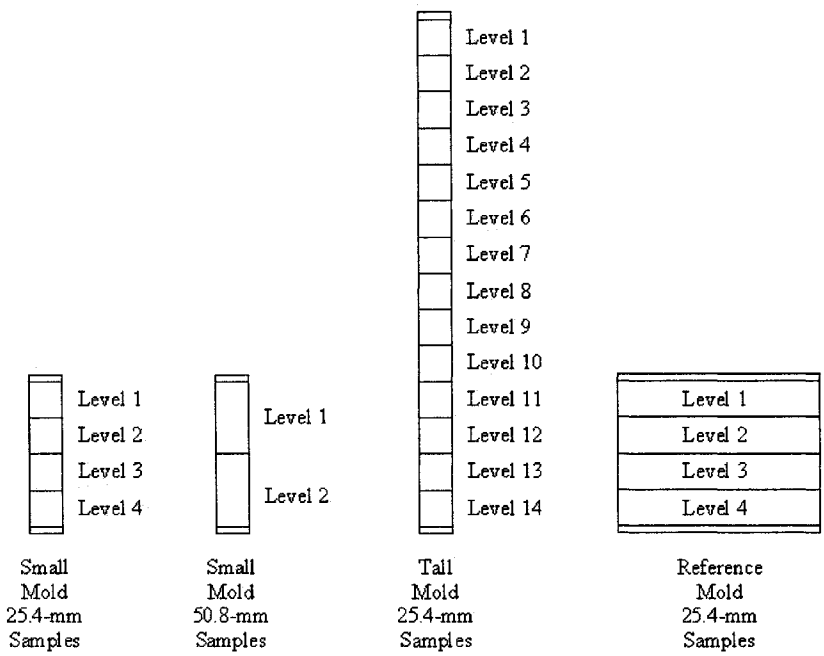

Figure-5.7: Diagram of Levels for the Small, Tall, and Reference Molds

It is shown by Figure-5.8, Figure-5.9, and Figure-5.10 that the average density does not change significantly with vertical position in the mold. As found by reference 7, the vertical density gradient is less evident for the small molds than for the reference batch.

Reproduced with permission of the copyright owner. Further reproduction prohibited without permission.

The same is shown in Figure-5.8 since the density is relatively the same for each level in the small molds but not for the reference where there is a definite increase in density in the fourth level. Interestingly, Figure-5.9 shows that there is a slight increase in density when comparing level 1 and level 14, but that there is actually more of an increase when comparing the top sample to the middle samples or the middle samples to the bottom samples. Figure-5.10, which shows the two levels of the small mold 50.8-mm samples, reveals that the there is only a slight increase in density from level 1 to level 2. It is better to look at the percent differences in density between the top and bottom of each type of mold and sample to ascertain a more accurate analysis since the densities are so uniform.

Table-5.4 shows percent differences in density between different levels for different batches. It shows that the small molds yield approximately the same average density increase from top to bottom regardless of measuring density in four increments or two. This restates the fact that density in the small molds is relatively uniform from top to

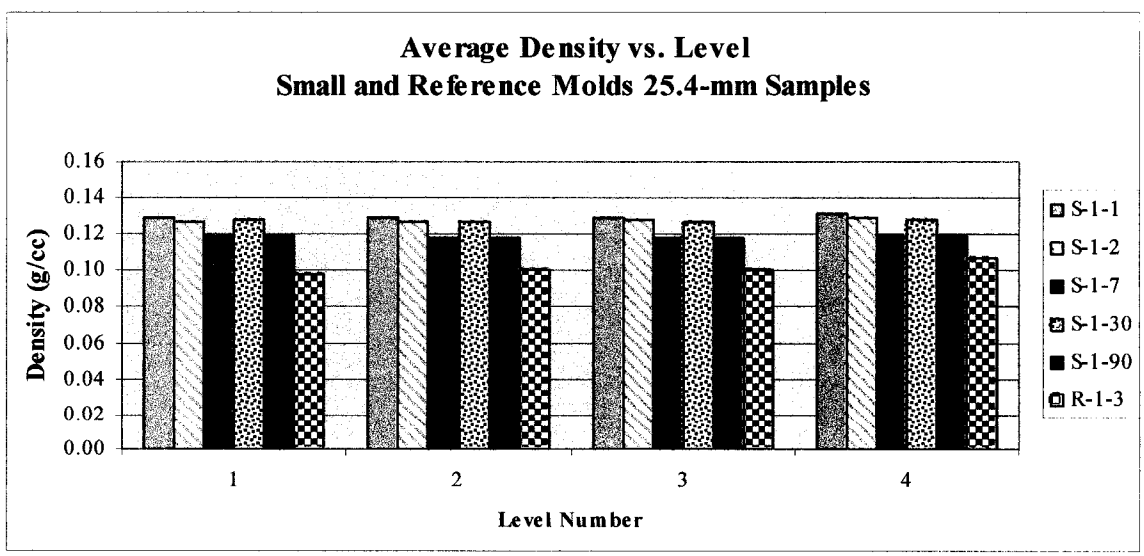

Figure-5.8: Average Density vs. Level: Small and Reference Molds 25.4-mm Samples

Reproduced with permission of the copyright owner. Further reproduction prohibited without permission.

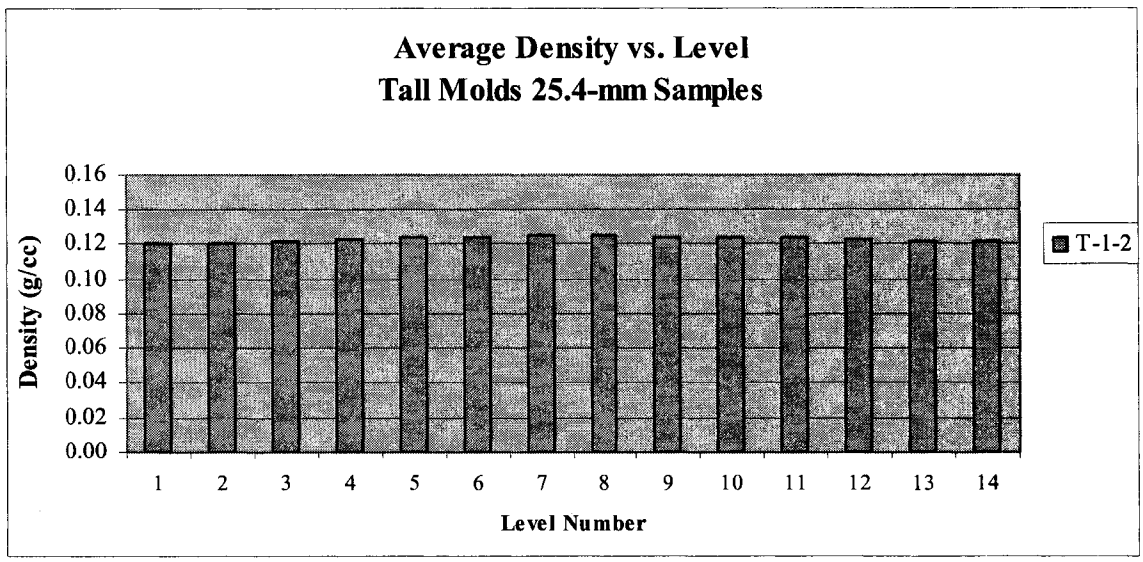

Figure-5.9: Average Density vs. Level: Tall Molds 25.4-mm Samples

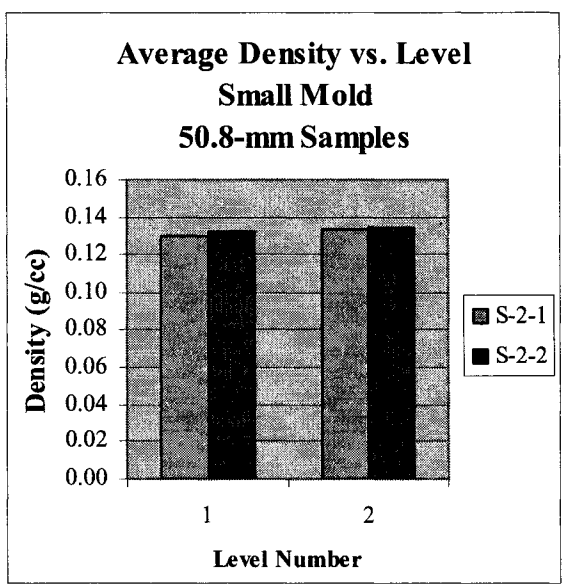

Figure-5.10: Average Density vs. Level: Small Mold 50.8-mm Samples

bottom. It also indicates that the gauge length does not alter the vertical density gradient. The tall mold yields foam that is less uniform than the small molds but still much more

Reproduced with permission of the copyright owner. Further reproduction prohibited without permission.

uniform than the reference mold. This means that the height of the mold is not the only influencing factor on the vertical density gradient. Interestingly, the difference in density is greater between the top sample and the middle of the mold. The highest value of density is seen at level 7, which coincidently enough is almost dead center in the mold.

Table-5.4: Differences in Vertical Density for Different Molds

Mold Type	Levels in Mold	Levels Compared	Increase from Top to Bottom
Small	2	1 and 2	0.82%
Small	4	1 and 4	0.84%
Tall	14	1 and 14	1.61%
Tall	14	1 and 7	3.69%
Reference	4	1 and 4	8.42%

Figures-5.11, 5.12, and 5.13 show the normalized modulus, peak yield, and collapse stress, respectively, of the small and reference molds with 25.4-mm samples. The modulus, yield, and collapse are all consistently lower at level 4 of the small molds. In addition, the yield and collapse at level 2 are larger for the small molds. It seems that aging the foam does not have a large impact on the mechanical properties. All five aging conditions yield mechanical properties that are within the same range of one another at each level. The reference batch shows a fairly consistent modulus with levels 3 and 4 being slightly larger. The yield and collapse are also fairly uniform with level 4 being slightly lower.

Reproduced with permission of the copyright owner. Further reproduction prohibited without permission.

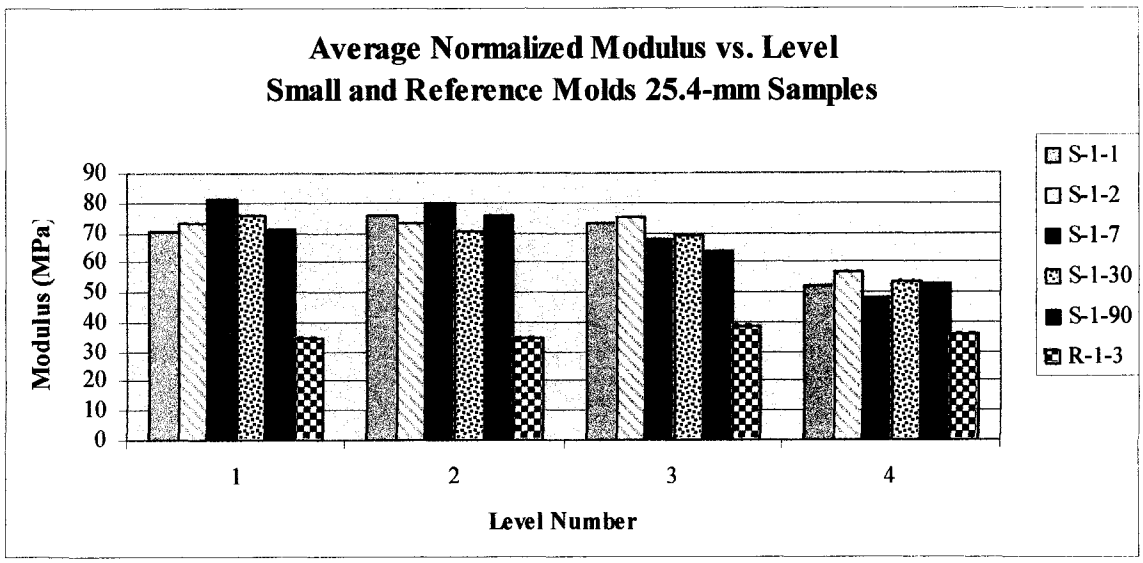

Figure-5.11: Average Normalized Modulus vs. Level:

Small and Reference Molds 25.4-mm Samples

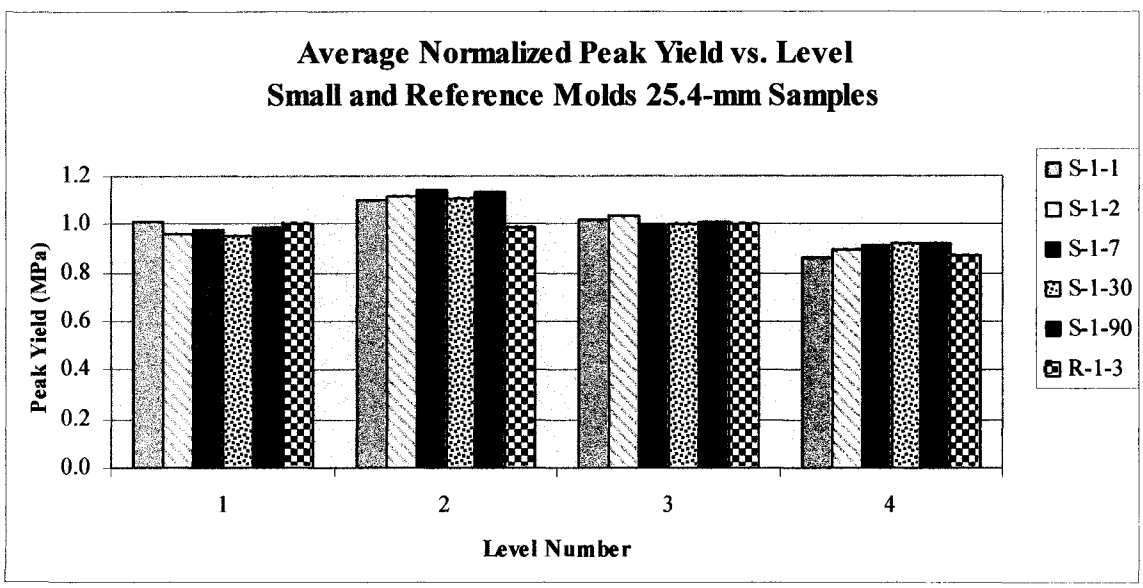

Figure-5.12: Average Normalized Peak Yield vs. Level:

Small and Reference Molds 25.4-mm Samples

Reproduced with permission of the copyright owner. Further reproduction prohibited without permission.

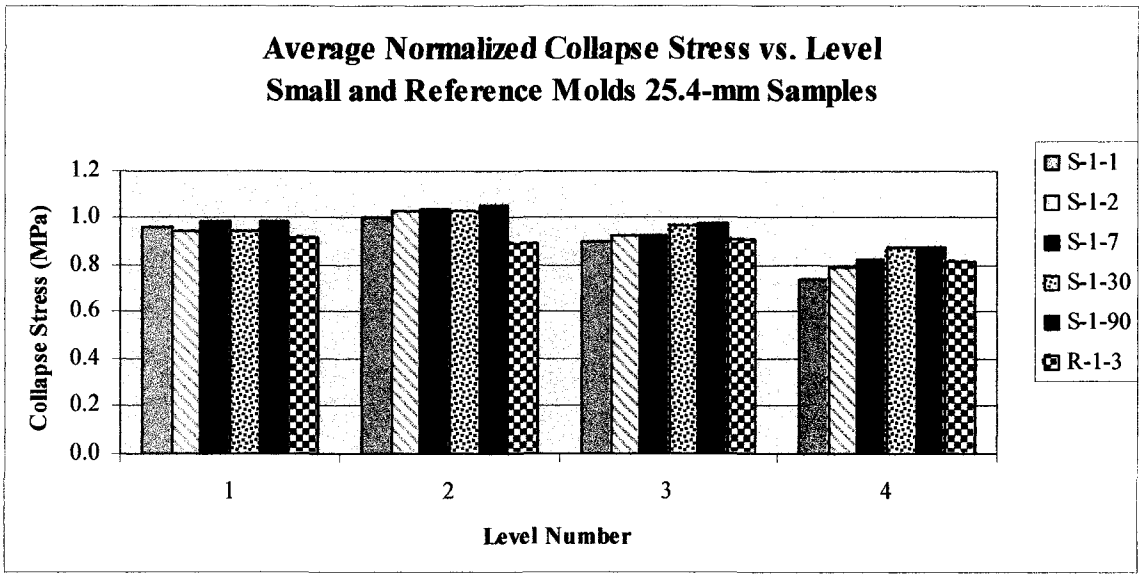

Figure-5.13: Average Normalized Collapse Stress vs. Level:

Small and Reference Molds 24.5-mm Samples

The normalized modulus, peak yield, and collapse stress of the tall molds are shown in Figure-5.14, 5.15, and 5.16, respectively. All mechanical properties are larger at levels 5, 6, and 7. This correlates approximately to level 2 in the small molds with 25.4-mm samples which is interesting because it is the level with the highest peak yield and collapse stress. This means that as the mold increases in size, the foam with the highest properties will be in the area that is 25-50% below the top of the mold. It is interesting that the properties of the tall molds tend to show a relatively smooth curve where as the small molds have properties that seem to be a bit uneven. This could be due to the fact that more increments of the tall molds are analyzed than the smaller molds.

Reproduced with permission of the copyright owner. Further reproduction prohibited without permission.

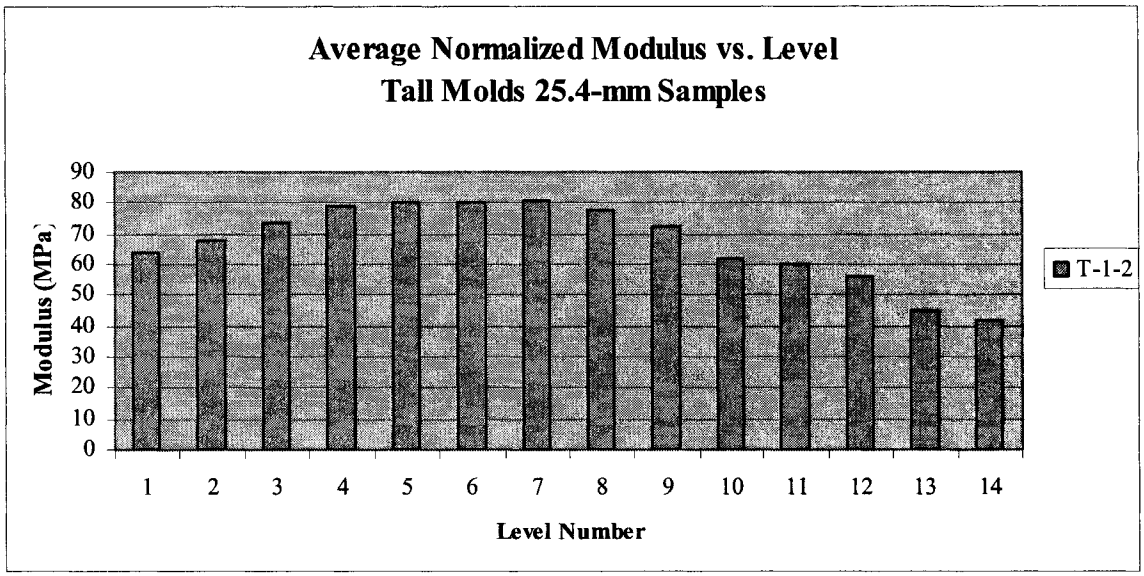

Figure-5.14: Average Normalized Modulus vs. Level:

Tall Molds 25.4-mm Samples

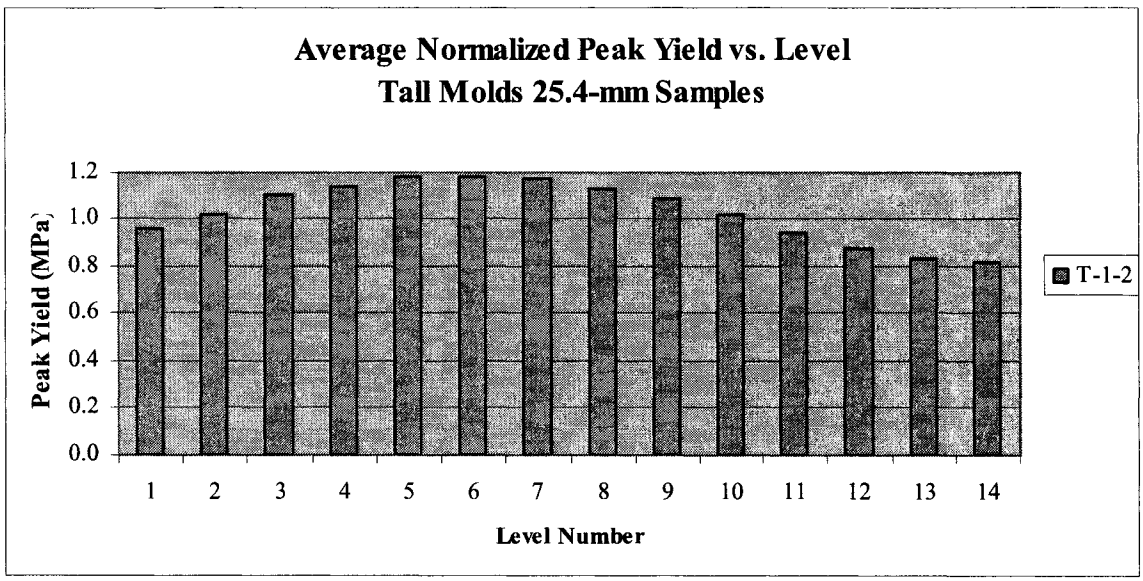

Figure-5.15: Average Normalized Peak Yield vs. Level:

Tall Molds 25.4-mm Samples

Reproduced with permission of the copyright owner. Further reproduction prohibited without permission.

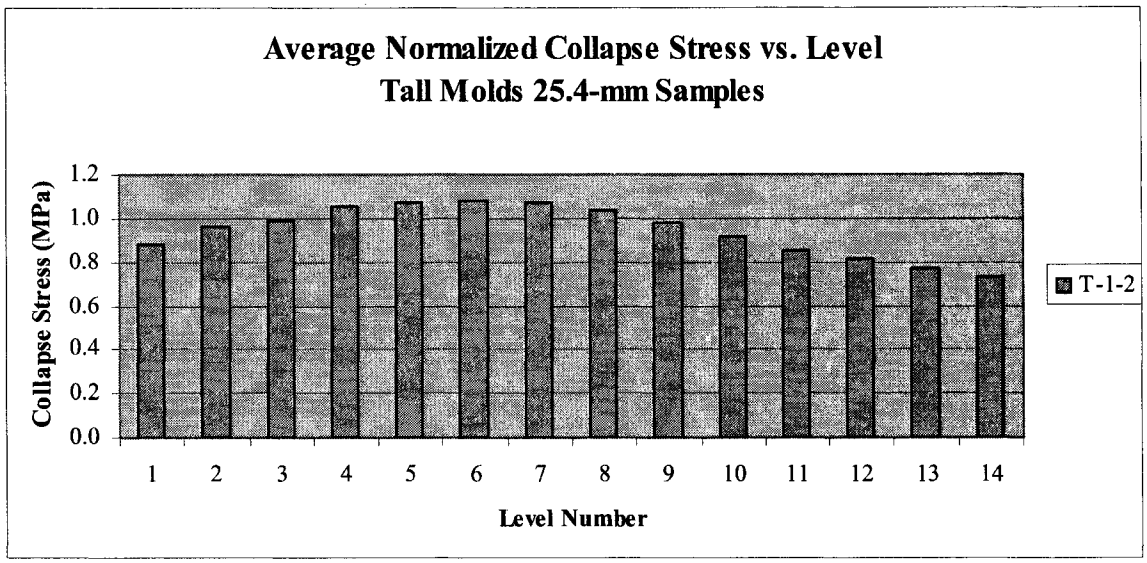

Figure-5.16: Average Normalized Collapse Stress vs. Level:

Tall Molds 25.4-mm Samples

The mechanical properties of the small molds with 50.8-mm samples are shown in Figure-5.17, 5.18, and 5.19. The normalized modulus, peak yield, and collapse are all lower for level 2 compared with level 1. This is consistent with the previous findings since the top 25-50% of the mold is usually seen as the highest in property values and the bottom 75-100% of the mold is usually seen as the lowest in property values. It is also seen that the property values for level 1 and level 2 are closer to one another than those seen for the other molds. It makes sense that the mold divided into two sections yields properties that have a smaller range between them than the mold divided into four or fourteen sections, which provides a more in-depth analysis of properties changing from the top to the bottom.

Reproduced with permission of the copyright owner. Further reproduction prohibited without permission.

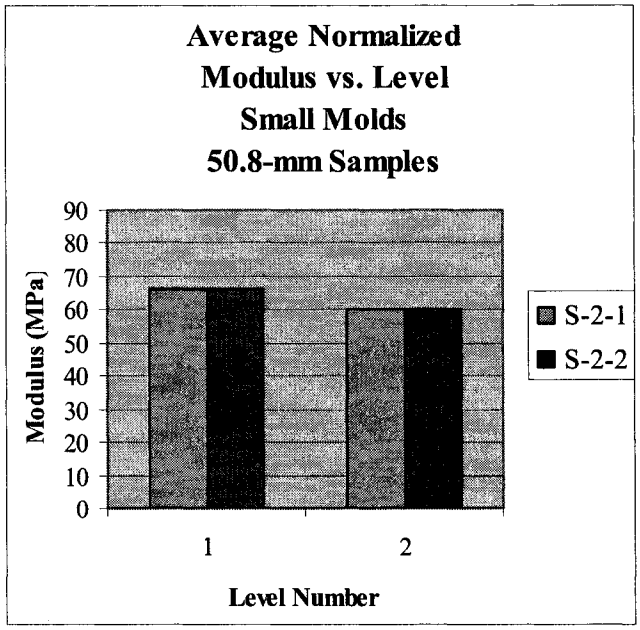

Figure-5.17: Average Normalized Modulus vs. Level:

Small Molds 50.8-mm Samples

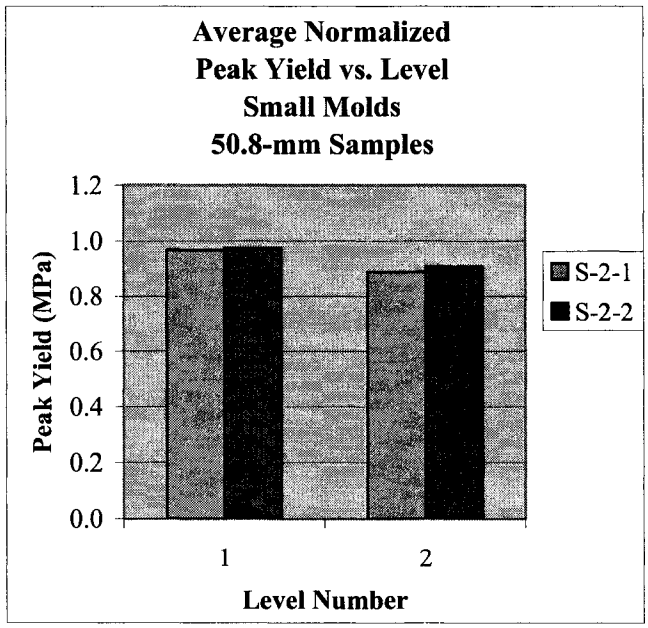

Figure-5.18: Average Normalized Peak Yield vs. Level:

Small Molds 50.8-mm Samples

Reproduced with permission of the copyright owner. Further reproduction prohibited without permission.

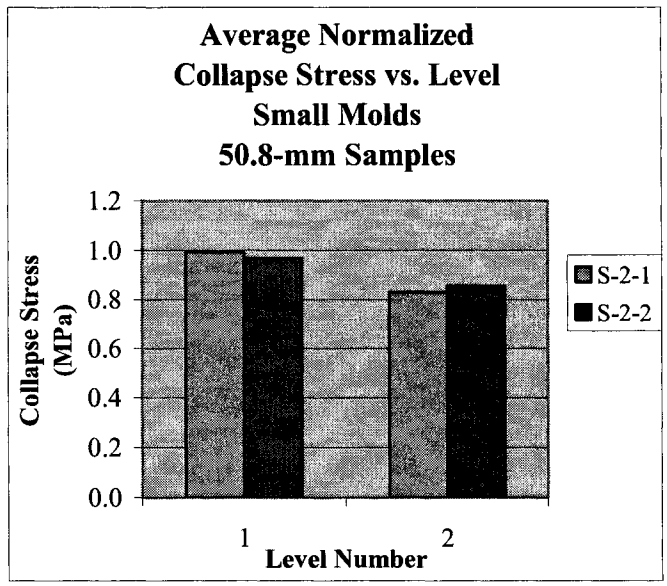

Figure-5.19: Average Normalized Collapse Stress vs. Level:

Small Molds 50.8-mm Samples

5.1.3 Effect of Mold Order on Density and Mechanical Properties

Figure-5.20 shows the density of each mold for all batches. Since the reference batch is only made in one mold, its average density is shown as a dotted straight line. There is no clear evidence that the order in which foam is poured has any effect on its density. There does seem to be variation in density from mold to mold, but the deviation is slight. Table-5.5 shows the percent difference in density between the mold with the smallest density and the mold with the largest density. As the data reveals, the differences are not consistent and vary from 0.6-7.5%.

Reproduced with permission of the copyright owner. Further reproduction prohibited without permission.

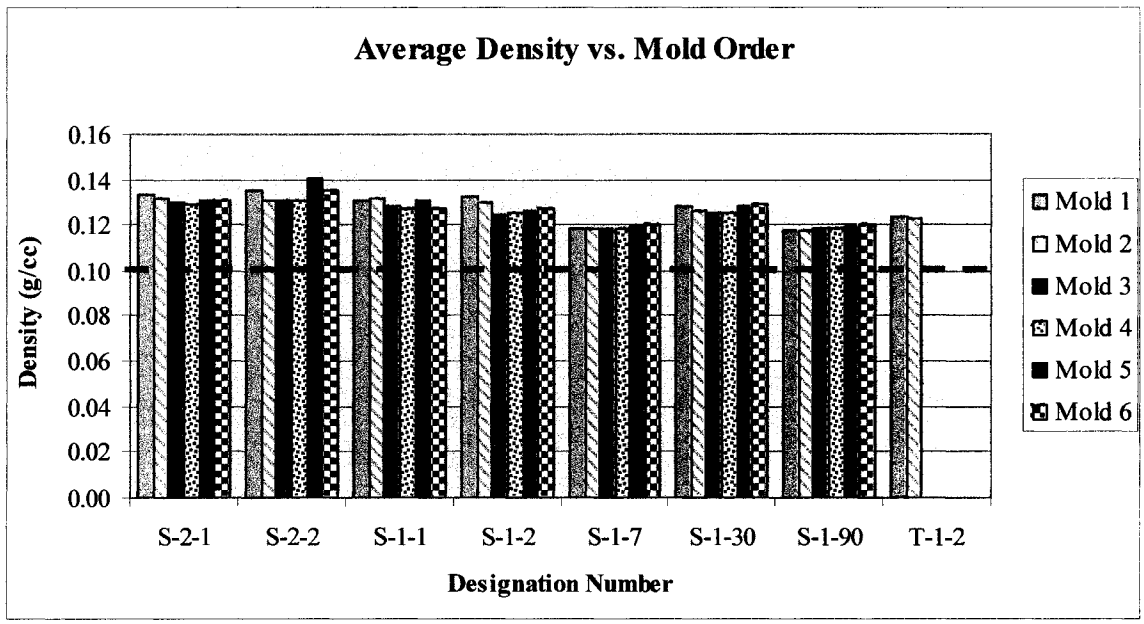

Figure-5.20: Average Density vs. Mold Order

Table-5.5: Differences in Properties for Different Mold Orders

Designation Number	Increase in Density	Increase in Modulus	Increase in Peak Yield	Increase in Collapse Stress
S-2-1	3.3%	9.2%	2.8%	2.8%
S-2-2	7.5%	5.9%	3.9%	7.7%
S-1-1	3.4%	9.6%	2.7%	2.9%
S-1-2	6.3%	11.4%	4.6%	6.1%
S-1-7	1.8%	16.8%	1.6%	3.7%
S-1-30	2.2%	21.7%	4.7%	3.7%
S-1-90	2.6%	21.0%	6.2%	5.0%
T-1-2	0.6%	8.2%	0.2%	0.0%

Figure-5.21, 5.22, and 5.23 show the normalized modulus, peak yield, and collapse stress of all batches, respectively. Again like the conclusion made about density, there is no clear evidence that the order in which foam is poured has any effect. Sometimes the properties are largest in the first mold, sometimes in the middle, and then still other times in the last mold poured. Table-5.5 includes percent differences between the lowest

Reproduced with permission of the copyright owner. Further reproduction prohibited without permission.

properties and the highest properties seen in different molds for the normalized modulus, peak yield, and collapse. Interestingly, it seems there is an increase in deviation of the normalized modulus as the foam ages. However, this could be an anomaly.

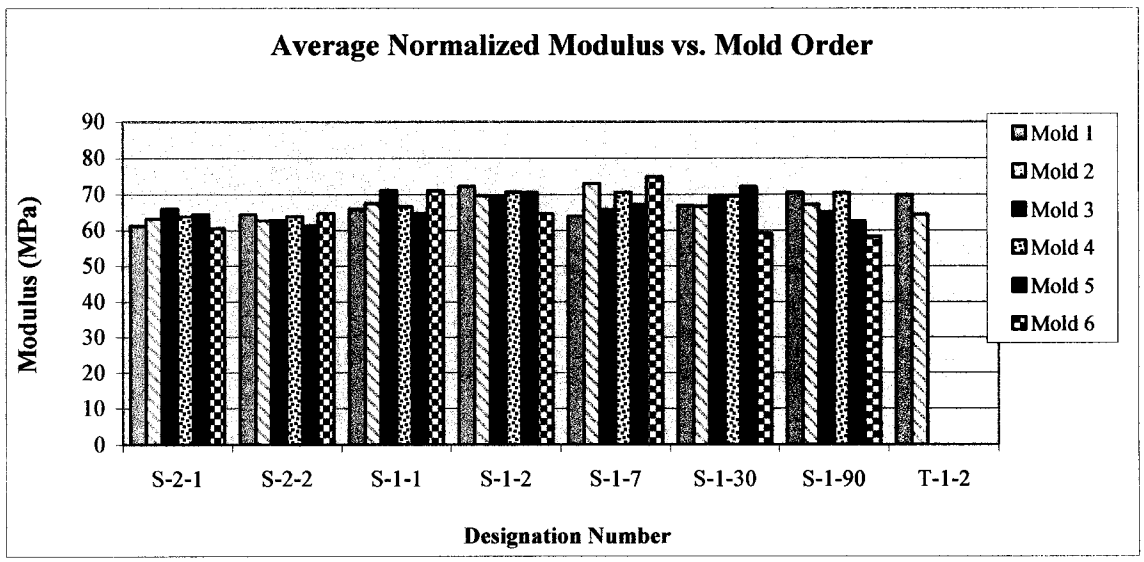

Figure-5.21: Average Normalized Modulus vs. Mold Order

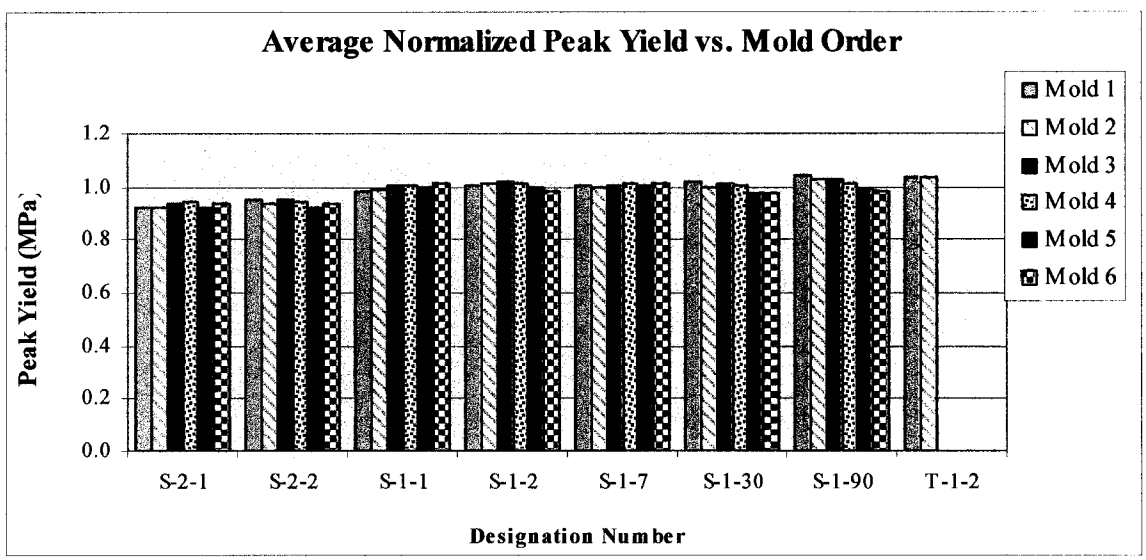

Figure-5.22: Average Normalized Peak Yield vs. Mold Order

Reproduced with permission of the copyright owner. Further reproduction prohibited without permission.

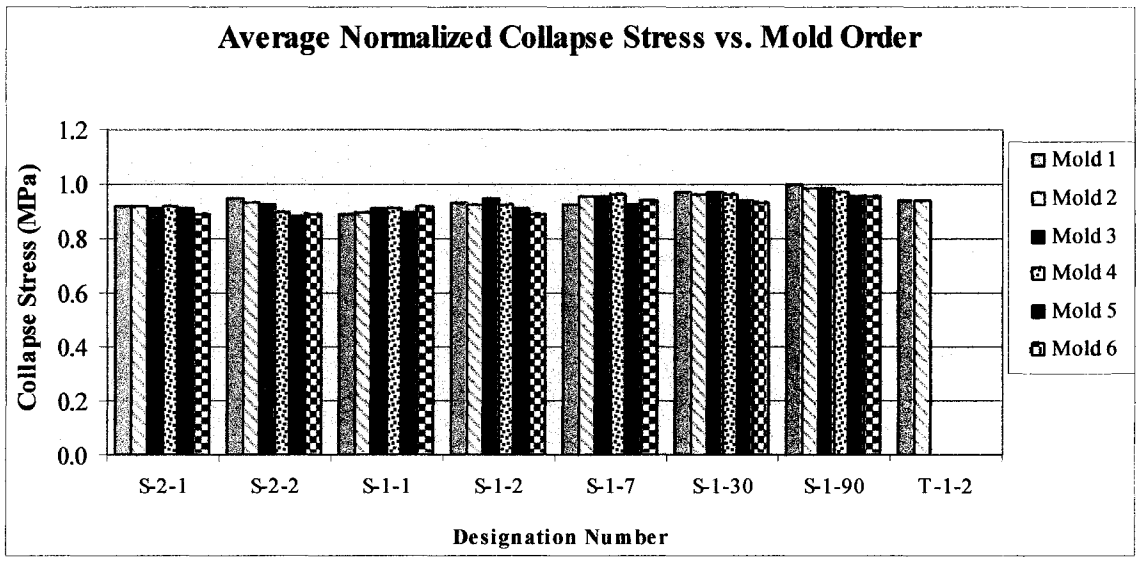

Figure-5.23: Average Normalized Collapse Stress vs. Mold Order

5.1.4 Discussion of Density and Mechanical Results

It is evident from the discussions above that density does not play an important roll since it is fairly uniform throughout the molds. In addition, the mechanical properties shown are all normalized for density so that the variable is not seen. Other studies show that mechanical properties increase with increasing density, [1] and this is clearly shown by the actual stress-strain curves in Appendix D. These non-normalized curves are broken into batches so it can be clearly seen that an increase in average density raises the non-normalized modulus, peak yield, and collapse. In addition, each graph shows the stress-strain curves according to level, which point out the definite impact of the vertical position.

The data presented in this section makes it clear that a specimen's level within the mold has more of an effect than its mold order. In previous studies, it was difficult to analyze the mechanical property data because of standard deviations up to 17% [6]. Even

Reproduced with permission of the copyright owner. Further reproduction prohibited without permission.

this current study saw standard deviations in the normalized modulus upwards of 20%, primarily because an outlier study is not performed. This is not done because it is important to analyze all specimens to see the effect of levels and molds. This high standard deviation is still seen when the data values are broken down into mold order but not so great. The standard deviations are actually lower when broken into levels, especially seen in the peak yield and collapse. This is important since it supports the finding that the levels have an important impact on the properties of the foam.

The aging study did not produce significant results. It is almost safe to say that within the first ninety days, the density and mechanical properties do not change significantly when aged at room temperature. This result is expected since reference 10 details a study at room temperature that reveals similar results except that the time periods used are much larger. The main reason for performing an aging study was to examine smaller time periods to provide reference information for the UNLV chemistry studies and to determine a suitable timeframe for taking initial measurements when doing a longer term aging study. One significant result from this study is that there is no rush to calculate density or mechanical properties within the first one or two days after making foam. Instead, the density and mechanical properties can be measured within the first thirty to ninety days with the assumption that they are about the same as when taken within the first two days.

The data also shows that the aged batches (S-1-7, S-1-30, and S-1-90) produce some of the highest standard deviations in the normalized modulus. This could be a coincidence or actually show that the modulus deviates more with an increase in time for the first ninety days.

Reproduced with permission of the copyright owner. Further reproduction prohibited without permission.

5.2 Cell Morphology Results

Imaging is performed on samples taken from three types of molds including the small molds, tall molds, and reference molds. These are the same molds used to process specimens for the mechanical data. Unfortunately, not as many samples can be produced because of the time consuming process of generating and analyzing images. Therefore, only eight samples are analyzed in the perpendicular and parallel directions. Figure-5.24 illustrates where each of the eight samples is taken from the respective molds. Also provided are the names of the samples to be used throughout the text. The first letter refers to the type of mold used (i.e. S=Small Mold, T=Tall Mold, and R=Reference Mold). The number after refers to the level at which the sample is taken from the mold, with exception of the reference batch where the letter "C" refers to its position in the center of the mold.

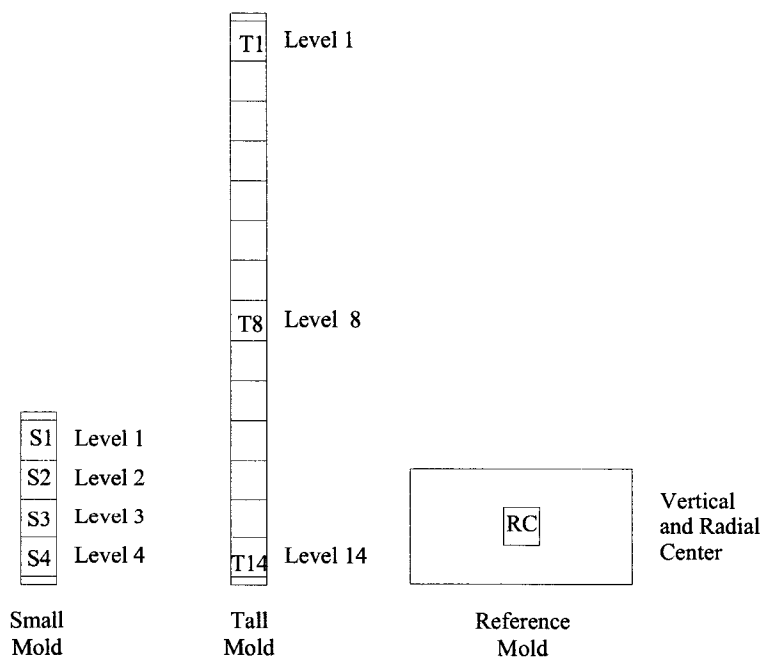

Figure-5.24: Location and Names of Samples to be Imaged

Reproduced with permission of the copyright owner. Further reproduction prohibited without permission.

Each sample produces a parallel and perpendicular slice for imaging. The location of each image taken is documented with a series of letters and numbers, and radial location numbers, as shown in Figure-5.25. The first letter indicates whether the image is located on a perpendicular ("A") slice or a parallel ("B") slice. The numbers that follow designate the location on the slice. The radial position numbers shown in parenthesis indicate the radial position of each image. Images with the same radial position number are averaged together. Though fourteen images are taken as seen in Appendix E, only half are analyzed because of the cumbersome and time-consuming nature of analysis. Figure-5.25 only shows those images that are analyzed.

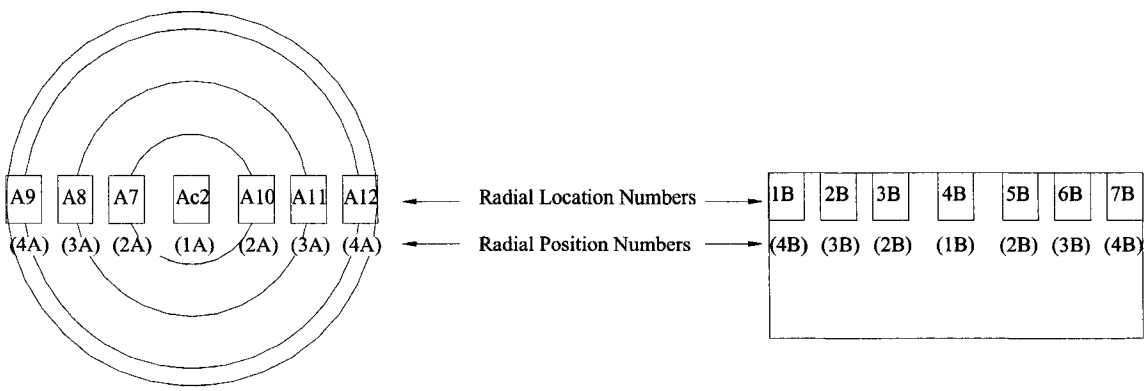

Figure-5.25: Location and Names of Images taken on Parallel and Perpendicular Slices

Appendix E shows all images that are taken with the SEM in addition to the average data calculated for each image analyzed. The parallel images are shown together in series to illustrate how the cells change as a function of vertical and radial positions. The perpendicular images are shown separately according to level. It is quite interesting to view and compare the parallel images from different mold sizes. Figure-5.26 and Figure-

Reproduced with permission of the copyright owner. Further reproduction prohibited without permission.

5.27 show all the parallel rows imaged for the small and tall molds, respectively. Figure-5.26 shows that the cells are more elongated at the bottom of the mold and that these cells tend to angle towards the center of the mold. Figure-5.27 further emphasizes this fact and shows that some of the images on the top row tend to slant towards the outside of the mold. This is particularly seen in the images in columns two and six. Figure-5.28 shows the parallel rows imaged for the reference mold. As seen in this image, all the cells are much larger and more uniform than the images seen in the small and tall molds. Keep these figures of the parallel images and the ones in Appendix E in mind when discussing measured properties of the images.

Visually, the perpendicular images are not as clear when looking for differences, particularly since it is not possible to arrange them in the same manner as the parallel images. Figure-5.29 shows the perpendicular images for the bottom sample from the tall mold. As shown, the images do not change significantly with radial position. All of the perpendicular images are included in Appendix E.

Reproduced with permission of the copyright owner. Further reproduction prohibited without permission.

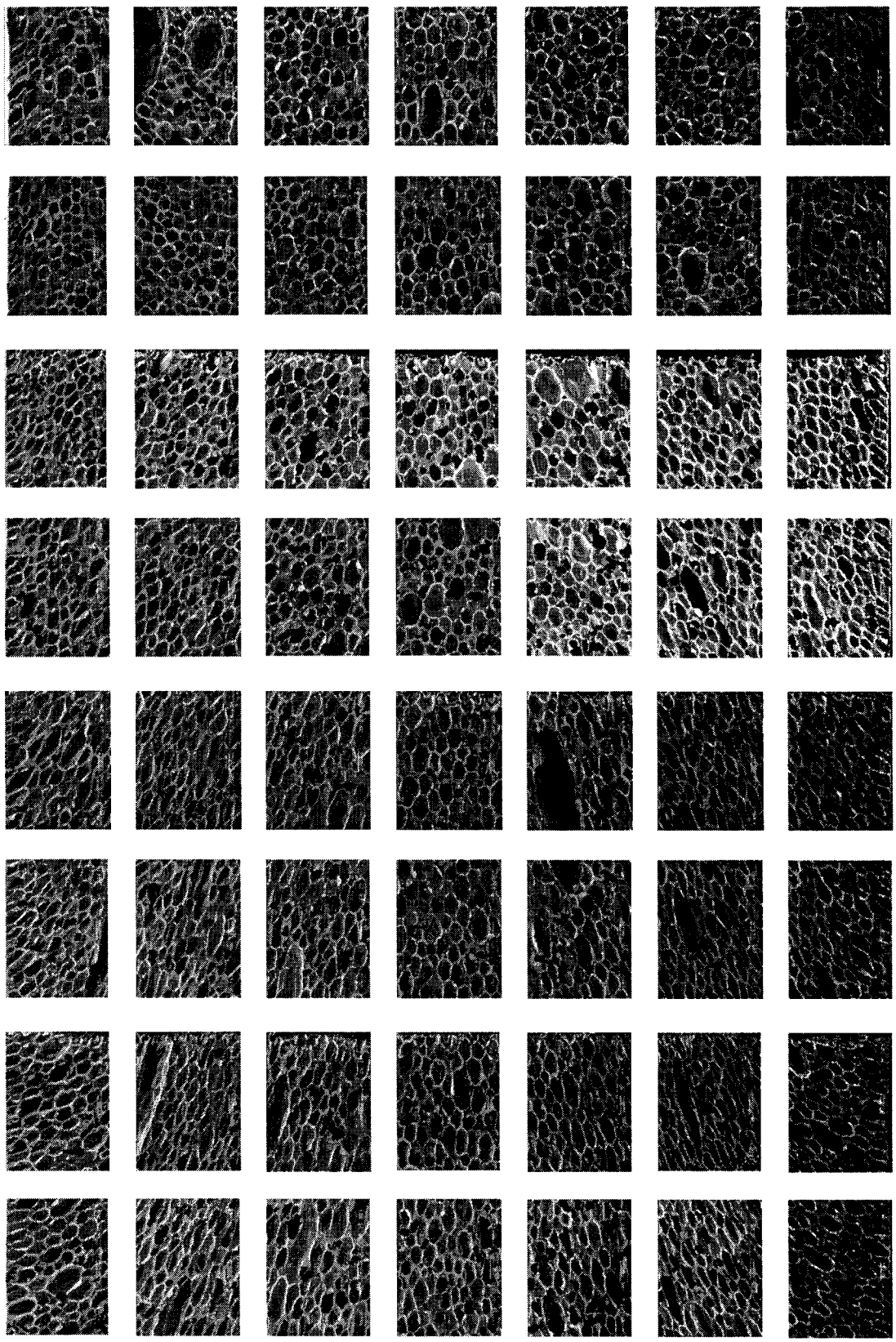

Figure-5.26: Small Mold Parallel Images

Reproduced with permission of the copyright owner. Further reproduction prohibited without permission.

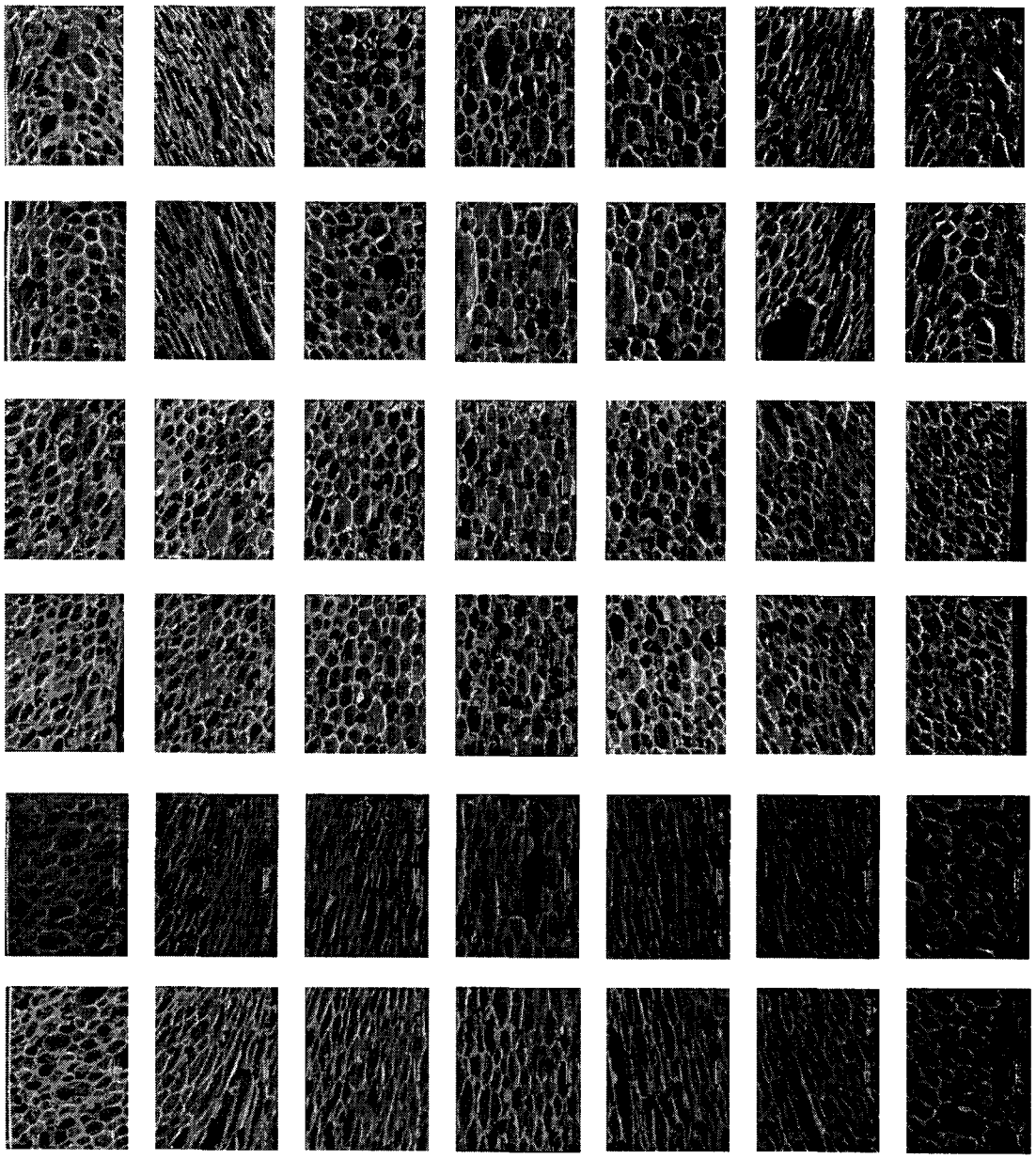

Figure-5.27: Tall Mold Parallel Images

Reproduced with permission of the copyright owner. Further reproduction prohibited without permission.

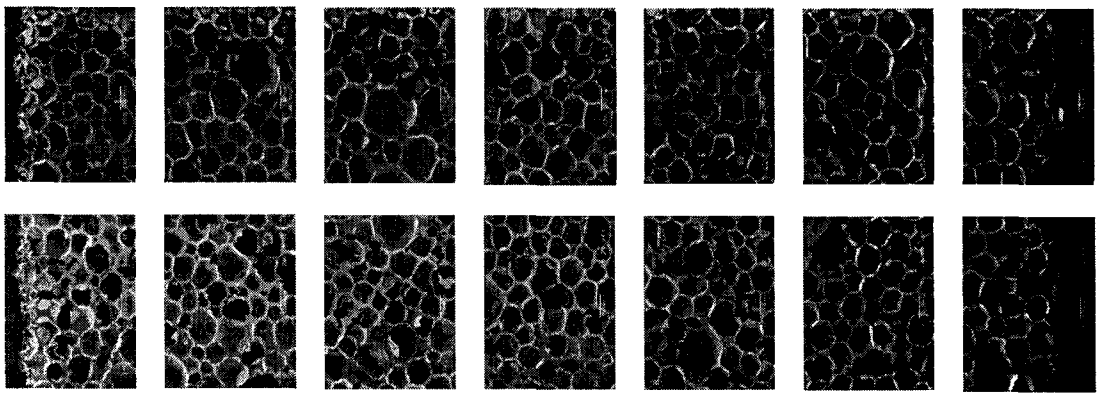

Figure-5.28: Reference Mold Parallel Images

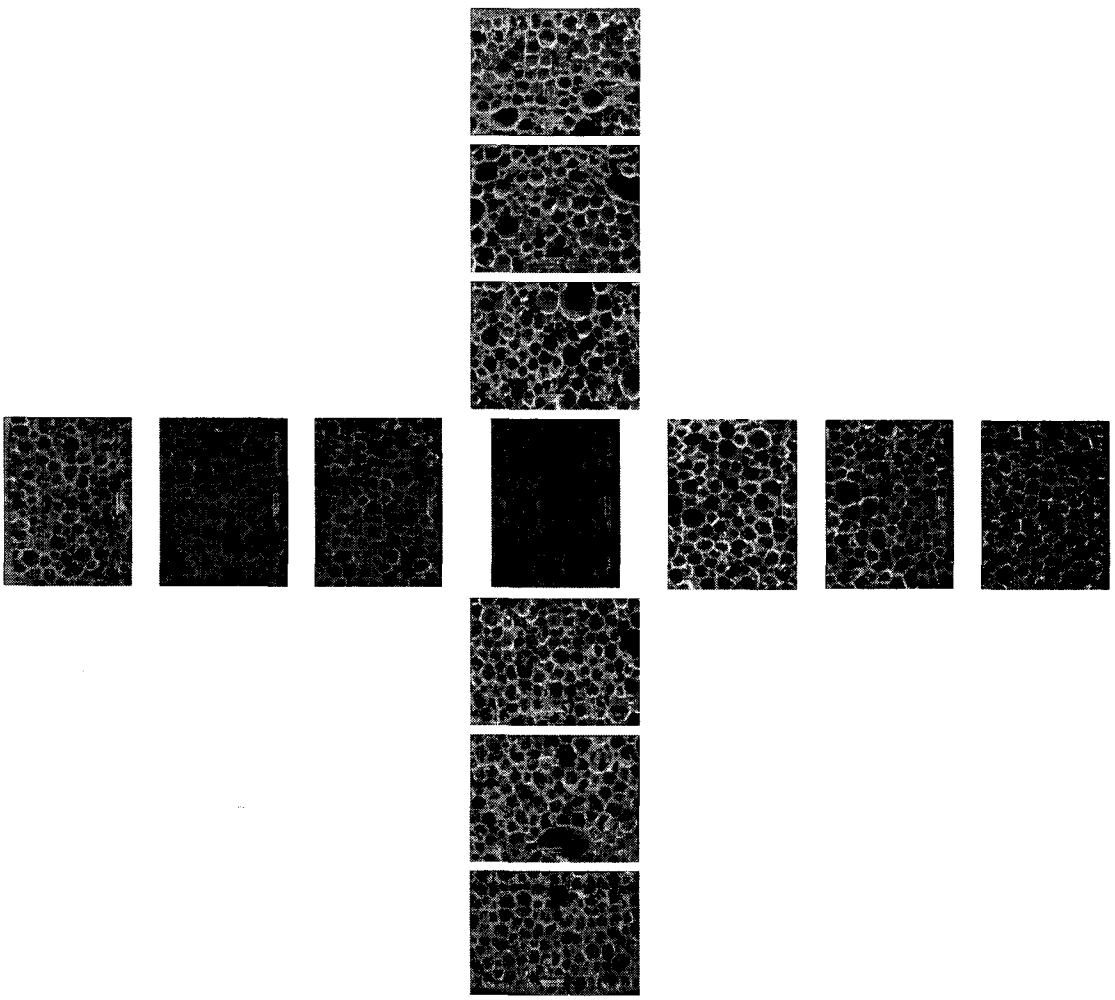

Figure-5.29: Tall Mold Bottom Sample Perpendicular Images

Reproduced with permission of the copyright owner. Further reproduction prohibited without permission.

Several properties of the images are measured automatically and manually using imaging software. Table-5.6 lists each property and how it is measured. The automatically measured properties are used to provide a quantitative analysis of the cell morphology from the top to the bottom of the mold (levels) and from the center to the side of the mold (radial). The manual measurements are also analyzed in the same manner as the automatic measurements except that they are also used to predict theoretical mechanical properties, which are discussed in the next section. This section is broken down into two subsections: level and radial positions. Each property shown in Table-5.6 is discussed in each section. Figure-5.30 shows visual definitions of each property listed in Table-5.6.

Table-5.6: Measured Properties

Property	Measured
Area of Cells	Automatically
Aspect Ratio	Automatically
Angle	Automatically
Diameter (Max)	Automatically
Diameter (Min)	Automatically
Diameter (Mean)	Automatically
Cell Edge Length	Manually
Cell Face Thickness	Manually
Edge Thickness	Manually

Reproduced with permission of the copyright owner. Further reproduction prohibited without permission.

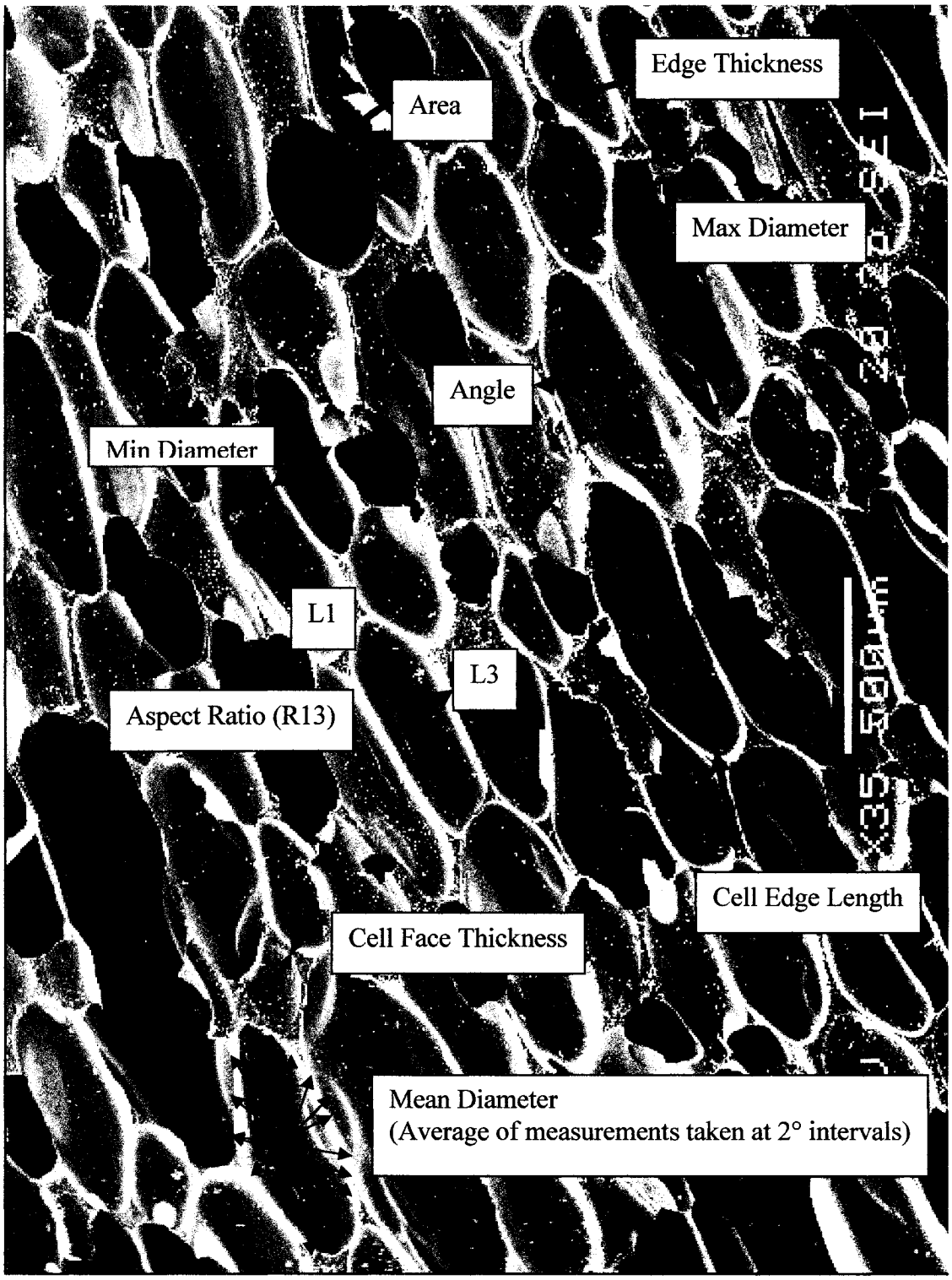

Figure-5.30: Visual Representation of Measurements

Reproduced with permission of the copyright owner. Further reproduction prohibited without permission.

5.2.1 Level Changes in Cell Morphology

To compare changes in levels, all measurements taken on each parallel or perpendicular slice is averaged. This eliminates radial positions, which will be discussed in the next subsection. Each graph in this subsection shows the average measurements per level for the parallel ("A") slices and perpendicular ("B") slices broken into sample numbers. All measurements are shown in micrometers.

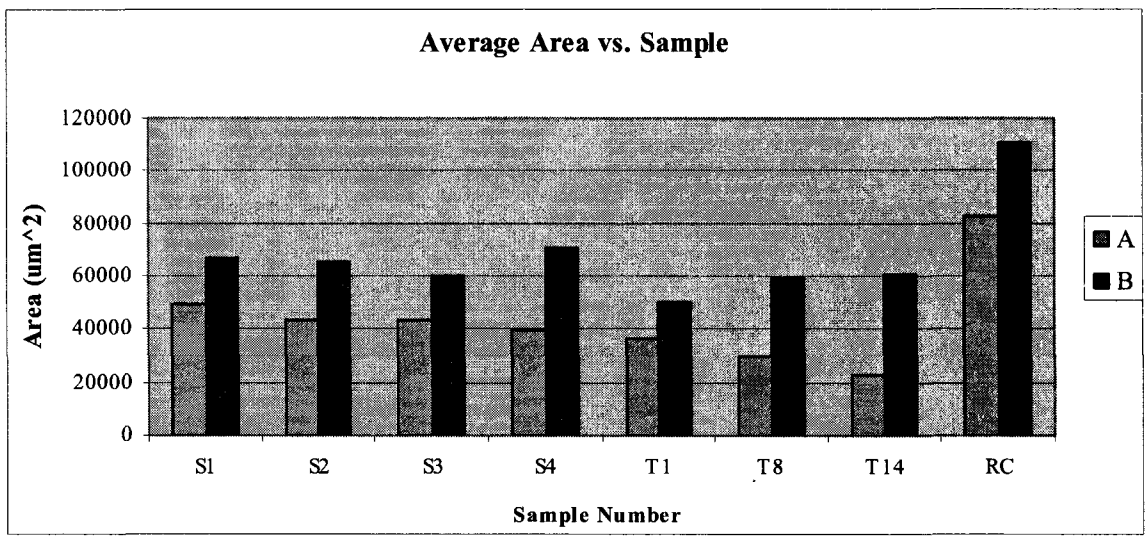

Figure-5.31: Average Area vs. Sample

Figure-5.31 shows the change of area for each sample. Of course, the reference sample, RC, has a much larger cell area than the other samples and is evident by viewing the images. This is clearly an effect of the mold size on the morphology of the foam. In addition, the areas of the tall mold are smaller than areas of the small mold indicating that the cells are smaller when the mold size increases vertically. Each sample reveals that the area in the parallel direction is smaller than in the perpendicular direction, which can be

Reproduced with permission of the copyright owner. Further reproduction prohibited without permission.

attributed to the elongation of the cells. As the cells elongate in the parallel direction the shape of the cells become elliptical instead of spherical making the area in the perpendicular direction area smaller and the parallel direction area larger. It even looks like there is some anisotropy in the reference batch which is expected since most polyurethane foams do have slight anisotropy [23]. It is interesting that the cell area tends to decrease towards the bottom of the mold for the perpendicular samples and tends to increase irregularly towards the bottom of the mold for parallel samples. This effect is probably due to the continued elongation of the cells toward the bottom of the molds. Whereas the cells are elongated all throughout the mold, the elongation of the cells increases more and more toward the bottom of the mold.

Figure-5.32 shows the average diameters for each sample. The average maximum and mean diameters follow the same pattern as seen for measurements of the area. However, the data for the average minimum diameter is scattered for the parallel slices. Even with this small inconsistency, it is evident that the measurements of the diameters further emphasize the statements made in reference to the area. Interestingly, it seems that the parallel samples in S4 and T14, which are samples at the bottom of the molds, show maximum diameter values larger than that of the reference sample, RC. This is due to the elongation of the cells in the small and tall molds, which produce much larger diameters in the major axis of the ellipse.

Reproduced with permission of the copyright owner. Further reproduction prohibited without permission.

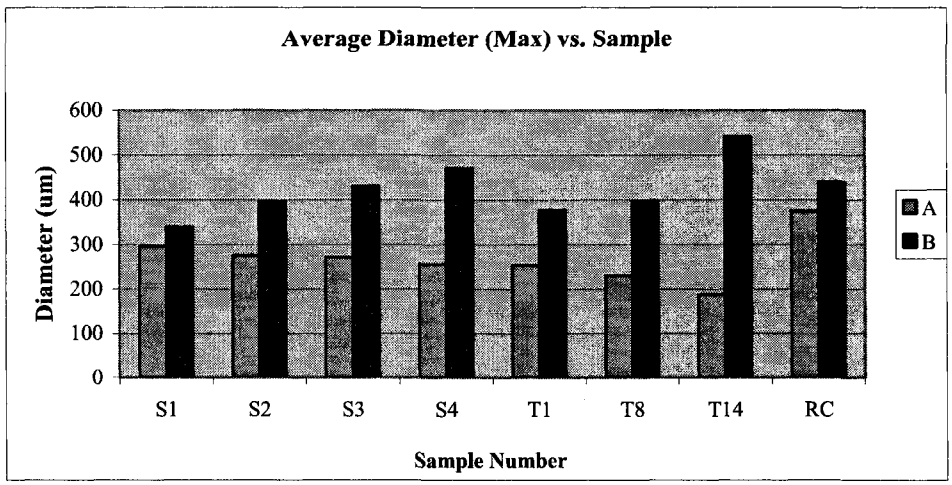

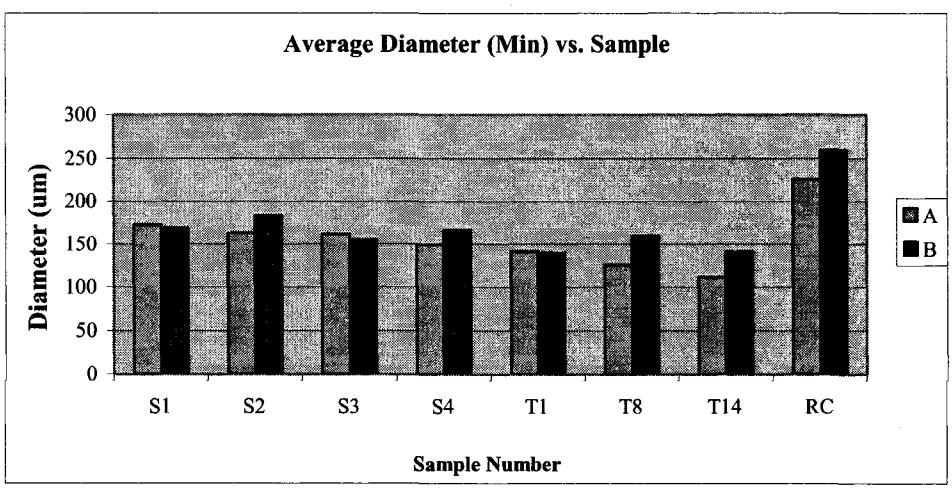

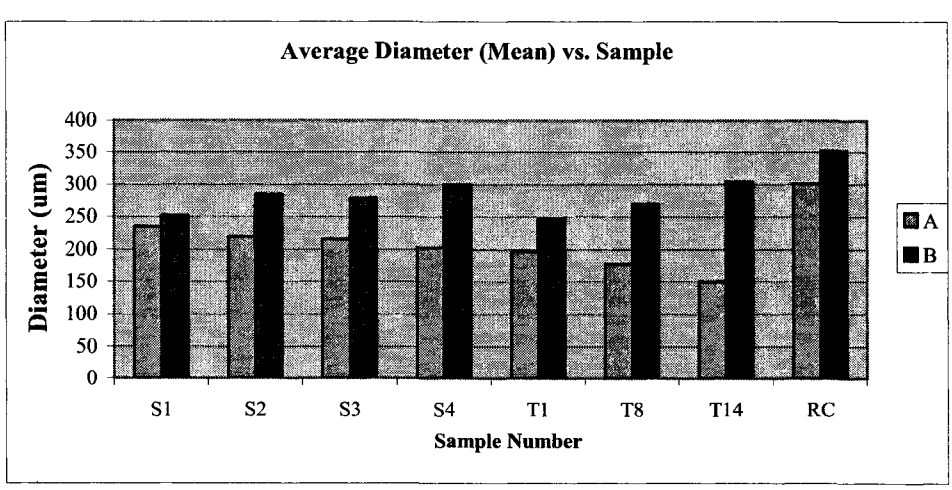

Figure-5.32: Average Maximum Diameter, Average Minimum Diameter, and Average Mean Diameter vs. Sample

Reproduced with permission of the copyright owner. Further reproduction prohibited without permission.

There are three types of aspect ratios, two of which are calculated and discussed in this section and shown in Figure-5.33. The aspect ratio usually of importance is L1/L3, which is labeled as R13. The second aspect ratio is L1/L2 labeled as R12. L1 is the diameter in the principal direction of the parallel slice and L3 is the diameter perpendicular to L1 also on the parallel slice. L2 is the mean diameter measured on the perpendicular slice. The third type of aspect ratio is L3/L2 and the reasoning for this ratio not being calculated is discussed.

The definitions of R13, R12, and R32 cannot be directly applied to the SEM images produced for this work because the cells are angled. Instead, the R13 ratio is calculated with respect to the major and minor ellipse axis instead of the rise direction. The angle of the cells is also provided to show how much the elongated cells are angled. The R13 ratio is calculated for each individual cell and than averaged for each image. The R12 ratio cannot be calculated for each individual cell since it is impossible to match cells from a perpendicular slice to a parallel slice. Therefore, this ratio is calculated from the average diameter of the perpendicular slice and the average major ellipse value from the parallel slice.

The average aspect ratio of importance, R13, is shown in Figure-5.33 according to sample number. The aspect ratio, R13, of an isotropic foam is 1.0 and the aspect ratio typical for polymer foams is 1.3 [23]. An anisotropic foam can reach an aspect ratio as high as 10 or more [23]. As seen in Figure-5.33, the aspect ratio for the reference mold is pushing 1.5; however this is lower than the aspect ratio of the small and tall molds. The aspect ratio of the T14 sample is simply startling at around 4.0. This is important since the other aspect ratios range from 1.5 to 2.5. This means that the bottom of the tall mold

Reproduced with permission of the copyright owner. Further reproduction prohibited without permission.

has an aspect ratio 2.5 times as large as the center of the reference mold. According to reference 5, a foam with an aspect ratio of 1.2 is almost twice as stiff in the rise direction as the other two directions. This means that a larger aspect ratio tends to make the foam stiffer in the rise direction. This is actually seen in the mechanical data presented in the previous section where the normalized modulus is larger in the small and tall molds than in the reference mold. However, it is shown that towards the bottom of the tall mold, the modulus approaches the values of the reference mold. This means that a higher aspect ratio only makes the foam stiffer to a certain point. The extremely high aspect ratio at the bottom of the tall molds could actually be a hindrance creating buckling much sooner in the cell walls and struts. It is also interesting to note that the samples in the middle of the small and tall molds also yield greater peak yield and collapse stress values and sometimes higher modulus values whereas the samples at the bottom yield low mechanical properties.

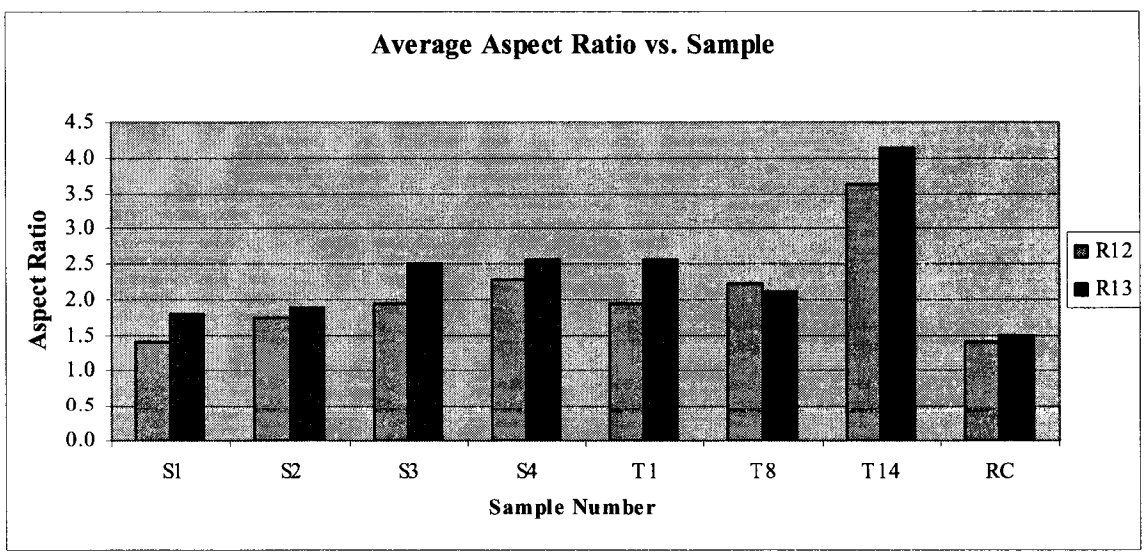

Figure-5.33: Average Aspect Ratio vs. Sample Number

Reproduced with permission of the copyright owner. Further reproduction prohibited without permission.

The second aspect ratio, R12, is also seen in Figure-5.33. Usually all three aspect ratios are calculated to indicate if the foam is axisymmetric (R32=1.0, R12=R13) or orthotropic (R32≠R12≠R13). However, the foam imaged for these calculations presents a slight problem. As seen by looking at the actual images, most of the cells are angled thereby giving incorrect data for the R12 aspect ratio. This is because the length L2 is actually measuring the horizontal distance of the ellipses shown in the parallel slices instead of the minor axes of the ellipses. In foam that shows cells that are not angled, L2 should equal the minor axis, L3, of the ellipse (for foams that are axisymmetric). The R12 ratio has been included in this discussion only because it is important to understand why the data for R12 is erroneous. Because of this, it makes sense that R32 not be calculated because it too will provide incorrect data. The angling of the cells creates a larger mean diameter, L2, since the measurement is taken with respect to the horizontal axis where as the diameter L3 is taken with respect the major and minor axis of the individual cells. So, already it is know the two diameters will create a ratio not equal to 1.0.

The angle at which the cells are aligned in the rise direction is important to consider. Usually, a foam's principal direction is in the rise direction. This means that the foam cells elongate so that the largest diameter of the ellipse corresponds with that of the axis of the principal direction. However, examination of the SEM images reveals that the elongated cells tend to form angles to the rise direction. Figure-5.34 shows the average angle of the cells at each level. Angles are calculated considering the horizontal is at 0-degrees and measuring clockwise. Therefore, a 90-degree angle indicates that the cells are aligned in the rise direction, an angle smaller than 90-degrees indicates that the cells are inclined toward the center of the mold, and an angle larger than 90-degrees indicates

Reproduced with permission of the copyright owner. Further reproduction prohibited without permission.

that the cells are inclined away from the center of the mold. Only the angles of the parallel samples are shown since angles of the perpendicular samples are not defined.

Figure-5.34 shows that for all but the top sample of the small and tall mold, cells tend to angle toward the center of the mold since angles are around 70 to 74-degrees. The top sample of the small mold, S1, tends to have cells that still angle slightly toward the center of the mold. Interestingly, the top sample of the tall mold, T1, shows the cells tend to angle slightly away from the center of the mold at 10-degrees to the vertical. This phenomenon is also visually illustrated in the SEM images. The reference sample, RC, shows that the cells angle slightly away from the center of the mold.

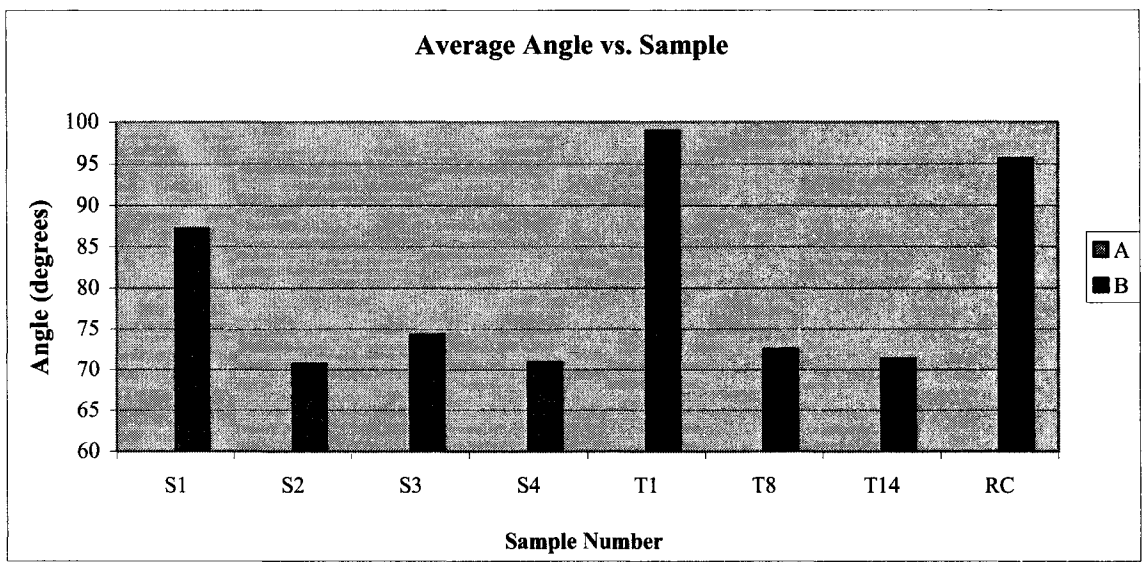

Figure-5.34: Average Angle vs. Sample Number

The remaining calculations are all made manually and are shown in Figure-5.35. These calculations typically have lower standard deviations than the calculations made automatically using the imaging software. This could be because there is less variation in

Reproduced with permission of the copyright owner. Further reproduction prohibited without permission.

the cells for these measurements or perhaps because there is human control over the measurements taken. Typically, twenty measurements are taken from each image. Sometimes fewer measurements are taken due to the fact that the image does not provide enough places to take accurate measurements.

The average cell edge length for all samples is shown in Figure-5.35. This graph shows that the small mold perpendicular samples have about the same cell edge length at around 200-um. The parallel samples of the small mold show an increase in length toward the bottom of the mold but levels off at the bottom sample, thereby increasing from 200-um to around 275-um. However, the same cannot be said about the tall molds, which show a decrease in cell edge length for the perpendicular samples toward the bottom of the mold. The parallel samples are also strange indicating that the length decreases at the center and shoots up to 325-um at the bottom of the mold. The reference sample shows that the cell edge length is larger for both the parallel and perpendicular slices than all the other samples save the T14 parallel slice. It makes sense that the cell edge length is larger for the reference mold since it has been shown that the average cell area is also larger. A possibility for the huge value of the tall mold could be because the cells are once again elongated, thereby producing large cell edge lengths. This could also account for the fact that the cell edge lengths in the parallel direction are larger than those in the perpendicular direction, since the cells are elongated more in the parallel direction than the perpendicular.

As shown by Figure-5.35, the average cell face thickness varies around 7-um to 8-um for most of the samples. The reference sample, RC, has values of about 6-um to 6.5-um which are lower but not too far off from the other values. Interestingly, the perpendicular

Reproduced with permission of the copyright owner. Further reproduction prohibited without permission.

values for T8 and T14, which are samples in the tall mold, have significantly lower values from all the other values in the small and tall molds. Sample T8 has a comparable value to that of the reference sample, and T14 is the lowest of all with a cell face thickness of 5-um. It is too early to tell, but this could have a considerable effect on the outcome of the theoretical calculations of density and mechanical properties for the perpendicular T8 and T14 samples. It also means that, for these samples only, the cell face thickness is larger for cells parallel to the rise direction. All other samples seem to have approximately the same cell face thickness in both directions.

The same type of phenomenon can be seen in the average edge thickness where most of the samples vary around 30-um to 35-um except for the T14 samples. The T8 sample is just a little off from the rest of the samples, but it is not as significant as the T14 sample in the perpendicular direction with an edge thickness of about 22.5-um. Strangely enough, the reference sample has the highest edge thickness where both the perpendicular and parallel samples are relatively equal. Even though the T8 and T14 parallel samples equal that of the reference sample, the parallel slices are much lower. This means that the struts of the cell structure in the reference mold have larger thicknesses. This is interesting since it would seem that having struts with larger thicknesses and therefore larger cross-sectional areas would produce foam with better properties, but this is actually the opposite of what is seen in the mechanical data where the reference mold and the bottom of the tall mold produce some of the smallest values in mechanical properties.

Reproduced with permission of the copyright owner. Further reproduction prohibited without permission.

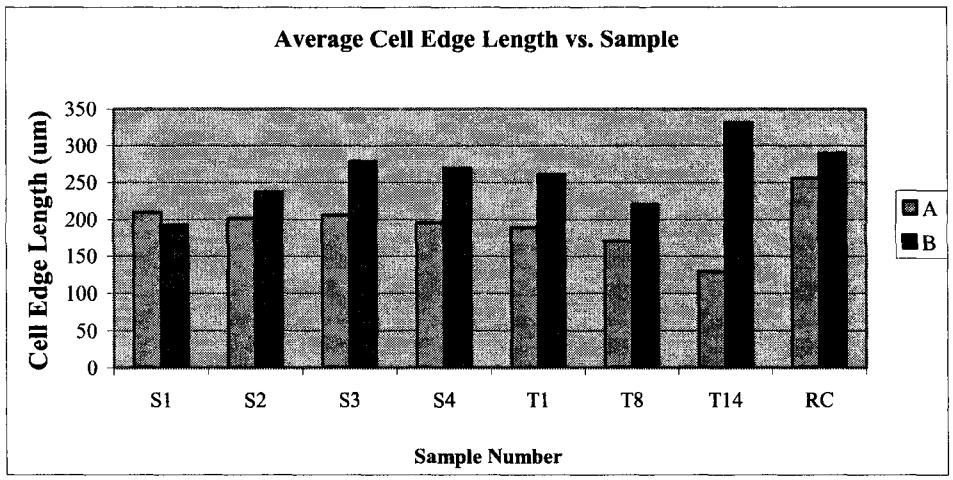

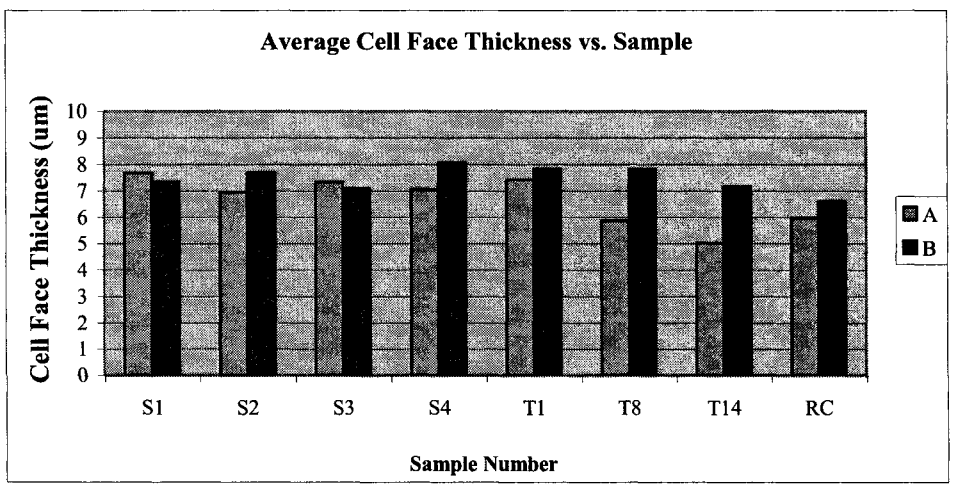

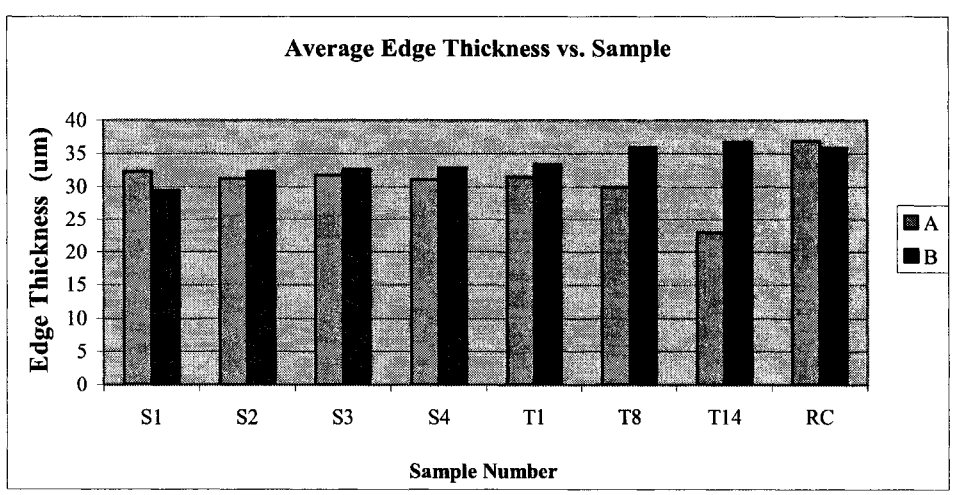

Figure-5.35: Average Cell Edge Length, Cell Face Thickness,

and Edge Thickness vs. Sample Number

Reproduced with permission of the copyright owner. Further reproduction prohibited without permission.

5.2.2 Radial Changes in Cell Morphology

Measurements averaged in the radial direction do not form patterns that are as clear as those in the vertical direction (levels). As shown by Figure-5.25, each parallel and perpendicular slice has seven images each that are analyzed. To provide radial positions, the center sample is designated as "1". The samples at continually larger radii are designated as "2", "3", and "4", respectively. Two samples at each radial position are averaged to provide four data points. To compare changes in the radial direction, all measurements taken in each mold at a certain position on the parallel or perpendicular slice are averaged. For example, consider the small mold samples S1, S2, S3, and S4. Each sample at the center position is averaged to provide one value for a particular slice, either parallel or perpendicular. This process is repeated for each subsequent radial position. Once the data points are calculated, they are then normalized to the full diameter of the mold. This gives a percentage of how close the data point is to the edge of the slice. In this case for the tall and small molds, it is possible to achieve values as close as 90% to the edge of the mold, measuring from the center of each image. The reference mold sample does not represent the entire cross-section of the mold since the sample imaged has a 28.7-mm diameter and the reference mold has a total diameter of 182-mm. Therefore, only 15% of the mold's center is analyzed.

Figure-5.36 shows the average area for each mold's perpendicular and parallel slices. Most of the curves tend to slope downward (decrease in area) from the center to the outside of the mold. The exceptions to this are the small mold perpendicular slices (S-A) that show a consistent area for all radial positions and the tall mold perpendicular slices (T-A) that show a slope upward from center to outside which is probably due to the

Reproduced with permission of the copyright owner. Further reproduction prohibited without permission.

elongation of the cells near the outside of the mold which increases the area. It is interesting to note that most of the curves are not linear but have a wave-like appearance. It is also interesting that the reference slices appear to decrease quite sharply in the first 15% from the mold's center. This is surprising since it has been seen that the reference mold provides fairly uniform density and mechanical properties.

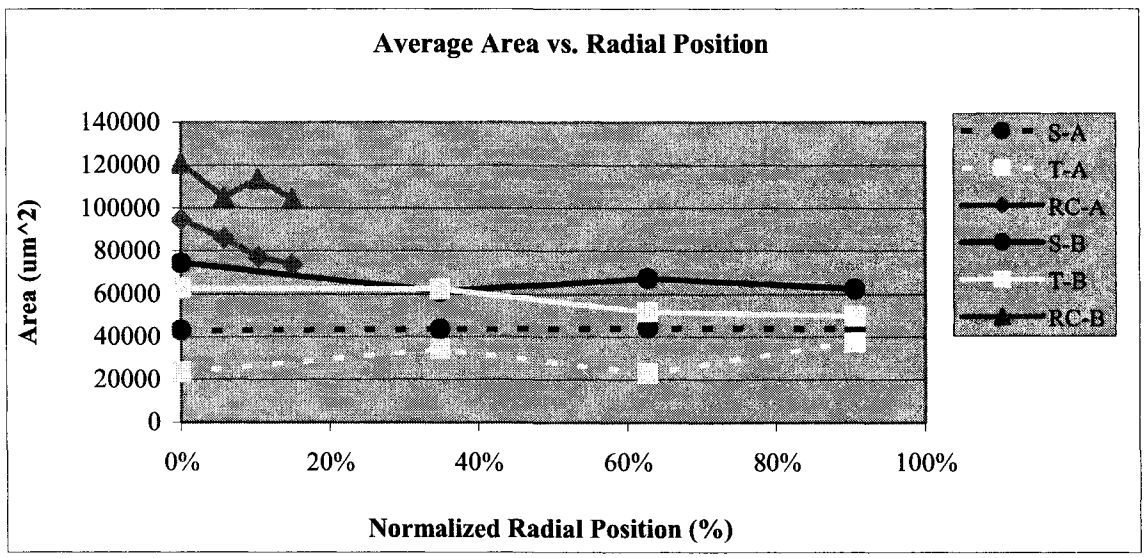

Figure-5.36: Average Area vs. Radial Position

A maximum, minimum, and mean diameter is calculated for each cell in the foam. These values are than averaged for the image to produce an average maximum, average minimum, and average mean diameter. The average maximum, average minimum, and average mean diameters of all the mold's perpendicular and parallel slices are shown in Figure-5.37. The small mold parallel and perpendicular slices have fairly uniform mean and minimum diameters with just a slight increase in maximum diameter from the center to the outside of the mold. This is in comparison with the diameters of the tall mold,

Reproduced with permission of the copyright owner. Further reproduction prohibited without permission.

which seem to exhibit erratic values usually in wave-like shapes. Interestingly, the maximum diameter for the perpendicular slices of the tall mold show an increase for the first three radial positions and then drastically drops 25% at the fourth position. The reference mold parallel and perpendicular slices show a fairly uniform mean and minimum diameter with an increase at the center.

The average aspect ratios, seen in Figure-5.38, show that the R12 and R13 ratios of the reference mold are fairly uniform for the first 15% of the mold radius. It is interesting to note that, even though the R12 ratio is erroneous, it follows the same radial pattern as the R13 ratio, except for one point in the tall mold. The small mold R13 ratio increases and drops slightly at the last point. This means that the cells become more elongated toward the outside of the mold and then suddenly become more uniform at the outside. The data for the tall molds is quite interesting and again shows wave-like appearances. The R13 ratios for the tall molds follow the same pattern as the small molds except the drop between the third and fourth data point is more drastic, dropping a staggering 45% compared to the small mold's 7% decrease. The R13 curves of the tall mold both show that the cells on the outer edge of the mold have more uniform cells than any other radial position.

Reproduced with permission of the copyright owner. Further reproduction prohibited without permission.

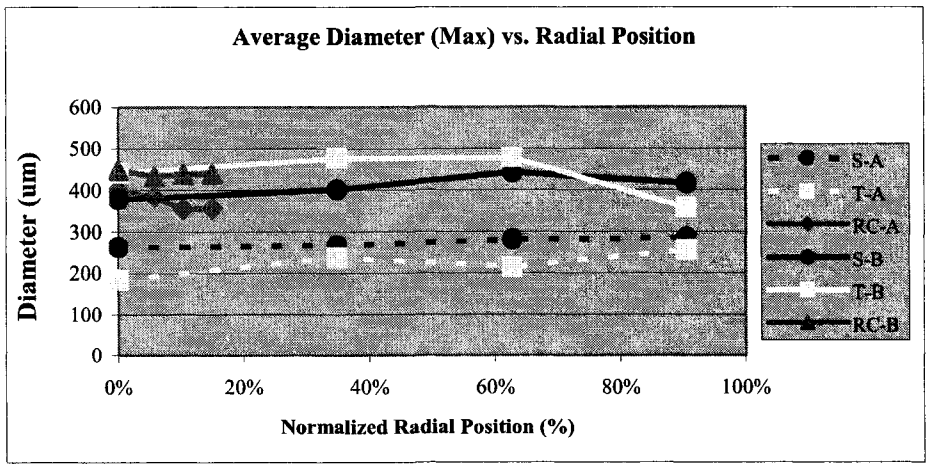

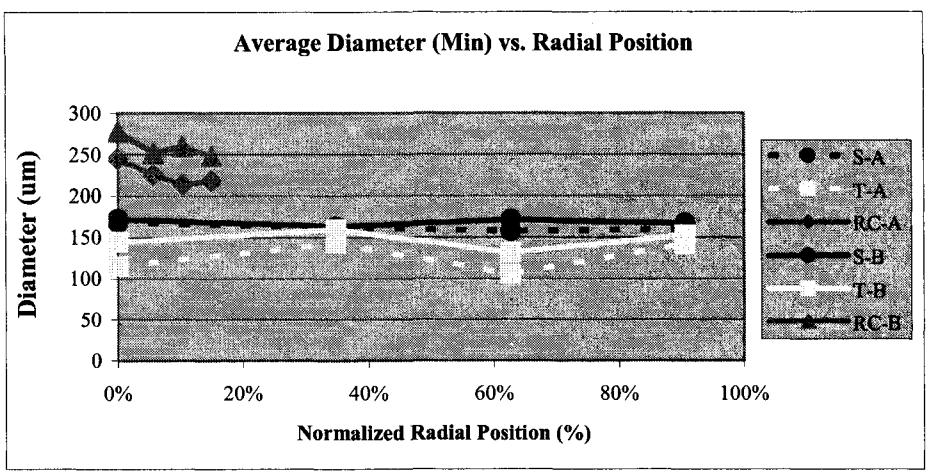

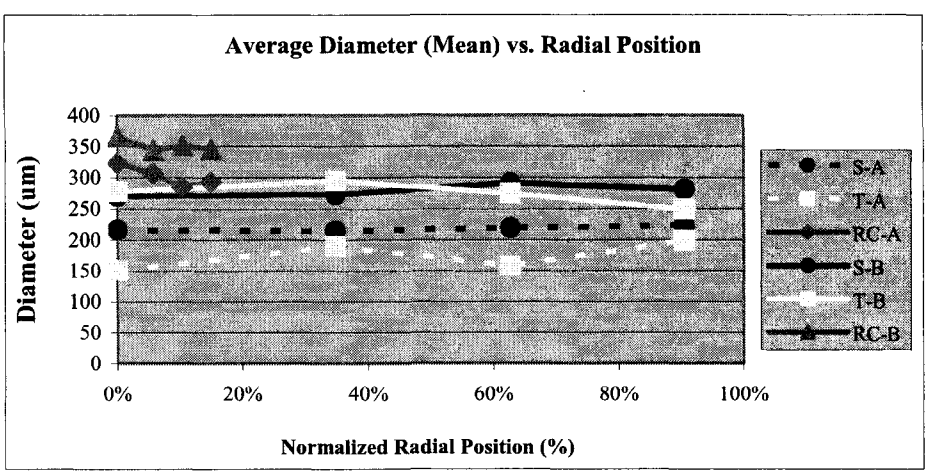

Figure-5.37: Average Maximum Diameter, Average Minimum Diameter, and Average Mean Diameter vs. Radial Position

Reproduced with permission of the copyright owner. Further reproduction prohibited without permission.

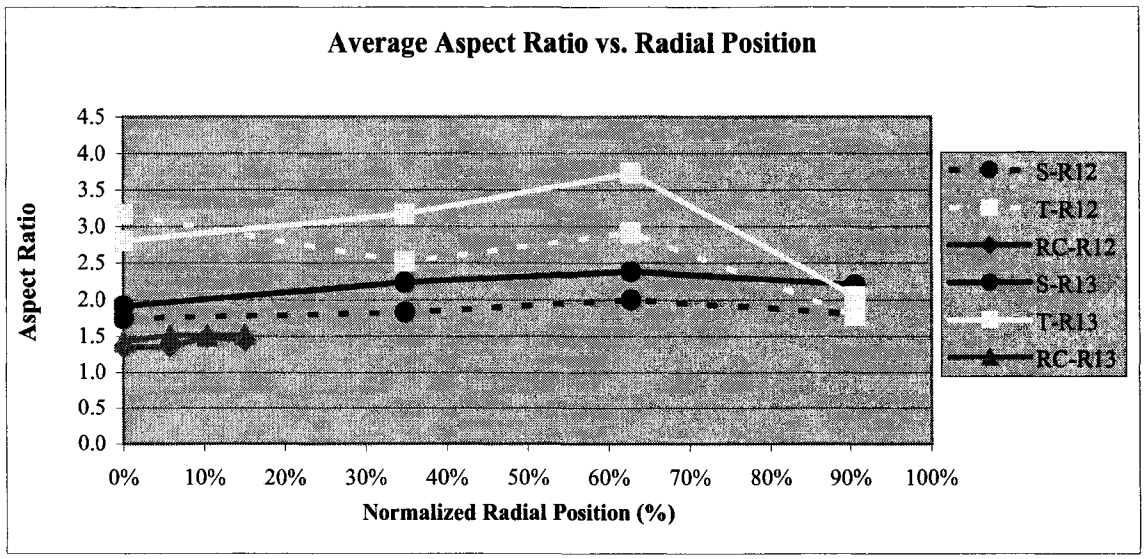

Figure-5.38: Average Aspect Ratio vs. Radial Position

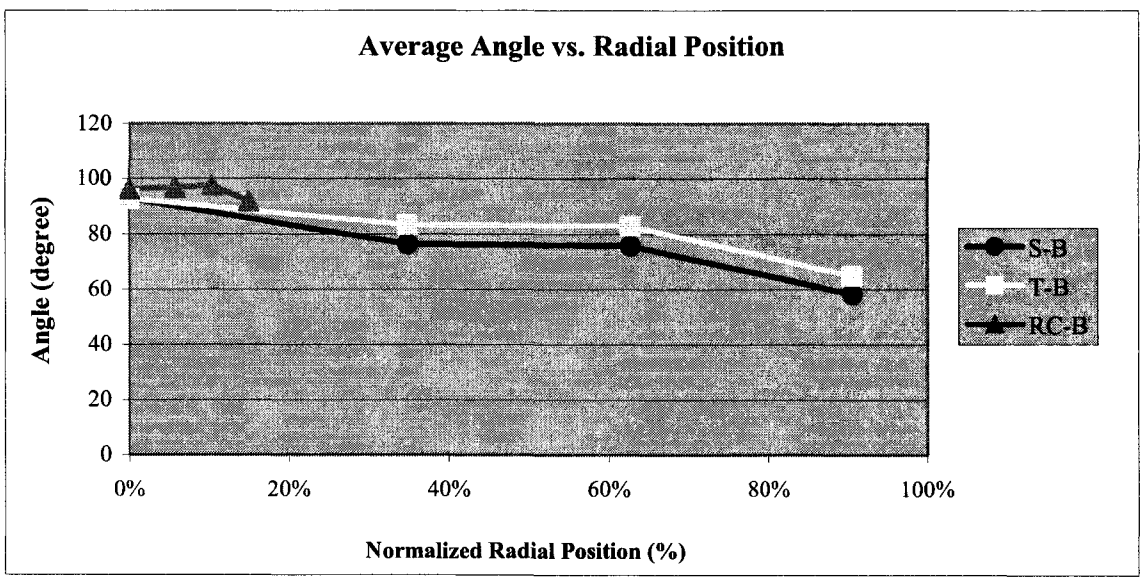

Figure-5.39: Average Angle vs. Radial Position

Figure-5.39 shows the angle at which the cells are inclined away from the rise direction. The angles shown are measured clockwise assuming 0-degrees is the horizontal. It is interesting that all three molds show approximately the same angle at the

Reproduced with permission of the copyright owner. Further reproduction prohibited without permission.

center of the mold, which is just slightly above 90-degrees indicating that that cells are angled away from the center of the mold. While the reference mold data is uniform for the first three points and then slightly decreases at the outermost point, the small and tall molds follow the same pattern of continually angling the cells toward the center of the mold. This can be seen visually in the SEM images provided in Appendix E.

The next figure, Figure-5.40, shows values of measurements made manually with the imaging software, which are used to predict density and mechanical properties. The small and tall molds show that cell edge length generally increases toward the outside of the mold, all except the tall mold parallel samples which decreases 20% from the third to forth data point. The reference mold has a fairly uniform cell edge length for the first 15% of the mold radius.

It seems that the cell face thickness is fairly uniform after the first data point, which is quite low. The tall mold parallel slice has the largest increase in cell face thickness from the first to second data point, which is 43%. The reference mold shows data for the cell face thickness that is really sporadic. This same behavior is seen in the average edge thickness values for the reference mold. Interestingly, the tall and small mold parallel slices follow the same pattern and the perpendicular slices follow the same pattern. The parallel samples tend to increase from the first to the second point and then begin the level off toward the outside of the mold. The perpendicular samples follow the same pattern except there is a decrease from point one to point two.

Reproduced with permission of the copyright owner. Further reproduction prohibited without permission.

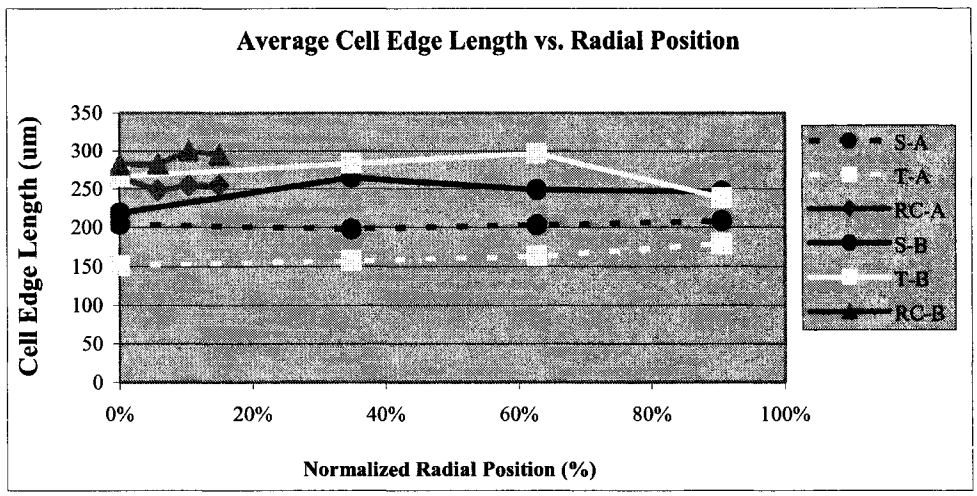

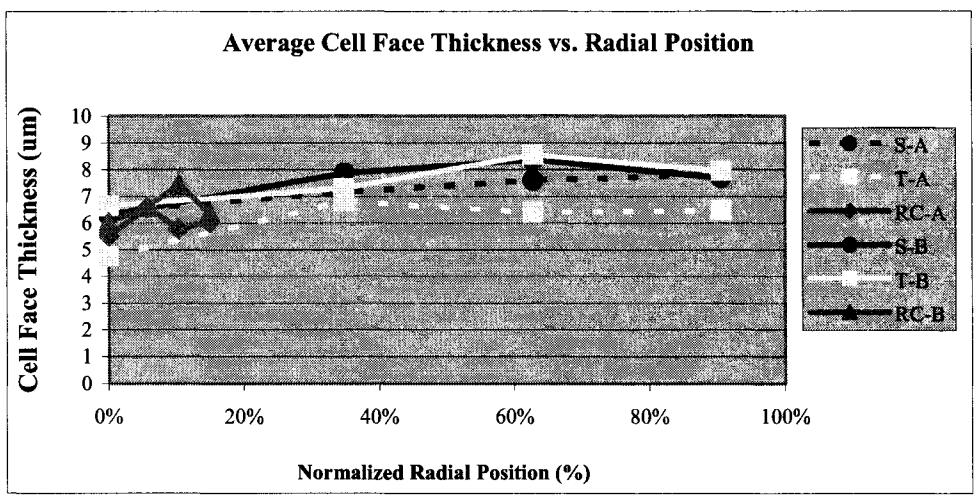

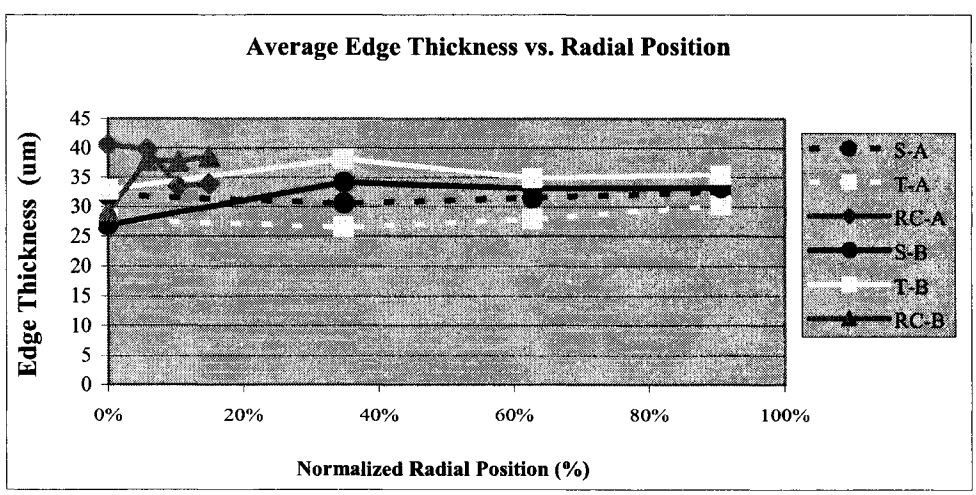

Figure-5.40: Average Cell Edge Length, Cell Face Thickness,

and Edge Thickness vs. Radial Position

Reproduced with permission of the copyright owner. Further reproduction prohibited without permission.

5.2.3 Discussion of Cell Morphology Results

This section discusses changes in cell morphology in reference to levels, mold sizes, and radial locations. There are visual differences in cell morphology depending on the mold size and location in the mold. Data analyzed from SEM images reinforce this finding, although it is clearer when dividing the molds into levels than into radial directions. This could be because the cells in the radial direction change at each level in addition to each radial position. Appendix E shows raw data of each radial position for each level. When looking at this data it is still unclear how the cells change in the radial direction. This could quite possibly be due to the large standard deviations of the data, which would mean more samples at the same level should be analyzed to produce a better result. This however is extremely time-consuming and may not even help the results. It is important to view the standard deviations more as a cell distribution than a statistical error since the cells in the foam at any location vary in size. This is the reason why averages are used to compare the data.

While the data analyzed according to level can be compared with experimental mechanical properties, the data analyzed according to radial positions can only be compared with density. This is because the data values according to levels are analyzed per sample, which is used to produce experimental mechanical properties. However, the mechanical properties are only measured in the rise direction. The data analyzed per radial position can be compared with experimental density because data has been produced using the coring method as described in Appendix C. Even though the experimental data values are limited, the next section describes how to achieve theoretical results of density and mechanical properties using cell morphology. Therefore,

Reproduced with permission of the copyright owner. Further reproduction prohibited without permission.

it is possible to see how the density and mechanical properties do or do not change according to levels and radial positions.

The main question to answer after the presentation of all the data in this section is, "why does the foam morphology change depending on level, mold size, or radial position?" This is a great question. One reason for the change in cell morphology could be that the foam, which is reacting at a high temperature, is poured into a cold mold. This means that the cells near the sides of the mold cool down and friction makes the cells drag on the sides of the molds. The cells in the center of the tube continue to push upward at a faster rate than the cells on the sides thereby forcing the cells on the sides to angle inward toward the center of the mold. The tall mold shows that cells at the top of the mold actually angle outward which is not seen in the small mold. This could be due to the outer cells dragging on the side of the mold near the completion of the reaction making the cells angle outward toward the mold walls. This is not seen in the small molds because the vertical length traveled by the cells is one-third of that traveled by the cells in the tall mold.

5.3 Theoretical Density and Mechanical Results

Theoretical results are tabulated only for levels as in the previous section except that the perpendicular ("A") and parallel ("B") samples are averaged together to produce one value per level. The values of cell edge length, cell face thickness, and edge thickness are the only measurements used to calculate theoretical values and are therefore the only values that have the parallel and perpendicular slices averaged. Radial positions are not shown because of the bad correlations between experimental and theoretical values as

Reproduced with permission of the copyright owner. Further reproduction prohibited without permission.

shown by the breakdown in levels. In this section, values of the volume fraction, density, modulus, and collapse stress are calculated theoretically and discussed. All theoretical mechanical properties are normalized for density so that a direct comparison to the normalized experimental mechanical properties can be made. This also allows the density to be disregarded as a variable.

5.3.1 Volume Fraction

Different values of Z_f (average number of faces that meet at an edge) and n (mean number of faces per cell) are used to calculate the volume fraction assuming the cell shapes are dodecahedron or tetrakaidekahedra. There are also values of Z_f and n found from averaging the values typically found in foams. For most foams Z_f=3 and n=5, for dodecahedral cells Z_f=3 and n=4, and for tetrakaidekahedral cells Z_f=3 and n=5.14 [5]. Again, the volume fraction is the sum of the area found in the edges divided by the area found in the edges and cell faces. The volume fractions found experimentally in this study using all three methods, shown in Figure-5.41, are around 50%, and the "most foams" and tetrakaidecahedra methods are very close to one another. However, Reference 22 shows that the volume fraction should be about 80%-90% and the theoretical value calculated using all three methods is not even close to this referenced value. This difference could only be due to error in the measured values of the cell edge length, cell face thickness, or edge thickness. However, it is interesting to note that only five cell wall and strut measurements each are taken from images of the polymer material for the study in reference 22. In addition, that study used embedded resin to help cut the foam surface to be viewed. Even though the effect is accounted for, there could still be an error in the method. It is also not evident that the volume fraction in this study should

Reproduced with permission of the copyright owner. Further reproduction prohibited without permission.

match that in reference 22 because the foam density is not the same and could perhaps have an affect.

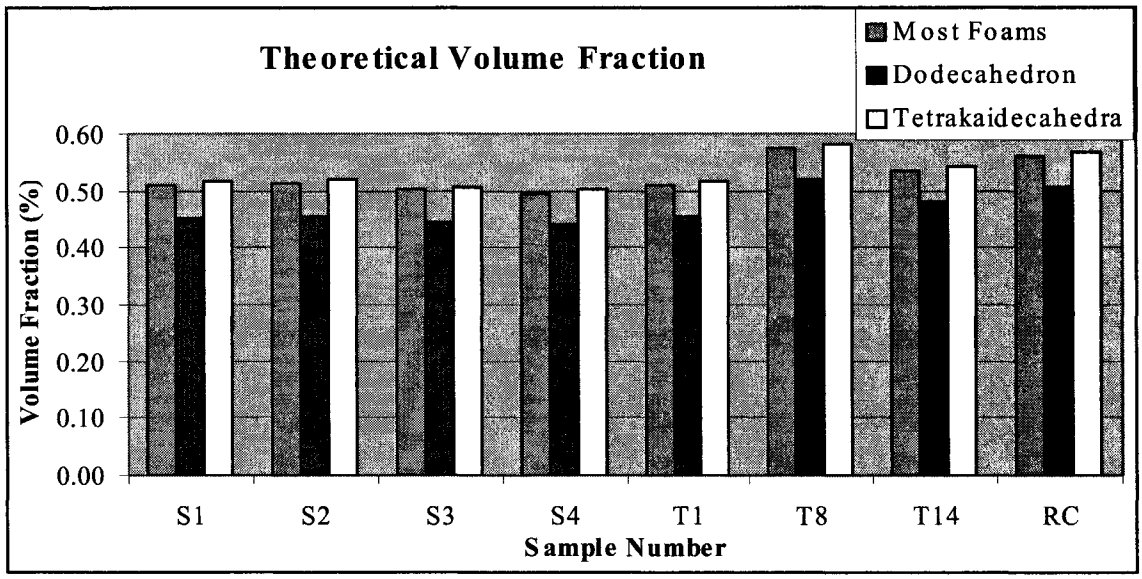

Figure-5.41: Theoretical Volume Fraction

The cell face thickness is possibly the measurement with the greatest error since it is so small. In order to get a good sample size for area, aspect ratio, etc. images are taken at X35 magnification. This may not be the best magnification to produce accurate values of cell face thickness as reference 22 uses 10X-4000X magnification to measure cell face thickness. Even though the measurements are taken with imaging software that allows zooming, there could be error due to shadowing and focusing. When the cell face thickness is taken at 50% of its original measured value, the volume fraction suddenly jumps up to 70%, which is a much better correlation with reference 22. It is important to note that the face thickness does vary along the length of the face, but the definition of face thickness indicates that the middle of the cell length be measured. If the face

Reproduced with permission of the copyright owner. Further reproduction prohibited without permission.

thickness was actually averaged along the length of the cell length then the value would be even larger and correlate even worse with the theoretical results.

Another possibility for the differences in measured volume fraction could be because of the density differences in the foam that is measured. Reference 22 uses foam that is 0.02 to 0.03-g/cc which is significantly lower than that used in this study (0.101 to 0.125-g/cc). It is agreed that this density difference could somehow affect the volume fraction of the foam.

5.3.2 Density

The density is also calculated using equations derived assuming cell shapes for "most foams", dodecahedron and tetrakaidecahedron. These equations use values of the cell edge length, cell face thickness, and edge thickness to calculate density. As with the volume fraction, all three methods yield a density that is far from the value expected. Figure-5.42 shows the theoretical density compared with the experimental density calculated for each sample. It is clear that the theoretical and experimental values do not match and the experimental density is sometimes 100% greater than the theoretical. Unfortunately, lowering the cell face thickness to 50% of its value like that done in the volume fraction calculations only further increases the gap between theoretical and experimental by lowering the theoretical density to values close to 0.045-g/cc. If the cell face thickness is raised by 50%, the density increases to just 0.075-g/cc. In this case, lowering the cell edge length by 30% corrects the theoretical density to a value more comparable to the experimental. The theoretical value of density corrects to 0.112-g/cc. By doing this the volume fraction also raises by 10%. However, there is more confidence

Reproduced with permission of the copyright owner. Further reproduction prohibited without permission.

in the cell edge length than the cell face thickness and changing it to obtain a better value is not as reasonable.

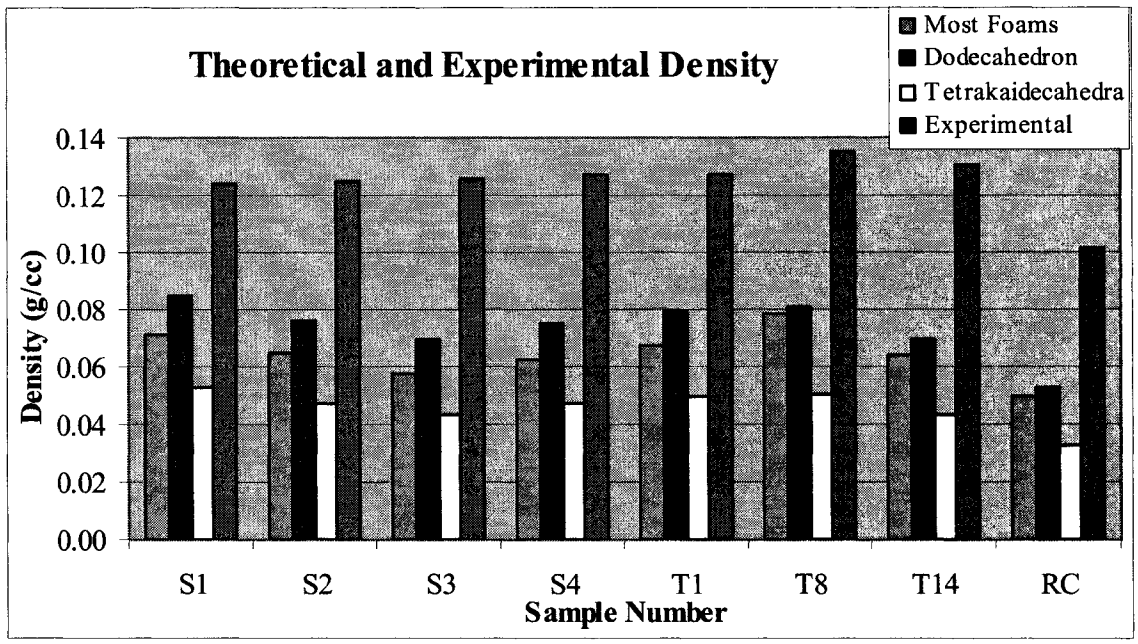

Figure-5.42: Theoretical and Experimental Density

5.3.3 Modulus

The modulus is calculated theoretically by using the volume fraction, relative density, and modulus of the solid material. Since it has been explained that the volume fraction and density do not match referenced and experimental values, respectively, it is correct to assume these values will have an adverse affect on the theoretical modulus value. This is the reason why other values are used to calculate the modulus. There are mainly two methods used to calculate the modulus. The first uses the volume fraction noted in reference 22 and the experimental density determined from the macroscopic 25.4-mm high 28.7-mm diameter samples while the second uses the theoretically calculated

Reproduced with permission of the copyright owner. Further reproduction prohibited without permission.

volume fraction and density. The volume fraction in the first method can either be 0.80 or 0.90 and the modulus of the solid material can be 1.6GPa to 2.7GPa for both methods. Using all these constraints, six theoretical values can be calculated as shown in Figure-5.43. The first four lines in the legend show the value of the volume fraction and modulus of solid material for the first method. The last two lines in the legend show the modulus of solid material used for the second method and also shows that the cell edge length, cell edge thickness, and cell face thickness are used to calculate the volume fraction by indicating the variables "l, t_e, t_f".

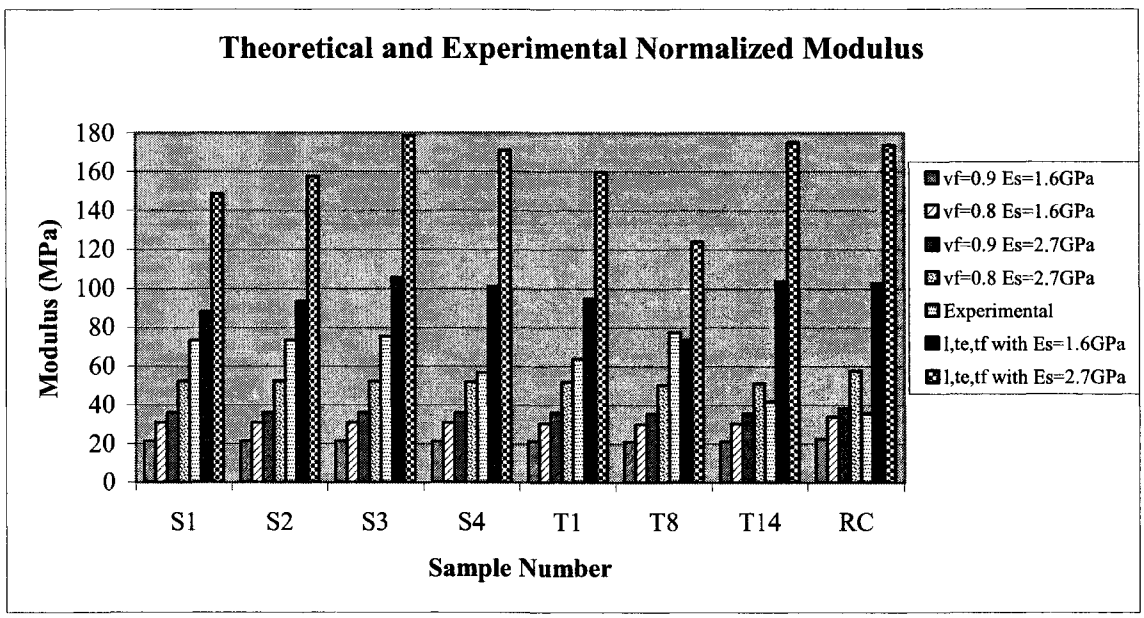

Figure-5.43: Theoretical and Experimental Normalized Modulus

As shown by Figure-5.43, the second method does not yield highly favorable results. Remember, the second method uses the actual measurements of cell edge length, cell edge thickness, and cell face thickness. By manipulating the modulus of the cell solid to

Reproduced with permission of the copyright owner. Further reproduction prohibited without permission.

the lower value, the experimental values are closer. Most of the samples are bounded by two methods, which are shown in Table 5-7 with percent differences between the experimental and theoretical values.

Table-5.7: Percent Differences between Theoretical and Experimental Modulus

Method	S1	S2	S3	S4	T1	T8	T14	RC
vf=0.8 Es=2.7GPa	28%	29%	31%	8%	19%	35%	22%	61%
l,te,tf with Es=1.6GPa	20%	27%	41%	79%	48%	5%	147%	188%

As shown by Table-5.7, most of the values for the first method correlate much better with the experimental data than the second method. It is interesting that the highest deviation is seen in the RC sample. This is because the RC sample is in the center of a large mold and should not have great effects from the mold. In theory, this sample should be the one that would most closely align with the theoretical value since the theoretical equations are based on foams that are uniform like the RC sample. The values for the small and tall molds do not match as well to the experimental data maybe because the equation for modulus does not account for the anisotropy of the cells or the angle at which the cells incline.

5.3.4 Collapse Stress

There is a conflict in the literature regarding the collapse stress. Fellow collaborators at Sandia National Labs use the elastic collapse equation to calculate the theoretical collapse stress [1]. This is an assumption that the foam behaves like an elastomeric foam, which is not the conclusion agreed upon by the mechanical engineering department at UNLV that believes the foam acts more like an elastic-plastic foam. The differences

Reproduced with permission of the copyright owner. Further reproduction prohibited without permission.

between these two types of foam are explained in Chapter 3. Assuming the foam is elastic-plastic requires a different equation to theoretically calculate collapse stress. Another reference studying the effects of anisotropy of foam properties uses both flexible and rigid polyurethane [23]. In this study, the collapse stress for the flexible foam is calculated using the elastomeric foam equation (σ_{el}) and the collapse stress for the rigid foam is calculated using the elastic-plastic foam equation (σ_{pl}). This would suggest that flexible polyurethane foam is elastomeric while the rigid polyurethane foam is elastic-plastic. However, the results of the Sandia National Labs theoretical data suggest that the elastomeric foam equation should be used because of the good correlation of the experimental data. Therefore, both σ_{el} and σ_{pl} equations are used to compute the theoretical collapse stress, which is then compared to the experimental collapse stress.

Figure-5.44 shows the theoretical and experimental normalized collapse stress using the elastic-plastic foam equation to calculate the theoretical values. As with the modulus, the volume fraction of the first method is changed to optimize the theoretical results. Since the modulus of the solid material is not used for the calculations, it is not a variable seen in the legend. The second method, which uses the values of cell edge length, edge thickness, and cell face thickness, found from the morphology measurements, is shown to have a huge disparity in values compared to the experimental data. The experimental data in this case is closest to the values calculated by the first method with a volume fraction of 0.90. This is not a good sign since the experimental modulus is closest to the second method using a volume fraction of 0.80. Though, the method using 0.80 for the collapse stress is not completely unreasonable. Percentage differences for the method using a 0.90 volume fraction range from 6% to 52%, whereas the differences for the method using a

Reproduced with permission of the copyright owner. Further reproduction prohibited without permission.

0.80 volume fraction range from 28% to 84%. The latter is not good but it is better than the 189% to 574% differences seen when comparing the second method to the theoretical data.

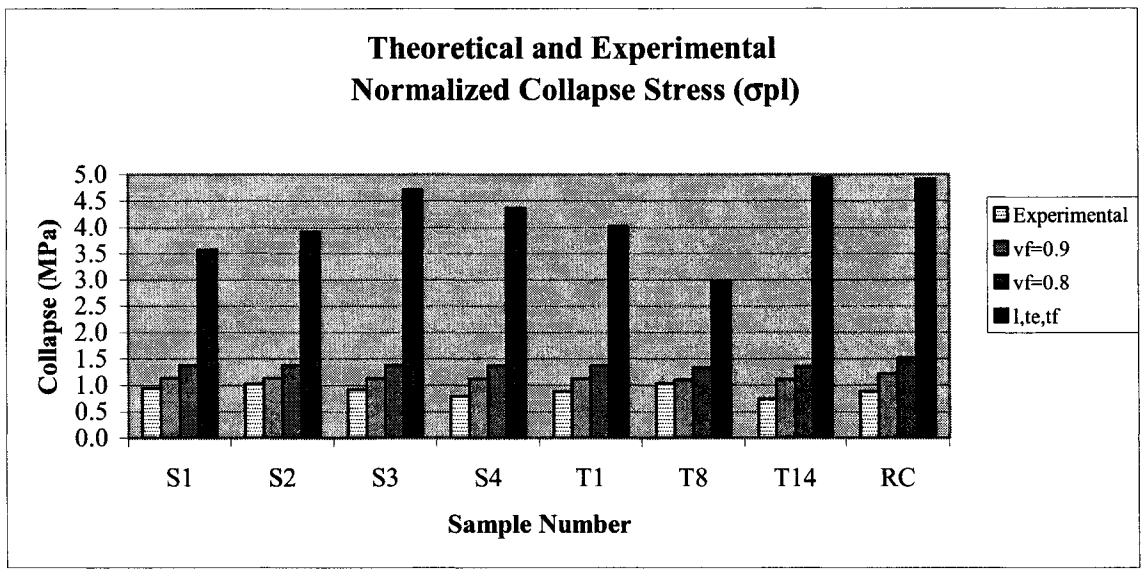

Figure-5.44: Theoretical and Experimental Normalized Collapse Stress (σ_{pl})

When looking at Figure-5.45, which shows the theoretical collapse stress, calculated from the elastomeric foam equation, it is not hard to see why Sandia National Labs used this theoretical value to compare to experimental data. This equation utilizes the modulus of the solid material to calculate the collapse stress and is therefore seen in the legend. However the volume fraction is not used so it is not seen in the legend. The second method utilizing values of cell edge length, edge thickness, and cell face thickness, shows a great correlation to the experimental values for most samples with percentage differences ranging from 1% to 24% which are the lowest of all methods when compared to the experimental values. It is not difficult to understand why the elastomeric foam

Reproduced with permission of the copyright owner. Further reproduction prohibited without permission.

equation is used even though the foam is rigid polyurethane and is considered elastic-plastic by one of the individuals who helped develop the two theoretical equations.

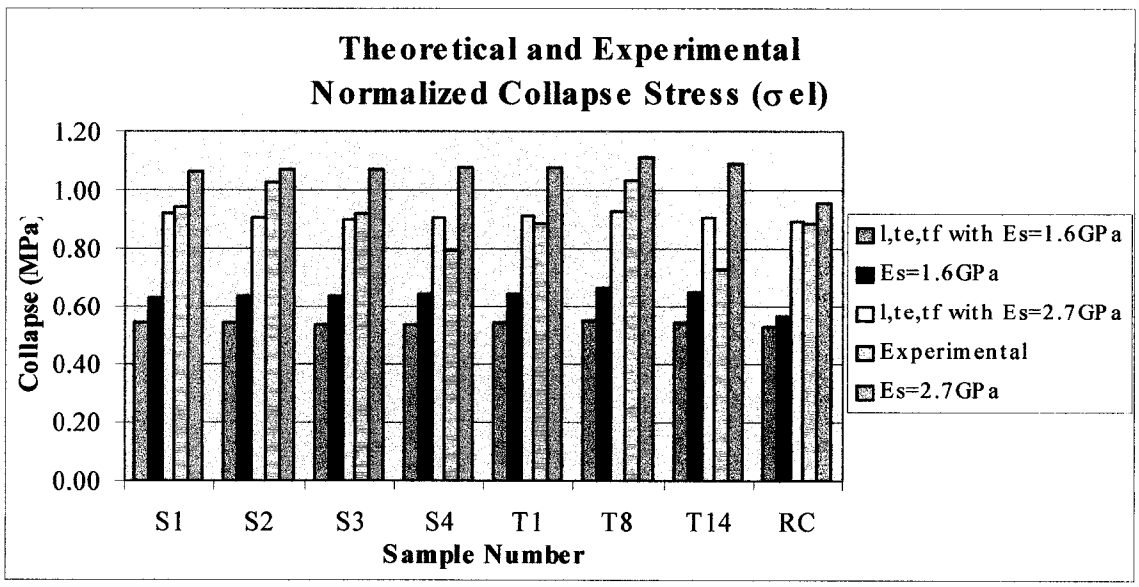

Figure-5.45: Theoretical and Experimental Normalized Collapse Stress (σ_{el})

5.3.5 Discussion of Theoretical Results

This section compares theoretical volume fraction, density, modulus, and collapse stress to experimental data. It is shown that one method cannot be used to calculate mechanical properties that agree with the experimental values. The easiest of values, the volume fraction, which depends mostly on the measurements taken from images, is not even correlating with previously found volume fractions for rigid polyurethane foam that indicate it should be within 80% to 90%. The density, dependent on the same values used to calculate the volume fraction, is also not correlating to the experimentally determined density. This is unfortunate since it was hoped the density of each radial position could be found to compare to experimental values of the radial density gradient. The theoretical

Reproduced with permission of the copyright owner. Further reproduction prohibited without permission.

values are not even shown in their radial form because of the awful correlation seen in levels. However, graphs of the radial positions in addition to tables of values are shown in Appendix F.

It is important to note that the theoretical values calculated using the first method do not show the same wave-like pattern that the second method values show. The first method shows values that are fairly uniform across the samples whereas the second method, which uses measurements from the images, shows definite deviations from one sample to the next. This implies that second method, however far from the experimental values in most cases, is superior because it shows the pattern in deviations per samples.

It is unfortunate that this section ends with a conclusion that the equations used do not provide theoretical data that correlates well to the experimental data. Perhaps the reason for this is the fact that all the equations rely on just the values of cell edge length, edge thickness, and cell face thickness. Most of the samples, especially those in the small and tall molds, show large aspect ratios and angles which might affect the experimental data. However, this does not explain why the RC sample did not correlate well to the theoretical data. There are theoretical equations to predict properties for anisotropic foams but these equations use the known property in the rise direction and the anisotropy ratio to predict properties in directions perpendicular to the rise. Therefore, these equations do not help in the calculation of theoretical properties in the rise direction where the cells are angled.

Reproduced with permission of the copyright owner. Further reproduction prohibited without permission.

CHAPTER 6

LINKING DENSITY AND MECHANICAL PROPERTIES TO CELL MORPHOLOGY

The main objective of this paper is to provide a reason for the variations in mechanical properties since density does not account for the differences. This is done primarily by providing mechanical data for different molds and conditions in addition to providing cell morphology data and theoretical data predicting mechanical properties. Another important aspect investigated is the room temperature aging affects on mechanical properties. This is undertaken because of the chemical differences found at room temperature [13].

The mechanical properties, compressive Young's modulus, peak yield, and collapse stress, change at different levels of a mold, but the order in which the foam is poured into the molds has no definite effect. The densities of the small and tall molds do not change significantly from level to level. The reference mold has a greater change in density from level to level, but the mechanical properties are more uniform. This suggests something else is changing the mechanical properties. Table-6.1 shows average percent differences for density and mechanical properties with respect to levels. Percent differences are calculated comparing the level with the lowest property (always the bottom of the mold) to the level with the highest property (always in the top 25% to 50% of the mold).

Reproduced with permission of the copyright owner. Further reproduction prohibited without permission.

Table-6.1: Percentage Differences in Properties per Level

Mold Type	Density	Modulus	Peak Yield	Collapse
Small Molds (2 Levels)	1%	10%	8%	16%
Small Molds (4 Levels)	2%	44%	24%	26%
Tall Molds (14 Levels)	4%	93%	45%	48%
Reference Mold (4 Levels)	8%	2%	14%	9%

The mechanical properties definitely decrease in mechanical properties at the bottom levels of the small and tall molds. When looking at the images of the parallel samples of the small and tall molds, cell morphology changes are visually evident from the top to the bottom of the molds. Data collected using imaging analysis software further supports this. The cell diameters of the parallel samples increase and the cell diameters of the perpendicular samples decrease toward the bottom of the mold. This further supports the fact that cells elongate more and more toward the bottom of the mold. This effect is seen in greater detail in the tall mold that yields an aspect ratio of around 4.0 which is almost twice that of all the other levels and molds. The angle of these elongated cells is also an important piece of information. If the unit cell has struts that act like beams and these beams are angled, then the load carried by these beams is going to be lower than for beams that are vertical, hence the lower mechanical properties. In addition, elongated cells create beams that are longer and therefore buckle under lower loads than shorter beams. The small and tall molds both have cells that angle around 15% to 20% from the vertical at all levels except the top.

Reproduced with permission of the copyright owner. Further reproduction prohibited without permission.

Radial changes in cell morphology are not as significant as those per level. The most mentionable is the aspect ratio of the tall mold, which is evident by viewing the SEM images. These images show that cells at around 60% of the mold radius are more elongated and that the cells around 90% of the mold radius are more angled. For example, cells in the tall mold increase in elongation by 83% from the 90% radial position to the 60% radial position. In addition, the cells in the tall mold increase in angle by 28% from the 60% to 90% radial position. These changes most likely affect the failure mechanism of the foam under compression more than anything. The samples at the bottom of the molds tend to snap or crackle during compression indicating that a group of cells collapsed catastrophically. However, this group of cells is most likely just those cells with large aspect ratios that are angled. The remainder of the cells continue to hold the foam at the collapse stress. Sometimes the effect is so great it can be seen on the actual stress-strain graphs. Figure-6.1 shows the stress-strain curves of Batch C5 and points out curves that show the snapping effect. The curves show sharp inverted peaks where the stress lowers sharply and then regains itself to match the collapse stress of the other curves at the same level. This snapping effect is not heard during compression of the upper level samples or seen on the stress-strain curves. The elongation of the cells toward the bottom of the molds could also cause the collapse to be lower as seen visually in Figure-6.1.

It is interesting to note that Lin [18] shows stress-strain curves of different density materials. It is concluded that higher density foams show a higher modulus, peak yield and collapse stress. In addition the peak yield is higher than the collapse for higher density foams. This is proven with this work when comparing the curves from the

Reproduced with permission of the copyright owner. Further reproduction prohibited without permission.

reference mold to the curves from the small and tall molds. The reference mold has a lower density so its curves show a peak yield close to the collapse and its modulus, peak yield and collapse stress are also lower. Huber and Gibson [23] also shows stress-strain curves but of materials tested in the rise direction and two directions perpendicular to the rise. The rise direction curve has a higher modulus, peak yield, and collapse than the other two curves. In addition, the rise direction has a peak yield that is higher than the collapse. Since deviations are seen in the stress-strain curves per level and the density of each level is fairly consistent, then the effect of the curves could be due to the angling of the cells. The rise direction produces higher properties than the other two directions. If the samples on the bottom of the mold show heavily angled and elongated cells this is almost like compressing the sample in a direction not parallel to the rise direction thereby producing properties that are lower.

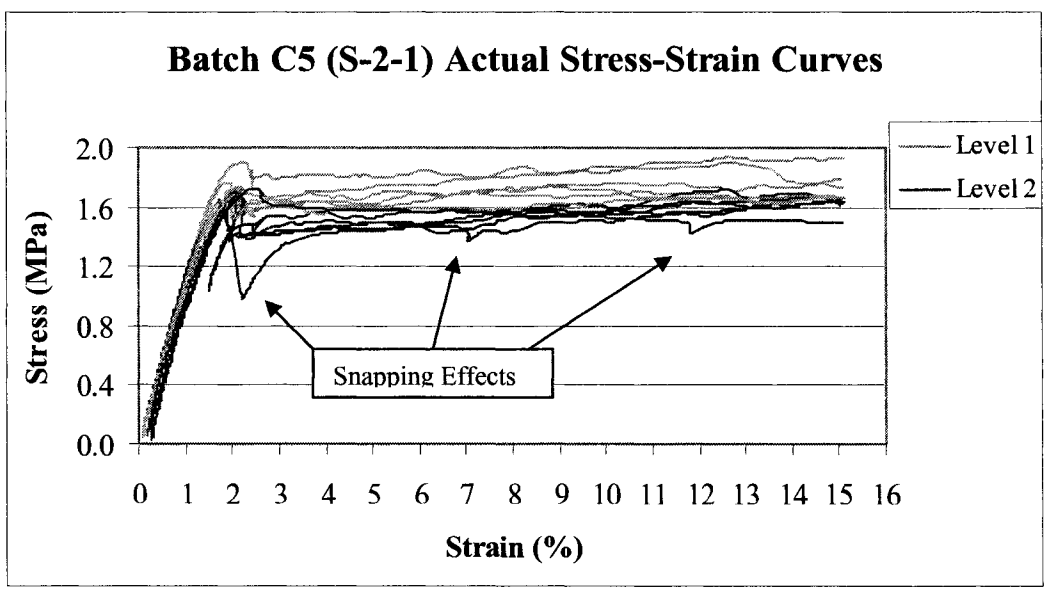

Figure-6.1: Actual Stress-Strain Curve of Batch C5 (S-2-1)

Reproduced with permission of the copyright owner. Further reproduction prohibited without permission.

Theoretical density, Young's modulus, peak yield, and collapse are all found using measurements of the cell edge length, cell face thickness, and edge thickness and equations set forth by Gibson and Ashby [5]. Unfortunately, results are not as expected, and the density calculated is far lower than the density measured of the actual sample. The density calculated using theoretical equations show a density of around 0.06-g/cc whereas the actual density of the foam samples is closer to 0.125-g/cc. The experimental density is just over two times greater than the density calculated theoretically. The volume fraction used to calculate the three mechanical properties is also far lower than the volume fraction found in Reitz et al [22]. The calculated volume fraction is around 50% whereas the referenced volume fraction used by Gibson and Ashby and Whinnery and Goods is reported as 80-90%. Interestingly, Lin [18] calculates the volume fraction for foamed plastics and shows it ranges from 8% to 50%. Unfortunately, a direct comparison can not be made because of the differences in material.

Since the theoretical results do not match the experimental results per level, there is no way that the results would give a clear picture of the mechanical properties per radial position. However, since density has been determined experimentally in other papers, it is worth comparing the theoretical density to the experimental density to see if the same slope exists. The experimental and theoretical radial densities are shown in Figure-6.2. Since the experimental radial density is an average taken from all levels, it makes since that the theoretical radial density should also be an average. Therefore, all perpendicular and parallel slices in each mold are averaged to provide the curves seen in Figure-6.2. Data for the experimental density is taken directly from reference 7 for the "S-Exp" data and from reference 6 for the "RC-Exp" data. The experimental density, "S-Exp" is taken

Reproduced with permission of the copyright owner. Further reproduction prohibited without permission.

from foam made at room temperature in a small mold and the experimental density, "RC-Exp", is taken from foam made at room temperature in a reference mold.

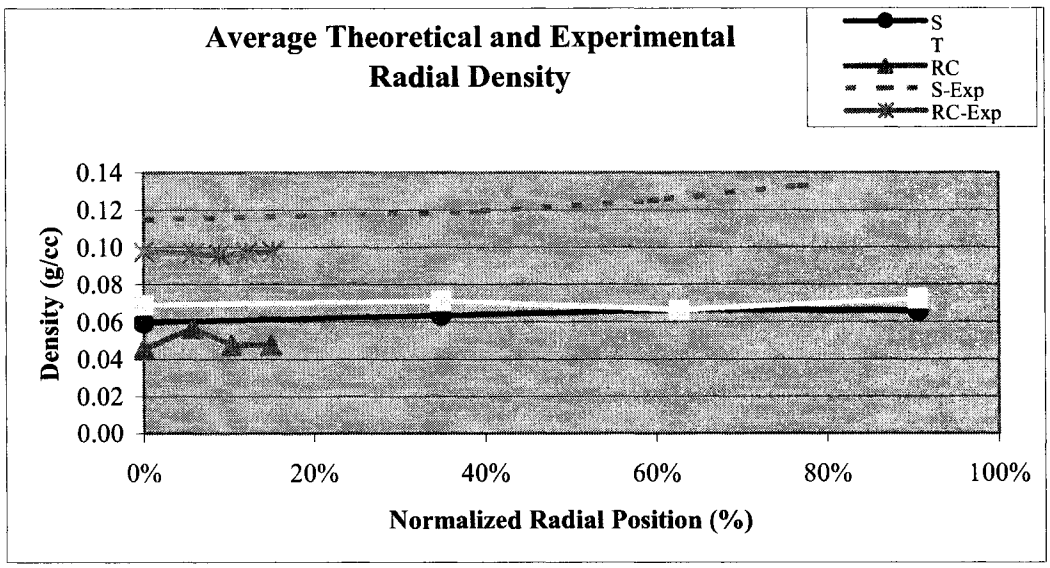

Figure-6.2: Average Theoretical and Experimental Radial Density

Visually, it seems that the experimental radial density for the small molds has a much greater slope than the theoretical density. Therefore, percentage differences are provided in Table-6.2 that shows the differences between the densities in the center of the mold compared to the densities at the last data point of the curve. Even though the experimental density is only measured to 77% of the mold radius, it has a 5% higher difference between center and outside than the theoretical density. It is clear that the theoretical density does not provide extremely accurate information.

Table-6.2: Percent Differences in Radial Density

Curve	S	S-Exp	RC	RC-Exp	T
% Difference	10.2%	15.7%	4.7%	0.0%	4.6%

Reproduced with permission of the copyright owner. Further reproduction prohibited without permission.

The theoretical modulus, peak yield, and collapse stress, even though incorrect are still compared with the experimental data collected for each mold. Several different methods are used to produce theoretical data that better matches the experimental. Unfortunately, a different method is better for each one of the mechanical properties. In some cases the experimental and theoretical properties vary by over 500%. In other instances the properties match quite well and had percent differences as low as 1%. It is unclear why the properties could not be predicted accurately using theoretical methods. It is thought that poor results could be attributed either to the measurements made from the SEM images or to the elongation and angling of the cells that is not taken into account by the theoretical equations. Another reason could be a chemical difference between the cell faces and the cell edges possibly creating a different modulus in these two areas. Even though matching the theoretical results to the experimental results did not occur, there is a qualitative correlation between mechanical properties and cell morphology just by looking at the experimental mechanical data, SEM images, and cell morphology calculations.

Reproduced with permission of the copyright owner. Further reproduction prohibited without permission.

CHAPTER 7

CONCLUSIONS

Polyurethane foam is used in industrial and military applications as a supporting or insulating material to protect sensitive components from shock, vibration, and/or thermal loading. Many foam components are formed into complex molds with significant variations in geometry and size. This work investigated the relationships between cell morphology, density, and mechanical properties in a molded polyurethane material using relatively small diameter cylindrical molds. These effects are important to understand so that mechanical designers can analyze and predict the response of foam components accurately.

It is reasonable to conclude that there is a relationship between cell morphology and mechanical data. It is evident that the shape and orientation of the cells has an affect on the mechanical data if not just by providing a different failure mechanism. It is unfortunate that the theoretical mechanical data could not directly relate cell morphology to differences in experimental mechanical data. In addition, the relationship between cell morphology and density could not be accurately made because of the incorrect theoretical density calculations.

Experimental mechanical data shows that vertical position in the small and tall molds have a significant effect on the mechanical properties. However, density in the small and tall molds does not change with respect to vertical position. Only in the reference mold

Reproduced with permission of the copyright owner. Further reproduction prohibited without permission.

does the density change by level. In addition, the mechanical data suggests the reference mold provides uniform properties. The mold order, the order the foam is poured in each successive mold, does not have a significant effect on mechanical properties or density in the small or tall molds. Unfortunately, the radial mechanical properties and density could not be accurately calculated theoretically. Finally, a definite change in cell morphology occurs per level and radial position of the small and tall molds. These changes most likely have an effect on the mechanical properties.

The mechanical data does not change significantly during the first ninety days of room temperature aging, even though significant changes in chemistry are seen [13]. These changes in chemistry do not affect the mechanical properties during the first ninety days. This study is performed because no data existed on the effect of room temperature aging on ReCrete. Sandia National Labs performed extensive thermal aging tests on TDI which show changes in mass and mechanical properties and shows insignificant effects on the properties at room temperature. However, it was thought that since the chemistry changed, the mechanical properties might also change and it was important to disprove this fact. Therefore, this work proves that chemistry changes have no effect on the mechanical properties for the first ninety days.

The main recommendation for further study is either to formulate equations that accurately describe the foam's density and mechanical properties or to take a magnified view of the SEM images to produce more accurate measurements for the theoretical calculations. In addition, it might be helpful to actually repeat the study done in reference 22 to see if replicating the results is possible. If replication is impossible, then maybe the calculation of the volume fraction for ReCrete polyurethane foam is correct. Especially

Reproduced with permission of the copyright owner. Further reproduction prohibited without permission.

since reference 18 shows volume fractions that range from 8-50% which is close to the value calculated in this work. The only discrepancy is that the foam used in reference 18 is not polyurethane foam.

Another important study to follow this one is to analyze the cell morphologies of foams that are processed at different temperatures. Documented in reference 28 is a study performed on foam under two different processing temperatures. It is shown that the skin thickness decreases and the cell size increases with increasing processing temperature. It would be interesting to see if this holds true for foam made in small diameter molds. In addition, it would be interesting to see if and how much the foam cells elongate or angle when the processing temperature is increased.

The data presented in this work shows that the cell morphology and mechanical properties are different for small diameter molds than for larger diameter molds. This could prove to be important because sometimes a mold is created with small and large crevices to be injected with foam. This means that the small crevices will most likely have foam of higher density and mechanical properties than the large crevices. In addition, the gradient of mechanical properties will be higher in the small crevices than in the larger ones and the density gradient will be more significant in the large crevices and almost non existent in the smaller ones. These effects should be accounted for when developing parts that are used to protect electronic equipment or for impact and absorption purposes. It can also help a designer that wishes one section of the foam to be stronger than another section. This can be accomplished simply by increasing or decreasing the volume of the mold in certain sections instead of changing the chemical formulation to produce the desired affect.

Reproduced with permission of the copyright owner. Further reproduction prohibited without permission.

APPENDIX A

MATERIALS AND EQUIPMENT

Foam Fabrication Chemicals

DOW CORNING® 193 SURFACTANT
Dow Corning Corporation
Silicone Glycol Copolymer
Average Hydorxyl Number: 75
Ashland Chemical
1-800-339-5502

POLYCAT® 17 CATALYST
Air Products and Chemicals Inc.
Tertiary Amine Catalyst (Trimethyl-N-Hydroxyethyl Propylene Diamine)
Average Hydroxyl Number: 400
Air Products and Chemicals Inc.
1-800-345-3107

RUBINATE® 1680
Dow Corning
Specific Gravity @ 25°C: 1.07
Viscosity 335.00 CST
Huntsman Polyurethanes
1-800-257-5547

VORANOL® 490 POLYOL
The Dow Plastic Company
Polyether Polyol
Density @ 25°C: 0.11 kg/cm^3
Typical Hydroxyl Number: 490 mg KOH equiv/g of resin
Functionality: 4.3 (calculated)
Average Molecular Weight: 460 g/mole
Viscosity @ 25°C: 5572 cups
Chem Central
1-602-751-9013

Reproduced with permission of the copyright owner. Further reproduction prohibited without permission.

Foam Fabrication Equipment

Arrow Overhead Mixer
VWR
Model# 2000
60Hz/ 115V/AC/ 2A

Blue M Oven
Model# DC-136-C
Temperature Range: 343°C

Conn Blade
Conn & Co., LLC
Intensive Type (IT)
2" diameter
Kimberly-Clark Kimwipes EXL
VWR
Model# 34256
1 ply/ 38.1 x 43.1 cm

Mettler Toledo Digital Scale (Chemical Scale)
VWR
Model# PB3002-S
Max: 3100g
Min: 0.5g
Readability: d= 0.01g

Microgrip Ambi Polyshield Latex Gloves, Powder Free
VWR

Mold Release
PTM&W Industries Inc
Model# PA0801-WAX
VOC: 20C-550 gm/lit
Vap Press: 2ml-Hg
65% light petroleum distillate

Puritan Wooden Applicators
VWR
Model# REF 807
Length: 15cm

VWR Thermo-Hygro
VWR
Catalog# 35519-049
Range: 0°C - 50°C
2% - 98% RH

Reproduced with permission of the copyright owner. Further reproduction prohibited without permission.

Foam Processing Equipment

Craftsman 11-in Band Saw
Sears Hardware
Model# 315.214500
3 wheel/ ⅓ HP
1/16" Blade

Craftsman Drill Press
Sears Hardware
Model# 137.219080
⅓ HP/ 5-Speed
½" Chuck

Delta 12" Disk Sander
Sears Hardware
Model# 31-120
½ HP/ 60Hz/ 120V/ 1725 RPM

Hole Saw
Abrasive Technology
Custom Order
1.13 x 2.5 x 0.375

Mettler Toledo Density Scale
VWR
Model# AG204 DeltaRange
Capability: Max 81g/210g
Readability: d= 0.1mg/1mg

Mitutoyo Absolute Digimatic Calipers
McMaster-Carr
Model# CD-6"C
Capability: 0-150mm
Resolution: 0.01mm
Accuracy: ±0.02mm
Repeatability: 0.01mm

Reproduced with permission of the copyright owner. Further reproduction prohibited without permission.

Mechanical Testing Equipment

Load Cell
United
Model# 1K T/C
4.4-kN Maximum

United Axial Loading Machine
United
Model# SSTM-1

United Laser
United
Model# EXT-62-LOE
Tolerances: ASTM E83

Morphology Equipment

Buehler EPOXIDE Resin and Hardener
Buehler
Resin ID no. 20-8130-128
Hardener ID no.20-8132-032

Buehler Epoxy Molds
Buehler
#20-8282
Disposable Cold MT Cups, 1-1/2"

Buehler Release Agent
Buehler
ID no. 20-8185-002

Cressington Sputter Coater
Cressington
108 auto

Image-Pro Plus 4.5
MediaCybernetics

JEOL-5600 Scanning Electron Microscope (SEM)
Resolution: 50nm at 100,000 times magnification

Lagun Mill
Lagun
#FTV-2S

Reproduced with permission of the copyright owner. Further reproduction prohibited without permission.

APPENDIX B

FOAM PROCESSING LOG

The following log includes all foam that has been processed at the University of Nevada, Las Vegas. Information includes batch number, date of processing, size of batch, and special conditions under which the foam is processed.

Reproduced with permission of the copyright owner. Further reproduction prohibited without permission.

Batch	Date	Size	Made By	Comments
1	8/16/00	1500-cc	John/Cameron	Airy
2	9/12/00	1500-cc	Linda/Cameron	Not mixed enough
3	9/21/00	1500-cc	Linda/Cameron/	Perfect
			O'Toole/Mike	
4	11/9/00	1500-cc	Mike/Linda	Made for Sci & Tech Day
5	11/9/00	1500-cc	Mike/Cameron	Made for Sci & Tech Day
				Too much Rubinate was added
6	11/13/00	1500-cc	Mike/Cameron	Made during Sci & Tech Day
7	12/12/00	3000-cc	Mike/Cameron	Scale not able to weigh Rubinate
8	12/19/00	3000-cc	Cosmo/Cameron	RT FR 3.8L
9	1/4/01	1500-cc	Mike/Cameron/Cosmo	RT FR Cyl Molds PKD
10	1/29/01	1500-cc	Mike/Cameron/Cosmo	RT FR Cyl Molds PKD Preheated
11	2/16/01	1500-cc	Mike/Cameron	Squares for United- 3.8L mold
12	5/14/01	1500-cc	Cameron/Mike	FR RT 1L
				(1st skin batch w/o water)
13	5/14/01	1500-cc	Mike/Cameron	Two Pour Cups- FR
14	5/16/01	1500-cc	O'Toole/Cameron/Mike	90C FR WB Cyl
15	5/17/01	1500-cc	Mike/Cameron/Dacia	RT FR Cyl
16	5/22/01	1500-cc	Mike/Dacia/Danny	RT FR 3.8L
17	5/22/01	1500-cc	Danny/ Dacia/ Mike	RT FR WB Cyl
18	5/23/01	1500-cc	Mike/ Danny/ Dacia	0C FR Cyl
19	5/25/01	1500-cc	Mike/ Danny	40C FR WB Cyl
20	6/13/01	1500-cc	Mike/Cameron	RT FR in square mold
21	6/14/01	1500-cc	Mike/ Bob	Attempt to make skin w/out water
				70C FR WB Cyl
22	6/20/01	1500-cc	Cameron/ Dacia/ Heidi	RT FR Cyl (For Bob's Analysis)
23	6/24/01	1500-cc	Mike/Cameron	RT FR Cyl
24	6/25/01	1500-cc	Cameron/ Mike	90C FR WB Cyl
25	6/26/01	1500-cc	Cameron/Dacia	0C FR Cyl
26	6/27/01	1500-cc	Cameron/Dacia	40C FR WB Cyl
27	6/28/01	1500-cc	Cameron/Dacia	RT FR Cyl WB
28	7/10/01	3000 cc	Mike/ Cameron/ Dacia	RT FR 1L (x4)
29	7/18/01	1500-cc	Cameron/ Mike	RT FR 1L molds for DA
30	7/27/01	1500-cc	Mike/ Heidi	RT FR 3.8L mold for DA
31	8/7/01	1500-cc	Cameron/ Mike	RT Air FR Cyl for DA
32	8/10/01	1500-cc	Cameron/ Mike/ Heidi	66C FR WB Cyl for DA
33	8/16/01	1500-cc	Cameron/Dacia	25 FR WB Cyl for DA
34	8/17/01	1500-cc	Cameron/Dacia	40C FR WB Cyl for DA
35	8/20/01	1500-cc	Cameron/Dacia	90C FR WB Cyl for DA
				(no mold release)
				(lathe experiment #1)

Reproduced with permission of the copyright owner. Further reproduction prohibited without permission.

Batch	Date	Size	Made By	Comments
36	8/27/01	1000-cc	Mike/ Dacia	66C FR WB Cyl for DA
37	9/5/01	1000-cc	Cameron/Dacia	90C FR WB Cyl for DA
				(water leak)
38	9/10/01	1000-cc	Cameron/ Dacia/ Gayani	0C FR IB Cyl (90min rise)
39	9/12/01	1000-cc	Cameron/Dacia	0C FR IB Cyl for DA (large voids)
40	9/17/01	1000-cc	Cameron/Dacia	66C FR WB Cyl
				(lathe experiment #2)
41	12/17/01	1500-cc	Cameron/ Mike	25C Air (aging study)
42	1/10/02	1500-cc	Cameron/Dacia	25C Air (strain rate study)
43	1/10/02	1500-cc	Cameron/Dacia	85C WB (temp test, molds 1,2,3)
				25C Air
				(new mold release, molds 4,5,6)
44	1/23/02	1500-cc	Cameron/Mike	85C WB (temp test, molds 1,2,3)
				25C Air
				(strain rate study, molds 4,5,6)
				1hr rise
D1	1/29/02	1500-cc	Cameron/Dacia	25C WB (1.13" small molds)
				All D batches for Dacia's thesis
D2	2/4/02	1500-cc	Cameron/Dacia	40C WB FR (1.13" small molds)
D3	2/11/02	1500-cc	Cameron/Dacia	65C WB FR (1.13" small molds)
D4	2/19/02	1500-cc	Cameron/Dacia	85C WB FR (1.13" small molds)
45	2/20/02	2500-cc	Cameron/Dacia	25C Air (1.6 dia tubes aging study)
D5	2/25/02	2500-cc	Cameron/Dacia	25C WB FR medium tubes
D6	3/4/02	2500-cc	Cameron/Dacia	40C WB FR medium tubes
D7	3/11/02	2500-cc	Cameron/Dacia	65C WB FR (1.6" med molds)
D8	3/18/02	2500-cc	Cameron/Dacia	85C WB FR (1.6" med molds)
46	4/1/02	2500-cc	Cameron/ Dacia	25C WB (2.0 dia tubes water leak)
D9	4/2/02	2500-cc	Cameron/Dacia	25C WB FR (2.0" large molds)
47	4/8/02	2500-cc	Cameron/Dacia	40C WB (2.0 dia tubes water leak)
D10	4/9/02	2500-cc	Cameron/Dacia	40C WB FR (2.0" large molds)
D11	4/16/02	2500-cc	Cameron/Dacia	65C WB FR (2.0" large molds)
D12	4/22/02	2500-cc	Cameron/Dacia	85C WB FR (2.0" large molds)
DR-1	5/21/02			25C Air FR, gallon mold for DA
				(Reference)
DR-2	5/28/02			25C Air FR, gallon mold for
				mech test (Reference)
48	6/6/02	1500-cc	Cameron/Dacia/	25C Air
			Gayani/Ellen	(long gauge length comp sample)
49	6/13/02	1500-cc	Cameron/Dacia/	25C Air (tension testing)
			Gayani/Ellen	

Reproduced with permission of the copyright owner. Further reproduction prohibited without permission.

Batch	Date	Size	Made By	Comments
50	6/20/02	1500-cc	Cameron/Dacia	25C Air (long gauge length comp.)
				Tube 1 = 90C WB for Chem IR
51	6/27/02	2500-cc	Dacia/ Cameron	Medium Tubes, RT Air FR
52	7/9/02	1500-cc	Guyani/Cameron/Ellen	Tubes 1-3 40C SandBath,1.13"dia.
				Tubes 4-6 RT Air FR, 1.13" dia.
53	7/16/02	2500-cc	Mike/Dacia	Large Tubes, Air RT FR,
				2" gauge samples
54	7/23/02	2500-cc	Cameron/Dacia	Tubes 1-5 2" gauge samples,
				Large Tubes
				Air RT FR, Tube 6 sample for chem
55	7/30/02	1500-cc	Mike/Cameron	RT Air FR - Rectangular mold
56	8/9/02	1500-cc	Cameron/Dacia	25C WB FR (Filmed)
57	9/10/02	1500-cc	Cameron/Dacia/Bob	#9 PKD foam, #2-6 FR Air RT
58			Cameron/Dacia	25C Air, small tubes
59			Cameron/Dacia	25C Air, small tubes
60	11/5/02	1500-cc	Cameron/Guyani	RT Air FR (Chemistry Analysis)
61	3/27/03	1500-cc	Cameron/Guyani	RT WB, 6 small tubes
				Guyani's thesis
C1	4/14/03	1500-cc	Cameron/Dacia	6", RT Air, 2" gauge, 1 day after
				All C Batches for Cameron's thesis
C2	4/16/03	1500-cc	Cameron/Dacia	6", RT Air, 1" gauge, 2 days after
C3	4/21/03	1500-cc	Cameron/Dacia	6", RT Air, 1" gauge, 1 day after
C4	4/22/03	1500-cc	Cameron/Dacia	6", RT Air, 2" gauge, 2 days after
C5	4/28/03	1500-cc	Cameron/Dacia	6", RT Air, 2" gauge, 1 day after
C6	4/29/03	1500-cc	Cameron/Dacia	6", RT Air, 1" gauge, 2 days after
C7	5/5/03	1500-cc	Cameron/Dacia	6", RT Air, 1" gauge, 1 day after
C8	5/6/03	1500-cc	Cameron/Dacia	6", RT Air, 2" gauge, 2 days after
C9	6/4/2003	1500-cc	Cameron/Dacia	18", RT Air, 1" gauge, 2 days after
C10	6/10/03	1500-cc	Cameron/Dacia	18", RT Air, 1" gauge, 2 days after
C11	6/11/03	1500-cc	Cameron/Dacia	6", RT Air, 1" gauge, 3 months after
C12	6/12/03	1500-cc	Cameron/Dacia	6", RT Air, 1" gauge, 3 months after
C13	6/16/03	1500-cc	Cameron/Dacia	6", RT Air, 1" gauge, 7 days after
C14	6/17/03	1500-cc	Cameron/Dacia	6", RT Air, 1" gauge, 7 days after
C15	7/9/03	1500-cc	Cameron/Dacia	6", RT Air, 1" gauge, 4 weeks after
C16	7/10/03	1500-cc	Cameron/Dacia	6", RT Air, 1" gauge, 4 weeks after
C17	8/7/03	1500-cc	Cameron/Dacia	SEM Imaging Batch -
				(2) small dia. 6" tubes
				(1) small dia. 18" tube

Reproduced with permission of the copyright owner. Further reproduction prohibited without permission.

APPENDIX C

RADIAL DENSITY GRADIENT SAMPLE PREPARATION

To calculate radial density gradients from the small mold, each cylindrical sample is cored into 13 samples as shown in Figure-C.1 (a). These samples are cored out of the cylindrical samples using a nickel-plated cork borer that is beveled on one side. Four radial positions are used to complete a radial density gradient graph. These positions are measured from the center of the cylindrical sample, the first position being dead center. The next three positions are at intervals of about 3-mm as shown in Figure-C.1 (b). Samples that are cored from the cylindrical samples have diameters of approximately 2.5-mm and heights of approximately 25.4-mm. The radial density gradient is also calculated from the reference mold in a similar manner as the small mold. Figure-C.2 shows the cored out foam.

After being extracted from the cylindrical samples, each cored sample is measured and weighed for a mean density calculation. Diameters and heights of each sample is measured four times with digital calipers and then averaged. Samples at the same radial position are averaged to provide a mean density at that particular radial position. Further information on sample preparation for radial density gradients can be found in Reference 6.

Reproduced with permission of the copyright owner. Further reproduction prohibited without permission.

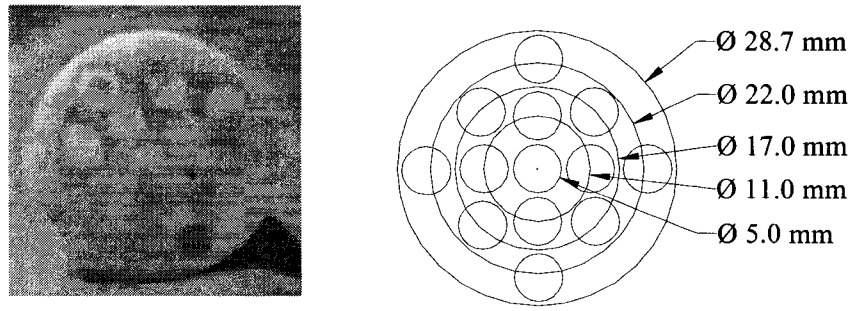

(a)

Figure-C.1: Cored Samples from Small Mold Cylindrical Sample

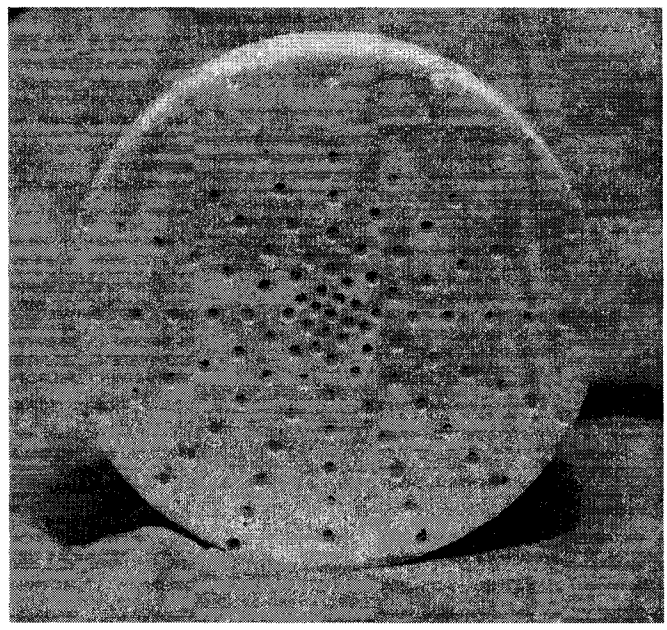

Figure-C.2: Cored Samples from Reference Mold

Reproduced with permission of the copyright owner. Further reproduction prohibited without permission.

APPENDIX D

DENSITY AND MECHANICAL PROPERTIES

Reproduced with permission of the copyright owner. Further reproduction prohibited without permission.

Table-D.1: S-2-1 Average Density, Modulus, Peak Yield, and Collapse

	Density	Modulus	Peak Yield	Collapse
Average	0.131	63.2	0.93	0.91
Std Dev	0.003	4.6	0.05	0.09
% Dev	1.9%	7.3%	5.9%	10.1%

Table-D.2: S-2-1 Level Density, Modulus, Peak Yield, and Collapse

		LEVEL 1	LEVEL 2
Density	Average	0.130	0.132
	Std Dev	0.003	0.002
	% Dev	2.0%	1.8%
Modulus	Average	66.2	60.3
	Std Dev	3.0	4.0
	% Dev	4.5%	6.7%
Peak Yield	Average	0.97	0.89
	Std Dev	0.03	0.04
	% Dev	2.9%	5.0%
Collapse	Average	0.99	0.83
	Std Dev	0.03	0.05
	% Dev	3.3%	5.7%

Table-D.3: S-2-1 Mold Order Density, Modulus, Peak Yield, and Collapse

		MOLD 1	MOLD 2	MOLD 3	MOLD 4	MOLD 5	MOLD 6
Density	Average	0.133	0.132	0.130	0.129	0.131	0.130
	Std Dev	0.001	0.002	0.001	0.003	0.003	0.003
	% Dev	0.5%	1.2%	0.9%	2.7%	1.9%	2.4%
Modulus	Average	61.2	63.2	66.1	63.9	64.6	60.5
	Std Dev	6.1	5.8	6.0	4.7	1.2	1.8
	% Dev	9.9%	9.1%	9.1%	7.3%	1.9%	2.9%
Peak Yield	Average	0.92	0.92	0.93	0.95	0.92	0.93
	Std Dev	0.09	0.05	0.08	0.04	0.05	0.03
	% Dev	9.8%	6.0%	8.4%	4.4%	5.1%	3.2%
Collapse	Average	0.92	0.92	0.91	0.92	0.91	0.89
	Std Dev	0.12	0.12	0.13	0.09	0.08	0.07
	% Dev	13.3%	12.8%	14.1%	10.0%	8.6%	7.7%

Reproduced with permission of the copyright owner. Further reproduction prohibited without permission.

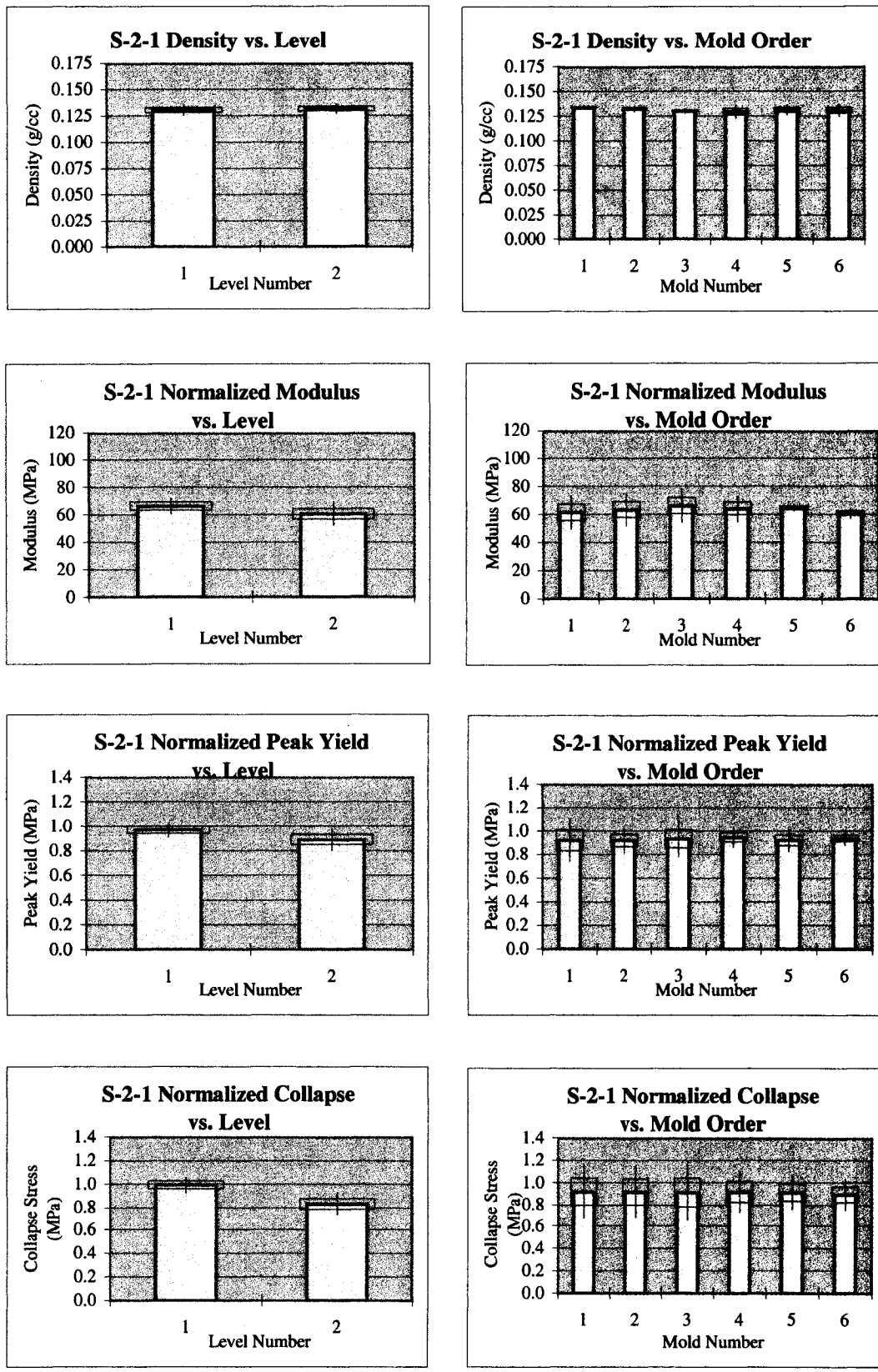

Figure-D-1: S-2-1 Density, Modulus, Peak Yield, and Collapse

Reproduced with permission of the copyright owner. Further reproduction prohibited without permission.

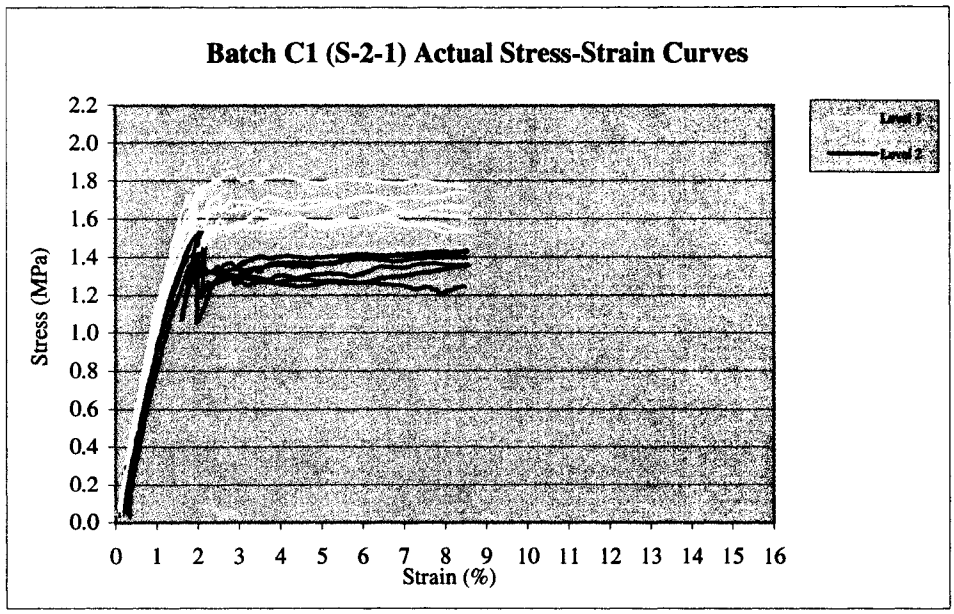

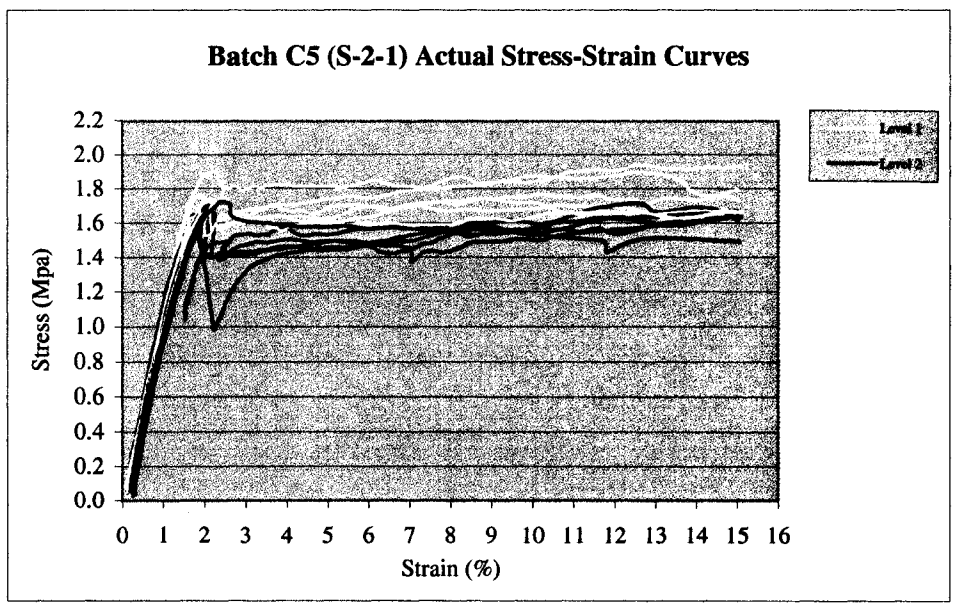

Figure-D-2: S-2-1 Actual Stress-Strain Curves (Not Normalized)

Reproduced with permission of the copyright owner. Further reproduction prohibited without permission.

Table-D.4: S-2-2 Average Density, Modulus, Peak Yield, and Collapse

	Density	Modulus	Peak Yield	Collapse
Average	0.134	63.3	0.94	0.91
Std Dev	0.010	5.7	0.04	0.07
% Dev	7.4%	9.0%	4.8%	7.7%

Table-D.5: S-2-2 Level Density, Modulus, Peak Yield, and Collapse

		LEVEL 1	LEVEL 2
Density	Average	0.134	0.135
	Std Dev	0.010	0.010
	% Dev	7.5%	7.5%
Modulus	Average	66.3	60.3
	Std Dev	4.0	5.7
	% Dev	6.0%	9.4%
Peak Yield	Average	0.97	0.91
	Std Dev	0.03	0.03
	% Dev	3.6%	2.8%
Collapse	Average	0.97	0.86
	Std Dev	0.04	0.04
	% Dev	4.4%	4.6%

Table-D.6: S-2-2 Mold Order Density, Modulus, Peak Yield, and Collapse

		MOLD 1	MOLD 2	MOLD 3	MOLD 4	MOLD 5	MOLD 6
Density	Average	0.135	0.131	0.131	0.131	0.141	0.136
	Std Dev	0.009	0.009	0.009	0.010	0.017	0.007
	% Dev	6.4%	6.8%	6.5%	7.6%	11.8%	5.2%
Modulus	Average	64.5	62.6	62.7	63.9	61.2	64.9
	Std Dev	6.7	4.1	4.7	6.0	8.8	6.1
	% Dev	10.4%	6.6%	7.4%	9.4%	14.4%	9.4%
Peak Yield	Average	0.96	0.94	0.95	0.95	0.92	0.94
	Std Dev	0.07	0.05	0.05	0.03	0.04	0.04
	% Dev	7.2%	5.3%	5.5%	3.2%	4.3%	4.7%
Collapse	Average	0.95	0.93	0.92	0.90	0.88	0.89
	Std Dev	0.08	0.05	0.10	0.06	0.08	0.06
	% Dev	8.4%	5.2%	11.3%	6.7%	9.3%	6.2%

Reproduced with permission of the copyright owner. Further reproduction prohibited without permission.

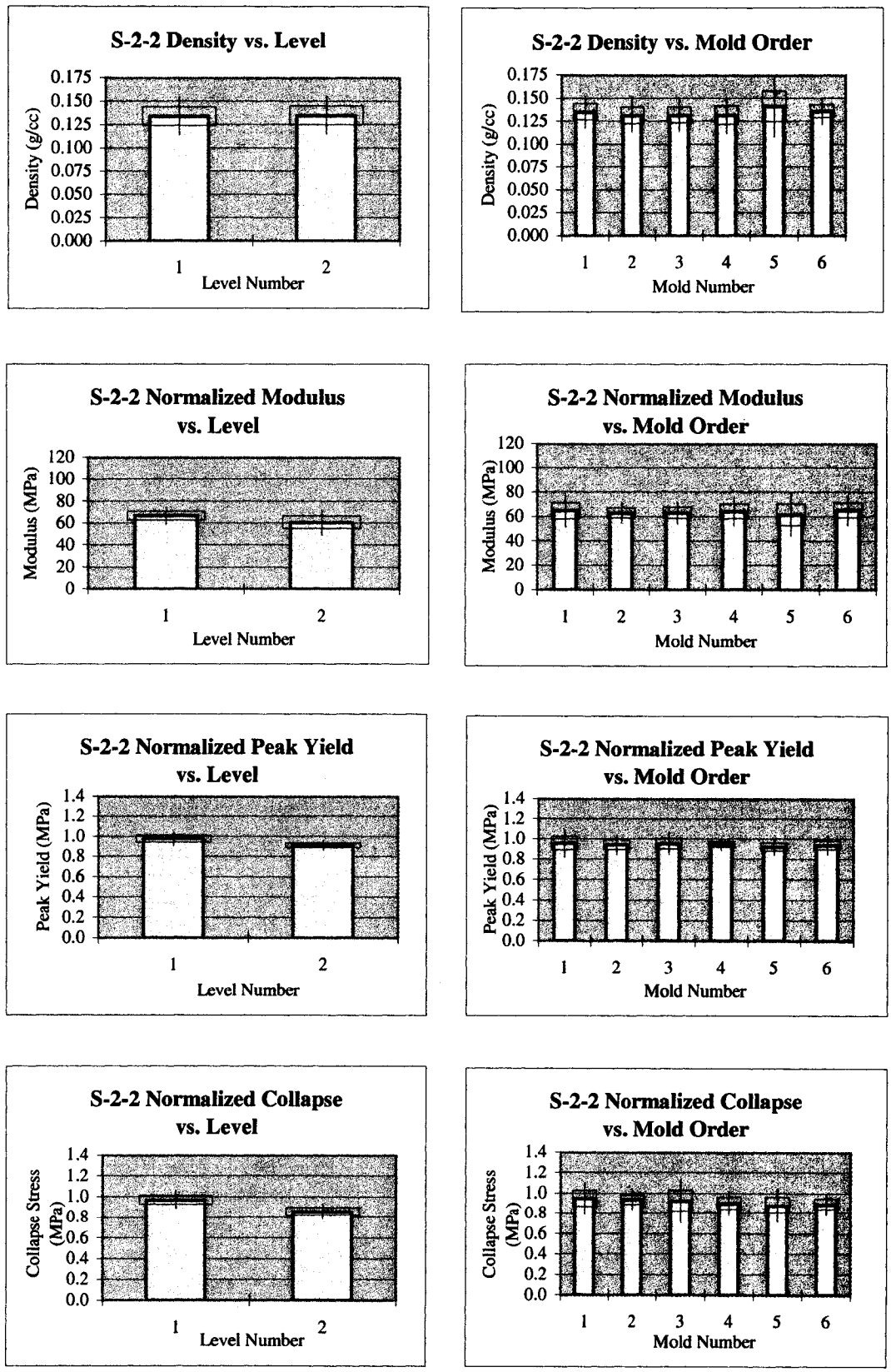

Figure-D-3: S-2-2 Density, Modulus, Peak Yield, and Collapse

Reproduced with permission of the copyright owner. Further reproduction prohibited without permission.

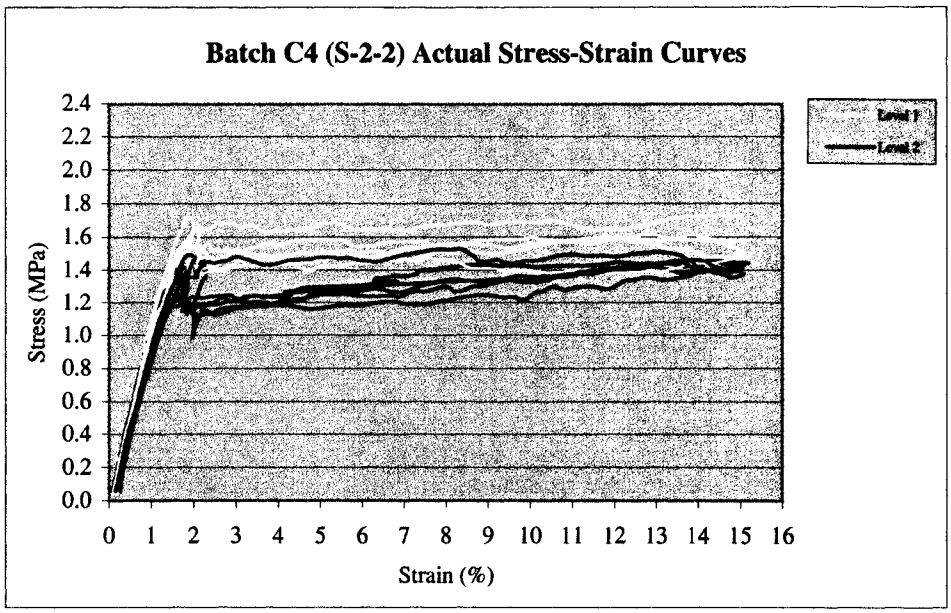

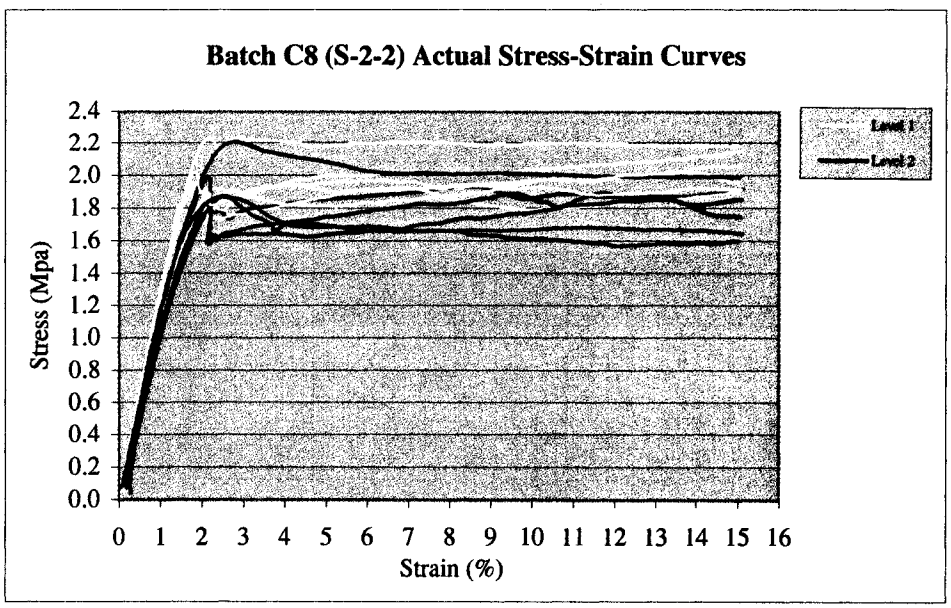

Figure-D-4: S-2-2 Actual Stress-Strain Curves (Not Normalized)

Reproduced with permission of the copyright owner. Further reproduction prohibited without permission.

Table-D.7: S-1-1 Average Density, Modulus, Peak Yield, and Collapse

	Density	Modulus	Peak Yield	Collapse
Average	0.130	67.8	1.00	0.90
Std Dev	0.007	12.1	0.10	0.11
% Dev	5.4%	17.9%	9.6%	12.2%

Table-D.8: S-1-1 Level Density, Modulus, Peak Yield, and Collapse

		LEVEL 1	LEVEL 2	LEVEL 3	LEVEL 4
Density	Average	0.129	0.129	0.129	0.131
	Std Dev	0.007	0.007	0.007	0.008
	% Dev	5.4%	5.4%	5.5%	5.8%
Modulus	Average	70.2	75.7	73.4	52.1
	Std Dev	8.7	8.2	8.1	6.4
	% Dev	12.4%	10.9%	11.0%	12.2%
Peak Yield	Average	1.01	1.10	1.02	0.87
	Std Dev	0.05	0.02	0.06	0.03
	% Dev	4.6%	1.8%	6.2%	3.7%
Collapse	Average	0.96	1.01	0.90	0.74
	Std Dev	0.05	0.03	0.06	0.02
	% Dev	5.5%	3.1%	6.7%	3.0%

Table-D.9: S-1-1 Mold Order Density, Modulus, Peak Yield, and Collapse

		MOLD 1	MOLD 2	MOLD 3	MOLD 4	MOLD 5	MOLD 6
Density	Average	0.131	0.132	0.128	0.128	0.131	0.127
	Std Dev	0.007	0.004	0.007	0.006	0.009	0.009
	% Dev	5.2%	3.3%	5.2%	4.8%	7.0%	6.9%
Modulus	Average	66.0	67.4	71.1	66.6	64.9	71.0
	Std Dev	9.1	11.9	12.8	13.4	11.6	15.6
	% Dev	13.7%	17.7%	17.9%	20.1%	17.9%	22.0%
Peak Yield	Average	0.98	0.99	1.01	1.01	1.00	1.01
	Std Dev	0.12	0.11	0.10	0.10	0.09	0.08
	% Dev	12.4%	10.7%	10.3%	9.5%	8.9%	8.4%
Collapse	Average	0.89	0.90	0.91	0.91	0.89	0.92
	Std Dev	0.12	0.12	0.12	0.12	0.11	0.11
	% Dev	13.6%	13.1%	13.6%	12.8%	11.9%	12.2%

Reproduced with permission of the copyright owner. Further reproduction prohibited without permission.

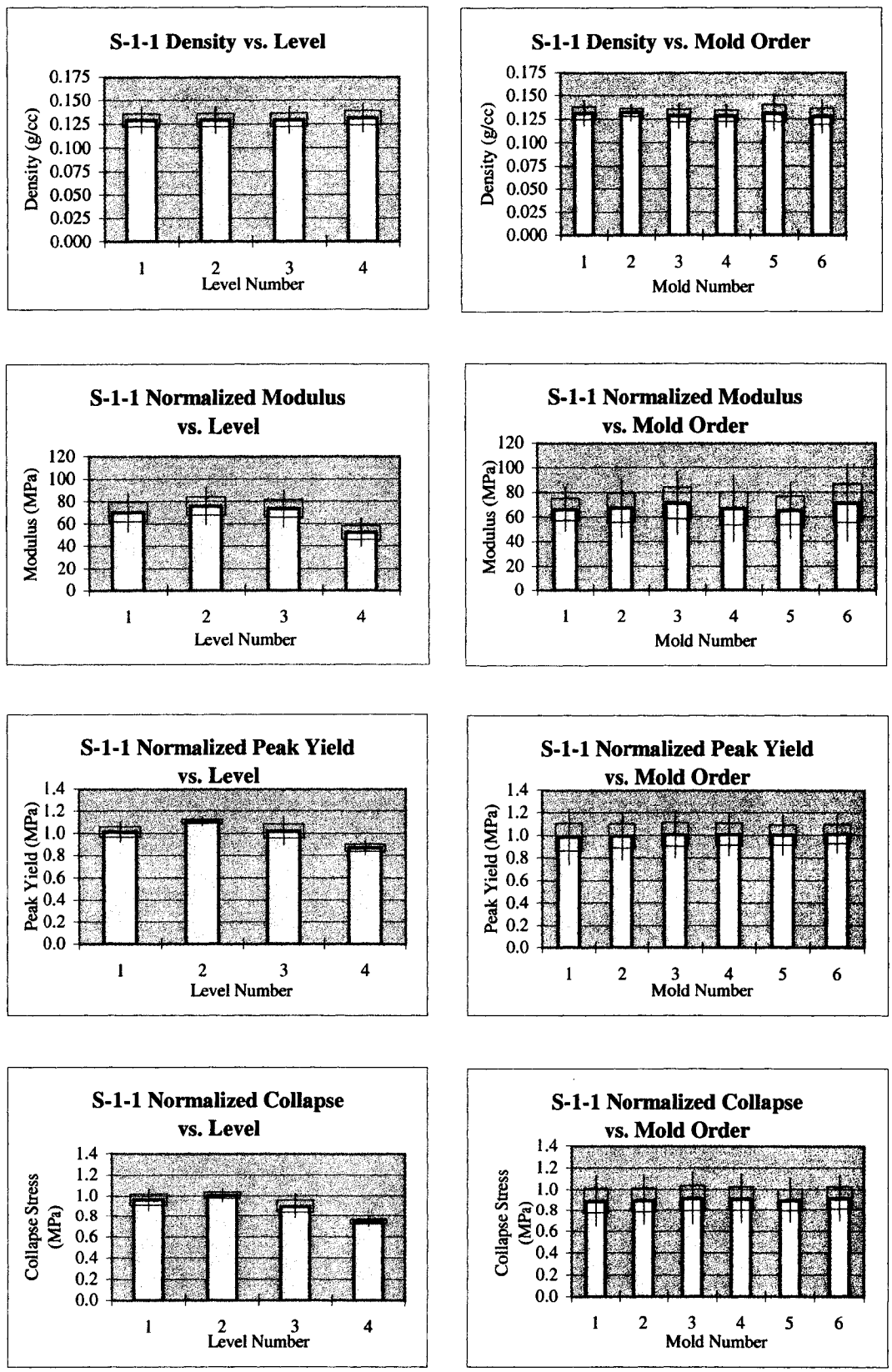

Figure-D-5: S-1-1 Density, Modulus, Peak Yield, and Collapse

Reproduced with permission of the copyright owner. Further reproduction prohibited without permission.

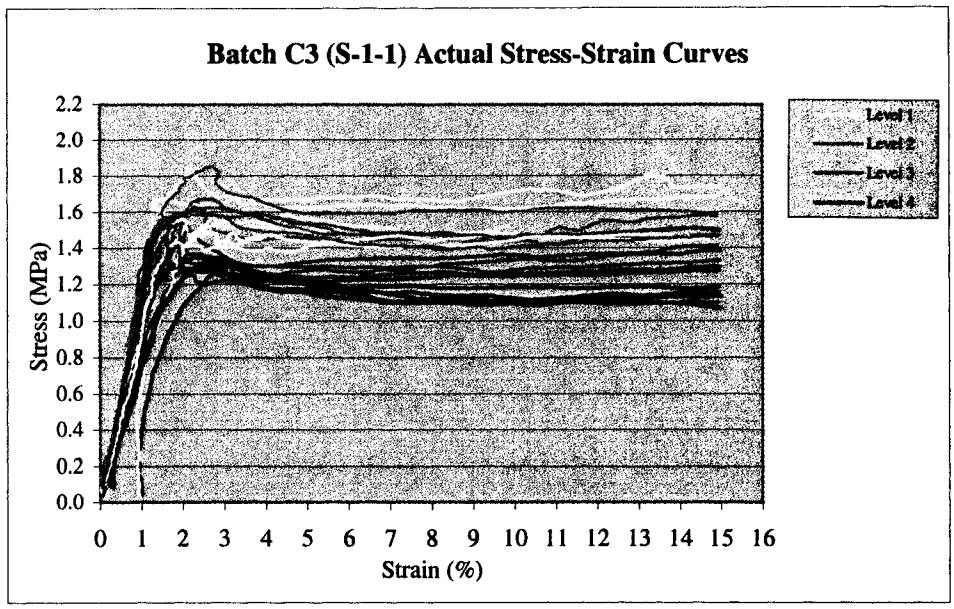

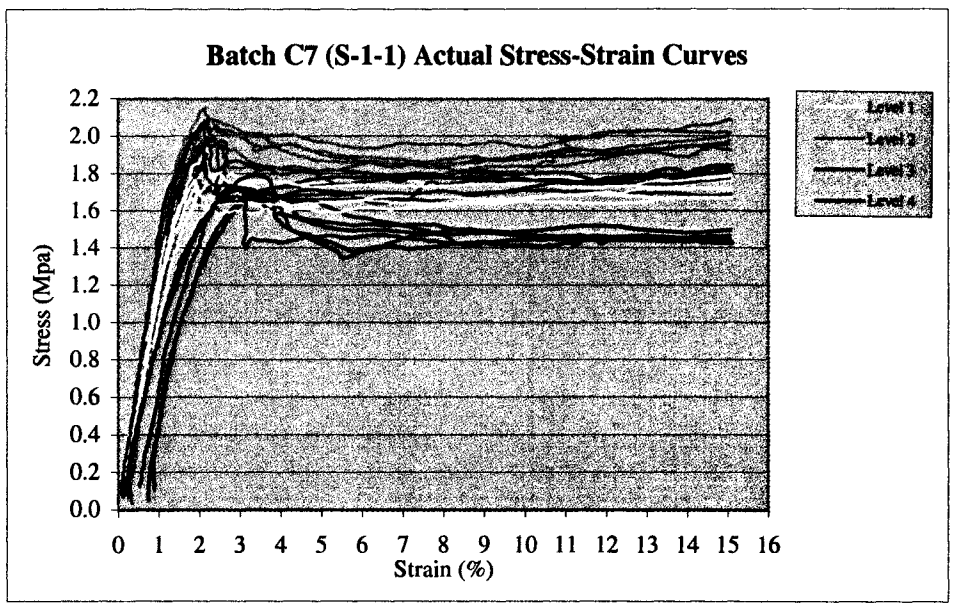

Figure-D-6: S-1-1 Actual Stress-Strain Curves (Not Normalized)

Reproduced with permission of the copyright owner. Further reproduction prohibited without permission.

Table-D.10: S-1-2 Average Density, Modulus, Peak Yield, and Collapse

	Density	Modulus	Peak Yield	Collapse
Average	0.128	69.5	1.00	0.92
Std Dev	0.005	10.8	0.09	0.09
% Dev	3.9%	15.5%	9.2%	10.2%

Table-D.11: S-1-2 Level Density, Modulus, Peak Yield, and Collapse

		LEVEL 1	LEVEL 2	LEVEL 3	LEVEL 4
Density	Average	0.127	0.127	0.128	0.129
	Std Dev	0.005	0.005	0.005	0.006
	% Dev	3.6%	4.0%	3.9%	4.3%
Modulus	Average	73.2	73.3	75.1	56.6
	Std Dev	8.3	7.8	8.7	6.8
	% Dev	11.4%	10.7%	11.5%	12.1%
Peak Yield	Average	0.96	1.12	1.04	0.89
	Std Dev	0.04	0.04	0.04	0.04
	% Dev	3.9%	3.1%	4.0%	4.0%
Collapse	Average	0.95	1.03	0.92	0.79
	Std Dev	0.04	0.05	0.03	0.05
	% Dev	4.6%	4.5%	3.4%	5.7%

Table-D.12: S-1-2 Mold Order Density, Modulus, Peak Yield, and Collapse

		MOLD 1	MOLD 2	MOLD 3	MOLD 4	MOLD 5	MOLD 6
Density	Average	0.132	0.130	0.124	0.125	0.127	0.127
	Std Dev	0.008	0.006	0.002	0.001	0.001	0.002
	% Dev	6.1%	4.7%	1.4%	1.2%	0.9%	1.9%
Modulus	Average	72.2	69.5	69.4	70.7	70.5	64.8
	Std Dev	15.4	10.5	13.8	8.8	7.7	8.7
	% Dev	21.3%	15.0%	19.8%	12.5%	10.9%	13.4%
Peak Yield	Average	1.01	1.01	1.02	1.01	0.99	0.98
	Std Dev	0.11	0.11	0.10	0.09	0.09	0.08
	% Dev	10.8%	10.4%	9.9%	9.4%	8.9%	8.2%
Collapse	Average	0.93	0.92	0.95	0.93	0.91	0.89
	Std Dev	0.12	0.11	0.12	0.09	0.08	0.07
	% Dev	12.7%	11.5%	12.3%	9.7%	8.6%	7.5%

Reproduced with permission of the copyright owner. Further reproduction prohibited without permission.

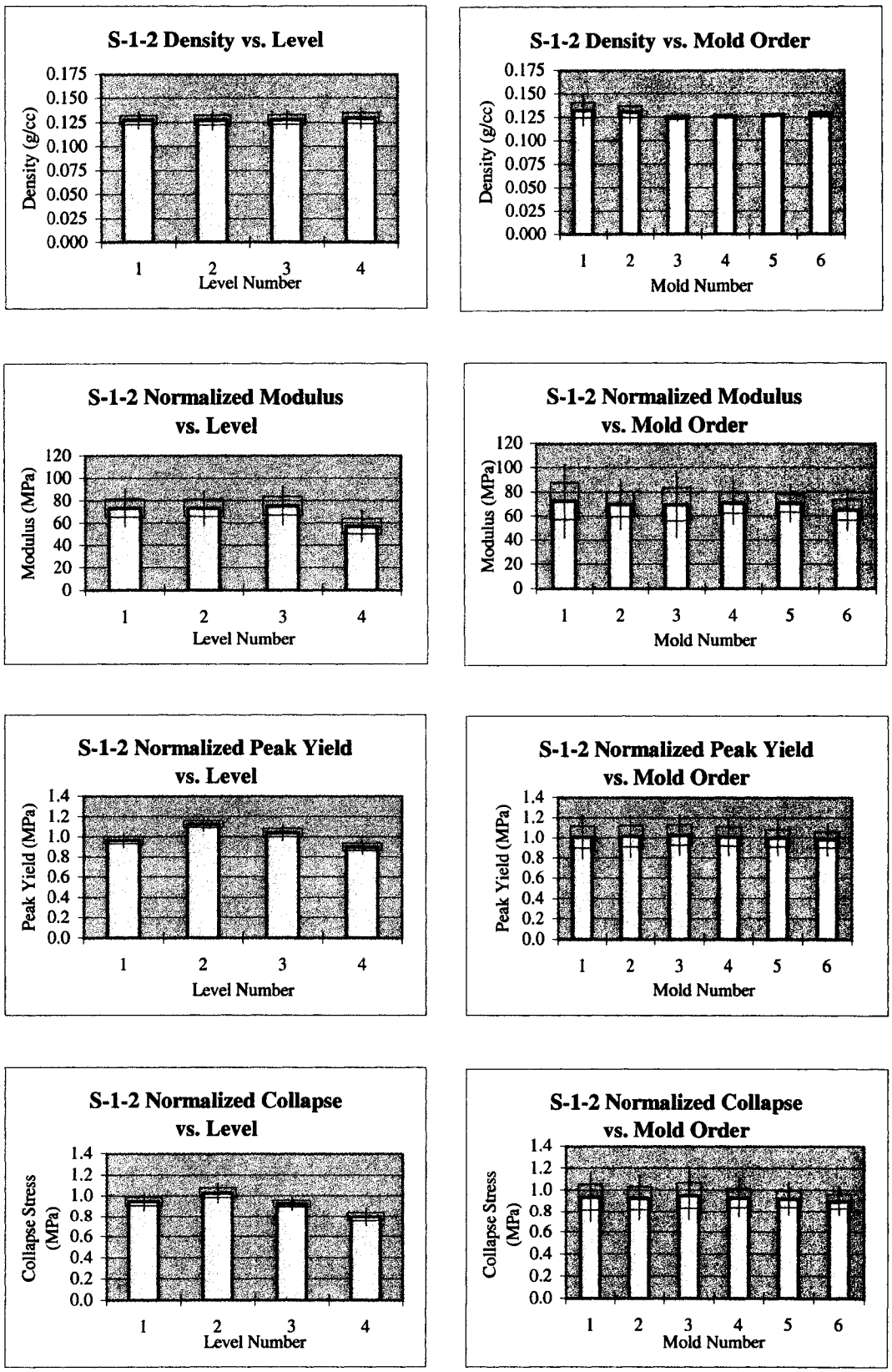

Figure-D-7: S-1-2 Density, Modulus, Peak Yield, and Collapse

Reproduced with permission of the copyright owner. Further reproduction prohibited without permission.

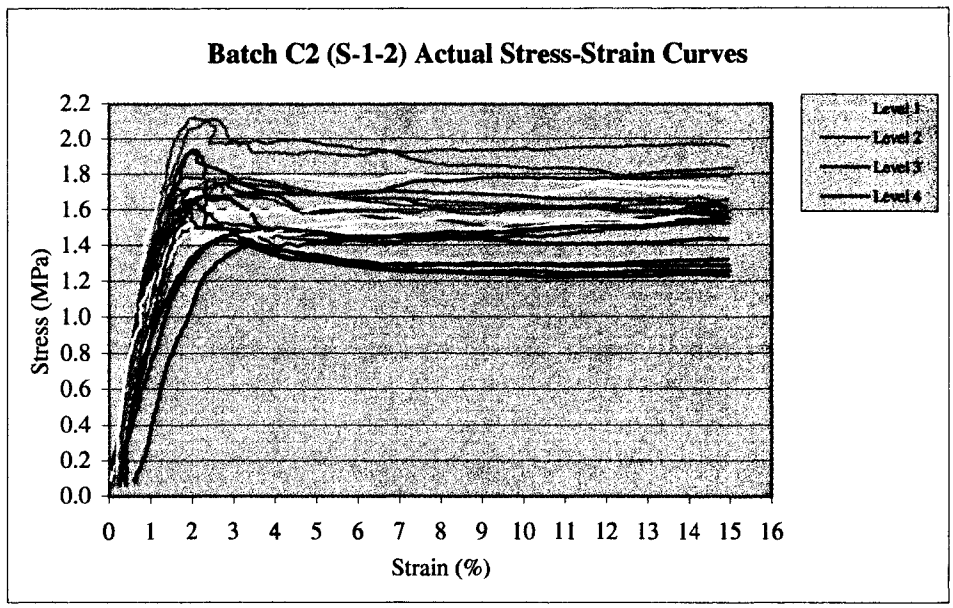

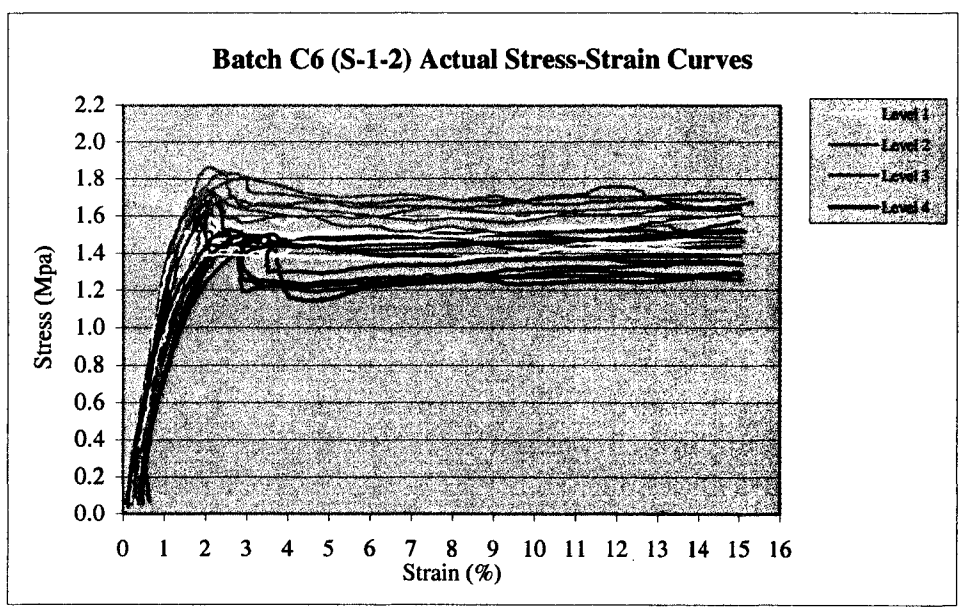

Figure-D-8: S-1-2 Actual Stress-Strain Curves (Not Normalized)

Reproduced with permission of the copyright owner. Further reproduction prohibited without permission.

Table-D.13: S-1-7 Average Density, Modulus, Peak Yield, and Collapse

	Original Density	Aged Density	Modulus	Peak Yield	Collapse
Average	0.119	0.119	69.2	1.01	0.94
Std Dev	0.006	0.006	18.2	0.10	0.09
% Dev	4.9%	4.9%	26.3%	9.6%	9.9%

Table-D.14: S-1-7 Level Density, Modulus, Peak Yield, and Collapse

		LEVEL 1	LEVEL 2	LEVEL 3	LEVEL 4
Original Density	Average	0.120	0.118	0.119	0.119
	Std Dev	0.006	0.006	0.006	0.006
	% Dev	5.0%	5.0%	4.9%	5.2%
Aged Density	Average	0.119	0.118	0.118	0.119
	Std Dev	0.006	0.006	0.006	0.006
	% Dev	5.0%	5.0%	4.9%	5.1%
Modulus	Average	81.5	80.1	67.5	47.8
	Std Dev	15.7	8.2	15.9	6.9
	% Dev	19.2%	10.3%	23.6%	14.5%
Peak Yield	Average	0.98	1.14	1.00	0.91
	Std Dev	0.07	0.03	0.06	0.02
	% Dev	6.9%	2.2%	6.3%	2.4%
Collapse	Average	0.98	1.04	0.93	0.82
	Std Dev	0.05	0.04	0.07	0.02
	% Dev	5.0%	3.9%	7.3%	2.0%

Table-D.15: S-1-7 Mold Order Density, Modulus, Peak Yield, and Collapse

		MOLD 1	MOLD 2	MOLD 3	MOLD 4	MOLD 5	MOLD 6
Original Density	Average	0.119	0.119	0.118	0.119	0.119	0.120
	Std Dev	0.003	0.004	0.005	0.007	0.007	0.009
	% Dev	2.6%	3.1%	4.1%	5.7%	6.1%	7.4%
Aged Density	Average	0.118	0.118	0.118	0.118	0.119	0.120
	Std Dev	0.003	0.004	0.005	0.007	0.007	0.009
	% Dev	2.7%	3.1%	4.1%	5.7%	6.0%	7.4%
Modulus	Average	64.1	73.0	65.8	70.5	67.1	74.8
	Std Dev	13.4	20.1	16.4	21.0	20.6	19.9
	% Dev	20.9%	27.6%	25.0%	29.8%	30.7%	26.5%
Peak Yield	Average	1.01	1.00	1.01	1.01	1.00	1.02
	Std Dev	0.12	0.11	0.10	0.09	0.09	0.10
	% Dev	11.9%	11.1%	9.8%	8.8%	9.2%	9.5%
Collapse	Average	0.93	0.95	0.95	0.96	0.93	0.94
	Std Dev	0.10	0.10	0.11	0.10	0.09	0.10
	% Dev	10.5%	10.0%	11.2%	10.2%	9.4%	10.6%

Reproduced with permission of the copyright owner. Further reproduction prohibited without permission.

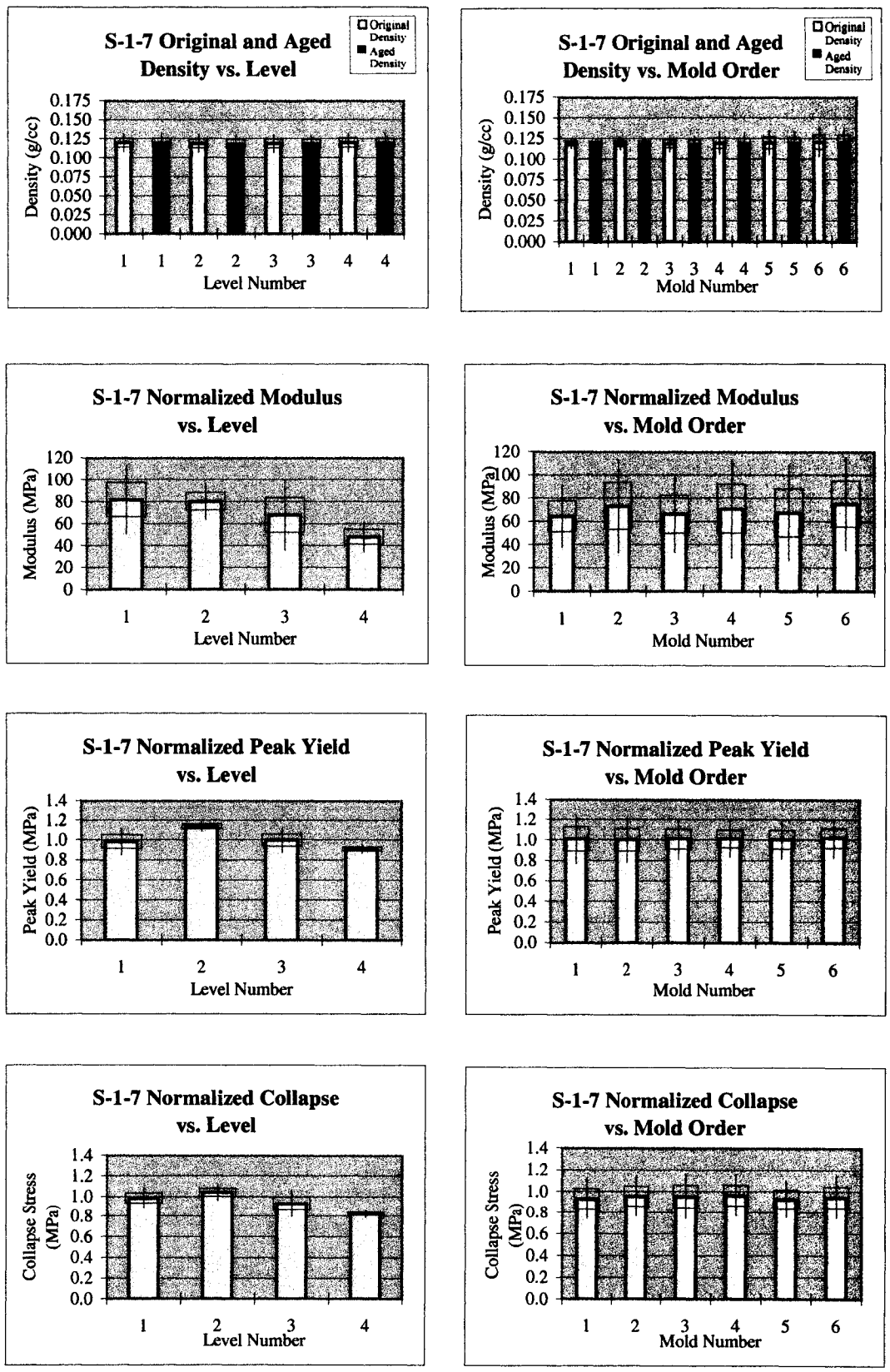

Figure-D-9: S-1-7 Density, Modulus, Peak Yield, and Collapse

Reproduced with permission of the copyright owner. Further reproduction prohibited without permission.

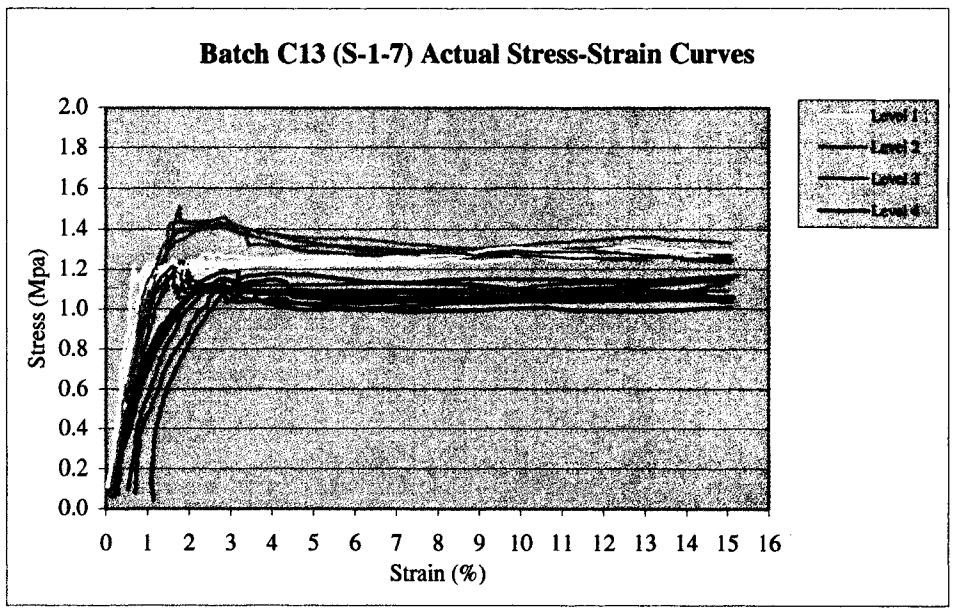

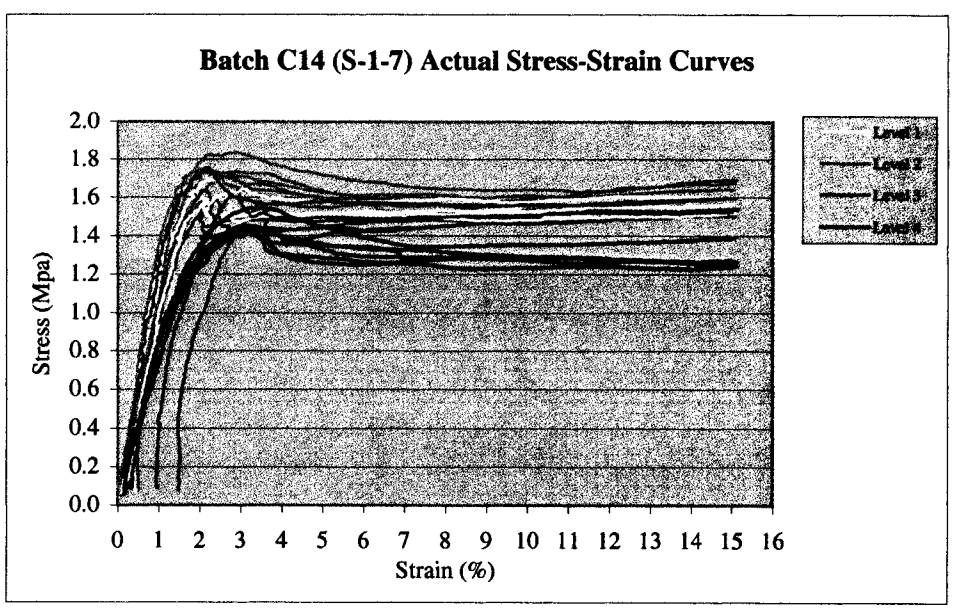

Figure-D-10: S-1-7 Actual Stress-Strain Curves (Not Normalized)

Reproduced with permission of the copyright owner. Further reproduction prohibited without permission.

Table-D.16: S-1-30 Average Density, Modulus, Peak Yield, and Collapse

	Original Density	Aged Density	Modulus	Peak Yield	Collapse
Average	0.127	0.127	67.2	1.00	0.95
Std Dev	0.013	0.013	14.9	0.09	0.08
% Dev	10.2%	10.1%	22.1%	9.1%	7.9%

Table-D.17: S-1-30 Level Density, Modulus, Peak Yield, and Collapse

		LEVEL 1	LEVEL 2	LEVEL 3	LEVEL 4
Original Density	Average	0.128	0.127	0.127	0.128
	Std Dev	0.013	0.013	0.013	0.014
	% Dev	10.4%	10.6%	10.4%	10.6%
Aged Density	Average	0.127	0.126	0.126	0.128
	Std Dev	0.013	0.013	0.013	0.013
	% Dev	10.4%	10.6%	10.3%	10.4%
Modulus	Average	75.5	70.6	69.2	53.6
	Std Dev	20.0	5.8	11.9	8.8
	% Dev	26.5%	8.3%	17.1%	16.4%
Peak Yield	Average	0.95	1.11	1.00	0.92
	Std Dev	0.07	0.07	0.04	0.03
	% Dev	7.3%	6.5%	3.8%	3.6%
Collapse	Average	0.95	1.03	0.97	0.87
	Std Dev	0.07	0.06	0.04	0.02
	% Dev	7.8%	5.8%	4.0%	2.2%

Table-D.18: S-1-30 Mold Order Density, Modulus, Peak Yield, and Collapse

		MOLD 1	MOLD 2	MOLD 3	MOLD 4	MOLD 5	MOLD 6
Original Density	Average	0.129	0.127	0.126	0.126	0.128	0.129
	Std Dev	0.014	0.013	0.014	0.015	0.013	0.013
	% Dev	10.7%	10.6%	10.8%	11.8%	10.4%	9.9%
Aged Density	Average	0.128	0.126	0.125	0.125	0.128	0.128
	Std Dev	0.014	0.013	0.013	0.015	0.013	0.013
	% Dev	10.6%	10.6%	10.7%	11.7%	10.4%	9.8%
Modulus	Average	66.8	66.7	69.3	69.4	72.0	59.2
	Std Dev	18.6	10.1	15.8	8.7	21.4	11.9
	% Dev	27.9%	15.2%	22.8%	12.5%	29.7%	20.1%
Peak Yield	Average	1.02	1.00	1.01	1.01	0.98	0.97
	Std Dev	0.11	0.10	0.10	0.09	0.08	0.08
	% Dev	10.9%	9.9%	10.0%	8.9%	8.4%	8.3%
Collapse	Average	0.97	0.96	0.97	0.97	0.94	0.93
	Std Dev	0.10	0.08	0.08	0.08	0.06	0.06
	% Dev	10.0%	8.5%	8.5%	8.0%	6.7%	6.9%

Reproduced with permission of the copyright owner. Further reproduction prohibited without permission.

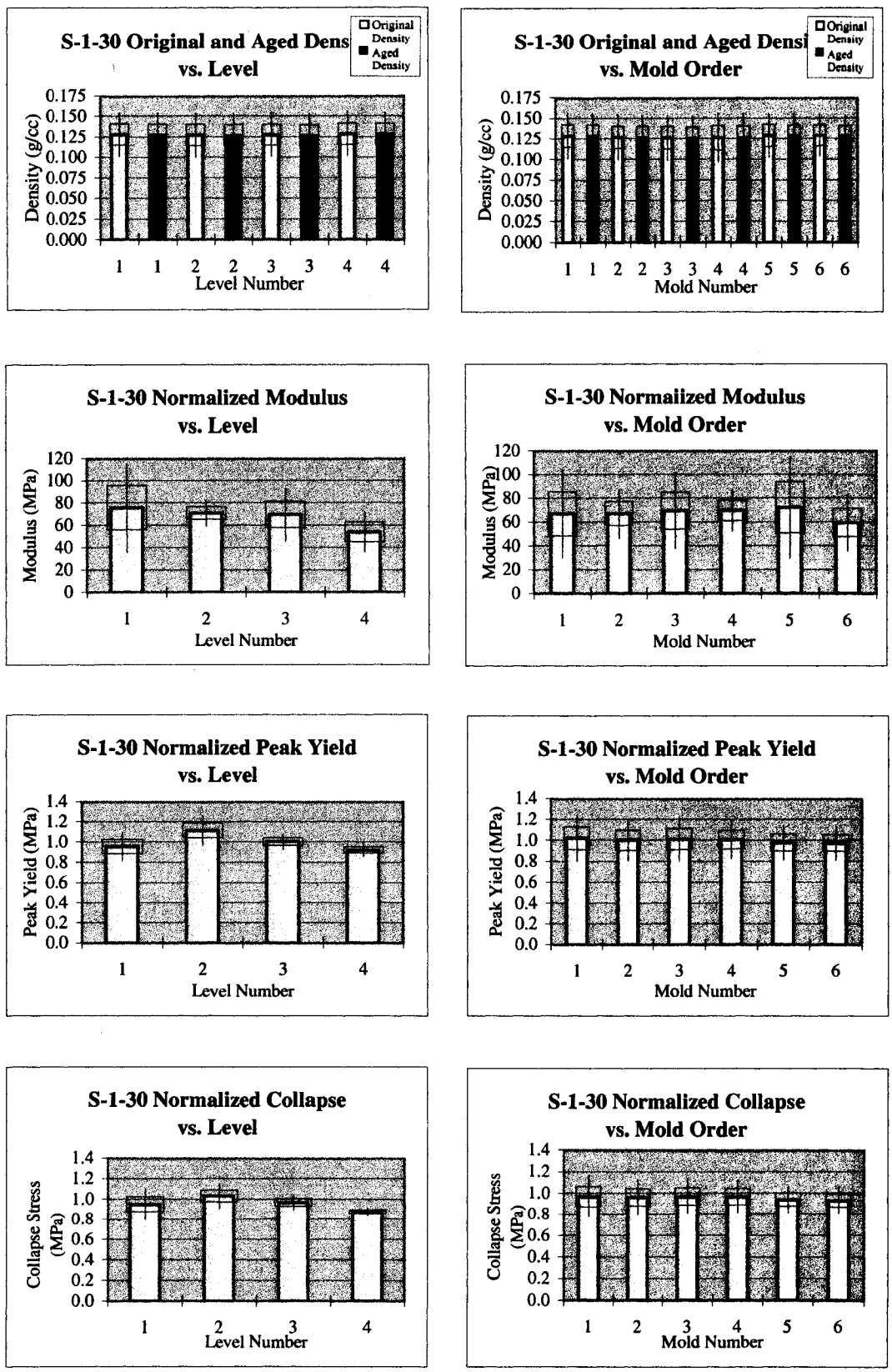

Figure-D-11: S-1-30 Density, Modulus, Peak Yield, and Collapse

Reproduced with permission of the copyright owner. Further reproduction prohibited without permission.

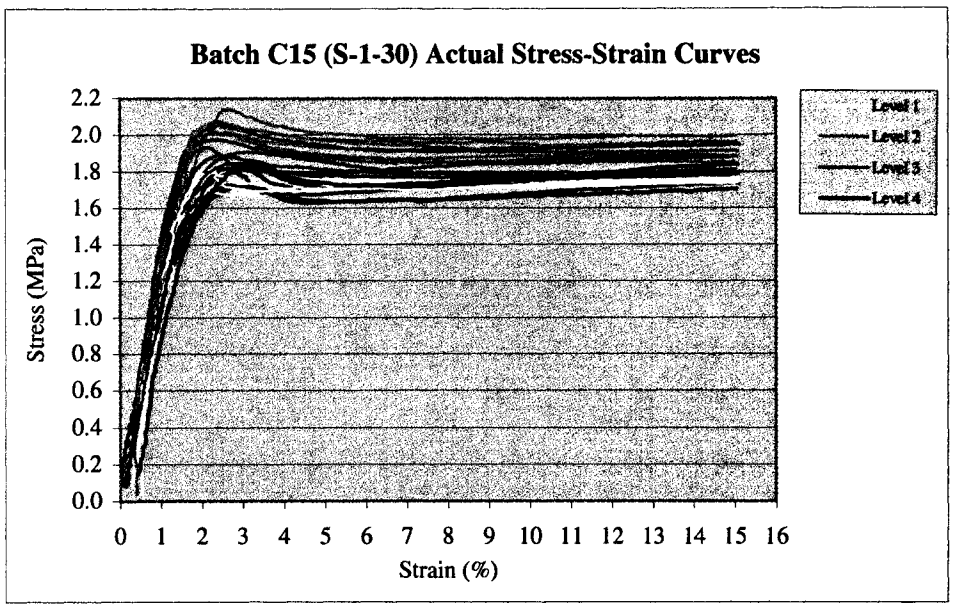

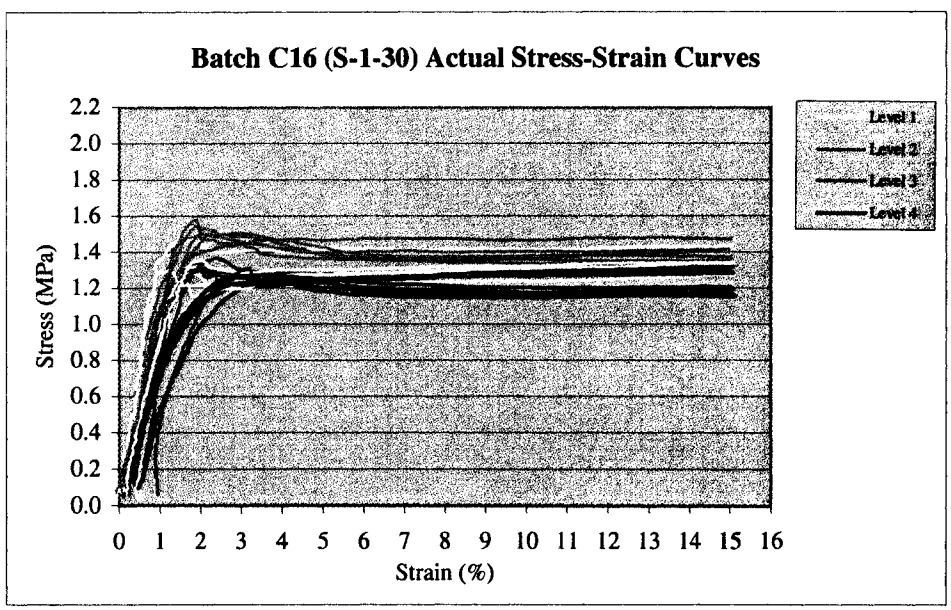

Figure-D-12: S-1-30 Actual Stress-Strain Curves (Not Normalized)

Reproduced with permission of the copyright owner. Further reproduction prohibited without permission.

Table-D.19: S-1-90 Average Density, Modulus, Peak Yield, and Collapse

	Original Density	Aged Density	Modulus	Peak Yield	Collapse
Average	0.119	0.119	65.5	1.01	0.97
Std Dev	0.002	0.002	15.3	0.09	0.07
% Dev	1.3%	1.3%	23.3%	9.0%	7.7%

Table-D.20: S-1-90 Level Density, Modulus, Peak Yield, and Collapse

		LEVEL 1	LEVEL 2	LEVEL 3	LEVEL 4
Original Density	Average	0.119	0.118	0.118	0.119
	Std Dev	0.002	0.002	0.001	0.001
	% Dev	1.6%	1.3%	1.1%	1.0%
Aged Density	Average	0.119	0.118	0.118	0.119
	Std Dev	0.002	0.002	0.001	0.001
	% Dev	1.6%	1.3%	1.1%	1.0%
Modulus	Average	70.7	75.8	63.5	52.5
	Std Dev	14.1	13.4	15.4	6.9
	% Dev	19.9%	17.7%	24.2%	13.1%
Peak Yield	Average	0.99	1.14	1.01	0.92
	Std Dev	0.03	0.05	0.06	0.02
	% Dev	3.3%	4.8%	5.9%	2.3%
Collapse	Average	0.99	1.06	0.98	0.87
	Std Dev	0.02	0.04	0.05	0.02
	% Dev	2.5%	3.5%	4.9%	2.5%

Table-D.21: S-1-90 Mold Order Density, Modulus, Peak Yield, and Collapse

		MOLD 1	MOLD 2	MOLD 3	MOLD 4	MOLD 5	MOLD 6
Original Density	Average	0.118	0.117	0.119	0.118	0.120	0.121
	Std Dev	0.001	0.001	0.000	0.001	0.001	0.001
	% Dev	1.2%	0.6%	0.4%	1.1%	0.9%	1.2%
Aged Density	Average	0.117	0.117	0.118	0.118	0.120	0.120
	Std Dev	0.002	0.001	0.001	0.001	0.001	0.001
	% Dev	1.3%	0.8%	0.5%	1.0%	0.9%	1.1%
Modulus	Average	70.5	67.1	65.1	70.4	62.5	58.2
	Std Dev	19.4	15.1	18.1	13.8	13.5	12.5
	% Dev	27.5%	22.5%	27.7%	19.6%	21.6%	21.5%
Peak Yield	Average	1.05	1.03	1.03	1.01	0.99	0.98
	Std Dev	0.11	0.10	0.09	0.08	0.08	0.09
	% Dev	10.7%	9.9%	9.1%	8.2%	8.5%	8.7%
Collapse	Average	1.00	0.98	0.99	0.97	0.96	0.95
	Std Dev	0.10	0.08	0.08	0.07	0.07	0.07
	% Dev	9.8%	8.2%	8.1%	6.9%	7.2%	6.8%

Reproduced with permission of the copyright owner. Further reproduction prohibited without permission.

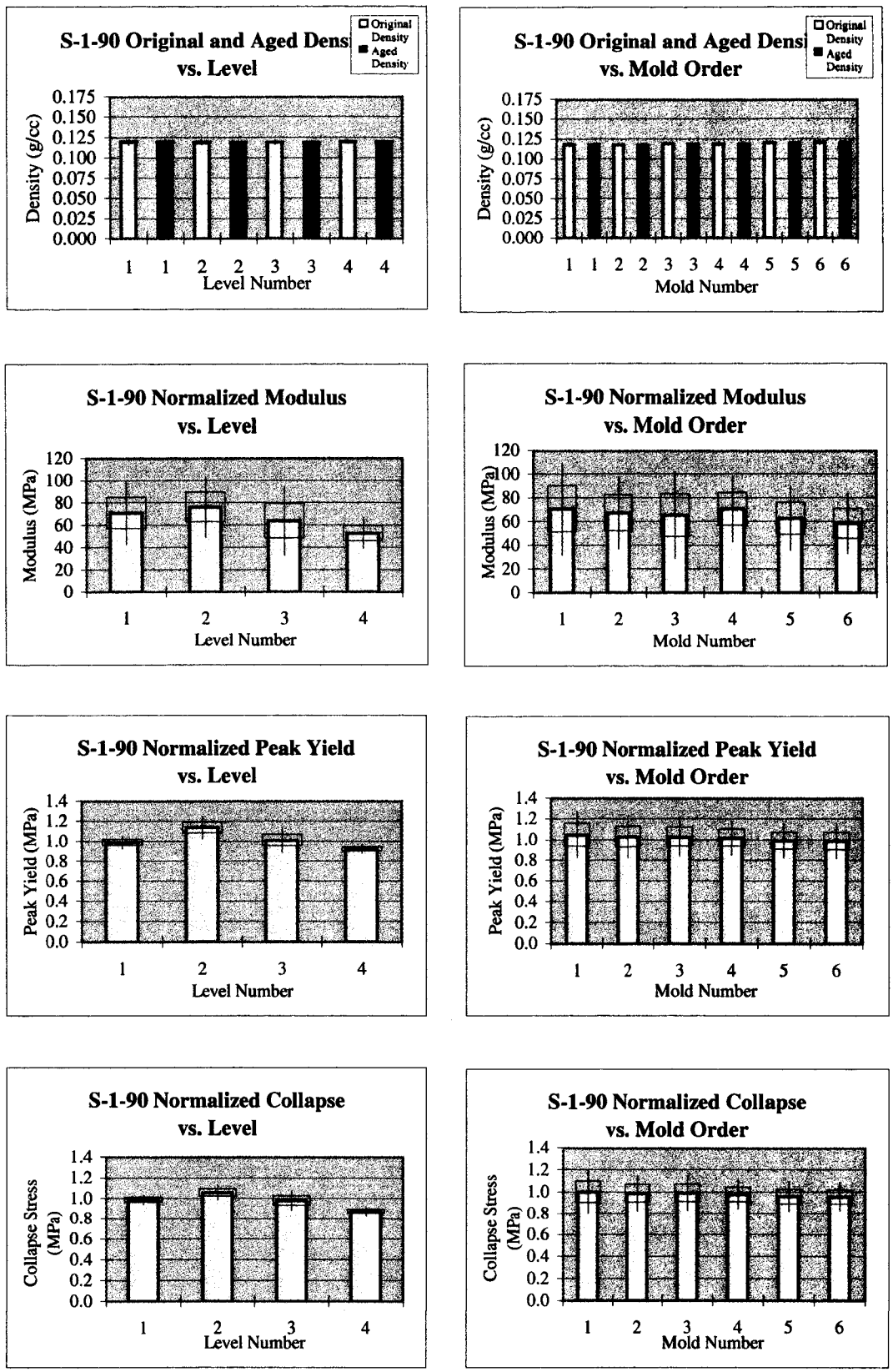

Figure-D-13: S-1-90 Density, Modulus, Peak Yield, and Collapse

Reproduced with permission of the copyright owner. Further reproduction prohibited without permission.

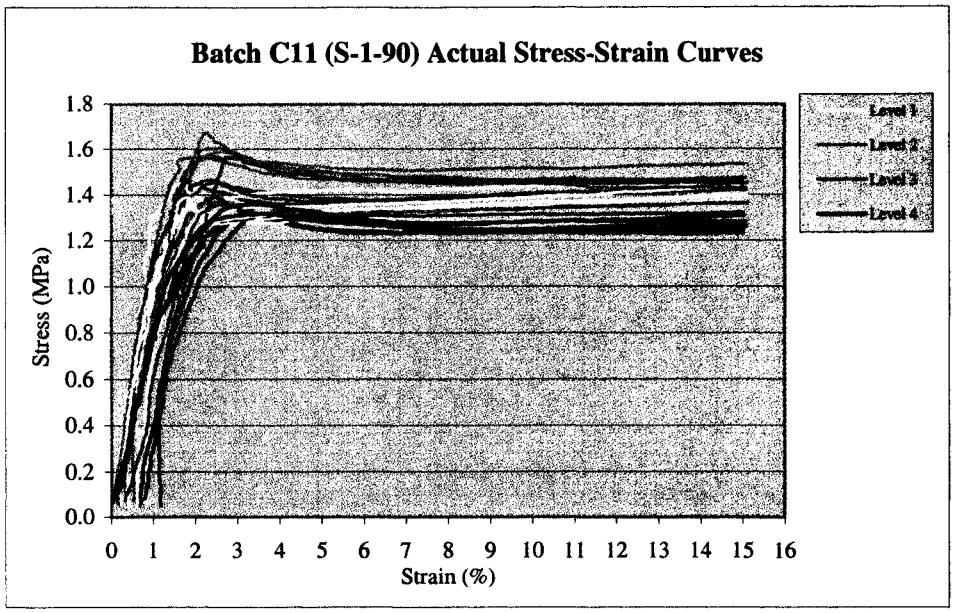

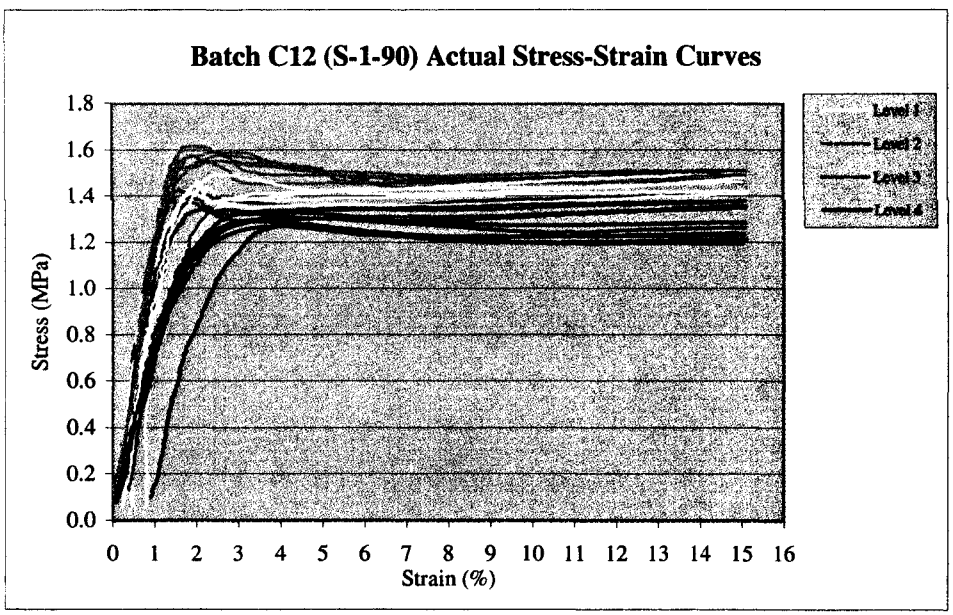

Figure-D-14: S-1-90 Actual Stress-Strain Curves (Not Normalized)

Reproduced with permission of the copyright owner. Further reproduction prohibited without permission.

Table-D-22: T-1-2 Average Density, Modulus, Peak Yield, and Collapse

	Density	Modulus	Peak Yield	Collapse
Average	0.123	67.2	1.03	0.94
Std Dev	0.010	16.4	0.13	0.12
% Dev	8.4%	24.3%	12.7%	12.9%

Table-D-23: T-1-2 Level Density, Modulus, Peak Yield, and Collapse

		LEVEL 1	LEVEL 2	LEVEL 3	LEVEL 4	LEVEL 5	LEVEL 6	LEVEL 7
Density	Average	0.120	0.121	0.122	0.123	0.124	0.124	0.125
	Std Dev	0.012	0.012	0.013	0.012	0.013	0.012	0.012
	% Dev	10.0%	10.0%	10.3%	10.1%	10.2%	10.0%	9.9%
Modulus	Average	63.8	67.6	73.9	79.0	80.2	80.3	81.1
	Std Dev	14.3	14.1	12.8	13.9	9.0	8.6	16.4
	% Dev	22.4%	20.9%	17.3%	17.6%	11.2%	13.1%	20.2%
Peak Yield	Average	0.97	1.02	1.10	1.14	1.18	1.18	1.17
	Std Dev	0.03	0.05	0.06	0.06	0.03	0.02	0.04
	% Dev	3.2%	5.1%	5.5%	5.2%	2.7%	1.9%	3.1%
Collapse	Average	0.88	0.96	0.99	1.05	1.07	1.08	1.07
	Std Dev	0.04	0.07	0.06	0.04	0.07	0.06	0.03
	% Dev	5.1%	7.8%	5.7%	4.3%	6.3%	5.2%	3.1%

		LEVEL 8	LEVEL 9	LEVEL 10	LEVEL 11	LEVEL 12	LEVEL 13	LEVEL 14
Density	Average	0.125	0.125	0.124	0.124	0.123	0.122	0.122
	Std Dev	0.012	0.012	0.011	0.011	0.011	0.010	0.010
	% Dev	9.7%	9.4%	9.1%	8.9%	8.7%	8.3%	8.1%
Modulus	Average	77.3	72.5	61.7	59.9	55.9	45.2	42.0
	Std Dev	12.3	15.1	11.8	12.2	9.3	6.7	1.5
	% Dev	15.9%	20.8%	19.1%	20.4%	16.6%	14.8%	3.7%
Peak Yield	Average	1.13	1.09	1.02	0.95	0.88	0.83	0.82
	Std Dev	0.04	0.03	0.01	0.03	0.02	0.07	0.06
	% Dev	3.7%	3.2%	0.7%	2.8%	1.9%	8.1%	7.8%
Collapse	Average	1.03	0.98	0.91	0.85	0.81	0.77	0.73
	Std Dev	0.06	0.03	0.02	0.01	0.03	0.05	0.06
	% Dev	5.5%	2.6%	2.1%	0.7%	3.2%	5.9%	7.9%

Table-D-24: T-1-2 Mold Order Density, Modulus, Peak Yield, and Collapse

		MOLD1	MOLD2
Density	Average	0.123	0.123
	Std Dev	0.010	0.011
	% Dev	7.7%	9.2%
Modulus	Average	69.8	64.5
	Std Dev	18.1	14.3
	% Dev	25.9%	22.1%
Peak Yield	Average	1.04	1.03
	Std Dev	0.13	0.13
	% Dev	13.0%	12.5%
Collapse	Average	0.94	0.94
	Std Dev	0.12	0.12
	% Dev	13.0%	13.0%

Reproduced with permission of the copyright owner. Further reproduction prohibited without permission.

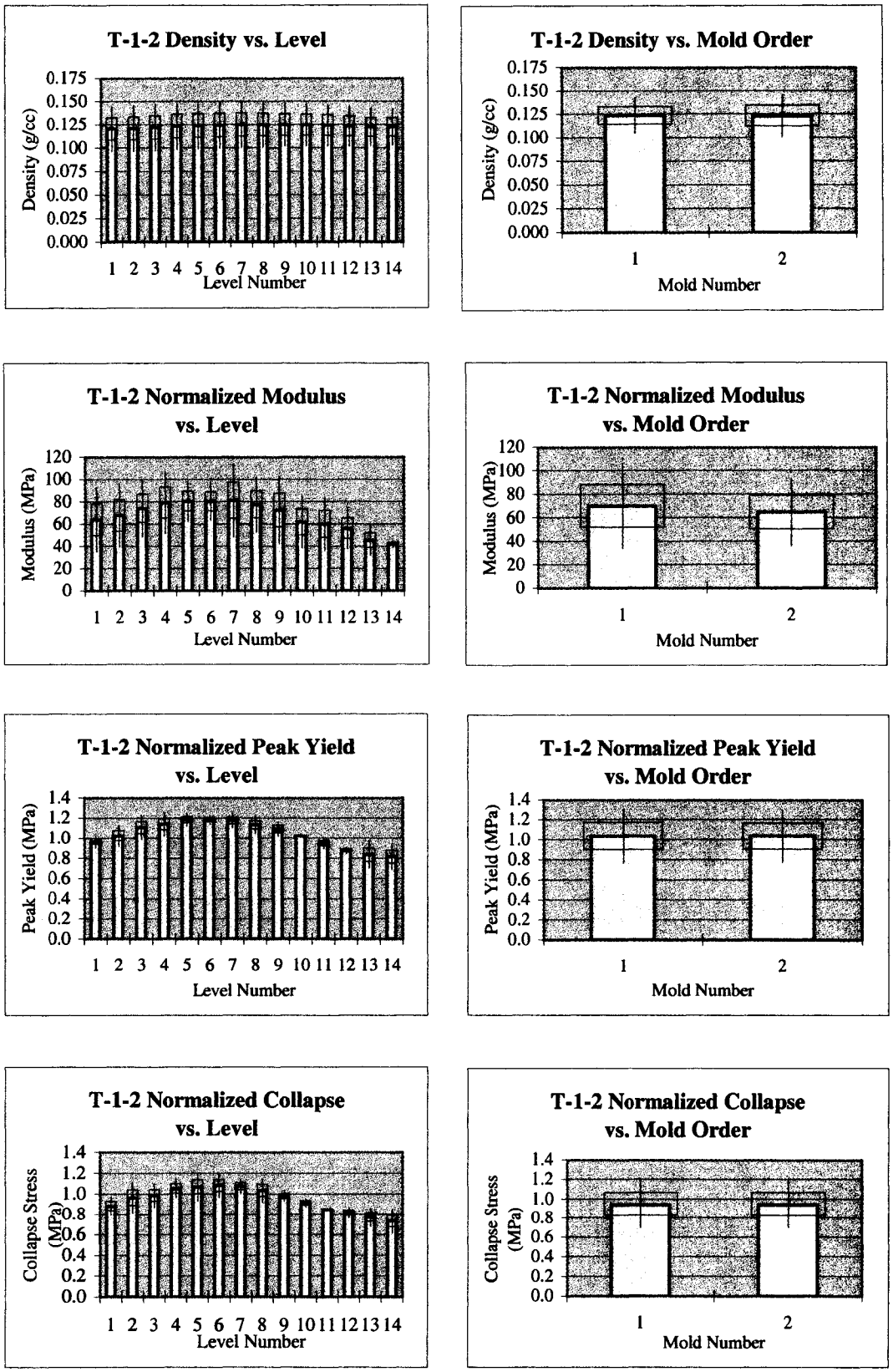

Figure-D-15: T-1-2 Density, Modulus, Peak Yield, and Collapse

Reproduced with permission of the copyright owner. Further reproduction prohibited without permission.

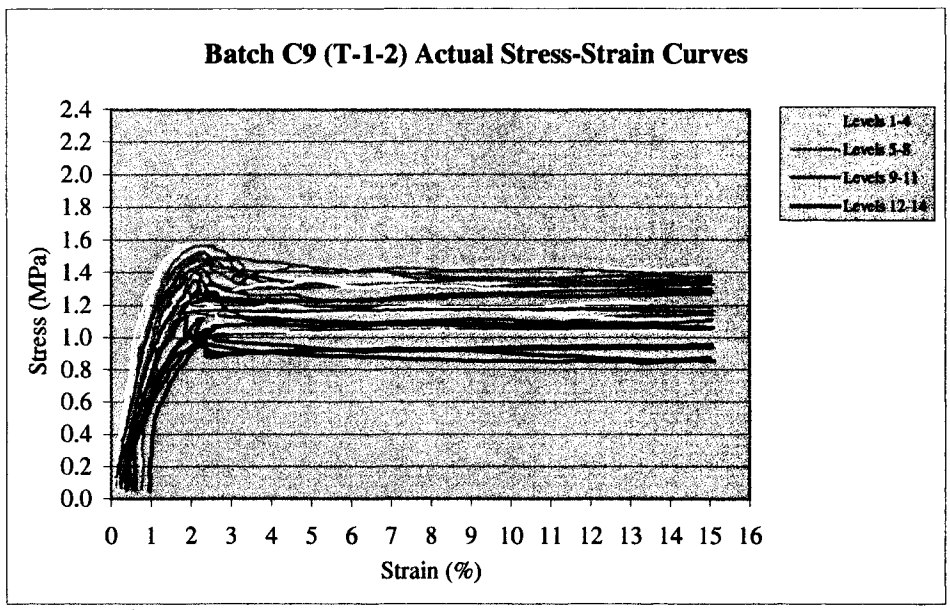

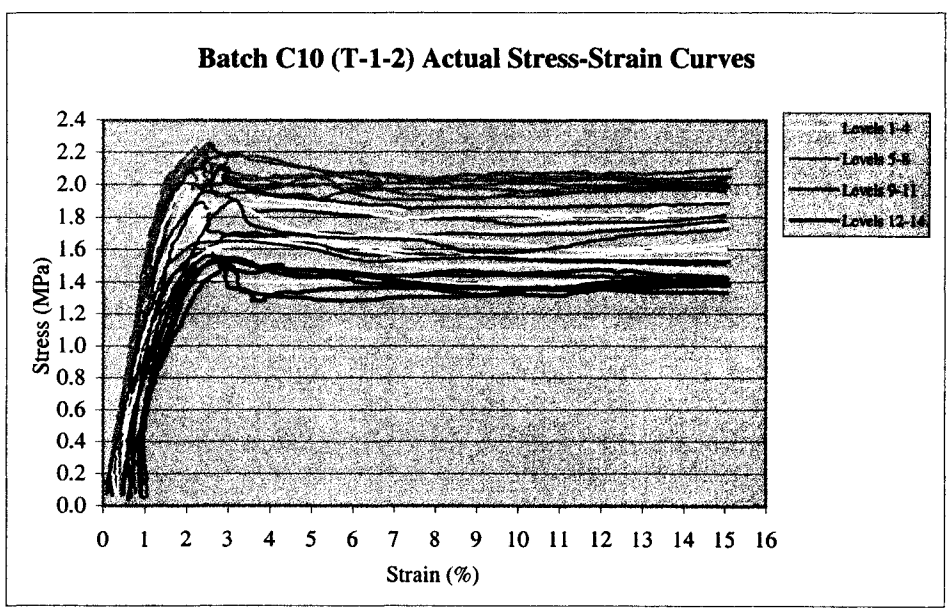

Figure-D-16: T-1-2 Actual Stress-Strain Curves (Not Normalized)

Reproduced with permission of the copyright owner. Further reproduction prohibited without permission.

Table-D-25: R-1-3 Average Density, Modulus, Peak Yield, and Collapse

	Density	Modulus	Peak Yield	Collapse
Average	0.101	35.7	0.97	0.88
Std Dev	0.004	3.9	0.07	0.05
% Dev	3.8%	10.9%	7.2%	5.7%

Table-D-26: R-1-3 Level Density, Modulus, Peak Yield, and Collapse

		LEVEL 1	LEVEL 2	LEVEL 3	LEVEL 4
Density	Average	0.099	0.100	0.100	0.107
	Std Dev	0.001	0.002	0.002	0.002
	% Dev	1.2%	2.3%	2.4%	1.5%
Modulus	Average	34.5	34.7	38.3	35.5
	Std Dev	2.4	2.1	4.6	4.9
	% Dev	6.9%	6.0%	12.1%	13.7%
Peak Yield	Average	1.00	0.99	1.00	0.87
	Std Dev	0.01	0.02	0.03	0.07
	% Dev	1.2%	2.1%	3.0%	8.4%
Collapse	Average	0.92	0.89	0.91	0.82
	Std Dev	0.01	0.03	0.02	0.05
	% Dev	1.4%	3.2%	2.7%	6.4%

Reproduced with permission of the copyright owner. Further reproduction prohibited without permission.

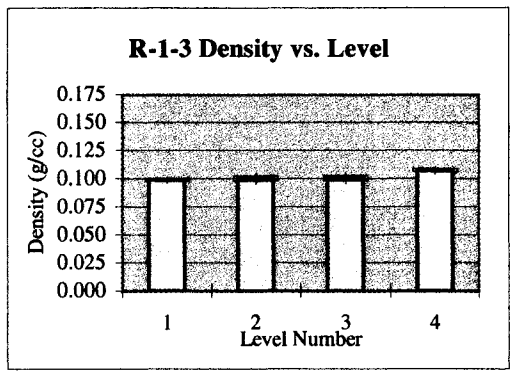

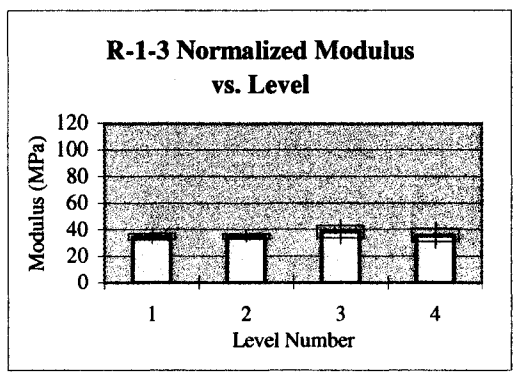

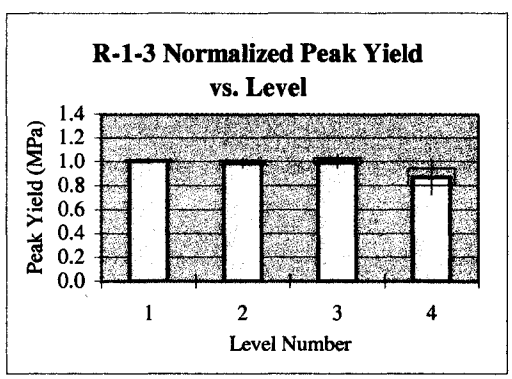

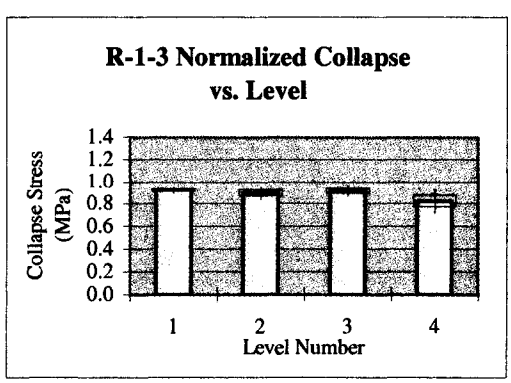

Figure-D-17: R-1-3 Density, Modulus, Peak Yield, and Collapse

Reproduced with permission of the copyright owner. Further reproduction prohibited without permission.

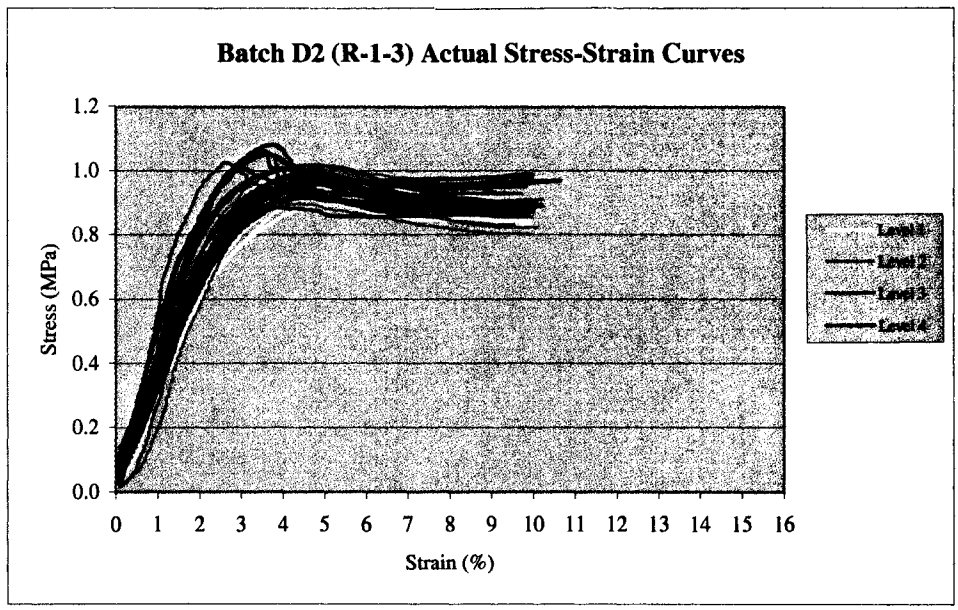

Figure-D-18: R-1-3 Actual Stress-Strain Curves (Not Normalized)

Reproduced with permission of the copyright owner. Further reproduction prohibited without permission.

APPENDIX E

CELL MORPHOLOGY IMAGES, TABLES, AND GRAPHS

Reproduced with permission of the copyright owner. Further reproduction prohibited without permission.

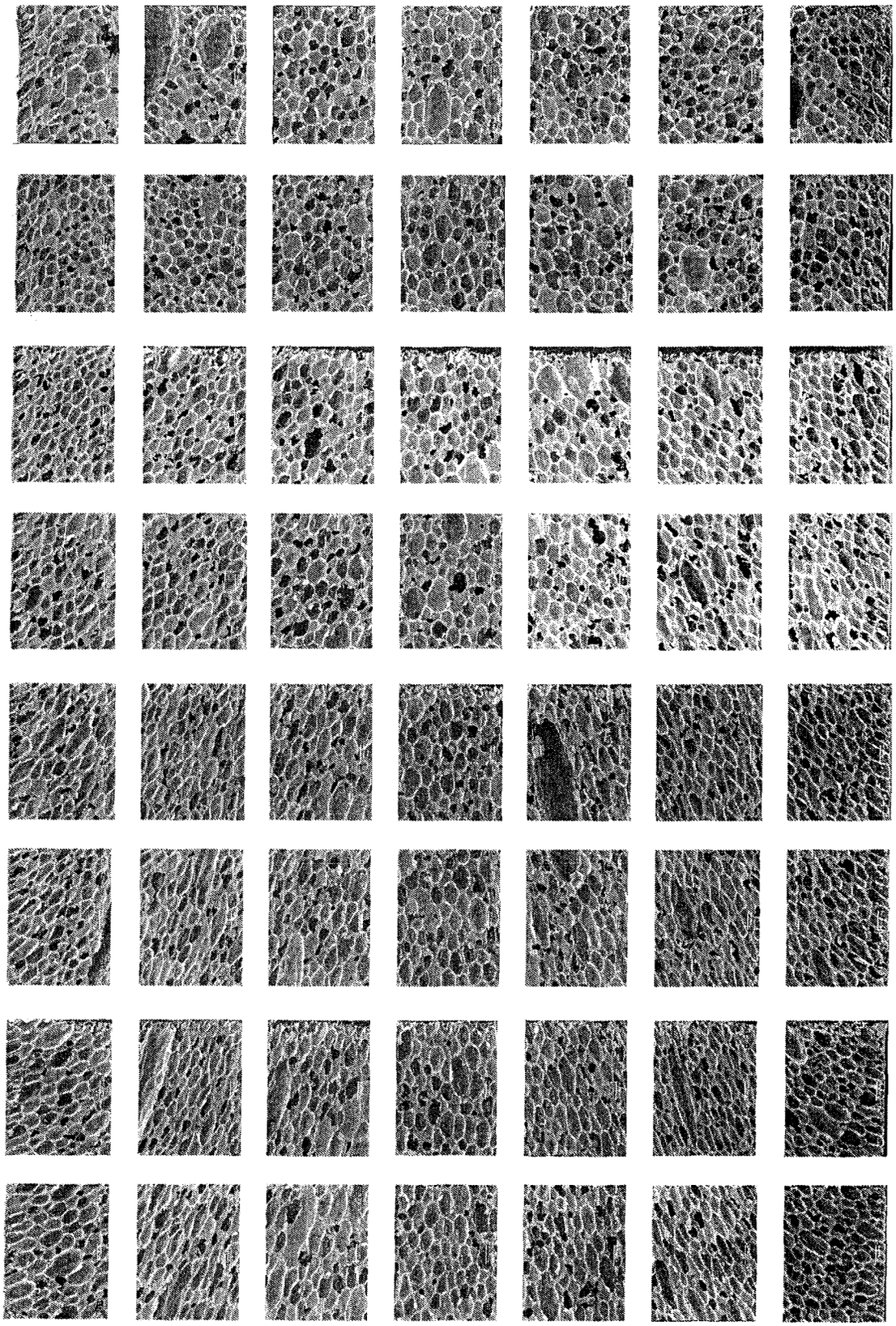

Figure-E.1: Small Mold Parallel Images

Reproduced with permission of the copyright owner. Further reproduction prohibited without permission.

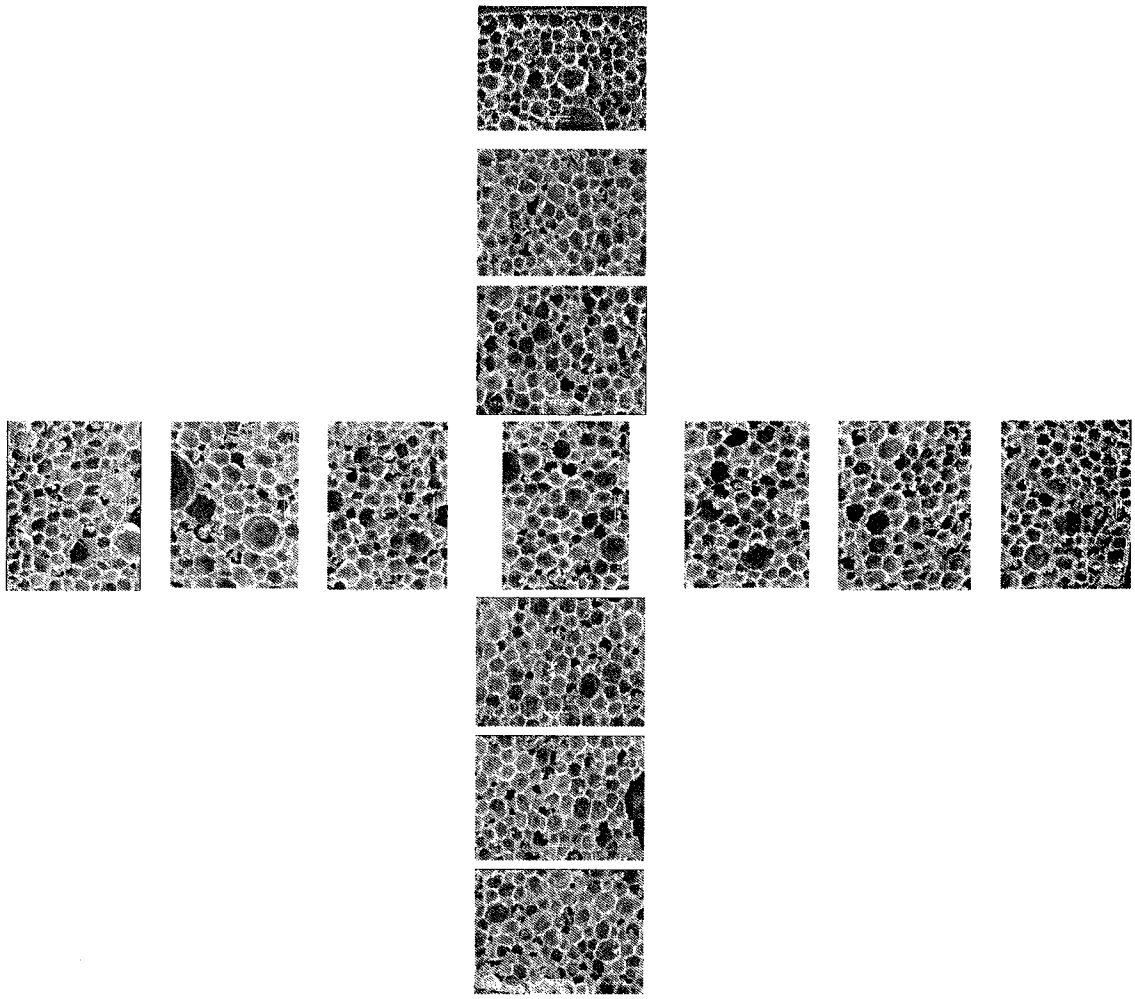

Figure-E.2: Small Mold Level 1 Perpendicular Sample

Reproduced with permission of the copyright owner. Further reproduction prohibited without permission.

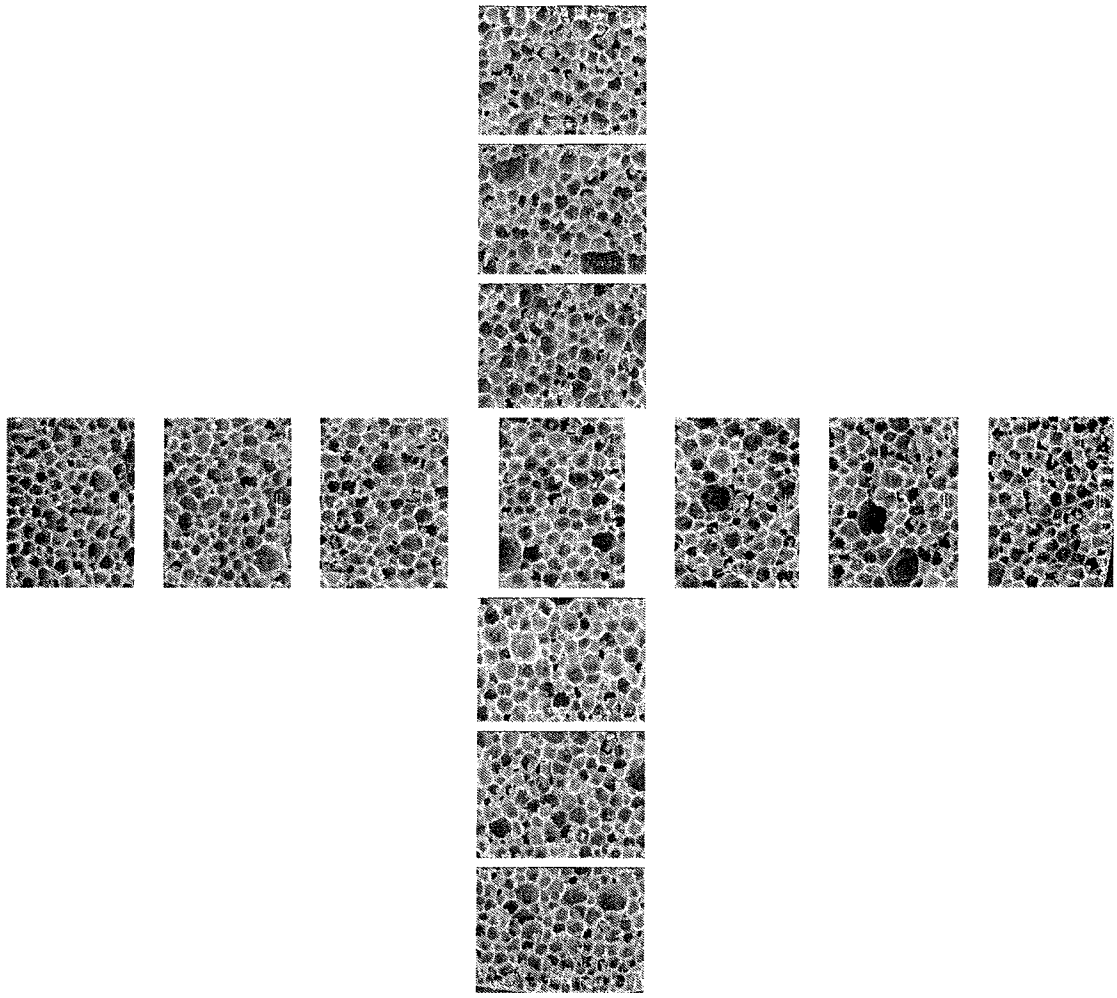

Figure-E.3: Small Mold Level 2 Perpendicular Sample

Reproduced with permission of the copyright owner. Further reproduction prohibited without permission.

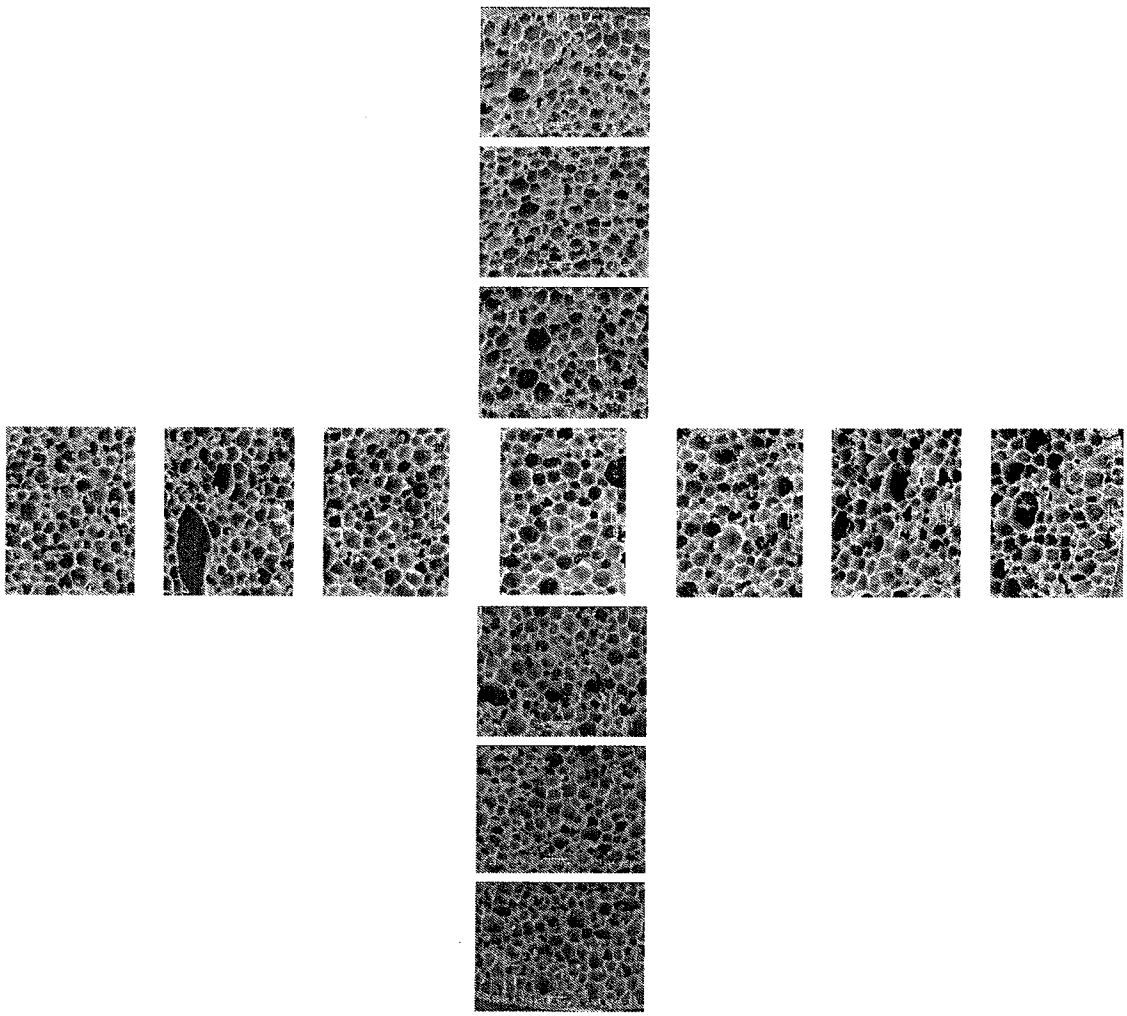

Figure-E.4: Small Mold Level 3 Perpendicular Sample

Reproduced with permission of the copyright owner. Further reproduction prohibited without permission.

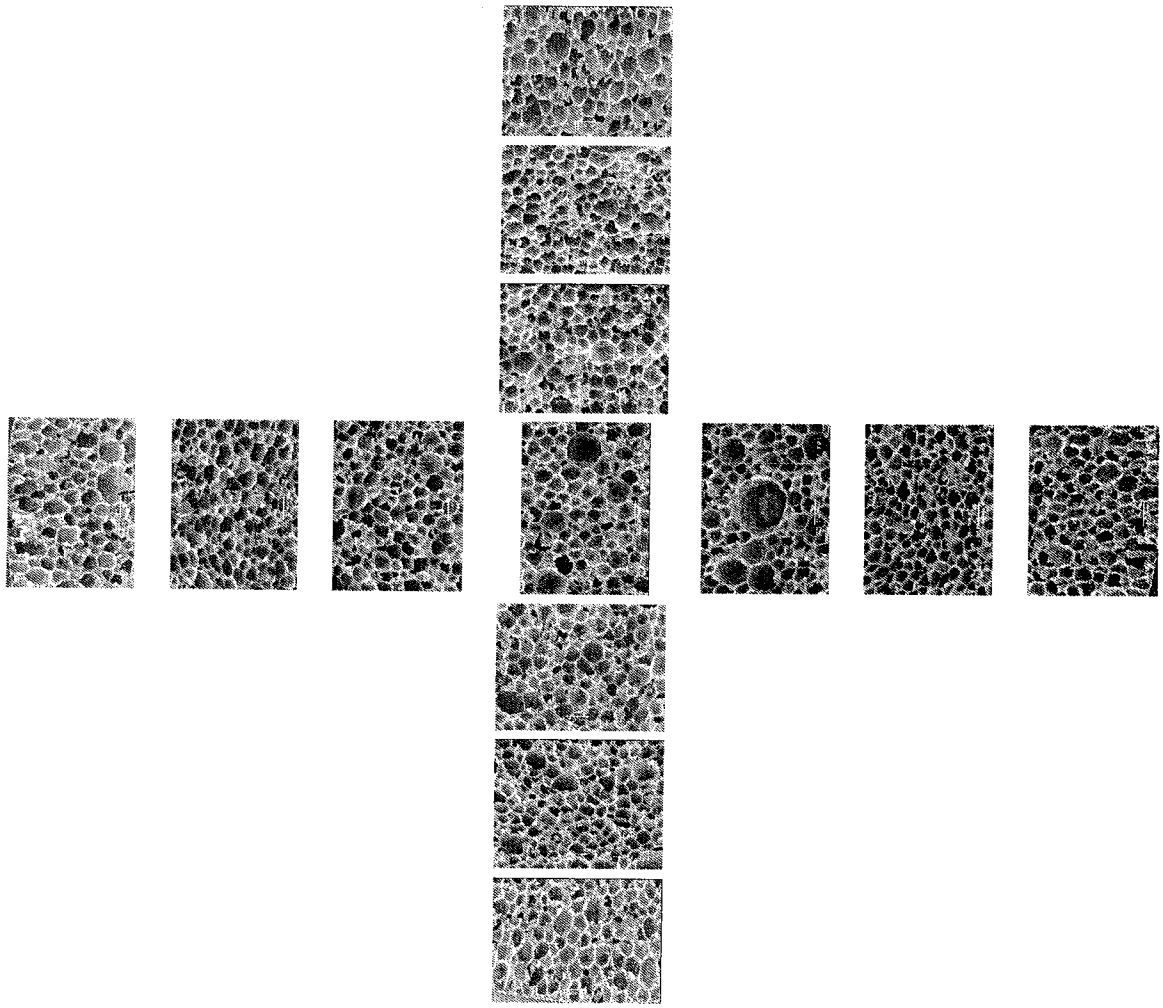

Figure-E.5: Small Mold Level 4 Perpendicular Sample

Reproduced with permission of the copyright owner. Further reproduction prohibited without permission.

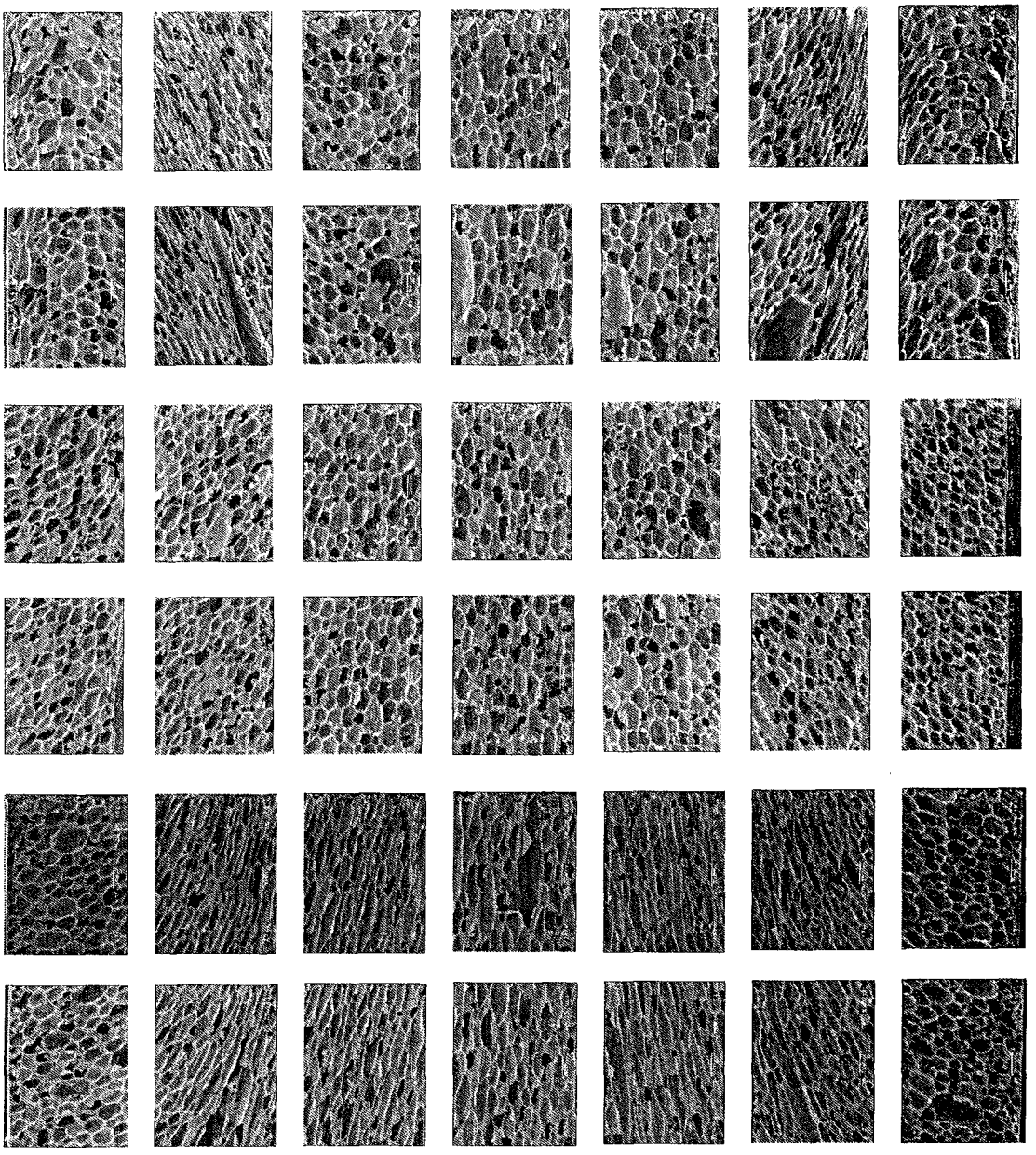

Figure-E.6: Tall Mold Parallel Images

Reproduced with permission of the copyright owner. Further reproduction prohibited without permission.

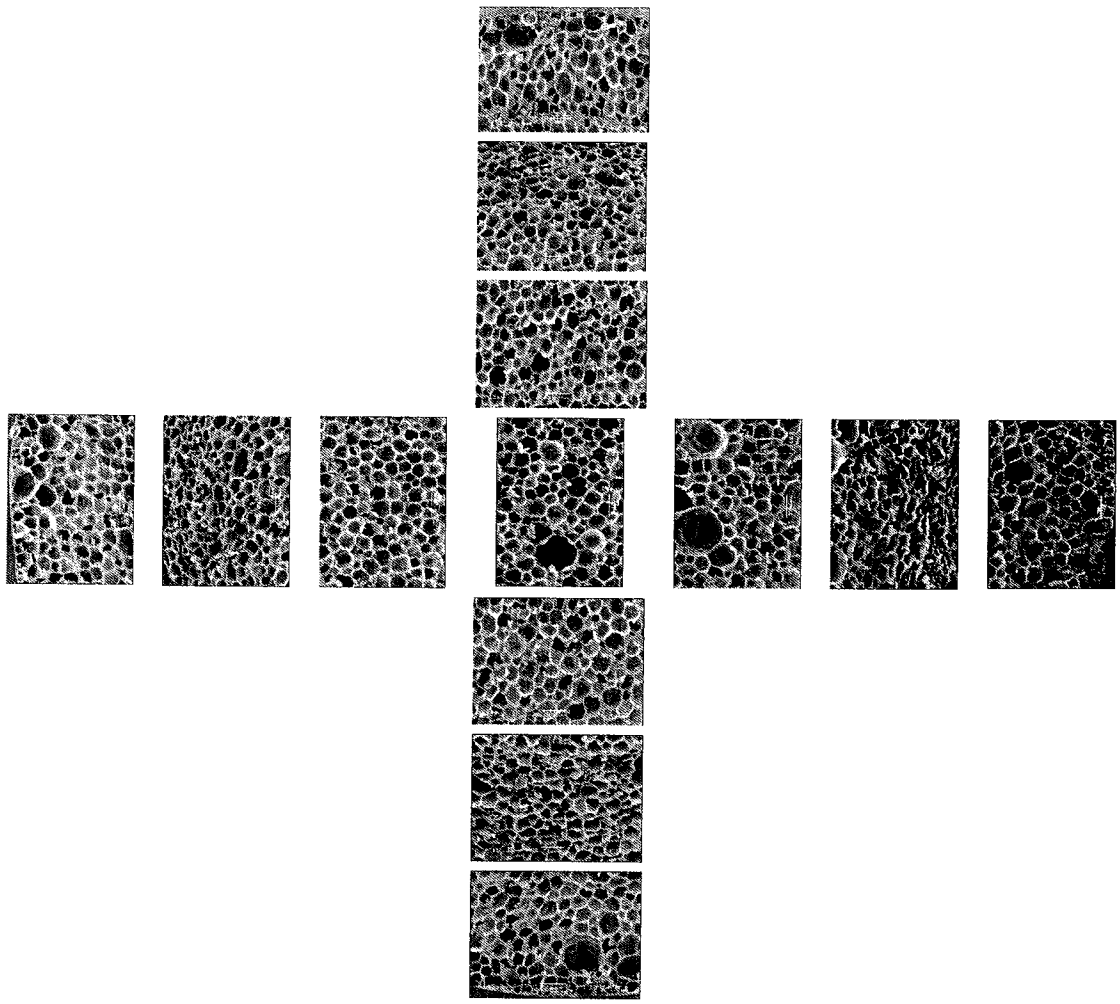

Figure-E.7: Tall Mold Level 1 Perpendicular Sample

Reproduced with permission of the copyright owner. Further reproduction prohibited without permission.

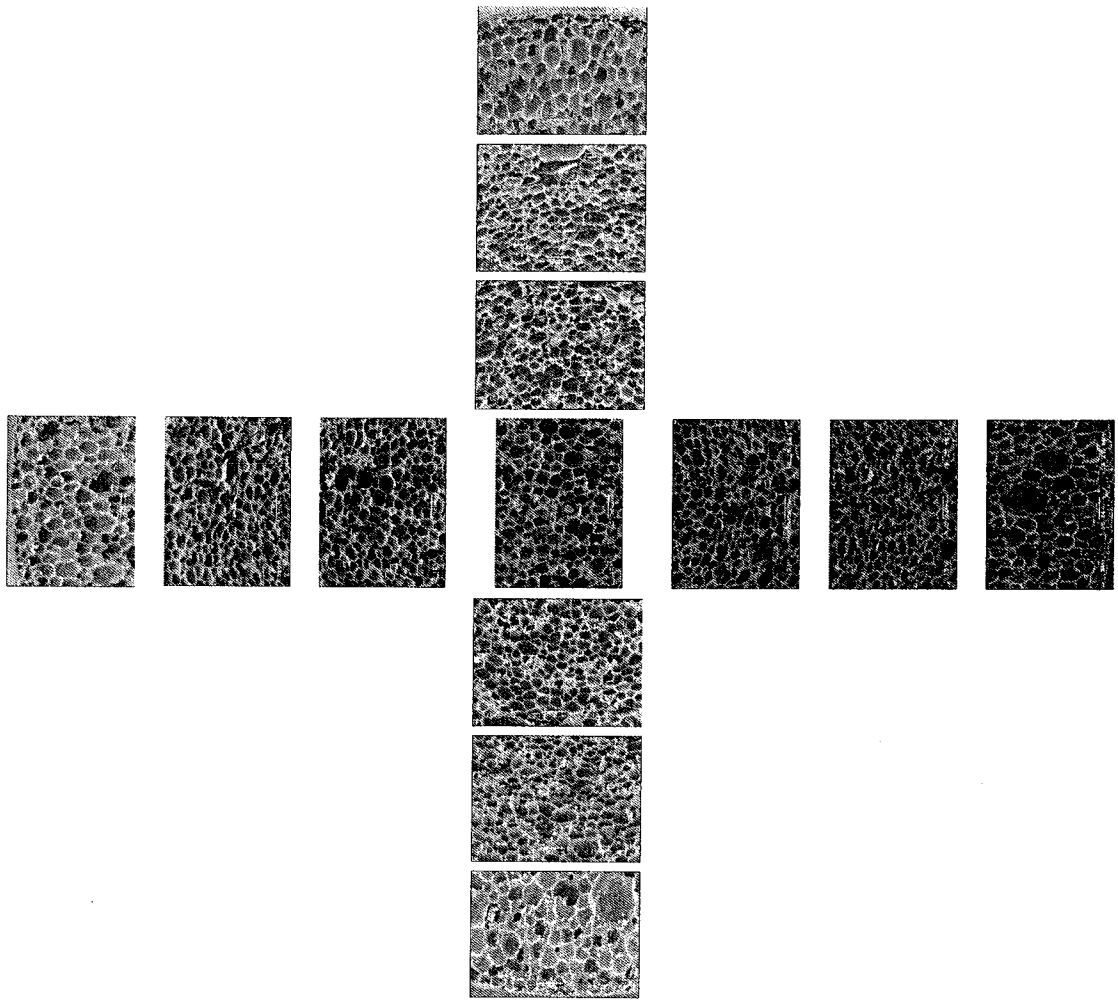

Figure-E.8: Tall Mold Level 8 Perpendicular Sample

Reproduced with permission of the copyright owner. Further reproduction prohibited without permission.

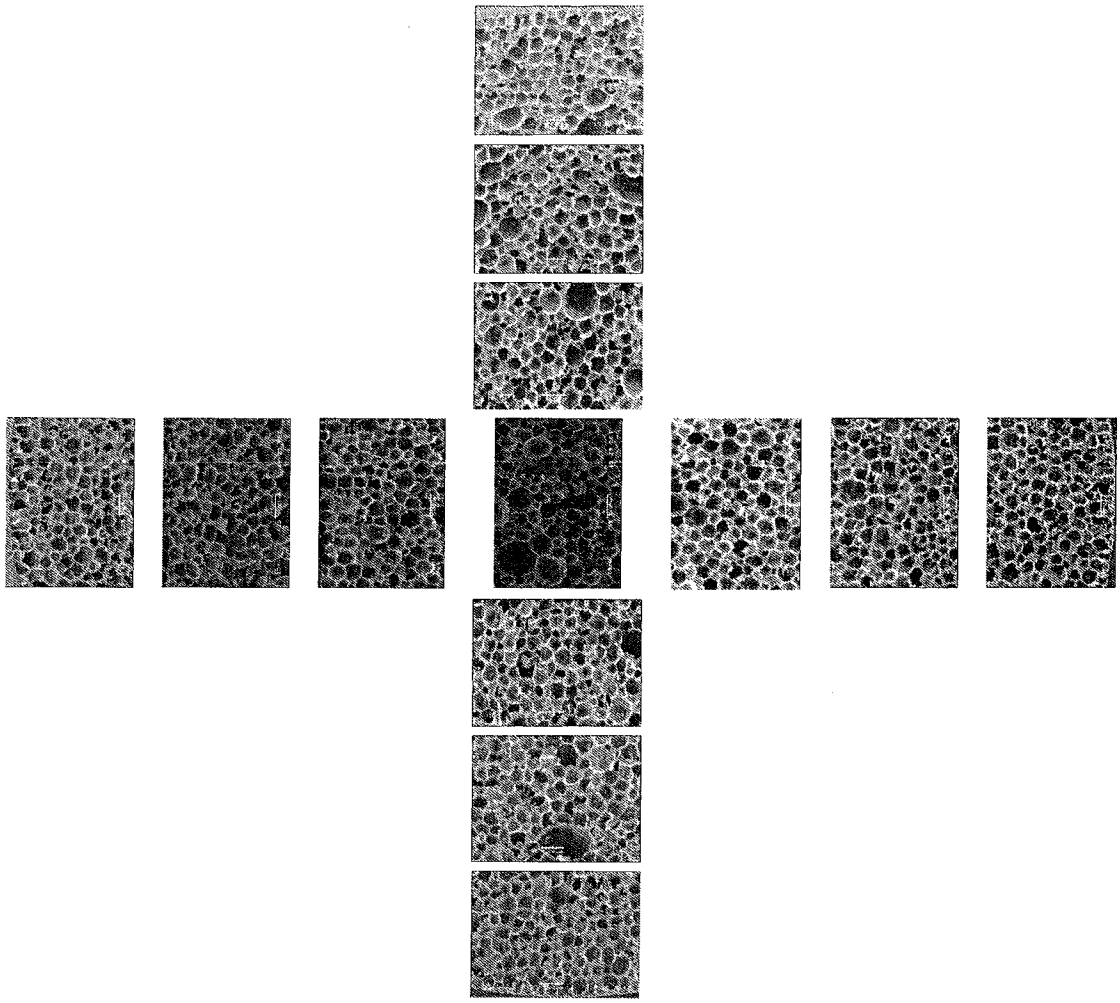

Figure-E.9: Tall Mold Level 14 Perpendicular Sample

Reproduced with permission of the copyright owner. Further reproduction prohibited without permission.

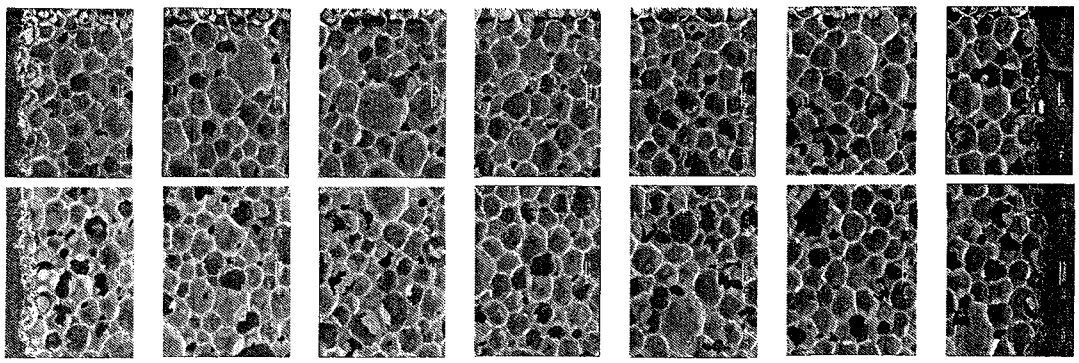

Figure-E.10: Reference Mold Parallel Sample

Reproduced with permission of the copyright owner. Further reproduction prohibited without permission.

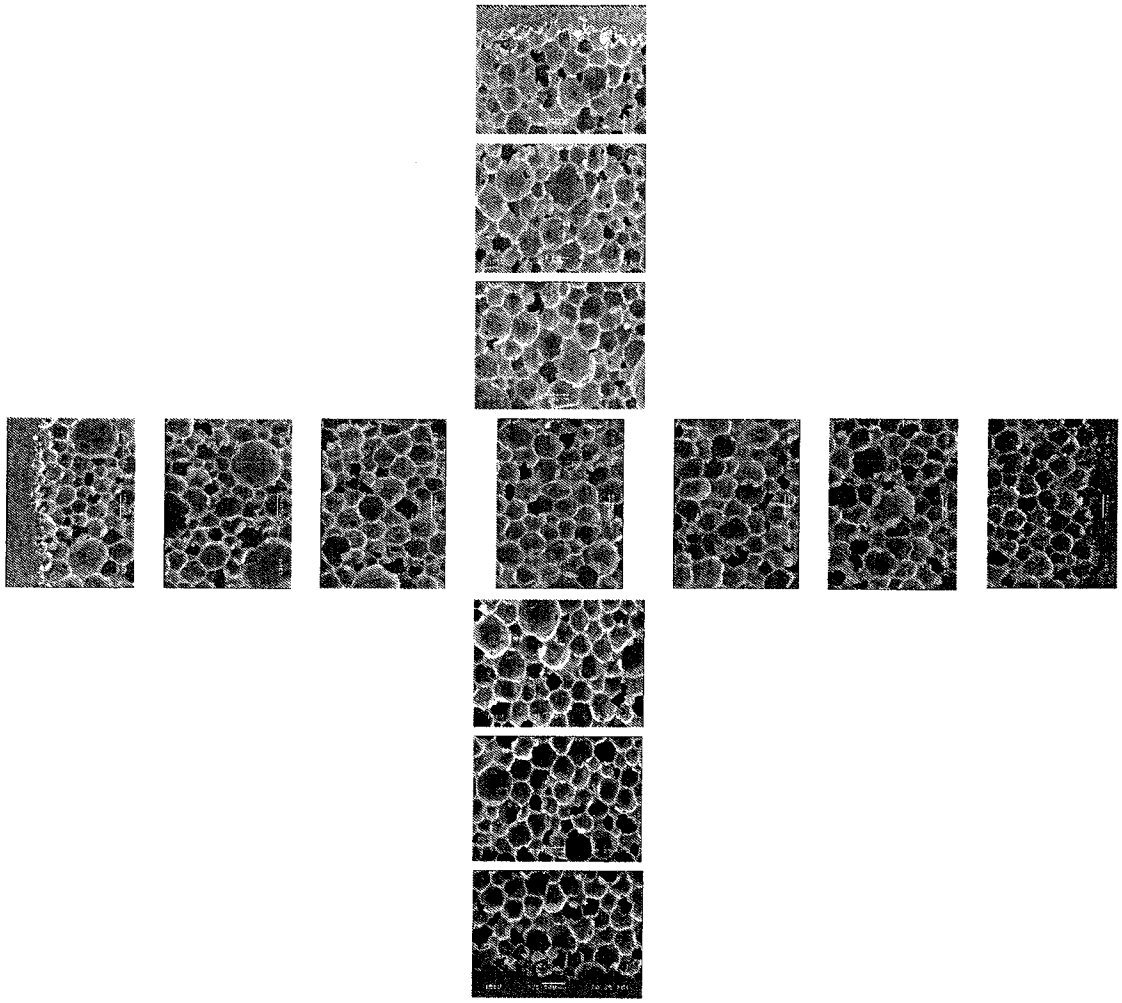

Figure-E.11: Reference Mold Perpendicular Sample

Reproduced with permission of the copyright owner. Further reproduction prohibited without permission.

Reproduced with permission of the copyright owner. Further reproduction prohibited without permission.

Table-E.1: Sample S1 Average Values

		Data used for Comparisons						Data used for Theoretical Calculations		
		Area (um^2)	Aspect Ratio	Angle (degree)	Dia (Max) (um)	Dia (Min) (um)	Dia (Mean) (um)	Cell Edge Length (um)	Cell Face Thickness (um)	Edge Thickness (um)
S1-1A	Average	48987	1.03	NA	289.26	179.60	235.72	214.19	6.70	31.71
	Std Dev	33158	NA	-	93.99	79.82	83.51	36.07	1.46	5.07
	% Diff	68%	-	-	32%	44%	35%	17%	22%	16%
S1-2A	Average	46504	1.59	NA	287.19	165.99	226.21	193.69	6.89	32.14
	Std Dev	34410	NA	-	119.30	84.11	92.29	48.37	3.44	7.73
	% Diff	74%	-	-	42%	51%	41%	25%	50%	24%
S1-3A	Average	55179	1.38	NA	310.20	178.77	245.61	220.39	8.35	31.43
	Std Dev	50719	NA	-	131.36	91.36	106.61	55.52	3.15	6.34
	% Diff	92%	-	-	42%	51%	43%	25%	38%	20%
S1-4A	Average	45602	1.63	NA	290.66	164.80	230.10	211.82	8.81	33.86
	Std Dev	30522	NA	-	102.45	70.52	78.28	40.00	4.13	7.59
	% Diff	67%	-	-	35%	43%	34%	19%	47%	22%
S1-1B	Average	27628	1.95	92.49	247.49	110.83	178.80	123.95	4.30	16.00
	Std Dev	25132	1.53	23.69	108.51	44.77	65.53	33.16	1.08	3.98
	% Diff	91%	78%	26%	44%	40%	37%	27%	25%	25%
S1-2B	Average	66921	1.71	79.90	369.28	186.27	276.90	227.46	9.14	36.86
	Std Dev	46050	0.63	32.00	152.49	82.08	104.73	76.86	3.11	6.33
	% Diff	69%	37%	40%	41%	44%	38%	34%	34%	17%
S1-3B	Average	69571	1.64	107.15	347.87	194.76	270.30	206.10	7.92	33.00
	Std Dev	89848	0.61	45.03	173.81	101.83	130.23	52.82	2.80	6.66
	% Diff	129%	37%	42%	50%	52%	48%	26%	35%	20%
S1-4B	Average	64755	1.89	69.11	391.66	182.24	279.41	214.75	7.99	32.00
	Std Dev	48842	0.72	35.91	171.24	77.33	101.63	61.79	3.33	6.96
	% Diff	75%	38%	52%	44%	42%	36%	29%	42%	22%

Reproduced with permission of the copyright owner. Further reproduction prohibited without permission.

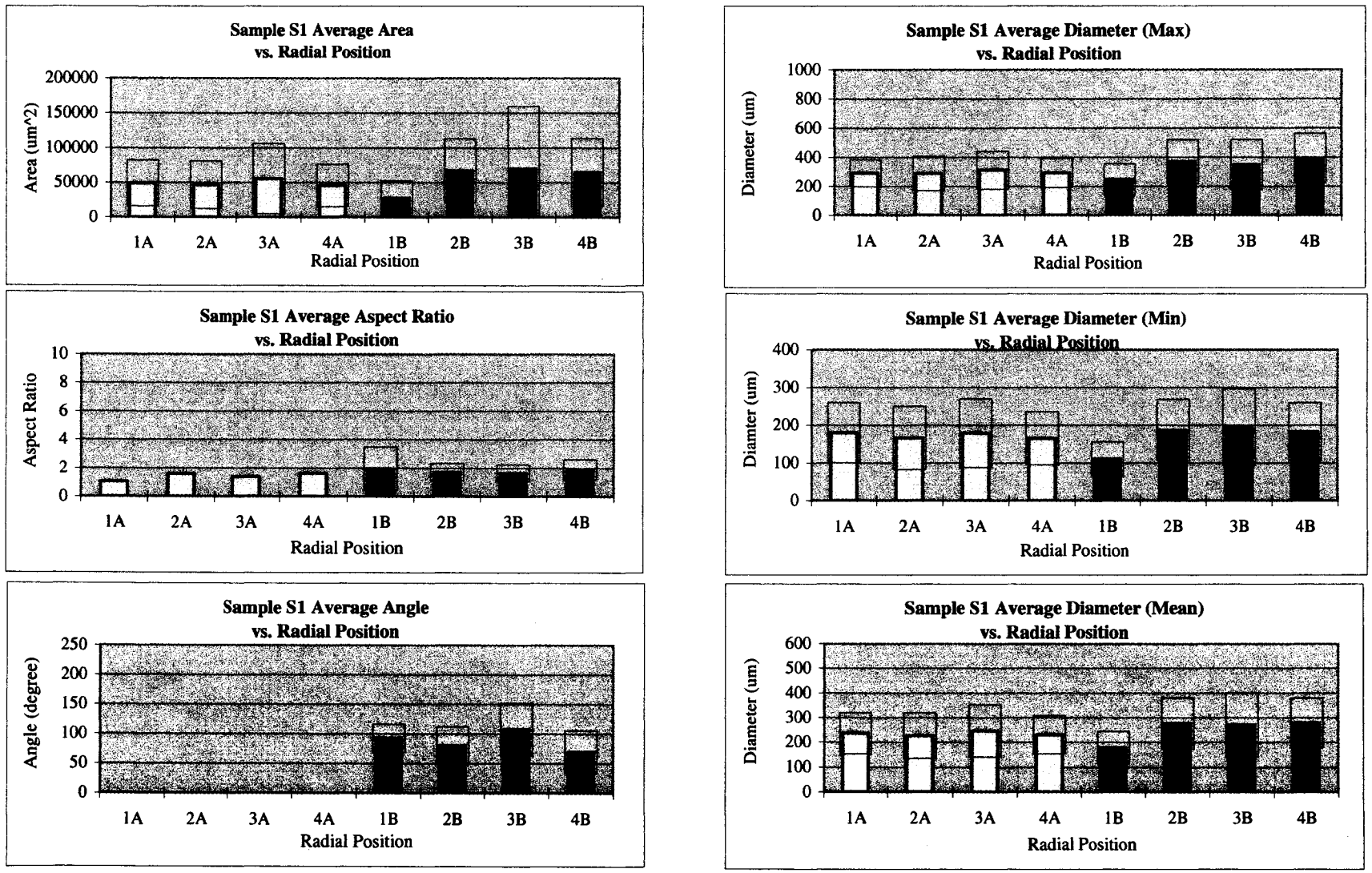

Figure-E.12: Graphs of Sample S1 Average Values used for Comparisons

Reproduced with permission of the copyright owner. Further reproduction prohibited without permission.

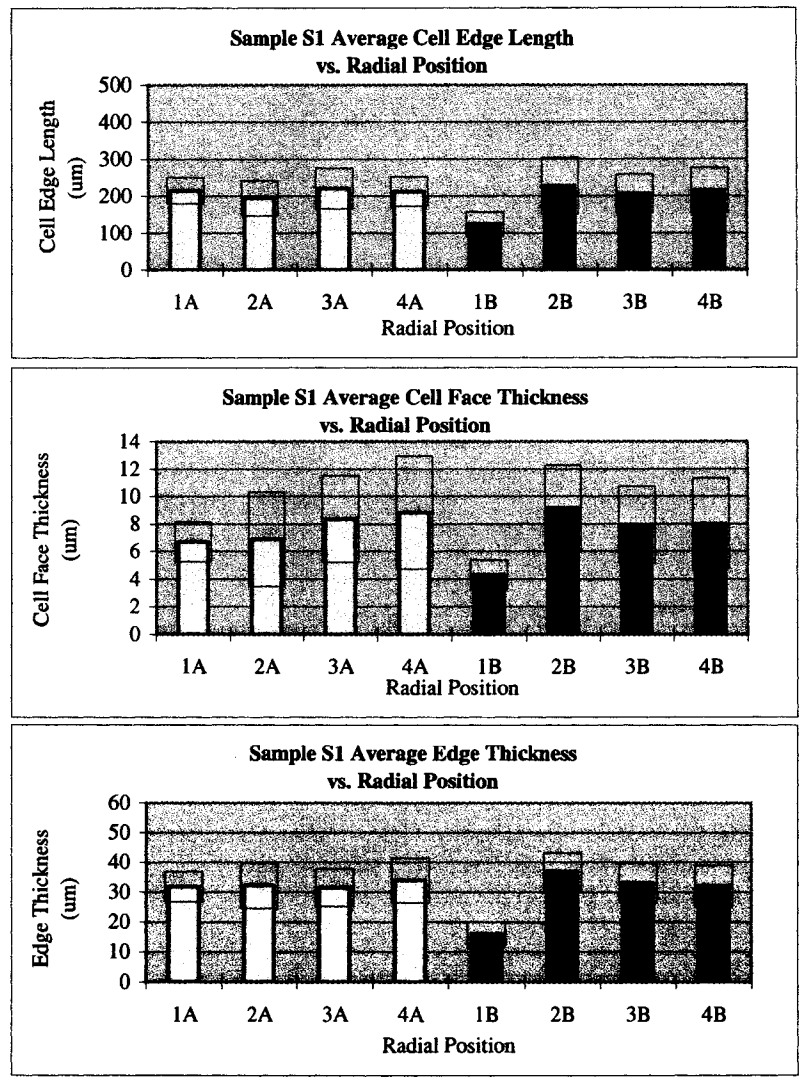

Figure-E.13: Graphs of Sample S1 Average Values used for Theoretical Calculations

Reproduced with permission of the copyright owner. Further reproduction prohibited without permission.

Table-E.2: Sample S2 Average Values

		Data used for Comparisons						Data used for Theoretical Calculations		
		Area (um^2)	Aspect Ratio	Angle (degree)	Dia (Max) (um)	Dia (Min) (um)	Dia (Mean) (um)	Cell Edge Length (um)	Cell Face Thickness (um)	Edge Thickness (um)
S2-1A	Average	42231	1.81	NA	267.06	166.17	218.91	199.16	6.24	31.71
	Std Dev	28375	NA	-	86.29	73.72	77.30	48.80	1.69	5.71
	% Diff	67%	-	-	32%	44%	35%	25%	27%	18%
S2-2A	Average	43304	1.57	NA	269.85	163.96	218.11	201.31	7.08	29.57
	Std Dev	33641	NA	-	98.12	76.45	84.83	50.12	2.40	5.16
	% Diff	78%	-	-	36%	47%	39%	25%	34%	17%
S2-3A	Average	45491	1.75	NA	281.74	162.12	220.44	203.89	7.03	31.57
	Std Dev	45180	NA	-	119.81	82.47	93.95	38.08	2.62	6.97
	% Diff	99%	-	-	43%	51%	43%	19%	37%	22%
S2-4A	Average	41234	1.87	NA	280.22	156.92	219.57	202.27	7.54	32.16
	Std Dev	25635	NA	-	92.02	65.84	71.48	48.34	3.03	7.34
	% Diff	62%	-	-	33%	42%	33%	24%	40%	23%
S2-1B	Average	74871	1.72	91.93	410.00	202.28	303.76	236.03	7.49	32.29
	Std Dev	43162	0.40	17.80	132.36	76.35	93.48	75.75	3.04	5.00
	% Diff	58%	23%	19%	32%	38%	31%	32%	41%	15%
S2-2B	Average	59000	1.74	72.68	351.97	172.09	261.03	233.46	7.55	33.80
	Std Dev	42256	0.55	30.42	142.02	75.05	99.87	79.43	2.43	9.13
	% Diff	72%	32%	42%	40%	44%	38%	34%	32%	27%
S2-3B	Average	65017	1.89	57.79	401.27	186.83	285.40	243.27	8.12	32.00
	Std Dev	33589	0.70	24.57	131.87	59.37	77.88	89.82	3.04	10.01
	% Diff	52%	37%	43%	33%	32%	27%	37%	37%	31%
S2-4B	Average	62005	2.18	60.28	425.80	170.14	286.23	238.30	7.68	31.18
	Std Dev	34264	0.62	19.45	132.82	49.71	79.55	93.32	2.40	5.77
	% Diff	55%	29%	32%	31%	29%	28%	39%	31%	19%

Reproduced with permission of the copyright owner. Further reproduction prohibited without permission.

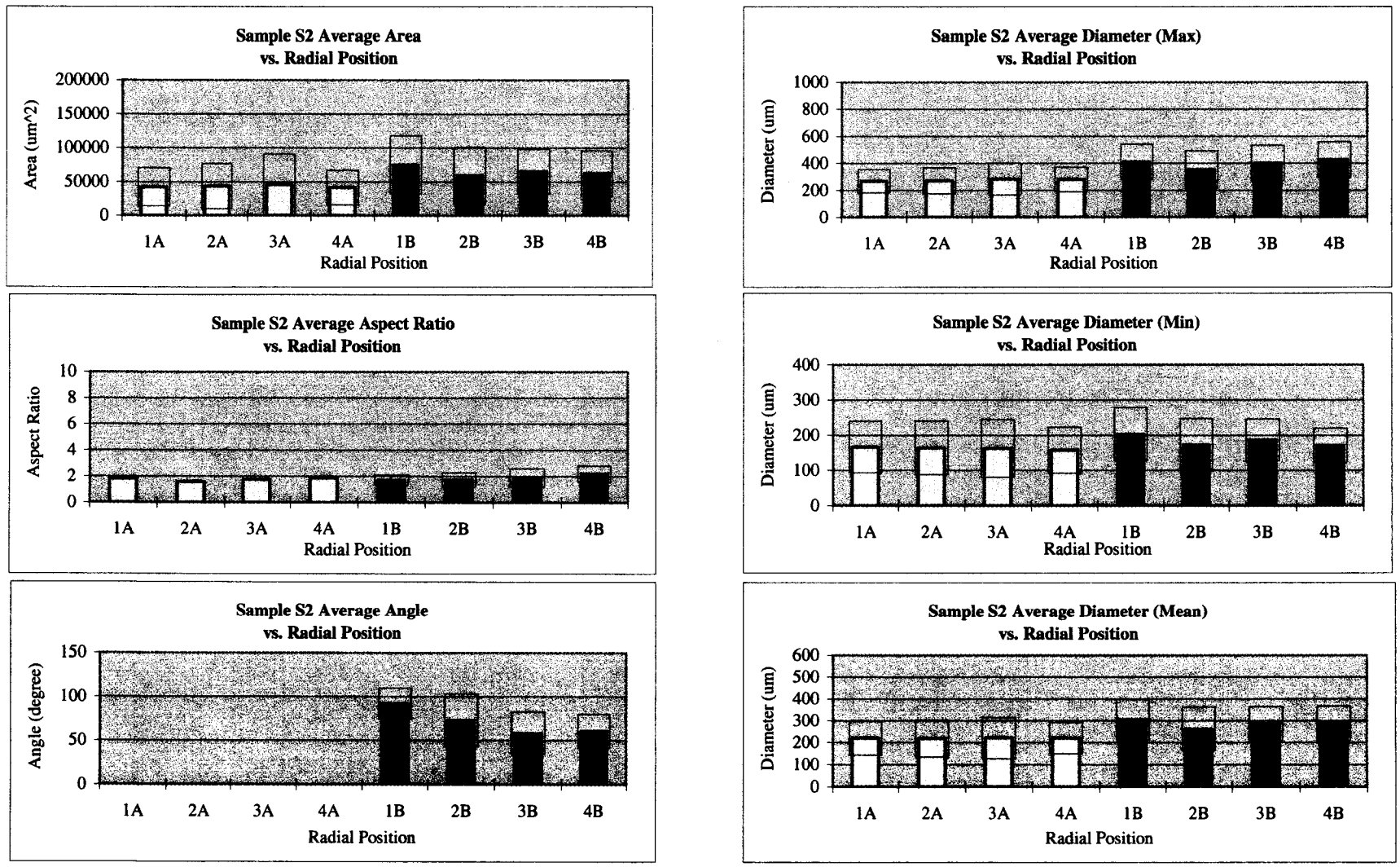

Figure-E.14: Graphs of Sample S2 Average Values used for Comparisons

Reproduced with permission of the copyright owner. Further reproduction prohibited without permission.

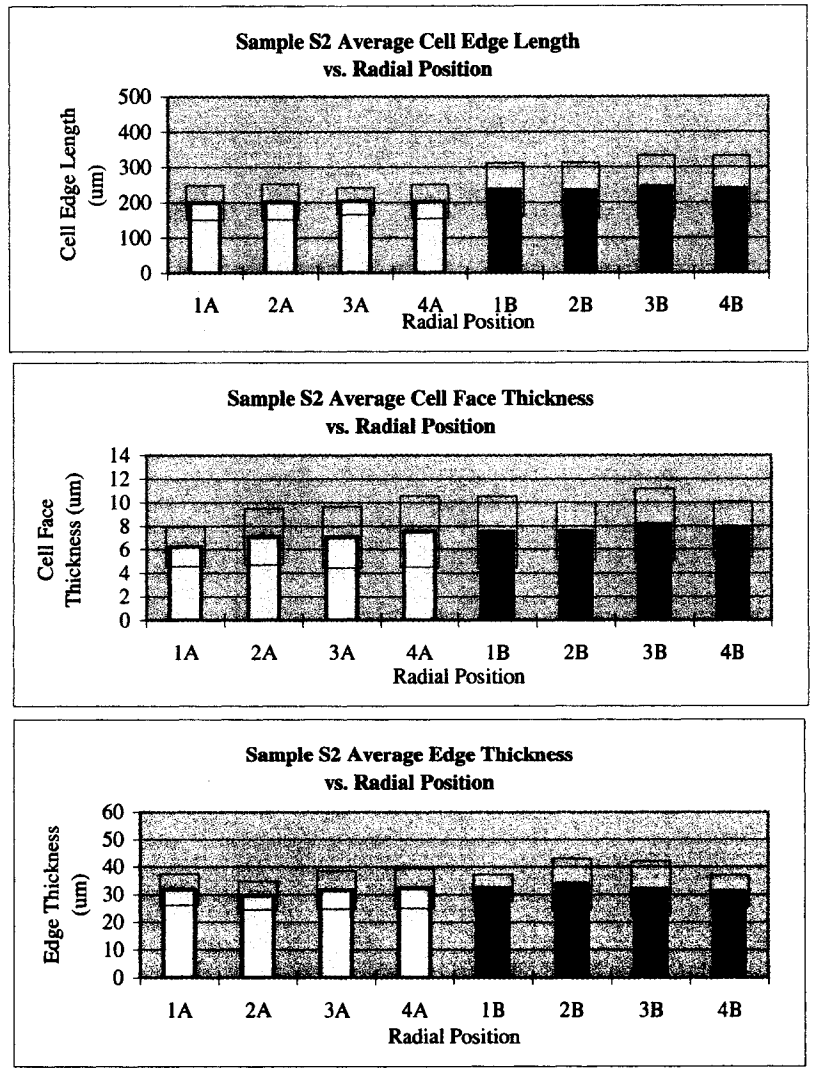

Figure-E.15: Graphs of Sample S2 Average Values used for Theoretical Calculations

Reproduced with permission of the copyright owner. Further reproduction prohibited without permission.

Table-E.3: Sample S3 Average Values

		Data used for Comparisons						Data used for Theoretical Calculations		
		Area (um^2)	Aspect Ratio	Angle (degree)	Dia (Max) (um)	Dia (Min) (um)	Dia (Mean) (um)	Cell Edge Length (um)	Cell Face Thickness (um)	Edge Thickness (um)
S3-1A	Average	46926	1.67	NA	274.42	177.78	224.52	212.15	6.68	32.00
	Std Dev	40738	NA	-	124.01	87.07	99.79	47.48	1.57	5.37
	% Diff	87%	-	-	45%	49%	44%	22%	24%	17%
S3-2A	Average	42087	1.64	NA	266.39	161.24	214.32	200.15	6.96	30.00
	Std Dev	34416	NA	-	109.32	77.72	90.80	44.11	2.19	7.18
	% Diff	82%	-	-	41%	48%	42%	22%	31%	24%
S3-3A	Average	41971	2.28	NA	277.19	153.45	214.38	205.13	7.78	32.16
	Std Dev	39426	NA	-	126.64	71.34	92.68	52.68	3.88	5.73
	% Diff	94%	-	-	46%	46%	43%	26%	50%	18%
S3-4A	Average	40893	2.14	NA	268.03	152.55	210.11	208.35	7.90	32.98
	Std Dev	40076	NA	-	118.01	69.86	87.85	62.24	3.23	7.47
	% Diff	98%	-	-	44%	46%	42%	30%	41%	23%
S3-1B	Average	64057	1.86	94.24	388.08	182.34	276.60	258.15	6.41	31.43
	Std Dev	46086	0.54	27.53	141.75	76.06	100.77	110.35	1.91	5.41
	% Diff	72%	29%	29%	37%	42%	36%	43%	30%	17%
S3-2B	Average	44525	2.62	73.48	365.34	126.67	236.22	296.15	6.27	32.65
	Std Dev	45850	1.17	21.08	182.18	71.63	115.29	143.38	2.26	7.01
	% Diff	103%	45%	29%	50%	57%	49%	48%	36%	21%
S3-3B	Average	67903	2.84	68.57	505.78	157.99	308.24	269.16	8.26	33.47
	Std Dev	42294	1.06	13.33	214.43	59.28	114.31	138.45	3.16	8.22
	% Diff	62%	37%	19%	42%	38%	37%	51%	38%	25%
S3-4B	Average	64617	2.68	60.72	462.64	153.30	293.10	292.79	7.48	32.98
	Std Dev	54387	1.11	21.67	236.76	65.95	132.11	138.24	2.51	7.08
	% Diff	84%	42%	36%	51%	43%	45%	47%	34%	21%

Reproduced with permission of the copyright owner. Further reproduction prohibited without permission.

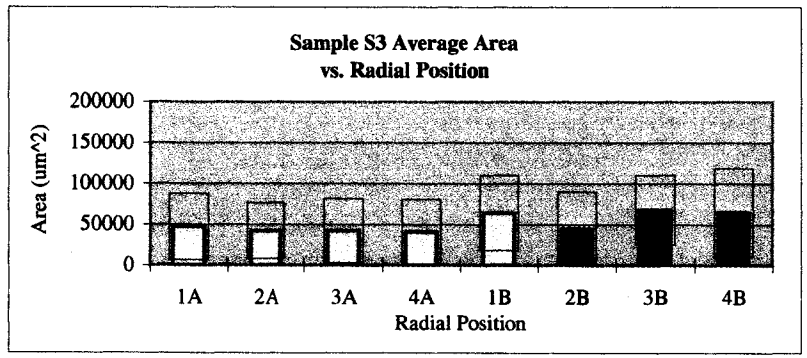

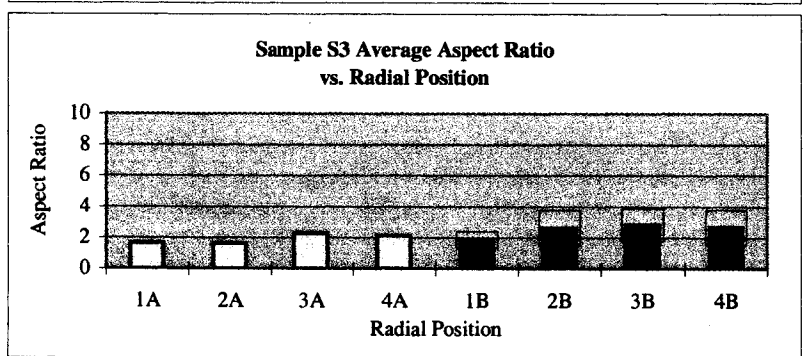

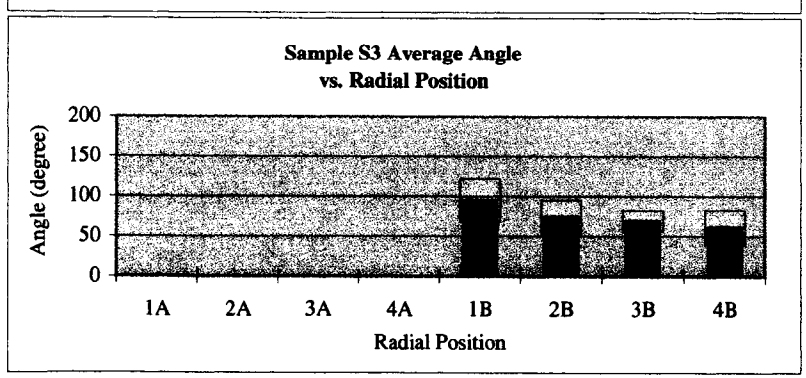

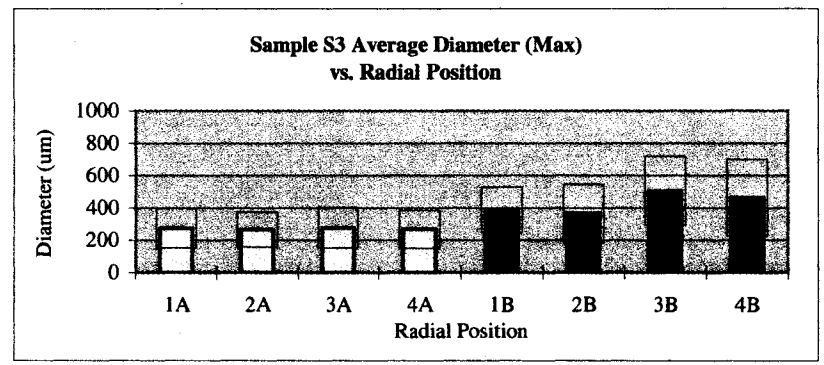

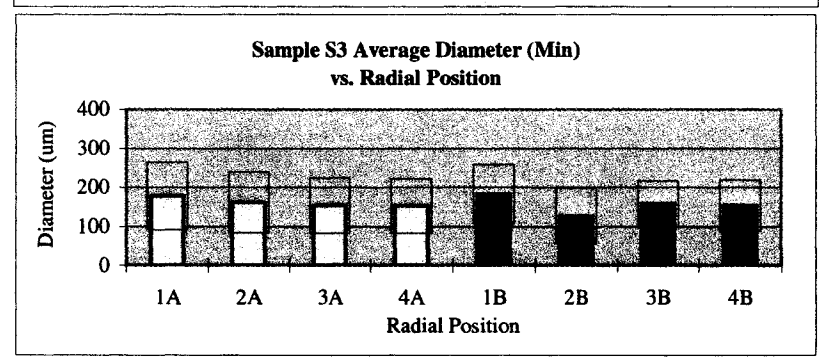

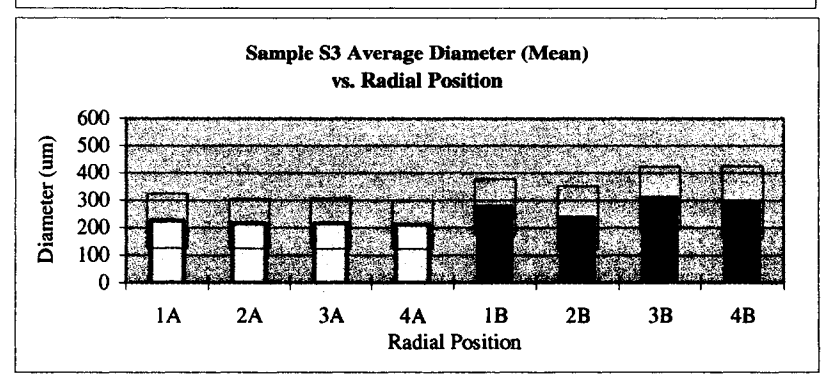

Figure-E.16: Graphs of Sample S3 Average Values used for Comparisons

Reproduced with permission of the copyright owner. Further reproduction prohibited without permission.

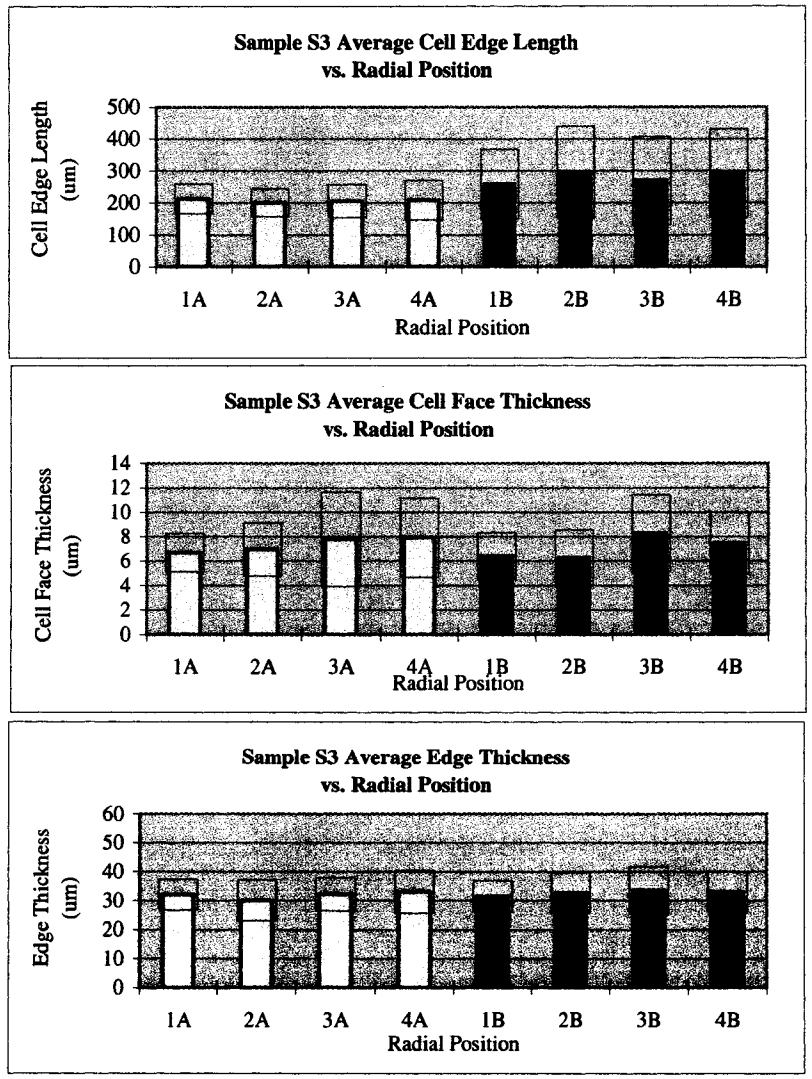

Figure-E.17: Graphs of Sample S3 Average Values used for Theoretical Calculations

Reproduced with permission of the copyright owner. Further reproduction prohibited without permission.

Table-E.4: Sample S4 Average Values

		Data used for Comparisons						Data used for Theoretical Calculations		
		Area (um^2)	Aspect Ratio	Angle (degree)	Dia (Max) (um)	Dia (Min) (um)	Dia (Mean) (um)	Cell Edge Length (um)	Cell Face Thickness (um)	Edge Thickness (um)
S4-1A	Average	34220	2.46	NA	222.83	146.81	184.12	190.82	6.23	32.29
	Std Dev	36119	NA	-	108.45	88.48	96.20	37.36	2.18	9.86
	% Diff	106%	-	-	49%	60%	52%	20%	35%	31%
S4-2A	Average	42246	2.51	NA	245.17	153.68	198.40	197.18	7.72	30.43
	Std Dev	73716	NA	-	139.61	105.49	118.35	49.91	3.09	6.89
	% Diff	174%	-	-	57%	69%	60%	25%	40%	23%
S4-3A	Average	33973	2.58	NA	255.55	133.64	194.93	183.78	7.22	30.71
	Std Dev	25240	NA	-	104.71	59.16	74.43	45.37	2.92	7.28
	% Diff	74%	-	-	41%	44%	38%	25%	40%	24%
S4-4A	Average	47894	1.59	NA	299.60	162.65	231.65	211.37	7.10	30.86
	Std Dev	37913	NA	-	122.41	75.86	90.64	51.60	3.51	10.25
	% Diff	79%	-	-	41%	47%	39%	24%	49%	33%
S4-1B	Average	84228	2.13	91.56	466.73	192.75	320.91	256.87	7.07	27.71
	Std Dev	70025	0.73	21.91	208.27	88.37	134.63	107.70	2.31	5.65
	% Diff	83%	34%	24%	45%	46%	42%	42%	33%	20%
S4-2B	Average	74107	2.88	79.27	517.41	165.97	316.64	303.50	8.48	33.14
	Std Dev	57596	1.06	17.73	259.40	73.94	141.56	161.68	3.26	10.07
	% Diff	78%	37%	22%	50%	45%	45%	53%	38%	30%
S4-3B	Average	66376	3.17	69.64	515.57	144.11	298.21	276.60	9.15	33.96
	Std Dev	79105	1.29	13.92	328.54	56.38	151.12	136.24	4.02	9.79
	% Diff	119%	41%	20%	64%	39%	51%	49%	44%	29%
S4-4B	Average	58491	2.08	43.04	384.18	159.97	264.21	240.60	7.58	36.57
	Std Dev	51550	0.65	33.82	179.83	78.03	120.34	81.02	3.09	9.92
	% Diff	88%	31%	79%	47%	49%	46%	34%	41%	27%

Reproduced with permission of the copyright owner. Further reproduction prohibited without permission.

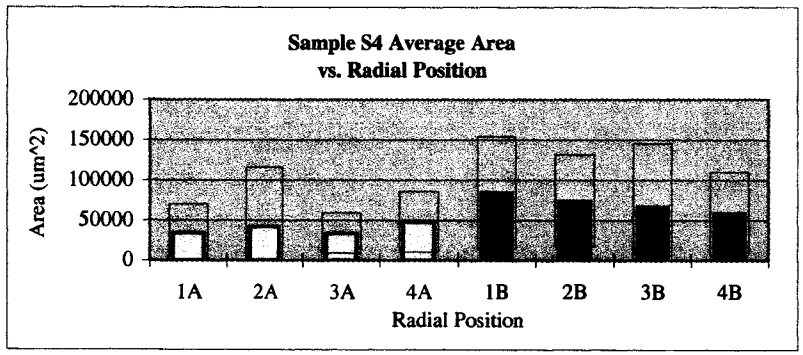

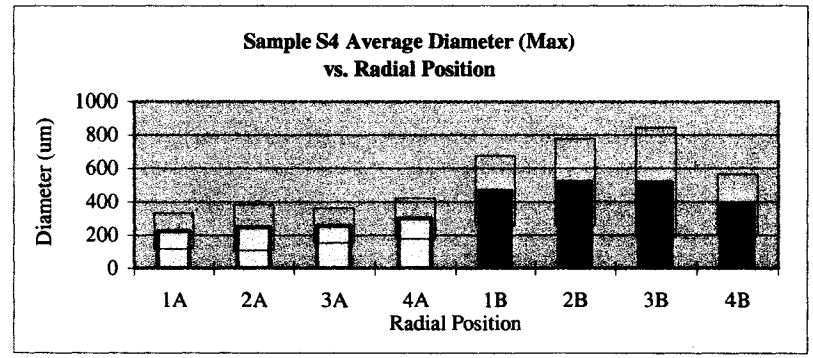

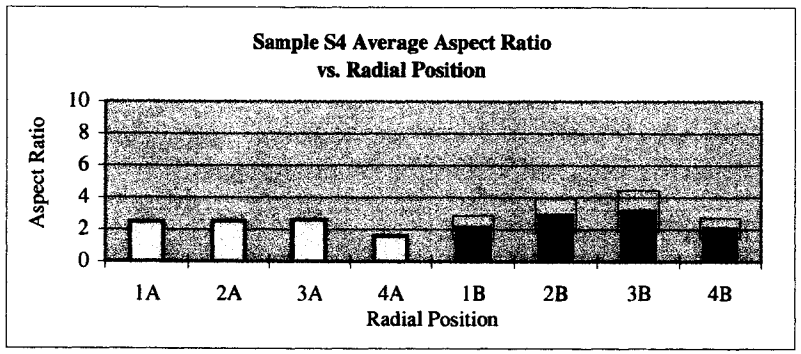

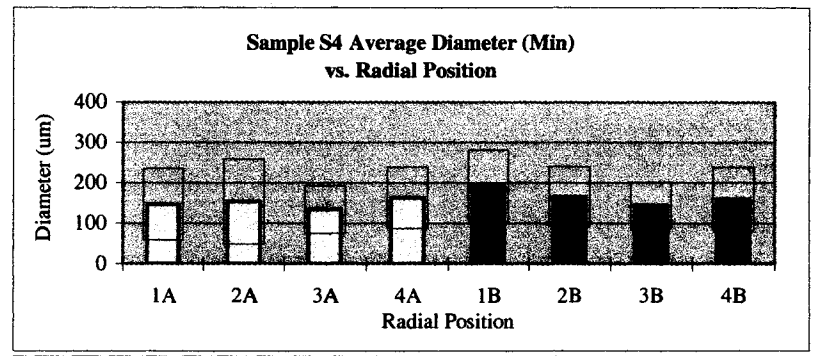

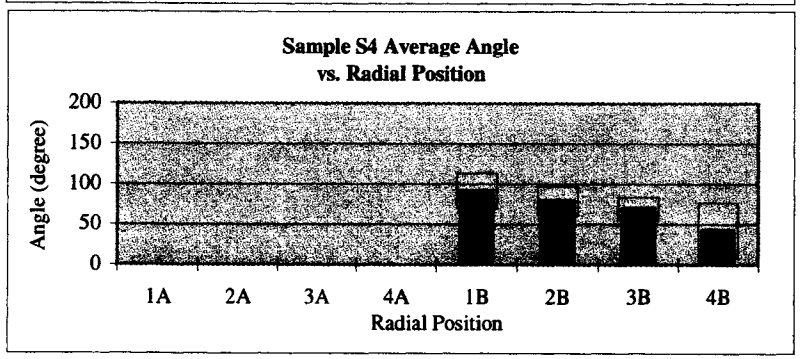

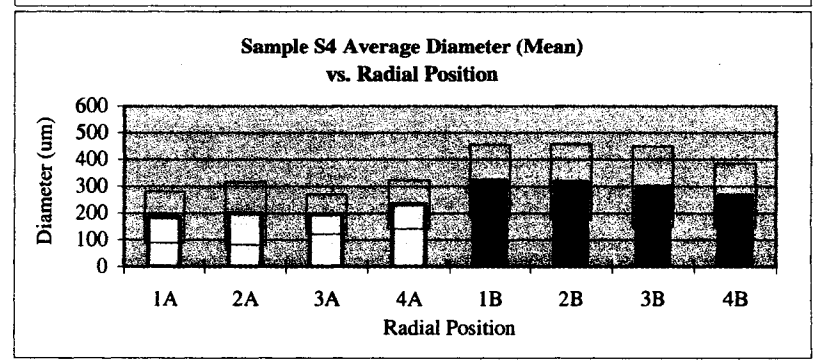

Figure-E.18: Graphs of Sample S4 Average Values used for Comparisons

Reproduced with permission of the copyright owner. Further reproduction prohibited without permission.

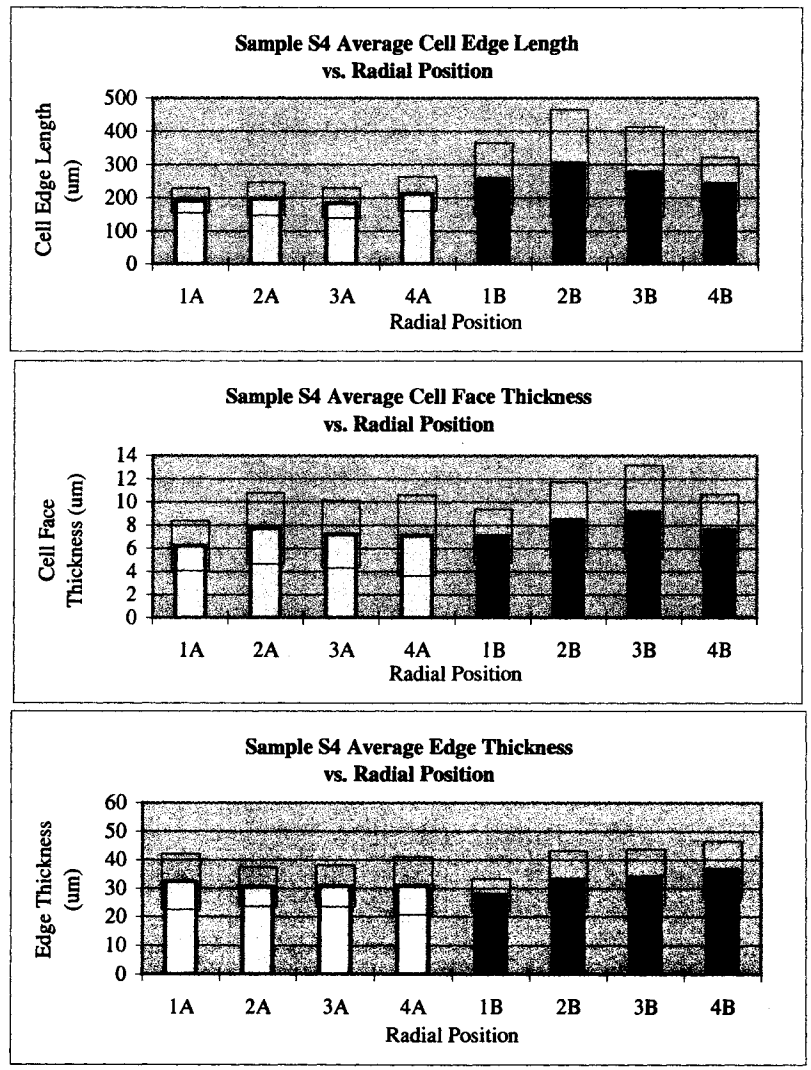

Figure-E.19: Graphs of Sample S4 Average Values used for Theoretical Calculations

Reproduced with permission of the copyright owner. Further reproduction prohibited without permission.

Table-E.5: Sample T1 Average Values

		Data used for Comparisons						Data used for Theoretical Calculations		
		Area (um^2)	Aspect Ratio	Angle (degree)	Dia (Max) (um)	Dia (Min) (um)	Dia (Mean) (um)	Cell Edge Length (um)	Cell Face Thickness (um)	Edge Thickness (um)
T1-1A	Average	34170	1.65	NA	229.80	140.00	187.70	193.97	5.90	32.57
	Std Dev	28636	NA	-	108.56	73.98	88.24	43.03	2.16	5.59
	% Diff	84%	-	-	47%	53%	47%	22%	37%	17%
T1-2A	Average	47066	1.63	NA	280.70	175.36	227.07	181.62	7.63	29.00
	Std Dev	37450	NA	-	111.17	75.41	86.92	41.43	2.93	6.26
	% Diff	80%	-	-	40%	43%	38%	23%	38%	22%
T1-3A	Average	21778	2.90	NA	224.94	96.37	156.42	190.22	7.72	31.53
	Std Dev	20478	NA	-	100.72	51.01	69.22	46.30	3.79	11.90
	% Diff	94%	-	-	45%	53%	44%	24%	49%	38%
T1-4A	Average	41875	1.54	NA	276.30	152.73	213.47	190.20	8.47	32.82
	Std Dev	39418	NA	-	125.02	75.24	92.19	43.29	3.11	12.65
	% Diff	94%	-	-	45%	49%	43%	23%	37%	39%
T1-1B	Average	42091	2.43	92.83	316.94	116.39	210.55	232.22	7.10	28.57
	Std Dev	58208	0.93	20.77	191.27	81.20	121.98	73.44	2.98	4.91
	% Diff	138%	38%	22%	60%	70%	58%	32%	42%	17%
T1-2B	Average	66754	1.80	93.60	377.83	182.80	280.25	236.34	6.60	37.43
	Std Dev	52987	0.60	36.31	147.05	79.78	104.04	96.33	1.73	10.10
	% Diff	79%	33%	39%	39%	44%	37%	41%	26%	27%
T1-3B	Average	45265	3.99	114.64	467.79	116.99	262.52	323.56	8.97	31.54
	Std Dev	34076	1.91	15.19	217.22	55.48	113.01	156.00	4.94	10.83
	% Diff	75%	48%	13%	46%	47%	43%	48%	55%	34%
T1-4B	Average	46501	2.07	94.59	342.59	143.27	234.93	254.59	8.72	35.92
	Std Dev	39102	1.06	44.00	157.24	69.73	95.70	83.73	3.65	13.69
	% Diff	84%	51%	47%	46%	49%	41%	33%	42%	38%

Reproduced with permission of the copyright owner. Further reproduction prohibited without permission.

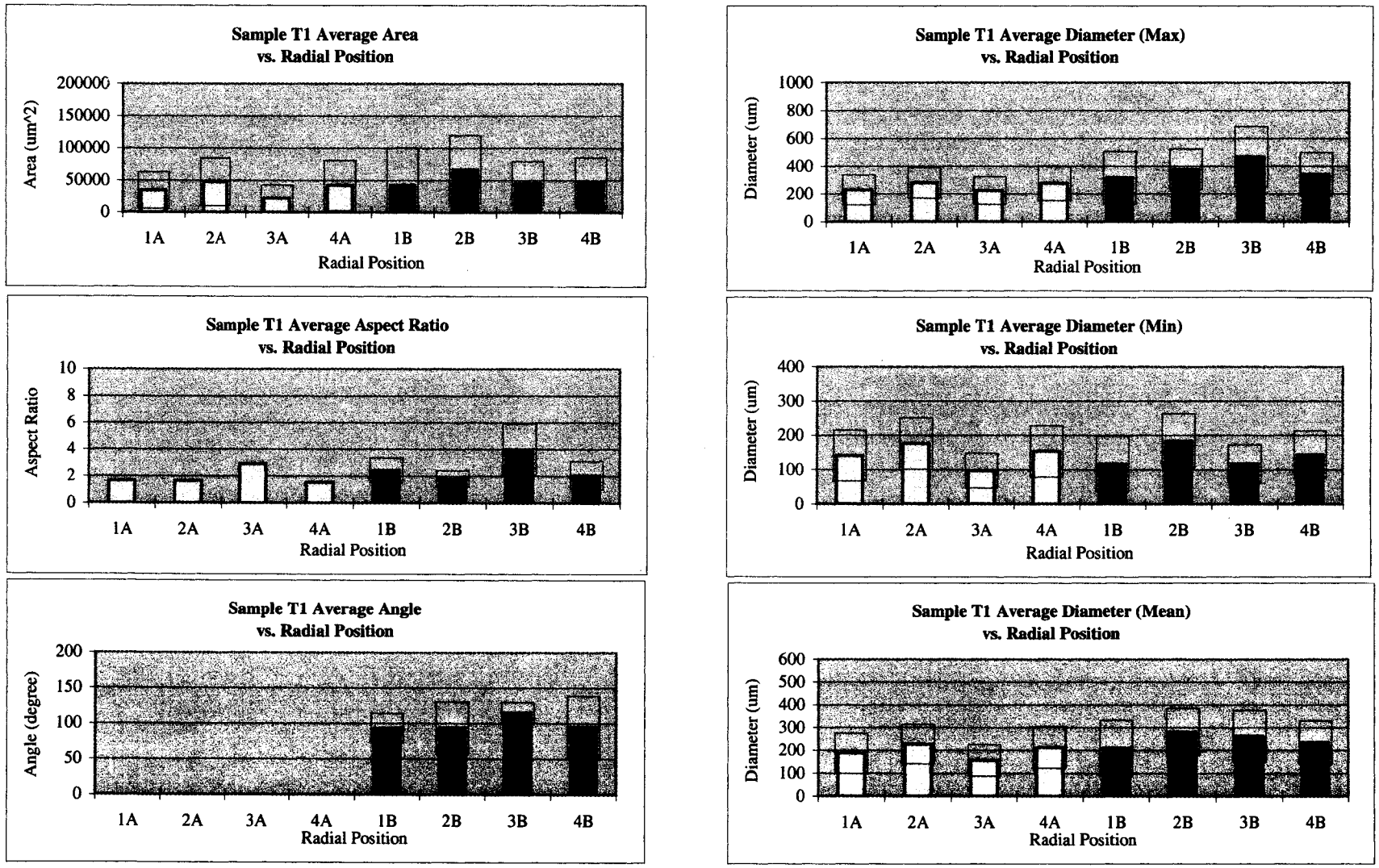

Figure-E.20: Graphs of Sample T1 Average Values used for Comparisons

Reproduced with permission of the copyright owner. Further reproduction prohibited without permission.

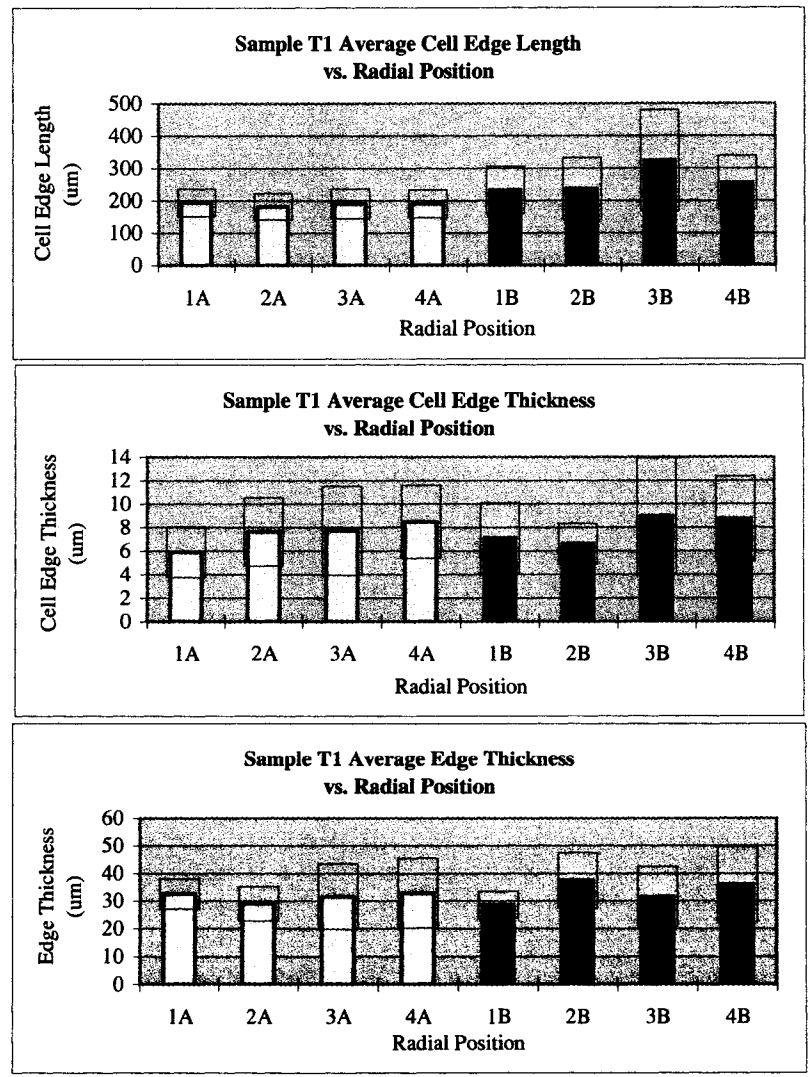

Figure-E.21: Graphs of Sample T1 Average Values used for Theoretical Calculations

Reproduced with permission of the copyright owner. Further reproduction prohibited without permission.

Table-E.6: Sample T8 Average Values

		Data used for Comparisons						Data used for Theoretical Calculations		
		Area (um^2)	Aspect Ratio	Angle (degree)	Dia (Max) (um)	Dia (Min) (um)	Dia (Mean) (um)	Cell Edge Length (um)	Cell Face Thickness (um)	Edge Thickness (um)
T8-1A	Average	24240	2.73	NA	192.54	121.35	158.12	168.06	5.29	33.71
	Std Dev	21549	NA	-	89.10	67.64	75.70	30.10	1.92	10.95
	% Diff	89%	-	-	46%	56%	48%	18%	36%	32%
T8-2A	Average	25254	2.13	NA	216.11	119.86	167.70	151.27	6.92	27.29
	Std Dev	19297	NA	-	92.14	53.38	66.32	38.10	2.72	5.56
	% Diff	76%	-	-	43%	45%	40%	25%	39%	20%
T8-3A	Average	21236	2.51	NA	216.82	102.83	157.54	155.17	5.62	26.78
	Std Dev	14716	NA	-	87.87	42.49	58.71	34.14	1.93	5.84
	% Diff	69%	-	-	41%	41%	37%	22%	34%	22%
T8-4A	Average	46542	1.55	NA	295.19	159.22	225.78	207.06	5.71	31.71
	Std Dev	51268	NA	-	130.66	80.32	96.86	53.74	1.89	7.65
	% Diff	110%	-	-	44%	50%	43%	26%	33%	24%
T8-1B	Average	73514	2.04	92.78	449.74	173.40	301.75	203.35	7.36	40.38
	Std Dev	43469	0.77	17.85	155.32	70.36	93.04	43.18	3.36	11.32
	% Diff	59%	38%	19%	35%	41%	31%	21%	46%	28%
T8-2B	Average	55748	2.00	79.11	368.99	161.69	258.92	210.29	6.72	35.43
	Std Dev	40090	0.70	22.76	134.78	72.59	94.96	52.54	1.75	7.23
	% Diff	72%	35%	29%	37%	45%	37%	25%	26%	20%
T8-3B	Average	60727	2.20	61.62	409.67	158.68	271.74	234.03	8.52	33.71
	Std Dev	49156	0.80	18.50	198.35	65.51	109.04	70.26	3.48	8.56
	% Diff	81%	36%	30%	48%	41%	40%	30%	41%	25%
T8-4B	Average	45792	2.21	56.57	365.11	144.71	245.93	233.56	8.70	34.12
	Std Dev	30772	0.70	19.39	133.45	52.97	82.04	65.87	3.16	8.14
	% Diff	67%	32%	34%	37%	37%	33%	28%	36%	24%

Reproduced with permission of the copyright owner. Further reproduction prohibited without permission.

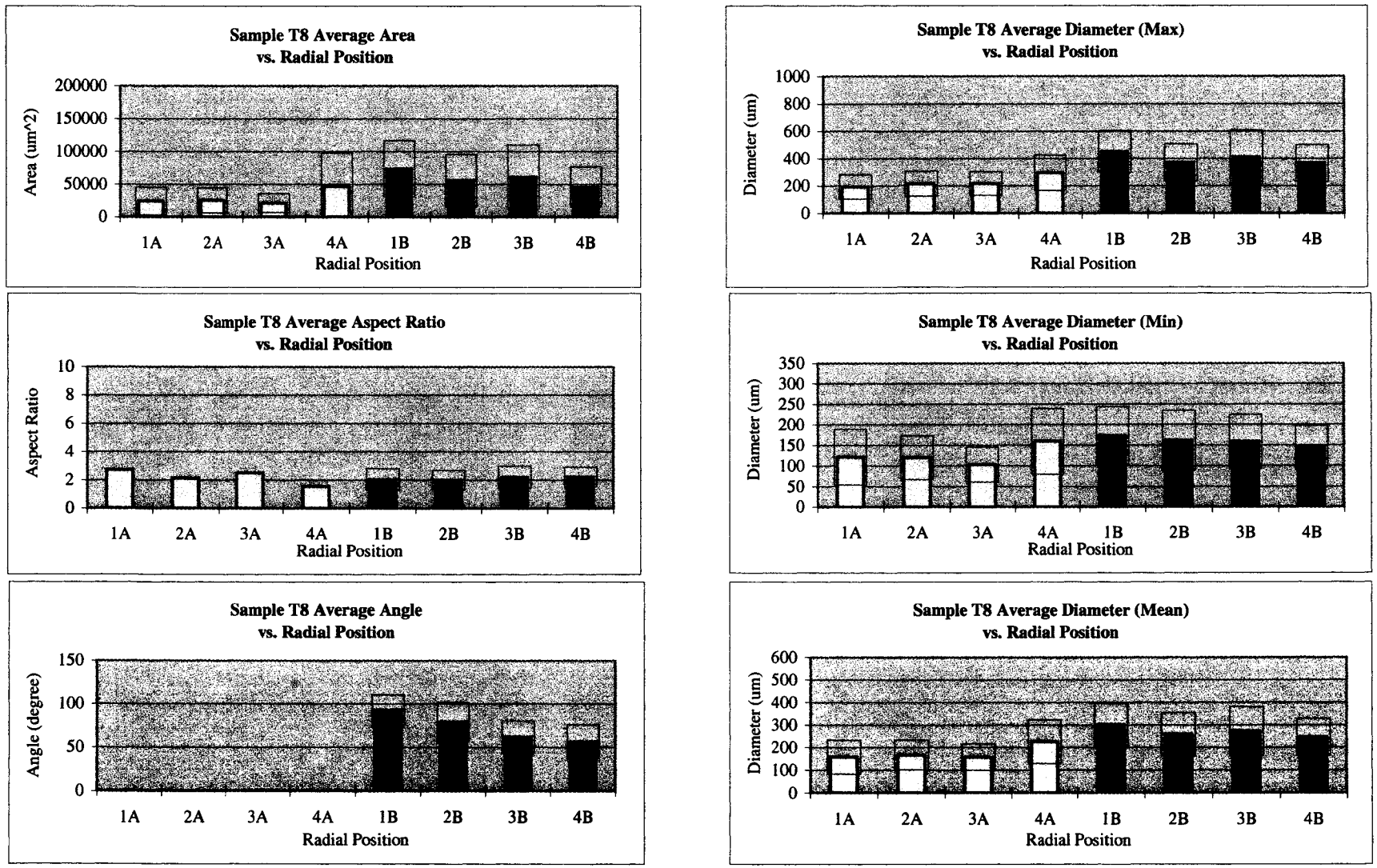

Figure-E.22: Graphs of Sample T8 Average Values used for Comparisons

Reproduced with permission of the copyright owner. Further reproduction prohibited without permission.

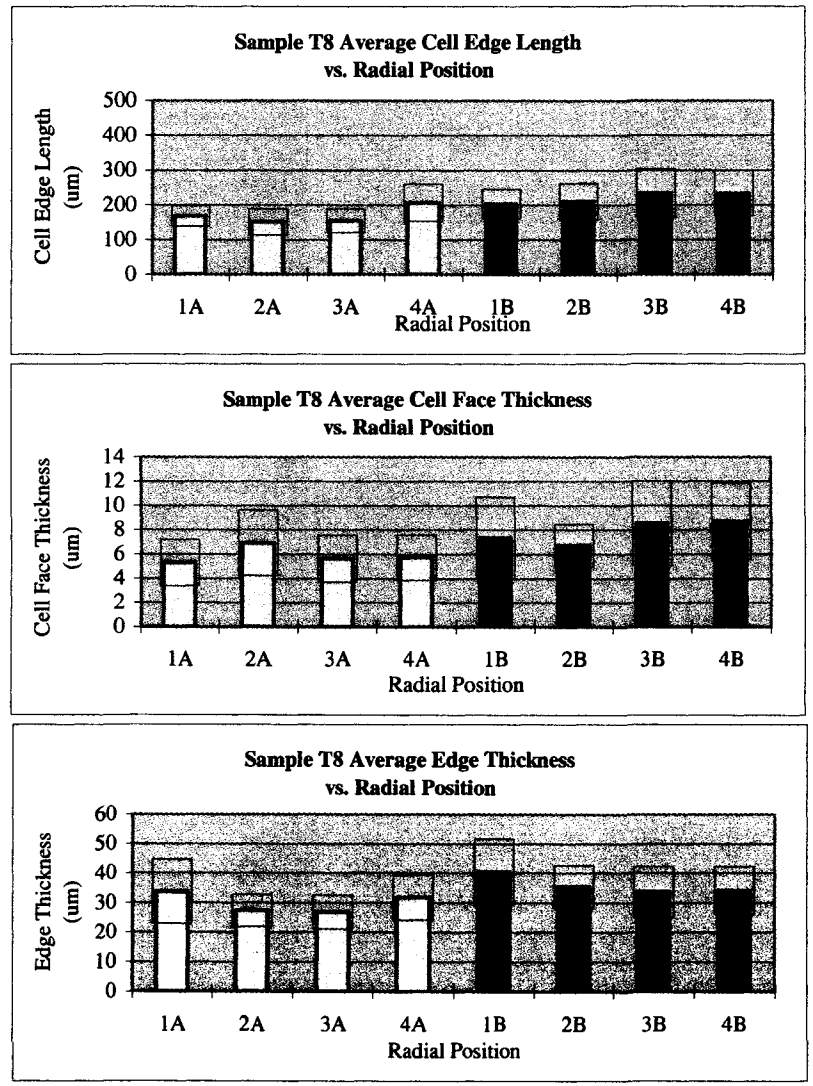

Figure-E.23: Graphs of Sample T8 Average Values used for Theoretical Calculations

Reproduced with permission of the copyright owner. Further reproduction prohibited without permission.

Table-E.7: Sample T14 Average Values

		Data used for Comparisons						Data used for Theoretical Calculations		
		Area (um^2)	Aspect Ratio	Angle (degree)	Dia (Max) (um)	Dia (Min) (um)	Dia (Mean) (um)	Cell Edge Length (um)	Cell Face Thickness (um)	Edge Thickness (um)
T14-1A	Average	11721	5.15	NA	132.26	84.55	108.17	92.31	3.09	17.14
	Std Dev	16050	NA	-	56.64	50.53	52.60	22.44	0.49	3.71
	% Diff	137%	-	-	43%	60%	49%	24%	16%	22%
T14-2A	Average	29861	3.81	NA	215.35	131.65	174.31	139.68	5.90	23.14
	Std Dev	30160	NA	-	110.27	74.76	88.66	59.68	3.15	10.10
	% Diff	101%	-	-	51%	57%	51%	43%	53%	44%
T14-3A	Average	26088	3.35	NA	205.33	116.67	161.59	144.36	5.90	25.43
	Std Dev	29127	NA	-	109.45	67.82	85.17	71.51	3.53	9.59
	% Diff	112%	-	-	53%	58%	53%	50%	60%	38%
T14-4A	Average	24273	2.26	NA	197.34	113.53	156.61	139.96	5.25	26.14
	Std Dev	23827	NA	-	99.17	65.47	79.01	60.01	2.71	10.10
	% Diff	98%	-	-	50%	58%	50%	43%	52%	39%
T14-1B	Average	72673	3.95	92.09	559.16	143.21	321.36	364.27	5.48	29.71
	Std Dev	66825	2.27	10.44	307.44	80.26	160.98	123.79	2.26	7.23
	% Diff	92%	57%	11%	55%	56%	50%	34%	41%	24%
T14-2B	Average	64239	5.73	77.44	683.44	132.93	345.43	404.27	8.59	41.67
	Std Dev	56227	3.25	11.60	441.16	69.56	211.64	225.21	3.20	7.81
	% Diff	88%	57%	15%	65%	52%	61%	56%	37%	19%
T14-3B	Average	49096	5.02	72.25	557.64	117.67	288.36	331.65	8.17	39.37
	Std Dev	38170	2.96	10.66	288.99	54.65	129.18	162.66	3.82	10.43
	% Diff	78%	59%	15%	52%	46%	45%	49%	47%	27%
T14-4B	Average	56994	1.86	43.39	365.88	169.36	265.01	227.21	6.43	36.29
	Std Dev	41903	0.59	29.96	154.07	71.38	101.25	65.20	2.40	6.79
	% Diff	74%	32%	69%	42%	42%	38%	29%	37%	19%

Reproduced with permission of the copyright owner. Further reproduction prohibited without permission.

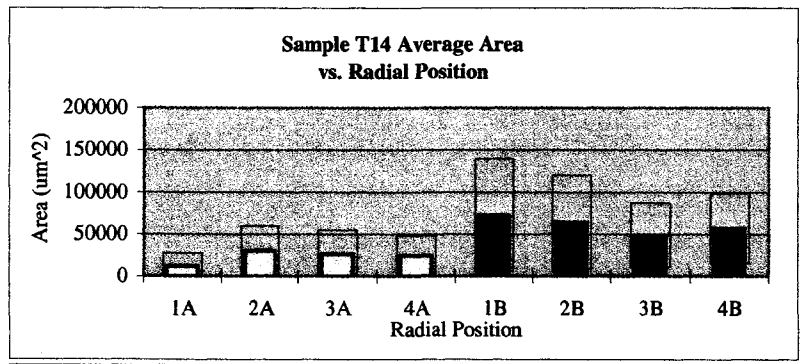

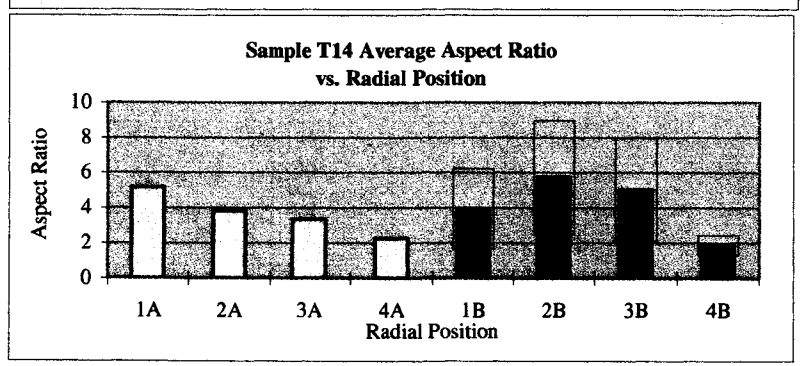

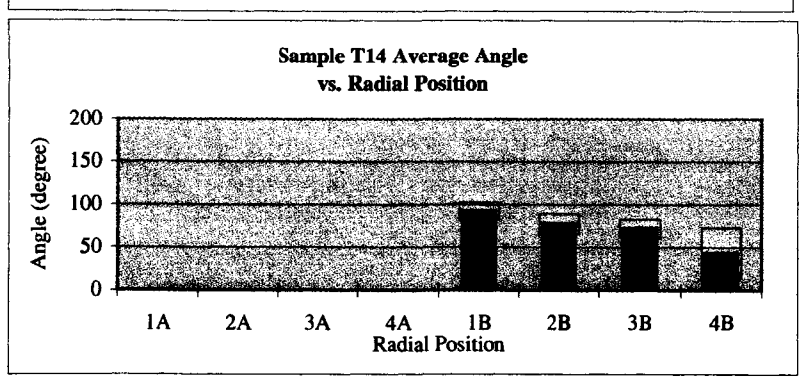

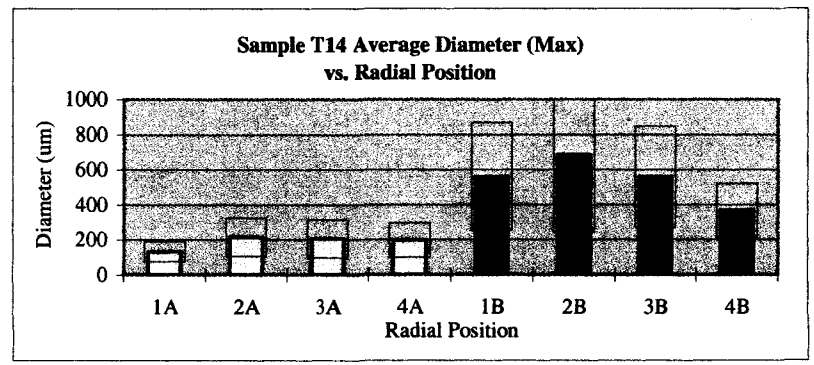

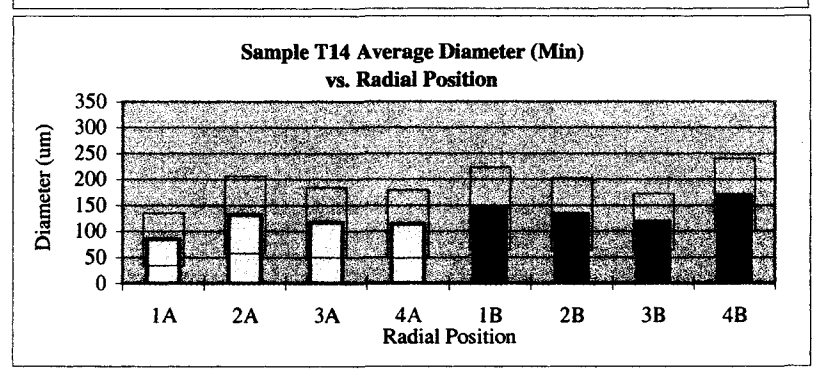

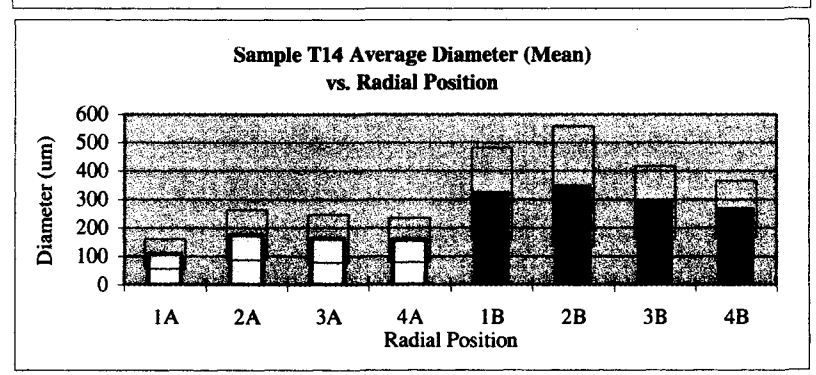

Figure-E.24: Graphs of Sample T14 Average Values used for Comparisons

Reproduced with permission of the copyright owner. Further reproduction prohibited without permission.

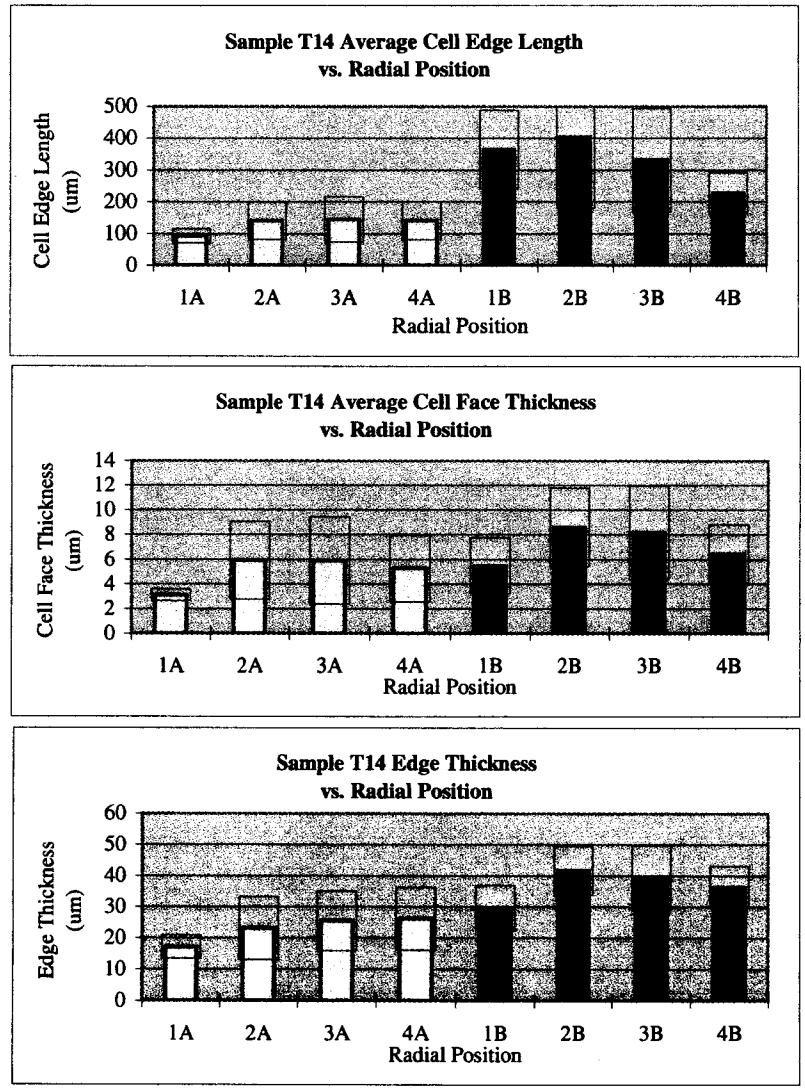

Figure-E.25: Graphs of Sample T14 Average Values used for Theoretical Calculations

Reproduced with permission of the copyright owner. Further reproduction prohibited without permission.

Table-E.8: Sample RC Average Values

		Data used for Comparisons						Data used for Theoretical Calculations		
		Area (um^2)	Aspect Ratio	Angle (degree)	Dia (Max) (um)	Dia (Min) (um)	Dia (Mean) (um)	Cell Edge Length (um)	Cell Face Thickness (um)	Edge Thickness (um)
RC-1A	Average	94577	1.34	NA	400.29	245.19	323.21	266.60	5.52	40.57
	Std Dev	68330	NA	-	158.10	109.04	133.78	67.35	1.36	5.83
	% Diff	72%	-	-	39%	44%	41%	25%	25%	14%
RC-2A	Average	85864	1.36	NA	383.39	225.67	305.99	248.16	6.58	39.71
	Std Dev	66051	NA	-	158.20	111.50	128.53	59.24	1.99	10.35
	% Diff	77%	-	-	41%	49%	42%	24%	30%	26%
RC-3A	Average	77035	1.49	NA	353.75	214.04	284.47	254.29	5.79	33.43
	Std Dev	83536	NA	-	165.52	120.71	139.24	60.16	2.18	7.50
	% Diff	108%	-	-	47%	56%	49%	24%	38%	22%
RC-4A	Average	73798	1.44	NA	356.70	218.89	292.16	255.20	6.03	33.86
	Std Dev	51776	NA	-	118.52	96.20	103.33	82.42	2.77	8.42
	% Diff	70%	-	-	33%	44%	35%	32%	46%	25%
RC-1B	Average	120884	1.43	96.08	448.64	277.58	366.16	281.90	6.02	29.14
	Std Dev	86681	0.29	42.32	173.50	137.88	148.92	74.98	1.62	4.50
	% Diff	72%	21%	44%	39%	50%	41%	27%	27%	15%
RC-2B	Average	105089	1.51	96.75	432.64	252.21	343.94	282.31	6.63	37.88
	Std Dev	91683	0.40	40.78	177.44	126.31	148.12	90.38	1.82	7.21
	% Diff	87%	27%	42%	41%	50%	43%	32%	27%	19%
RC-3B	Average	113543	1.51	97.51	438.22	259.74	351.51	299.36	7.42	37.71
	Std Dev	99461	0.45	40.85	192.27	140.84	155.35	83.27	2.82	10.42
	% Diff	88%	30%	42%	44%	54%	44%	28%	38%	28%
RC-4B	Average	104298	1.52	91.84	439.93	248.19	345.60	295.22	6.39	38.48
	Std Dev	82847	0.46	42.60	180.76	119.89	141.91	98.12	2.25	16.30
	% Diff	79%	30%	46%	41%	48%	41%	33%	35%	42%

Reproduced with permission of the copyright owner. Further reproduction prohibited without permission.

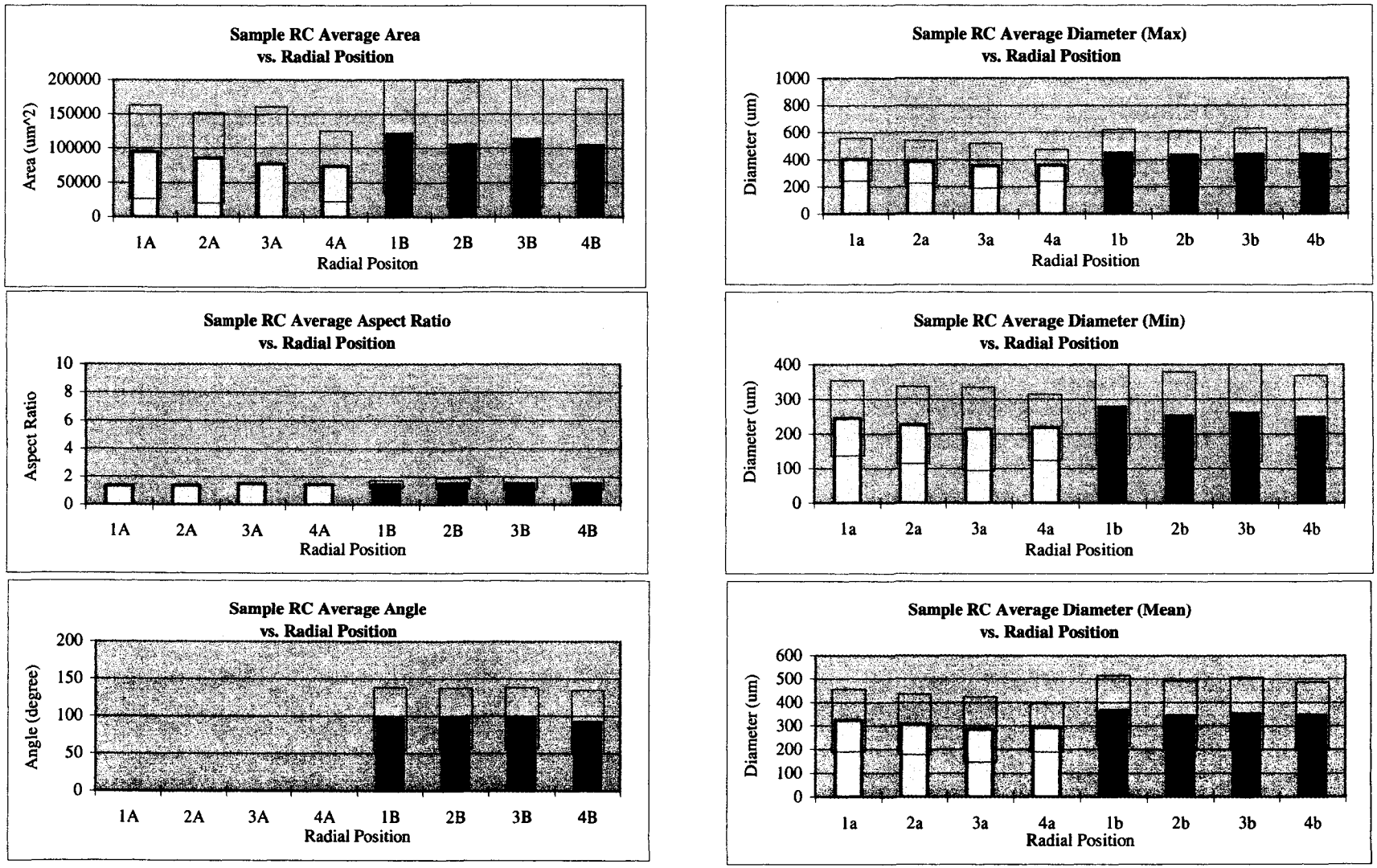

Figure-E.26: Graphs of Sample RC Average Values used for Comparisons

Reproduced with permission of the copyright owner. Further reproduction prohibited without permission.

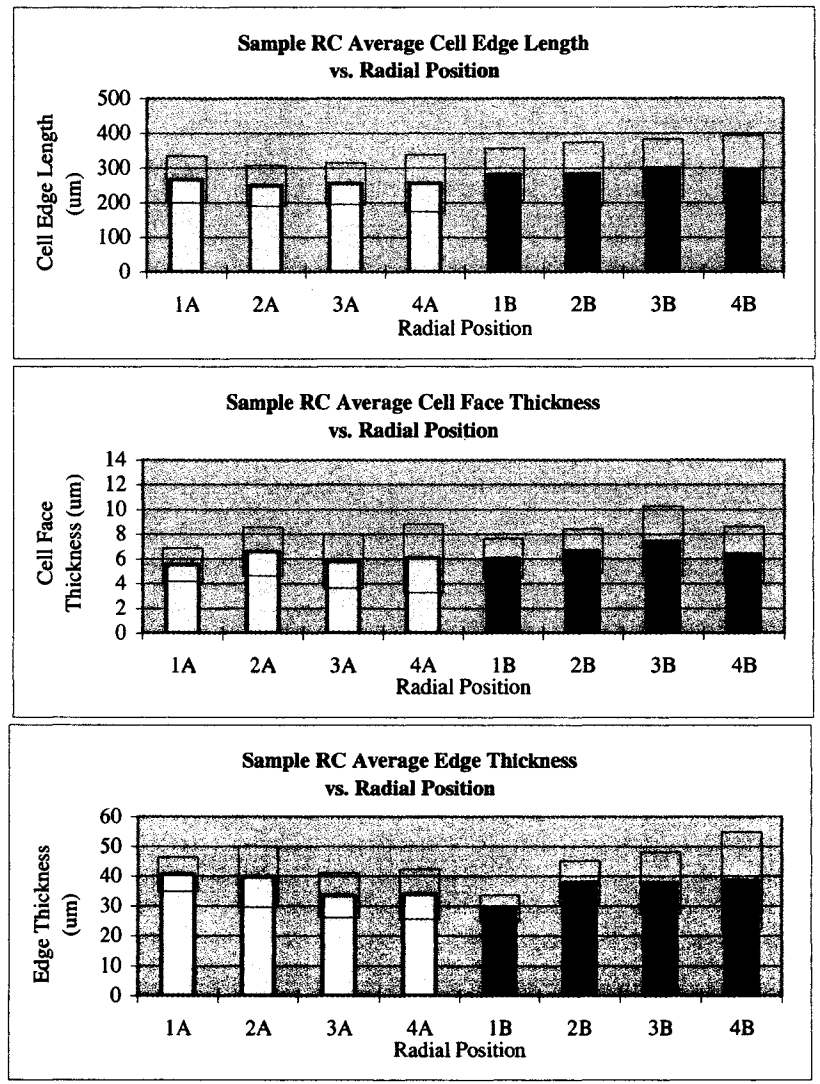

Figure-E.27: Graphs of Sample RC Average Values used for Theoretical Calculations

APPENDIX F

THEORETICAL CALCULATIONS

Reproduced with permission of the copyright owner. Further reproduction prohibited without permission.

Table-F.1: Theoretical Volume Fraction of Samples from Small Mold

	Volume Fraction (%)		
	Most Foams	Dodecahedron	Tetrakaidecahedra
S1-1A	53.9%	48.3%	54.6%
S1-2A	56.3%	50.8%	57.0%
S1-3A	47.2%	41.7%	47.9%
S1-4A	50.6%	45.0%	51.3%
S1-1B	44.5%	39.0%	45.1%
S1-2B	52.1%	46.5%	52.8%
S1-3B	52.6%	47.1%	53.3%
S1-4B	49.9%	44.3%	50.5%
S2-1A	57.4%	51.9%	58.1%
S2-2A	50.6%	45.0%	51.3%
S2-3A	53.7%	48.1%	54.4%
S2-4A	53.1%	47.5%	53.8%
S2-1B	49.6%	44.0%	50.3%
S2-2B	51.9%	46.4%	52.6%
S2-3B	46.4%	40.9%	47.0%
S2-4B	47.0%	41.5%	47.6%
S3-1A	54.6%	49.1%	55.3%
S3-2A	51.9%	46.3%	52.6%
S3-3A	51.9%	46.4%	52.6%
S3-4A	52.4%	46.8%	53.1%
S3-1B	49.9%	44.3%	50.6%
S3-2B	48.9%	43.3%	49.6%
S3-3B	45.7%	40.2%	46.3%
S3-4B	45.3%	39.8%	46.0%
S4-1A	59.4%	53.9%	60.1%
S4-2A	50.3%	44.8%	51.0%
S4-3A	54.2%	48.7%	54.9%
S4-4A	51.4%	45.8%	52.1%
S4-1B	41.3%	36.0%	42.0%
S4-2B	41.6%	36.3%	42.2%
S4-3B	43.2%	37.8%	43.9%
S4-4B	55.0%	49.4%	55.7%

Reproduced with permission of the copyright owner. Further reproduction prohibited without permission.

Table-F.2: Theoretical Volume Fraction of Samples from Tall Mold

	Volume Fraction (%)		
	Most Foams	Dodecahedron	Tetrakaidecahedra
T1-1A	60.7%	55.3%	61.4%
T1-2A	50.3%	44.7%	51.0%
T1-3A	53.0%	47.4%	53.7%
T1-4A	52.7%	47.1%	53.4%
T1-1B	45.2%	39.8%	45.9%
T1-2B	59.9%	54.5%	60.6%
T1-3B	36.4%	31.4%	37.0%
T1-4B	49.2%	43.6%	49.9%
T8-1A	68.1%	63.0%	68.7%
T8-2A	54.3%	48.7%	54.9%
T8-3A	57.8%	52.3%	58.5%
T8-4A	58.6%	53.1%	59.3%
T8-1B	64.5%	59.2%	65.1%
T8-2B	59.7%	54.2%	60.3%
T8-3B	48.7%	43.2%	49.4%
T8-4B	48.8%	43.3%	49.5%
T14-1A	63.2%	57.8%	63.8%
T14-2A	52.0%	46.4%	52.7%
T14-3A	55.9%	50.3%	56.5%
T14-4A	60.8%	55.3%	61.4%
T14-1B	42.4%	37.1%	43.1%
T14-2B	45.4%	40.0%	46.1%
T14-3B	48.8%	43.3%	49.5%
T14-4B	60.0%	54.6%	60.7%

Table-F.3: Theoretical Volume Fraction of Samples from Reference Mold

	Volume Fraction (%)		
	Most Foams	Dodecahedron	Tetrakaidecahedra
RC-1A	65.1%	59.9%	65.7%
RC-2A	61.7%	56.3%	62.3%
RC-3A	55.8%	50.3%	56.5%
RC-4A	55.4%	49.8%	56.1%
RC-1B	45.5%	40.0%	46.2%
RC-2B	56.1%	50.6%	56.8%
RC-3B	51.6%	46.1%	52.3%
RC-4B	56.7%	51.1%	57.4%

Reproduced with permission of the copyright owner. Further reproduction prohibited without permission.

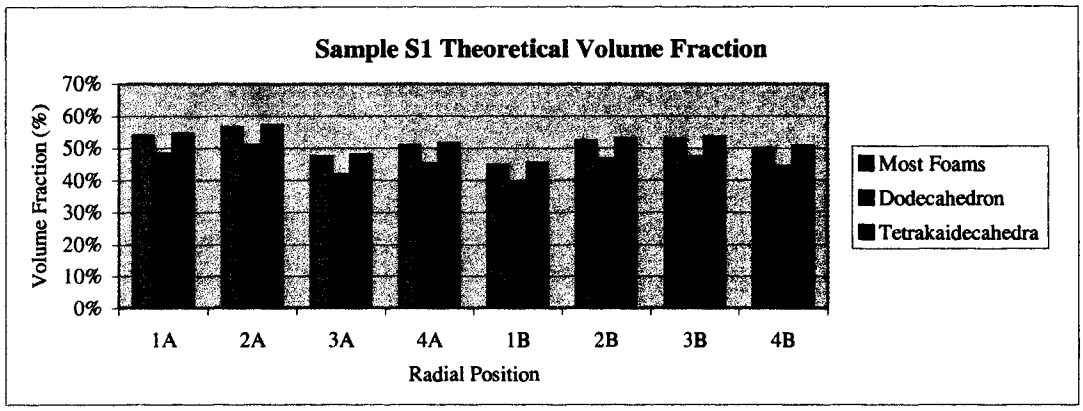

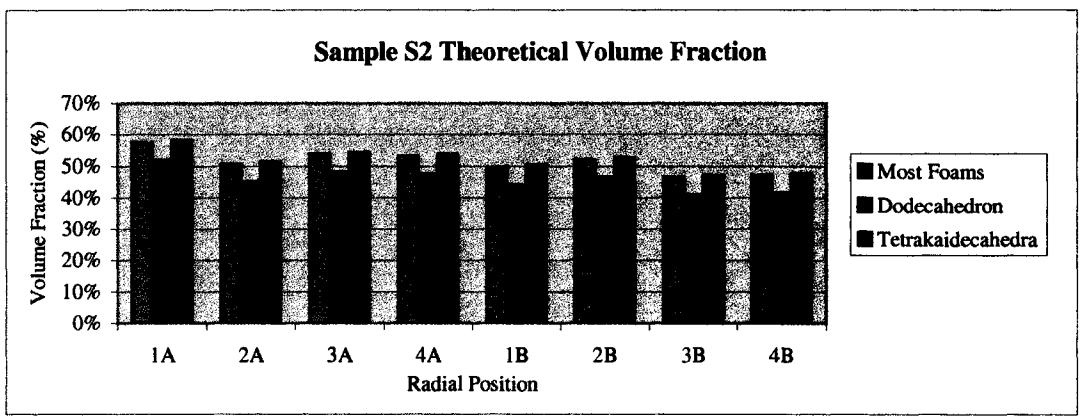

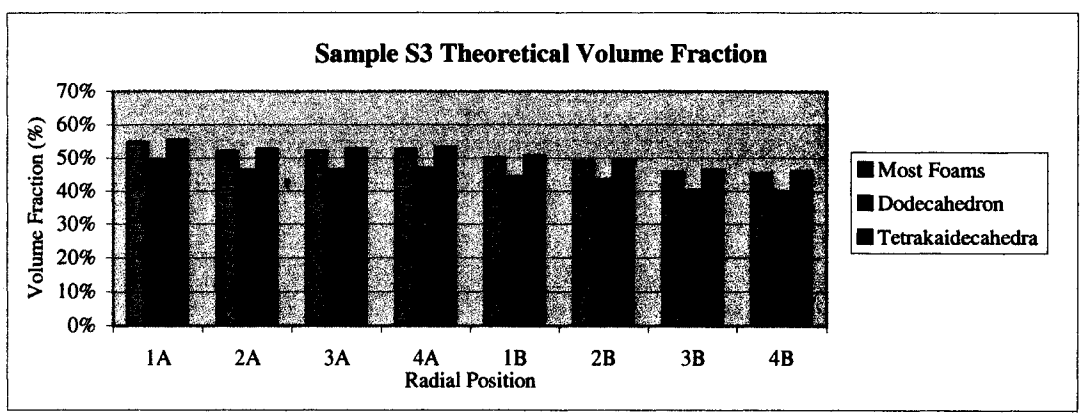

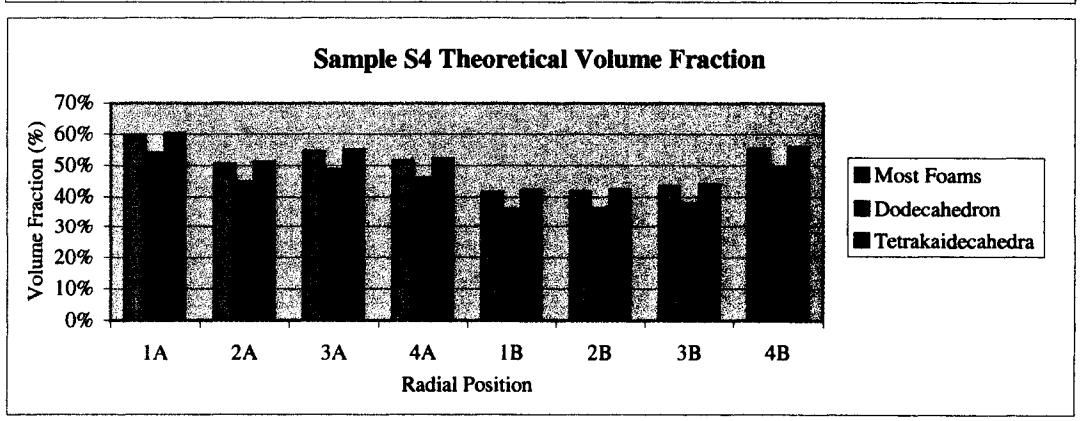

Figure-F.1: Theoretical Volume Fraction for Small Mold Samples

Reproduced with permission of the copyright owner. Further reproduction prohibited without permission.

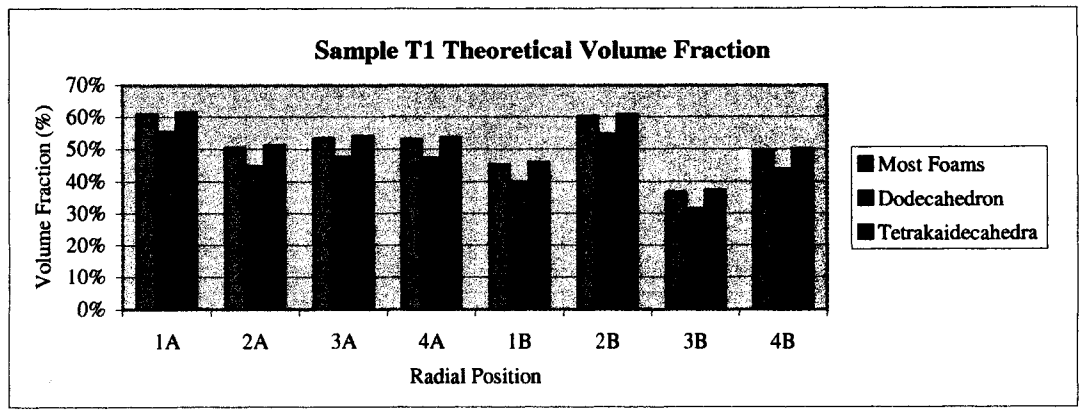

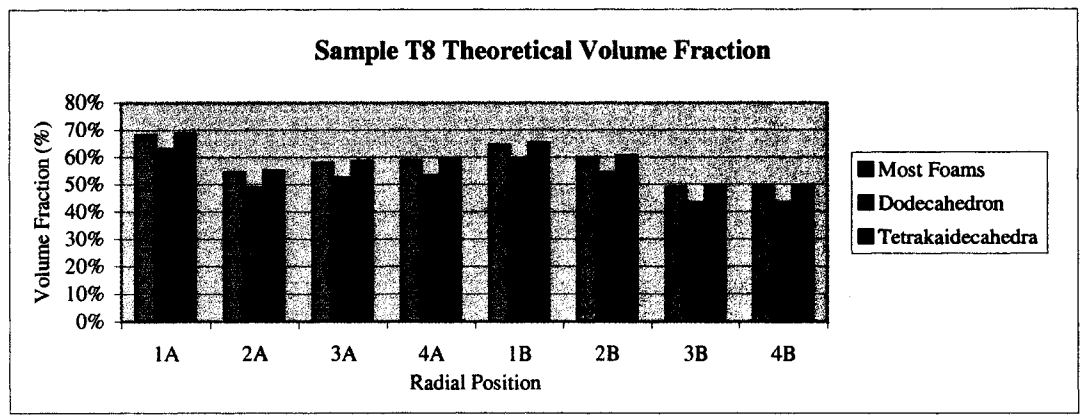

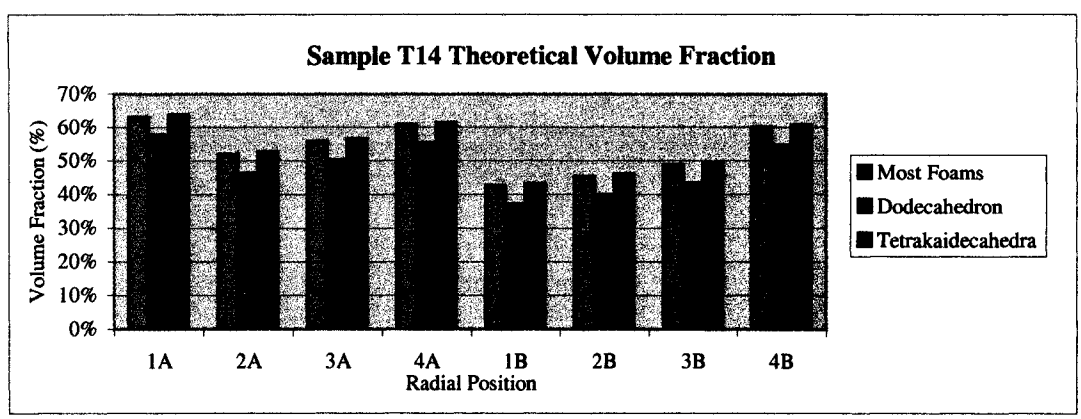

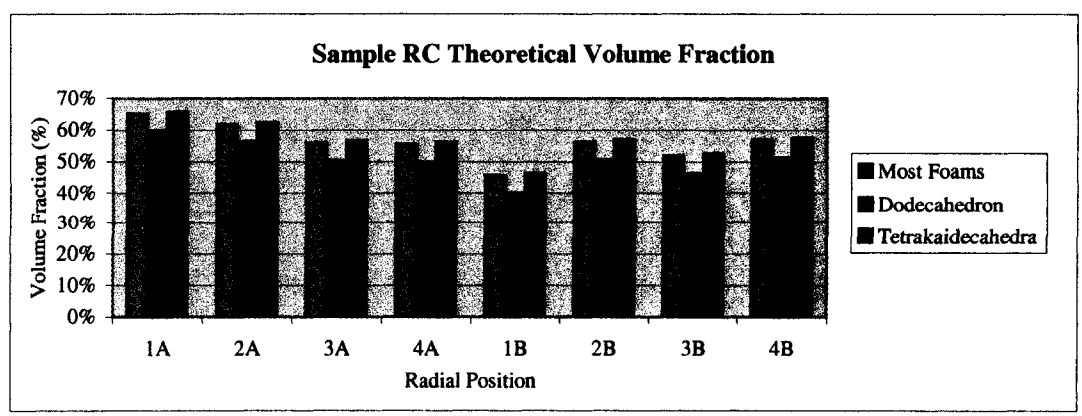

Figure-F.2: Theoretical Volume Fraction for Tall and Reference Mold Samples

Reproduced with permission of the copyright owner. Further reproduction prohibited without permission.

Table-F.4: Theoretical Density of Samples from Small Mold

	Density (g/cc)		
	Most Foams	Dodecahedron	Tetrakaidecahedra
S1-1A	0.063	0.071	0.044
S1-2A	0.076	0.081	0.050
S1-3A	0.067	0.086	0.054
S1-4A	0.079	0.095	0.059
S1-1B	0.059	0.079	0.049
S1-2B	0.078	0.092	0.057
S1-3B	0.076	0.088	0.054
S1-4B	0.069	0.085	0.053
S2-1A	0.068	0.071	0.044
S2-2A	0.067	0.080	0.050
S2-3A	0.069	0.079	0.049
S2-4A	0.074	0.085	0.053
S2-1B	0.059	0.072	0.045
S2-2B	0.063	0.074	0.046
S2-3B	0.059	0.076	0.047
S2-4B	0.057	0.074	0.046
S3-1A	0.064	0.072	0.045
S3-2A	0.067	0.079	0.049
S3-3A	0.074	0.086	0.054
S3-4A	0.074	0.086	0.054
S3-1B	0.046	0.057	0.035
S3-2B	0.039	0.048	0.030
S3-3B	0.053	0.070	0.043
S3-4B	0.044	0.058	0.036
S4-1A	0.074	0.074	0.046
S4-2A	0.074	0.089	0.055
S4-3A	0.080	0.090	0.056
S4-4A	0.065	0.077	0.048
S4-1B	0.045	0.063	0.039
S4-2B	0.045	0.064	0.040
S4-3B	0.055	0.075	0.047
S4-4B	0.065	0.072	0.045

Reproduced with permission of the copyright owner. Further reproduction prohibited without permission.

Table-F.5: Theoretical Density of Samples from Tall Mold

	Density (g/cc)		
	Most Foams	Dodecahedron	Tetrakaidecahedra
T1-1A	0.071	0.069	0.043
T1-2A	0.079	0.096	0.059
T1-3A	0.080	0.093	0.057
T1-4A	0.088	0.102	0.063
T1-1B	0.053	0.070	0.043
T1-2B	0.064	0.064	0.040
T1-3B	0.042	0.063	0.039
T1-4B	0.063	0.078	0.049
T8-1A	0.090	0.072	0.045
T8-2A	0.093	0.104	0.065
T8-3A	0.079	0.083	0.051
T8-4A	0.062	0.063	0.039
T8-1B	0.093	0.083	0.051
T8-2B	0.073	0.073	0.045
T8-3B	0.067	0.083	0.052
T8-4B	0.068	0.085	0.053
T14-1A	0.083	0.076	0.047
T14-2A	0.082	0.096	0.060
T14-3A	0.086	0.093	0.058
T14-4A	0.088	0.086	0.053
T14-1B	0.025	0.034	0.021
T14-2B	0.037	0.048	0.030
T14-3B	0.045	0.056	0.035
T14-4B	0.065	0.065	0.040

Table-F.6: Theoretical Density of Samples from Reference Mold

	Density (g/cc)		
	Most Foams	Dodecahedron	Tetrakaidecahedra
RC-1A	0.054	0.047	0.029
RC-2A	0.064	0.060	0.038
RC-3A	0.048	0.052	0.032
RC-4A	0.049	0.054	0.033
RC-1B	0.037	0.049	0.030
RC-2B	0.050	0.054	0.033
RC-3B	0.048	0.057	0.035
RC-4B	0.046	0.049	0.031

Reproduced with permission of the copyright owner. Further reproduction prohibited without permission.

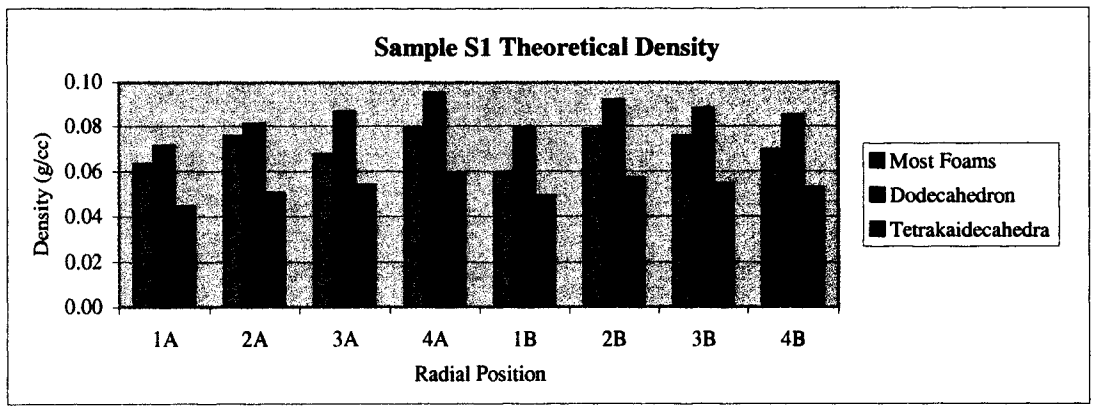

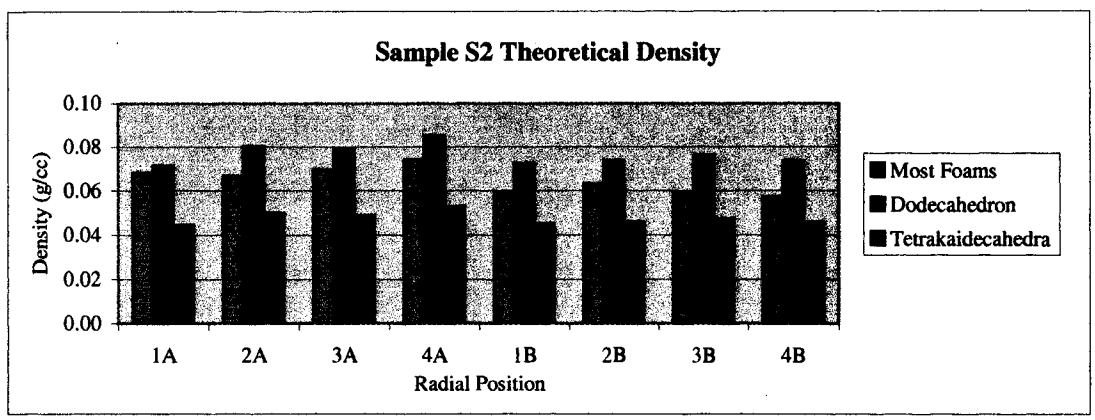

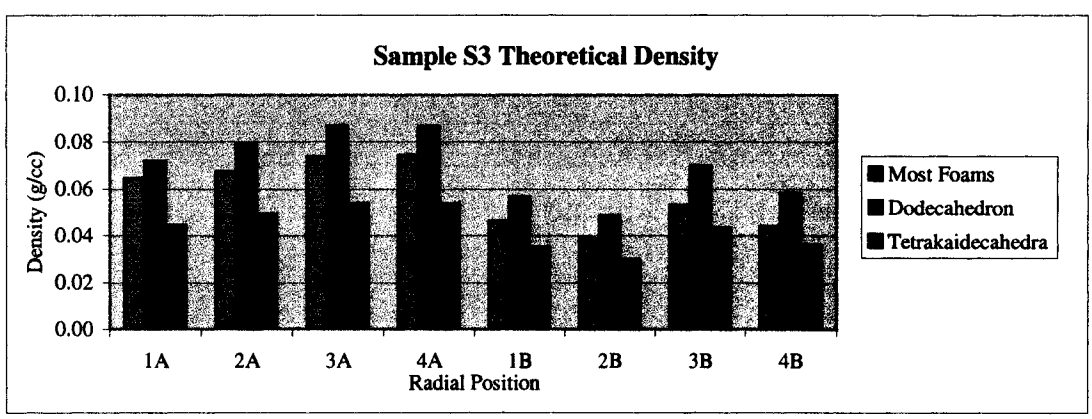

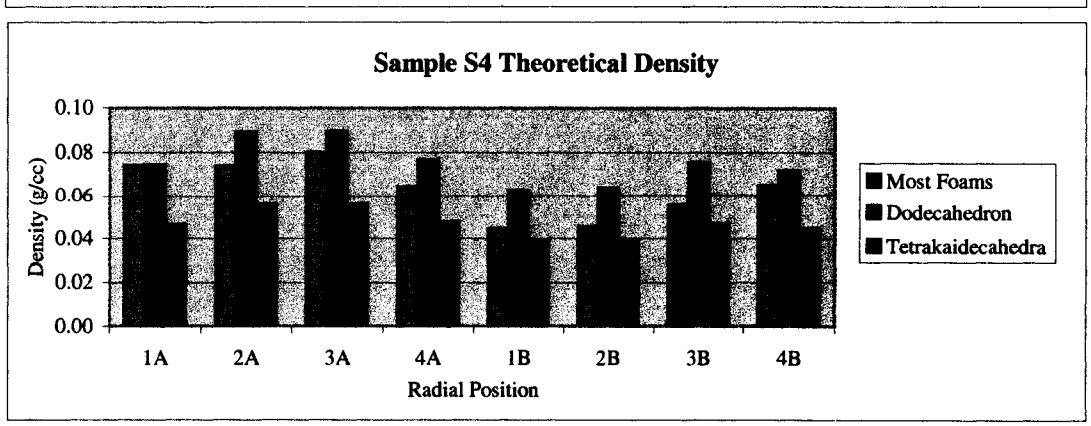

Figure-F.3: Theoretical Density for Small Mold Samples

Reproduced with permission of the copyright owner. Further reproduction prohibited without permission.

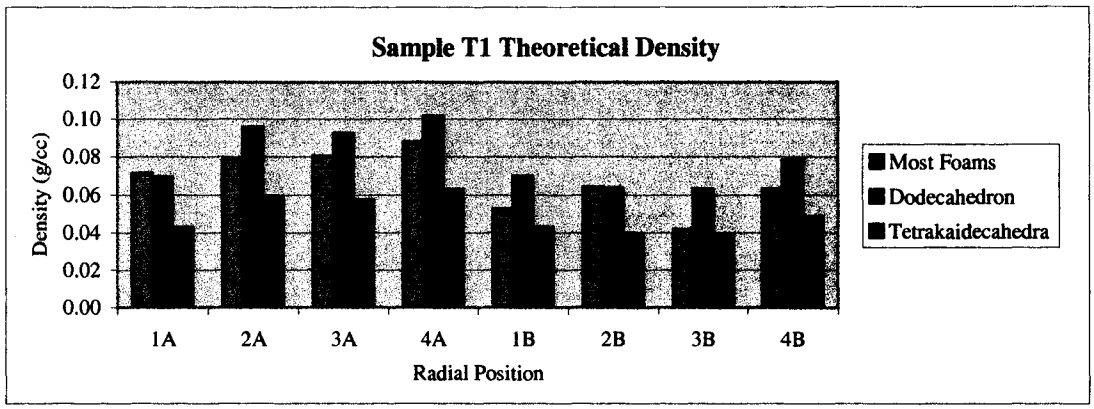

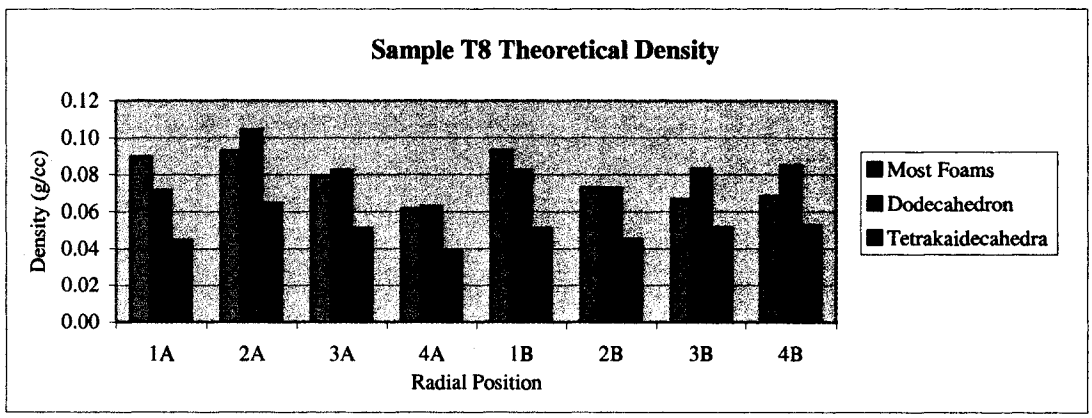

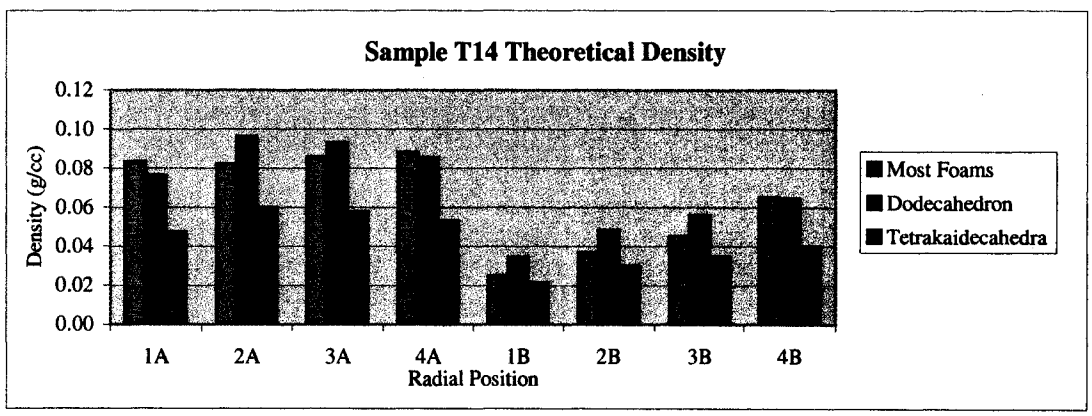

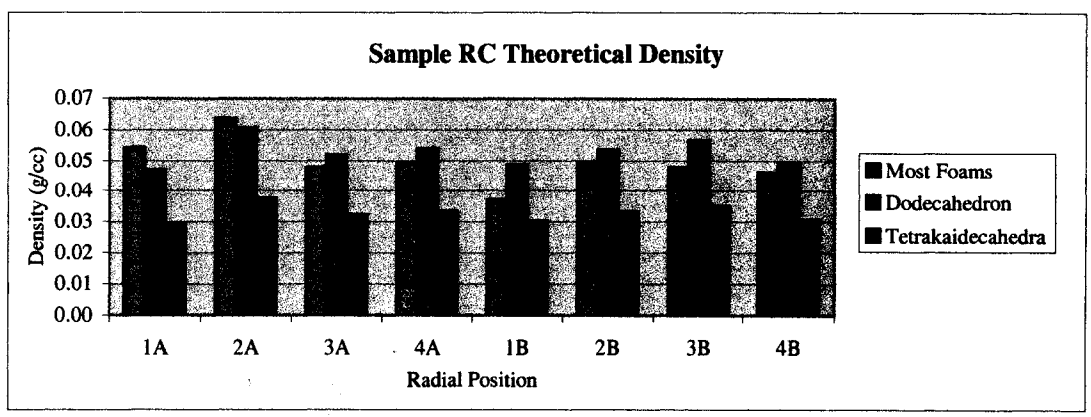

Figure-F.4: Theoretical Density for Tall and Reference Mold Samples

Reproduced with permission of the copyright owner. Further reproduction prohibited without permission.

Table-F.7: Theoretical Mechanical Properties of Samples from Small Mold

	Normalized Modulus (MPa)		Normalized σpl Collapse (MPa)	Normalized σel Collapse (MPa)	
	Es=1.6	Es=2.7	σys=1.27	Es=1.6	Es=2.7
S1-1A	89.2	150.5	3.80	0.54	0.91
S1-2A	75.4	127.2	3.04	0.55	0.92
S1-3A	96.5	162.9	3.90	0.54	0.91
S1-4A	81.9	138.2	3.17	0.55	0.93
S1-1B	110.9	187.2	4.67	0.54	0.90
S1-2B	79.9	134.8	3.12	0.55	0.93
S1-3B	80.9	136.6	3.20	0.55	0.92
S1-4B	90.2	152.3	3.64	0.54	0.92
S2-1A	78.9	133.1	3.32	0.54	0.92
S2-2A	91.7	154.8	3.78	0.54	0.91
S2-3A	84.1	142.0	3.46	0.54	0.92
S2-4A	81.5	137.5	3.26	0.55	0.92
S2-1B	101.4	171.1	4.35	0.54	0.90
S2-2B	93.0	156.9	3.93	0.54	0.91
S2-3B	107.9	182.0	4.59	0.54	0.90
S2-4B	108.5	183.1	4.66	0.53	0.90
S3-1A	86.6	146.1	3.67	0.54	0.91
S3-2A	88.8	149.8	3.66	0.54	0.91
S3-3A	83.5	141.0	3.33	0.55	0.92
S3-4A	82.3	138.9	3.28	0.55	0.92
S3-1B	118.6	200.2	5.57	0.53	0.89
S3-2B	136.4	230.1	6.81	0.52	0.88
S3-3B	116.6	196.8	5.13	0.53	0.90
S3-4B	133.6	225.4	6.30	0.52	0.89
S4-1A	71.6	120.8	2.95	0.55	0.92
S4-2A	86.0	145.0	3.40	0.55	0.92
S4-3A	75.8	127.9	2.96	0.55	0.93
S4-4A	92.2	155.5	3.85	0.54	0.91
S4-1B	141.7	239.1	6.58	0.52	0.89
S4-2B	139.4	235.2	6.43	0.53	0.89
S4-3B	118.8	200.5	5.12	0.53	0.90
S4-4B	85.5	144.2	3.62	0.54	0.91

Reproduced with permission of the copyright owner. Further reproduction prohibited without permission.

Table-F.8: Theoretical Mechanical Properties of Samples from Tall Mold

	Normalized Modulus (MPa)		Normalized σpl Collapse (MPa)	Normalized σel Collapse (MPa)	
	Es=1.6	Es=2.7	σys=1.27	Es=1.6	Es=2.7
T1-1A	71.3	120.3	3.01	0.54	0.92
T1-2A	82.1	138.6	3.17	0.55	0.93
T1-3A	77.1	130.2	2.99	0.55	0.93
T1-4A	73.3	123.7	2.75	0.56	0.94
T1-1B	118.4	199.7	5.22	0.53	0.90
T1-2B	77.6	130.9	3.38	0.54	0.91
T1-3B	160.5	270.9	7.56	0.52	0.88
T1-4B	97.4	164.3	4.06	0.54	0.91
T8-1A	51.8	87.4	2.12	0.56	0.94
T8-2A	68.6	115.7	2.53	0.56	0.95
T8-3A	70.8	119.4	2.82	0.55	0.93
T8-4A	82.1	138.6	3.61	0.54	0.91
T8-1B	55.2	93.1	2.16	0.56	0.95
T8-2B	71.8	121.1	2.98	0.55	0.92
T8-3B	94.8	160.0	3.87	0.54	0.91
T8-4B	93.0	156.9	3.77	0.54	0.92
T14-1A	61.0	102.9	2.47	0.55	0.93
T14-2A	77.6	131.0	2.97	0.55	0.93
T14-3A	70.0	118.1	2.68	0.56	0.94
T14-4A	62.2	104.9	2.43	0.56	0.94
T14-1B	208.8	352.4	12.16	0.51	0.86
T14-2B	150.9	254.6	7.62	0.52	0.88
T14-3B	123.3	208.1	5.83	0.53	0.89
T14-4B	76.7	129.4	3.33	0.54	0.91

Table-F.9: Theoretical Mechanical Properties of Samples from Reference Mold

	Normalized Modulus (MPa)		Normalized σpl Collapse (MPa)	Normalized σel Collapse (MPa)	
	Es=1.6	Es=2.7	σys=1.27	Es=1.6	Es=2.7
RC-1A	76.7	129.4	3.67	0.53	0.90
RC-2A	75.1	126.7	3.32	0.54	0.91
RC-3A	103.2	174.1	4.90	0.53	0.89
RC-4A	102.3	172.6	4.80	0.53	0.89
RC-1B	150.3	253.6	7.57	0.52	0.88
RC-2B	100.1	169.0	4.70	0.53	0.89
RC-3B	112.3	189.6	5.25	0.53	0.89
RC-4B	103.6	174.9	5.01	0.53	0.89

Reproduced with permission of the copyright owner. Further reproduction prohibited without permission.

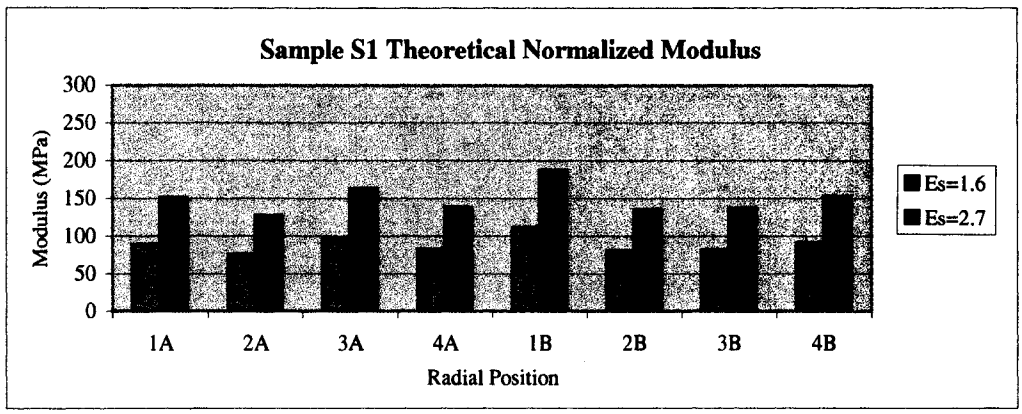

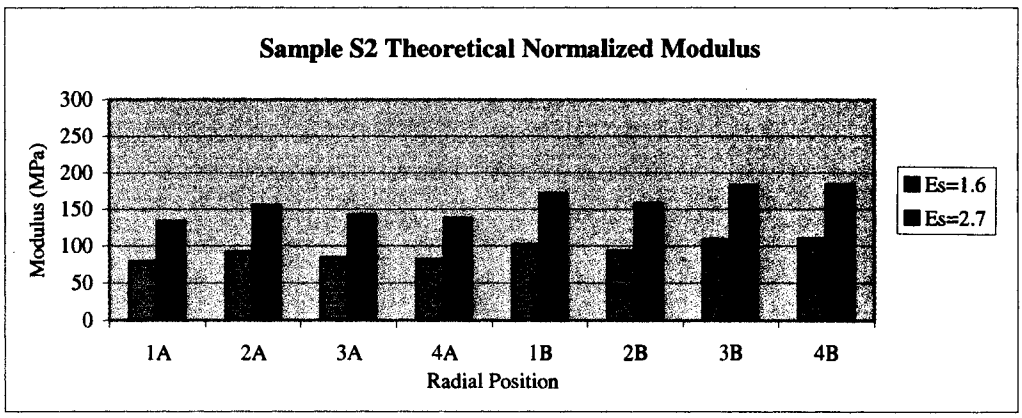

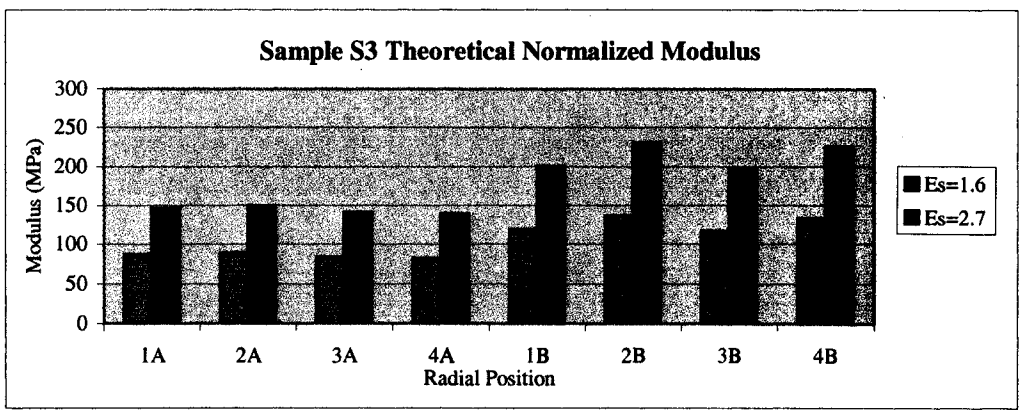

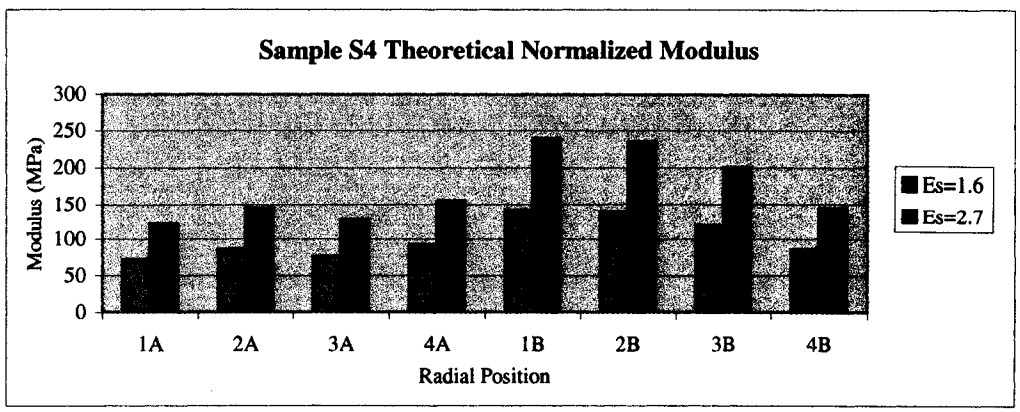

Figure-F.5: Theoretical Modulus for Small Mold Samples

Reproduced with permission of the copyright owner. Further reproduction prohibited without permission.

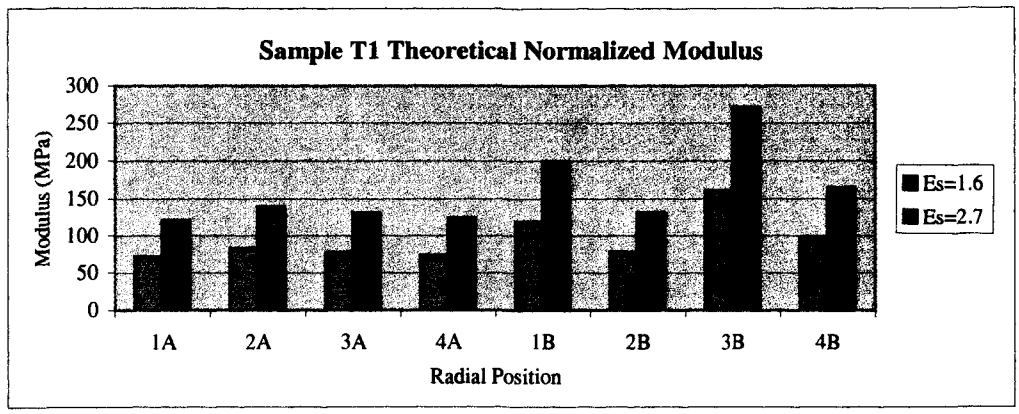

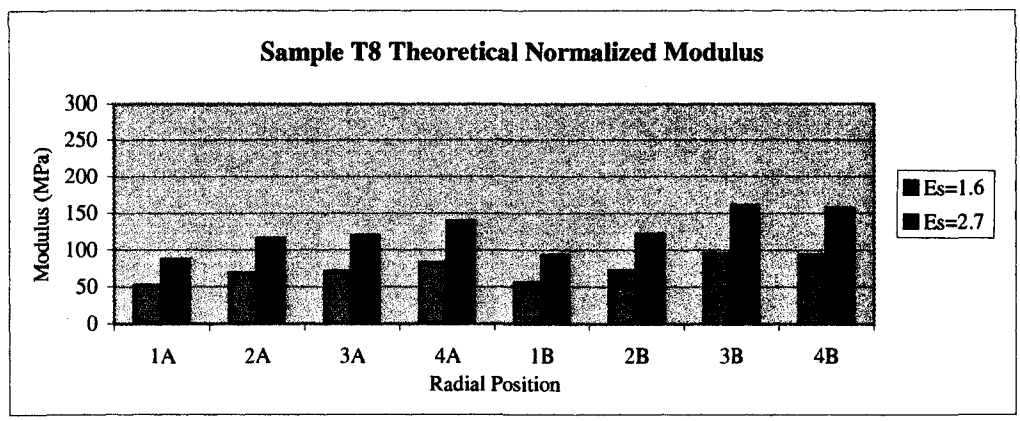

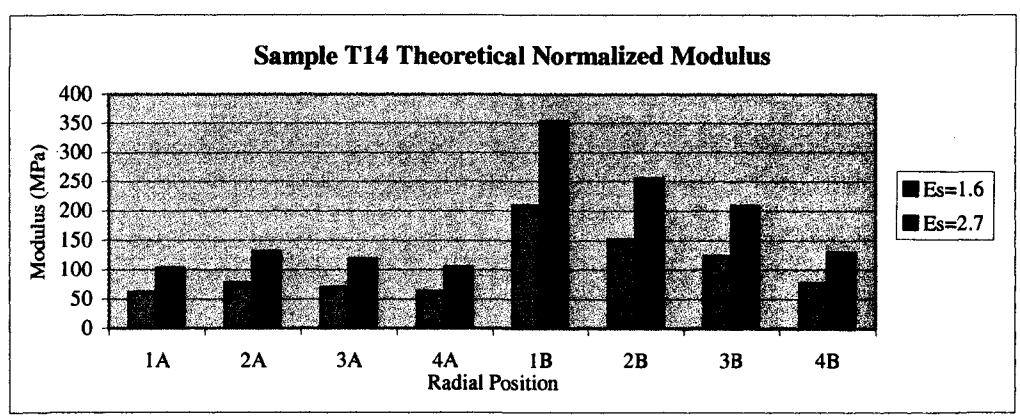

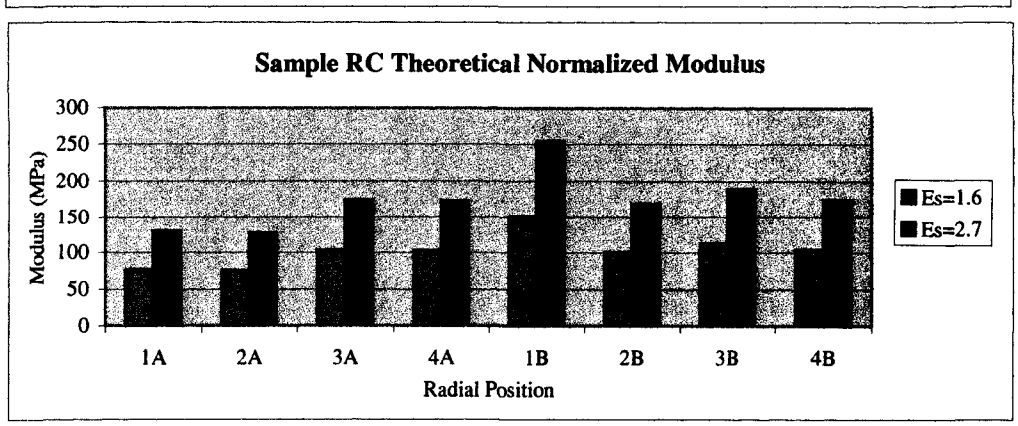

Figure-F.6: Theoretical Modulus for Tall and Reference Mold Samples

Reproduced with permission of the copyright owner. Further reproduction prohibited without permission.

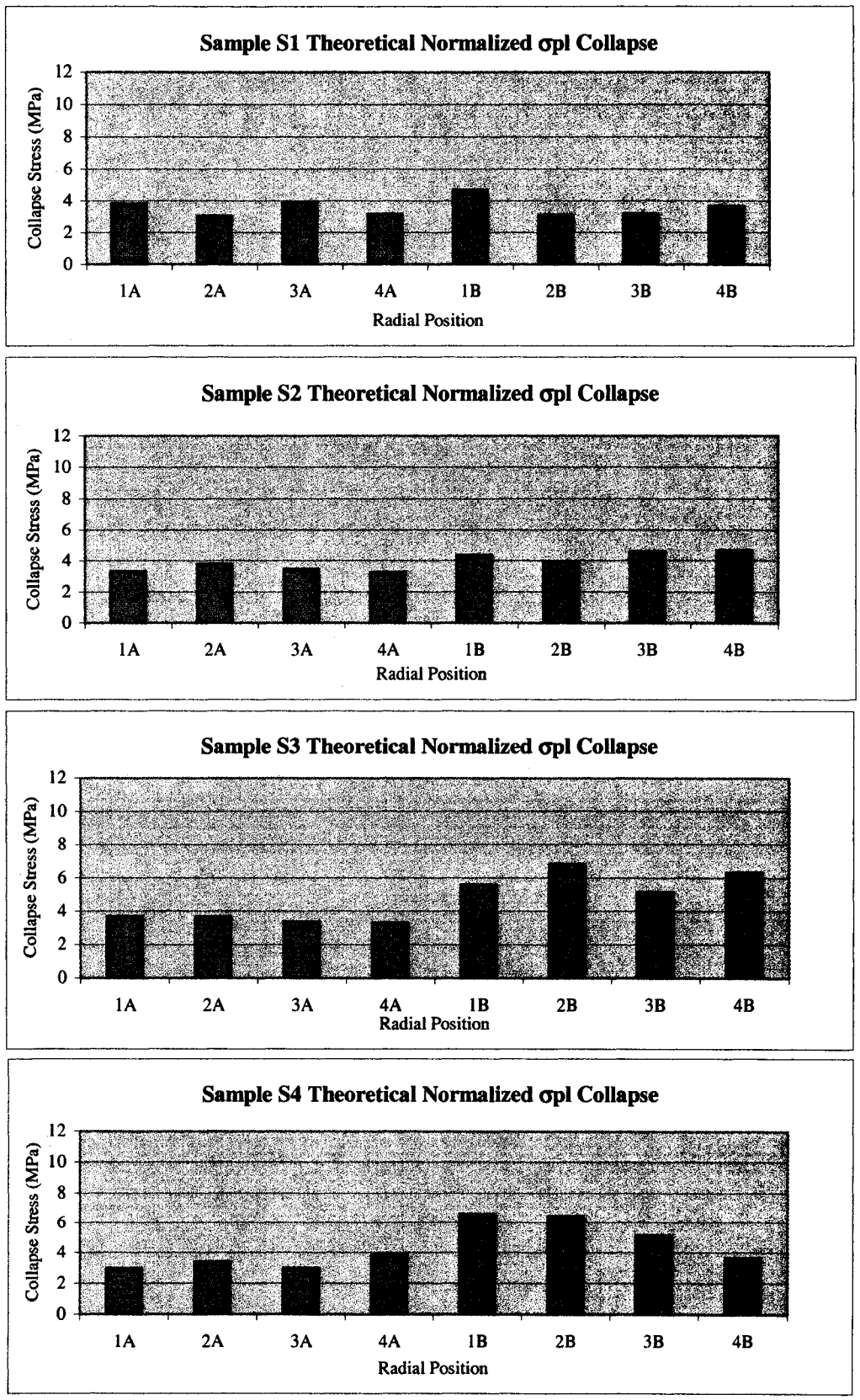

Figure-F.7: Theoretical σpl Collapse for Small Mold Samples

Reproduced with permission of the copyright owner. Further reproduction prohibited without permission.

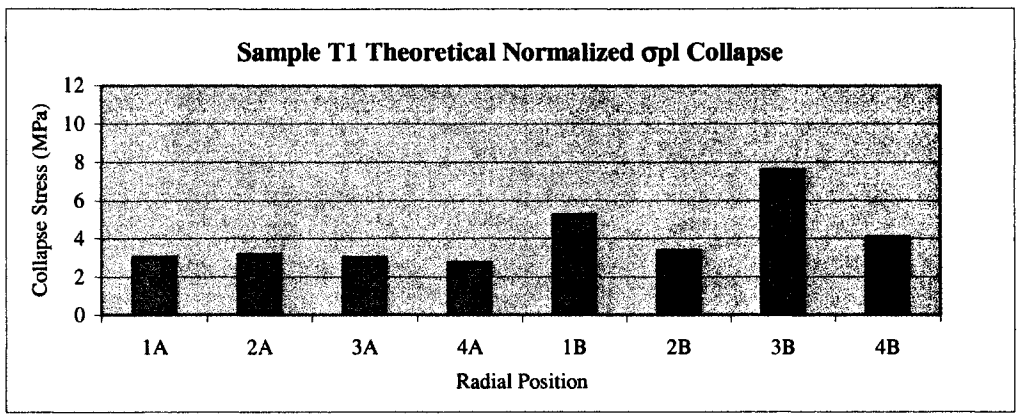

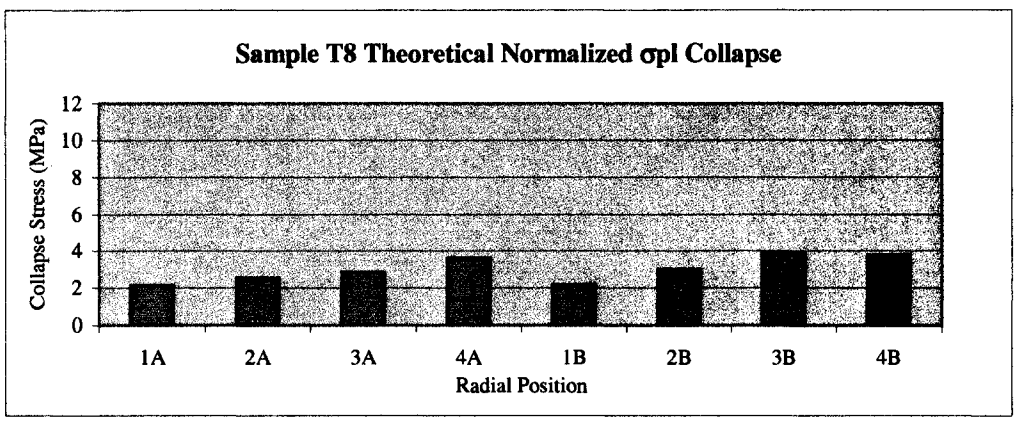

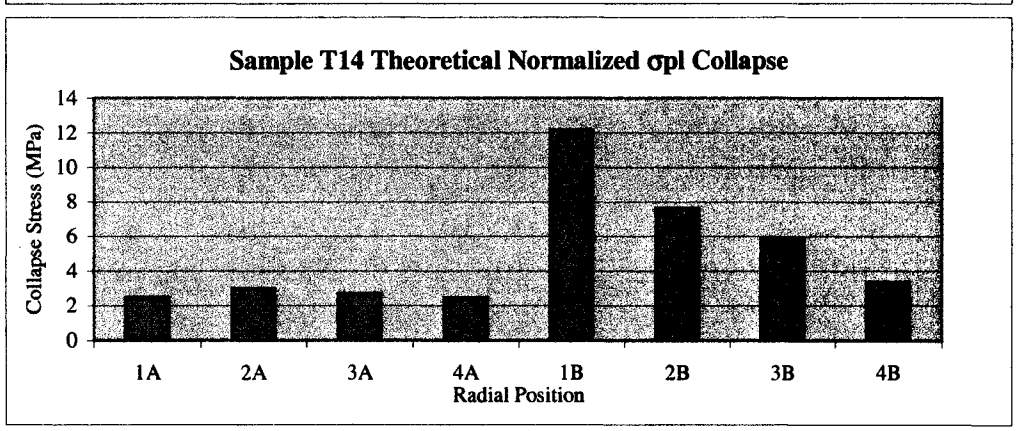

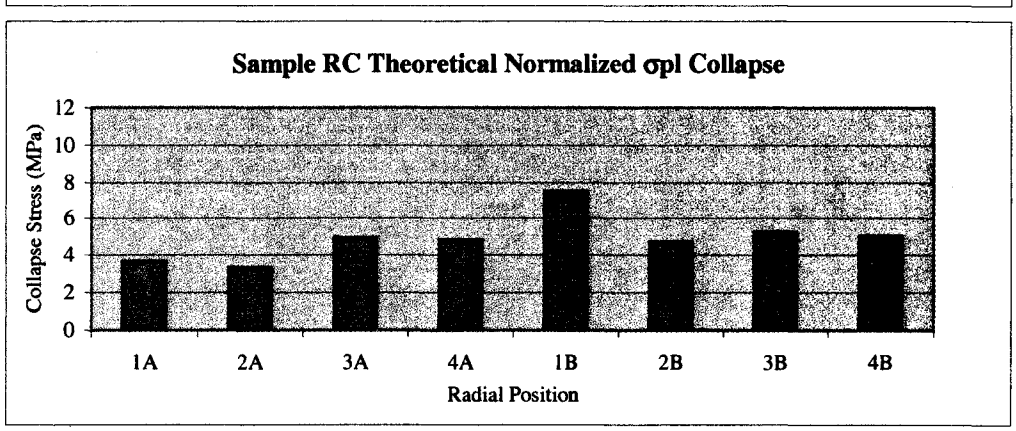

Figure-F.8: Theoretical σpl Collapse for Tall and Reference Mold Samples

Reproduced with permission of the copyright owner. Further reproduction prohibited without permission.

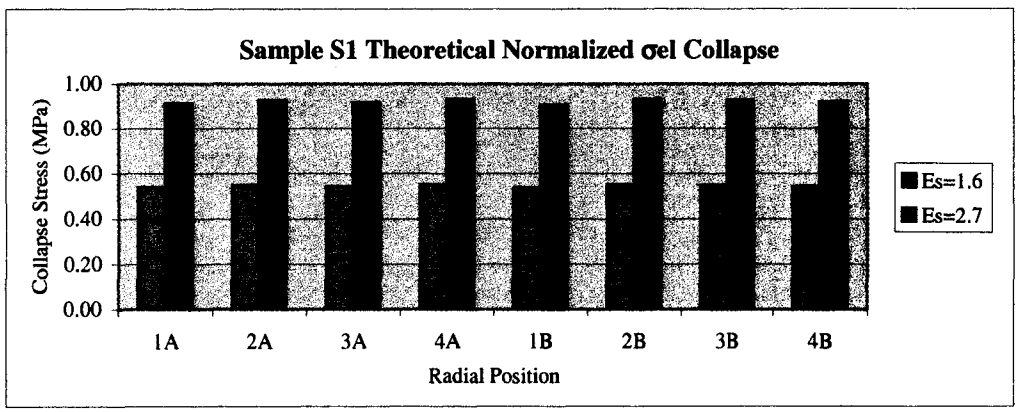

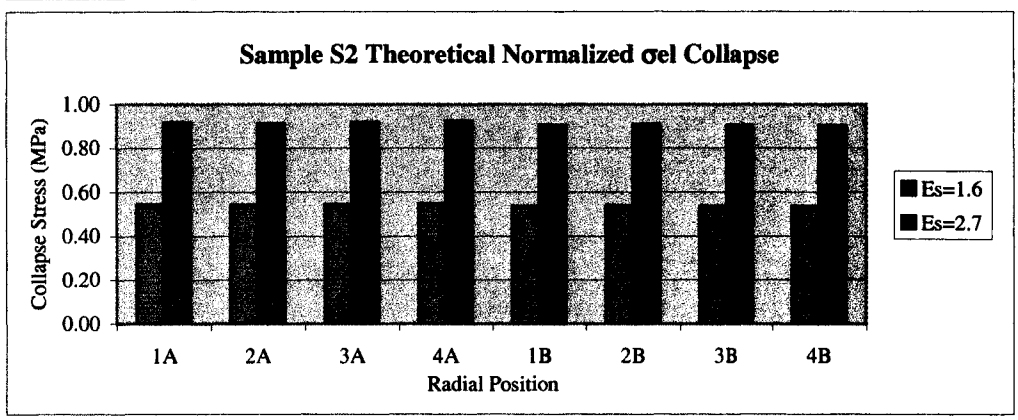

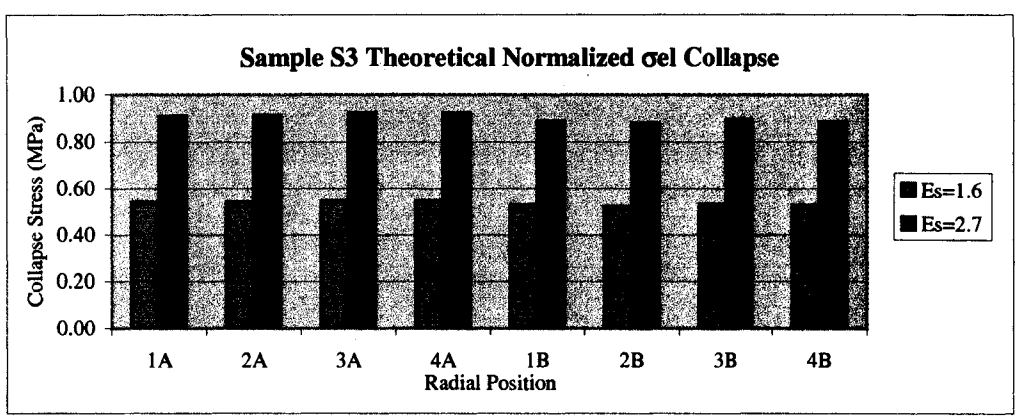

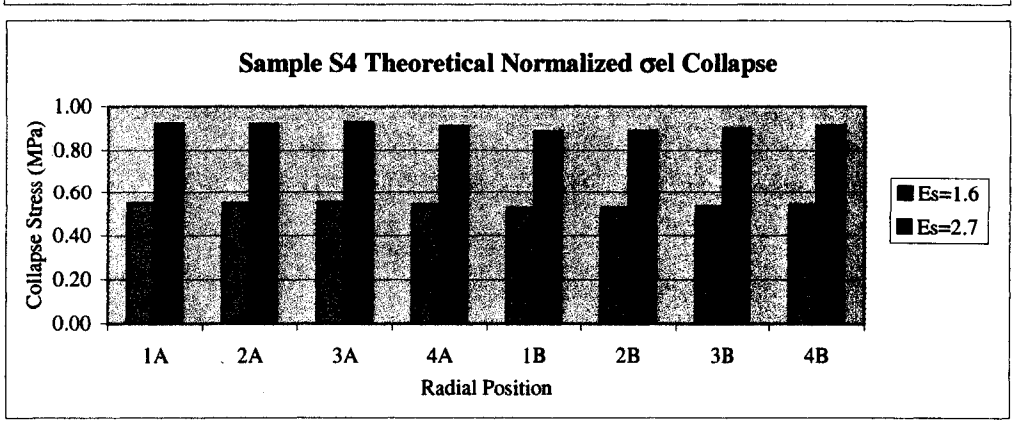

Figure-F.9: Theoretical σel Collapse for Small Mold Samples

Reproduced with permission of the copyright owner. Further reproduction prohibited without permission.

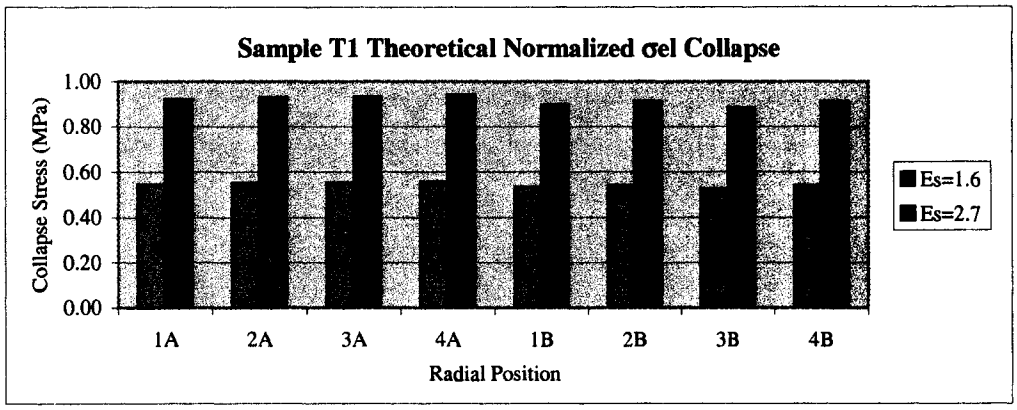

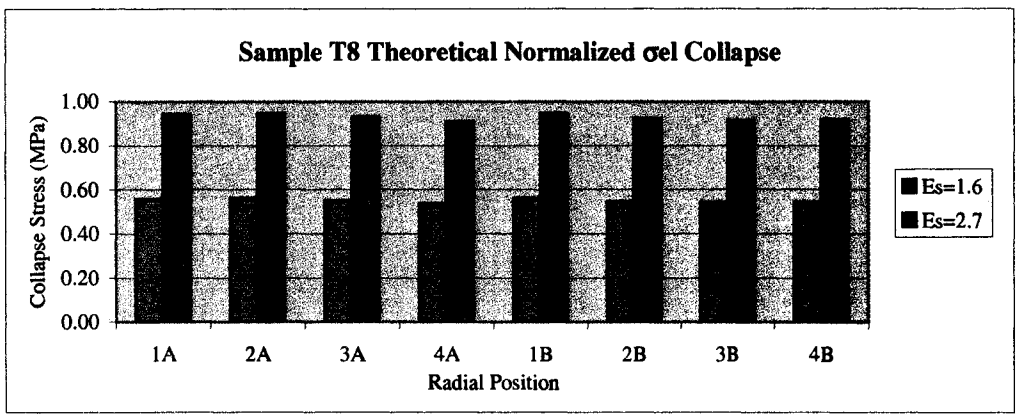

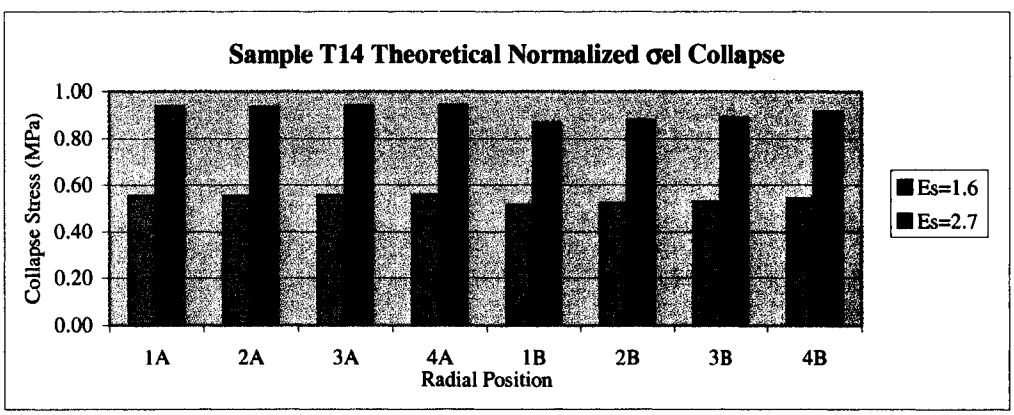

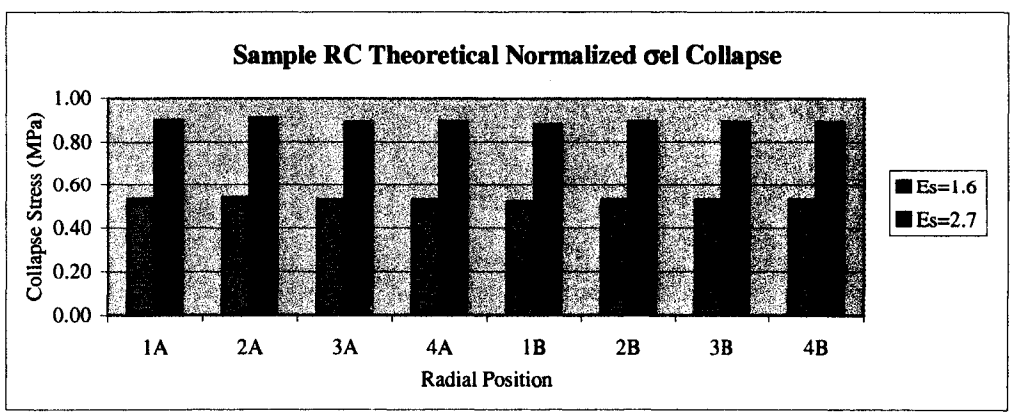

Figure-F.10: Theoretical σel Collapse for Tall and Reference Mold Samples

Reproduced with permission of the copyright owner. Further reproduction prohibited without permission.

APPENDIX G

PERMISSION TO USE COPYRIGHTED MATERIAL

Reproduced with permission of the copyright owner. Further reproduction prohibited without permission.

Permission to Use Copyrighted Material

University of Nevada, Las Vegas

I, Marion B. Rhodes holder

of copyrighted material entitled Characterization of Polymeric Structures

authored by M. B. Rhodes

and originally published in Low Density Cellular Plastics

hereby give permission for the author to use the above described material in total or in part for inclusion in a master's thesis/ doctoral dissertation at the University of Nevada, Las Vegas.

I also agree that the author may execute the standard contract with University Microfilms, Inc. For microform reproduction of the completed dissertation, including the materials to which I hold copyright.

Marion B. Rhodes 11/14/03

Signature Date

Marion B. Rhodes Professor of Chemistry.

Name (Typed) Title

Chemistry Dept. Univ. of Massachusetts

Representing

Reproduced with permission of the copyright owner. Further reproduction prohibited without permission.

REFERENCES

[1] Goods, S.H., Neuschwanger, C.L., Henderson, C., Skala, D.M., March 1997, "Mechanical Properties and Energy Absorption Characteristics of a Polyurethane Foam," Sandia National Laboratory report 97-8490.

[2] Honkomp, D.J., Casagrande, G., October 2002, "All-MDI Fully Water Blown Molded Flexible Foam Systems for the North American ("Technical Bulletin 117") Furniture Market," Proceedings of the 2002 Polyurethanes Conference. Salt Lake City, Utah, pp.393-408.

[3] Bailey, R.E., Robert, W.P., October 2002, "MDI, TDI and the Environment," Proceedings of the 2002 Polyurethanes Conference. Salt Lake City, Utah, pp. 106-109.

[4] Whinnery, L.L., Goods, S.H., Irvin, D.J., Skala, D.M., Leonard, C.M., April 27-30 1999, "A Replacement Polyurethane Foam for Stockpile Applications," Twenty-Second Aging, Compatibility and Stockpile Stewardship Conference. Oak Ridge, Tennessee.

[5] Gibson, L.J., Ashby, M.F., 1997, *Cellular Solids, Structures and Properties*, 2nd Edition Cambridge University Press, Cambridge, UK.

[6] Jackovich, D., 2003, "Temperature and Mold Size Effects on Density Gradients and Mechanical Properties in a Polyurethane Foam System," University of Nevada Las Vegas Masters Thesis.

[7] O'Toole, B., Mullin, M., Nelson, M.C., Jackovich, D., Mohan, R., May 2002,"Effect of Mold Size on the Average Density and Density Gradients in a Polyurethane Foam System," Proceedings of the Annual Technical Conference for the Plastics Industry, ANTEC. San Francisco, California.

[8] O'Toole, B., Nelson, M.C., M. Mullin, D. Jackovich, R. Mohan, et al., May 2002,"Correlation of Processing Temperature, Density Gradients, and Mechanical Properties in a Molded Polyurethane Foam System," Proceedings of the Annual Technical Conference for the Plastics Industry, ANTEC. San Francisco, California.

[9] Goods, S.H., Neuschwanger, C.L., Henderson, C., Skala, D.M., 1998, "Mechanical Properties of CRETE, a Polyurethane Foam," Journal of Applied Polymer Science, Vol. 68, pp. 1045-1055.

Reproduced with permission of the copyright owner. Further reproduction prohibited without permission.

[10] Goods, S.H., Whinnery, L.L., June 2000, "The Effect of Thermal Aging on the Mechanical Properties of a Stockpile Polyurethane Foam," Sandia National Laboratory report 2000-8245.

[11] Mallick, P.K., 1993, *Fiber-Reinforced Composites*, 2nd ed., Marcel Dekker, Inc., New York.

[12] Nelson, M.C., December 2000, "The Effects of Skin on a Polyurethane Foam," unpublished report for National Science Foundation Research Program (NSF).

[13] Kodippili, G.C., May 2003, "Structural Characterization of Polyurethane Foam and Implications of Aging," University of Nevada Las Vegas Masters Thesis.

[14] Harbron, D.R., Page, C.J., Scarrow, K.R., Jan 2001,"Methods of Minimising Density Gradients in Rigid Polyurethane Foams," Journal of Cellular Plastics, Vol. 37, pp. 43-57.

[15] Weaire, D., May 21,1994, "Froths, Foams and Heady Geometry," New Scientist, pp. 34-37.

[16] Rhodes, M.B., June 1994 "Characterization of Polymeric Cellular Structures", *Low Density Cellular Plastics (Physical Basis of Behavior)*, Ed. N.C. Hilyard and A. Cunningham, Pubs Chapman and Hall, pp. 56-77.

[17] Rompala, T.A., Sulzbach, M., Wirth, J., October 2002, "Polyurethane Raw Material Frothing Process and Acceptable Blowing Agents," Proceedings of the 2002 Polyurethanes Conference. Salt Lake City, Utah, pp. 177-185.

[18] Lin, Hong-Ru, 1997, "The Structure and Property Relationships of Commercial Foamed Plastics", Polymer Testing, Vol. 16 (Issue 5), pp. 429-443.

[19] Alberts, B., Bray, D., Lewis, J., Raff, M., Roberts, K., Watson, J.D., 1994, *Molecular Biology of The Cell*, 3rd Edition Garland Publishing, Inc., New York.

[20] Rhodes, M.B., 1997, "A Perspective on Cell Morphology and Foam Properties," *Polymeric Foams*, American Chemical Society, pp. 178-194.

[21] Chan, N., Evans, K.E., 1997, "Microscopic Examination of the Microstructure and Deformation of Conventional and Auxetic Foams," Journal of Materials Science, Vol. 32, pp. 5725-5736.

[22] Reitz, D.W., Schuetz, M.A., Glicksman, L.R., March-April 1984, "A Basic Study of Aging of Foam Insulation," Journal of Cellular Plastics, Vol. 20, n 2, pp. 104-113.

[23] Huber, A.T., Gibson, L.J., Aug 1988, "Anisotropy of Foams" Journal of Materials Science, Vol. 23, pp. 3031-3040.

Reproduced with permission of the copyright owner. Further reproduction prohibited without permission.

[24] Schwartz, N.V., Bomberg, M.T., Oct 1991, "Image Analysis and the Characterization of Cellular Plastics," Journal of Thermal Insulation, Vol. 15, pp. 153-171.

[25] ASTM Standards, "Standard Test Method for Apparent Density of Rigid Cellular Plastics," Designation: D1622-93, Vol. 14.02, pp. 349-351.

[26] ASTM Standards, "Standard Test Method for Compressive Properties of Rigid Cellular Plastics," Designation: D1621-94, Vol. 03.01, pp. 346-348.

[27] United Optical Extensometer (EX-62-LOE) Manual, prepared by United Calibration Corporation.

[28] Wang, C.S., April 1982, "Effects of Foaming Variables on Density and Morphology of Expanded Ethylene-Propylene Terpolymers," Journal of Applied Polymer Science, Vol. 27, n 4, pp. 1205-1215.

Reproduced with permission of the copyright owner. Further reproduction prohibited without permission.

VITA

Graduate College
University of Nevada, Las Vegas

Michelle Cameron Nelson

Home Address:
720 Forest Haven Way
Henderson, Nevada 89015

Degrees:
Bachelor of Science, Mechanical Engineering, 2002 (Magna Cum Laude)

Special Honors and Awards:
Harold J. and Mayme Stocker Scholarship, Fall 1998 to Spring 2003
Royal Academy of Dancing Vocational Graded Examinations in Dance,
Classical Ballet Advanced I- Passed with Merit (2003)
Tau Beta Pi, Nevada Beta, President-2001 to 2002
Tau Beta Pi, Student Member of the Year, 2001 and 2002
Tau Beta Pi, R.H. Nagel Most Improved Chapter Award, 2002
Order of the Engineer, 2003
Engineer Intern (EI#0T3999), December 2000

Publications:
1. B. O'Toole, M. Mullin, M.C. Nelson, D. Jackovich, and R. Mohan, "Effect of Mold Size on the Average Density and Density Gradients in a Polyurethane Foam System," Proceedings of the Annual Technical Conference for the Plastics Industry (ANTEC), San Francisco, CA, May 5-9, 2002.
2. B. O'Toole, M.C. Nelson, M. Mullin, D. Jackovich, R. Mohan, et al., "Correlation of Processing Temperature, Density Gradients, and Mechanical Properties in a Molded Polyurethane Foam System," Proceedings of the Annual Technical Conference for the Plastics Industry (ANTEC), San Francisco, CA, May 5-9, 2002.

Thesis Title: The Relationship of Cell Morphology, Density, and Mechanical Properties in a Rigid Polyurethane Foam

Thesis Examination Committee:
Chairperson, Dr. Brendan O'Toole, Ph. D.
Committee Member, Dr. Mohamed Trabia, Ph. D.
Committee Member, Dr. William Culbreth, Ph. D.
Graduate Faculty Representative, Dr. Malcolm Nicol, Ph. D.

Reproduced with permission of the copyright owner. Further reproduction prohibited without permission.